INSIGHTS INTO PROTEROZOIC TECTONICS FROM THE SOUTHERN EYRE PENINSULA, SOUTH AUSTRALIA

Bruce F Schaefer B.Sc. (Hons)

Department of Geology and Geophysics
The University of Adelaide
South Australia

August 1998

Thesis submitted in fulfilment of requirements for the degree of Doctor of Philosophy in the Faculty of Science, University of Adelaide

Table of Contents

List of Figures

List of Tables

Statement of originality

This work contains no material which has been accepted for the award of any other degree or diploma in any university or Tertiary institution, and, to the best of my knowledge and belief, contains no material previously published or written by another person, except where due reference has been made in the text.

I hereby consent to this copy of my thesis, when deposited in the University Library, being available for loan and photocopying

..... 28/8/98.....

Bruce F Schaefer

Abstract

The understanding of processes responsible for driving crustal growth and tectonism during the Proterozoic is still open to debate, and nonuniformitarian processes may be responsible for some of the features observed in Precambrian terrains. An investigation of Palaeoproterozoic magmatism, crustal growth and tectonism on southern Eyre Peninsula, part of the Gawler Craton, South Australia is made.

The southern Eyre Peninsula comprises a terrain which underwent extension and sedimentation from ~2000 - ~1850 Ma, prior to voluminous felsic magmatism of the Lincoln Batholith at 1853-1848 Ma. Emplacement of the tholeiitic Tournefort Dykes at 1812±5 Ma was the result of impingement of a mantle plume upon ancient lithospheric mantle and juvenile asthenosphere frozen to the base of thinned continental lithosphere. The Kimban Orogeny (1750-1700 Ma) was responsible for mid-upper amphibolite to lower granulite facies metamorphism, as well as generating the syn-post orogenic Moody Suite magmas. Sedimentation, magmatism and deformation were all controlled to differing degrees by the Kalinjala Shear Zone, a feature manifested in the present outcrop distribution of the Precambrian geology on southern Eyre Peninsula.

The Lincoln Batholith comprises voluminous felsic even-grained and rapakivi textured charnockites and granite gneisses with subordinate syn-plutonic mafic magmatism of the Jussieu Dykes. Granite gneisses are typically retrogressed equivalents of the charnockites, however primary hydrous melts are observed in the Colbert Suite. The Lincoln Batholith is chemically and isotopically homogeneous, containing elevated K, LREE and Y and negative Nb, Sr, P and Ti anomalies. $\varepsilon_{Nd(1850)}$ values range from -2.1 to -4.2. The Jussieu Dykes preserve isotopic mixing trends between the contemporary depleted mantle and local upper crust, implying asthenospheric involvement in Lincoln Batholith generation. The total area of preserved Lincoln Batholith magmatism is large, exceeding 5000km^2, and was probably emplaced in an extensional intracontinental setting over a short period of time. Trace element geochemistry and Nd isotopic signatures suggest the source for felsic Lincoln Batholith magmatism was enriched in incompatible elements, of intermediate composition and had experienced a prolonged prehistory isolated from the depleted mantle. Crustal contamination of the Lincoln Batholith is not likely to exceed 30%, with the remainder of the batholith representing the addition of new material to the continental crust.

The Tournefort Dykes comprise four geochemical groups; high Magnesium tholeiites, Iron rich tholeiites, high Barium tholeiites and a group comprising remaining unassigned tholeiites. Pb-Pb zircon evaporation geochronology suggests an emplacement age of 1812±6 Ma for the Tournefort Dykes, comparable to a Rb-Sr isochron age of 1817±43 Ma. The Tournefort Dykes contain two isotopic groups; primitive dykes with $\varepsilon_{Nd(1812)}$ ranging from +1.8 to -1.8, and more evolved dykes with $\varepsilon_{Nd(1812)}$ values from -2.9 to -6.2. Low compatible element ratios such as Ti/V and Zr/Y and depleted mantle-like geochemistry of non-cumulate dykes suggests the evolved signatures are not a product of crustal contamination. Nd-Sr isotope relationships preclude simple depleted mantle - continental crust mixing. An enriched lithospheric mantle source is therefore required to generate the evolved isotopic signature of the Tournefort Dykes. The low $\varepsilon_{Nd(1812)}$ dykes also display ocean island basalt affinities, suggestive of a mantle plume, which is also a plausible source

of thermal energy to drive Tournefort magmatism. High $\varepsilon_{Nd(1812)}$ dykes exhibit a tendency towards depleted mantle - continental lithospheric mantle mixing arrays, suggesting that asthenosphere was involved in their genesis. This is likely to be asthenosphere frozen onto the base of extended lithosphere between ~2000 - 1850 Ma. The Tournefort Dykes therefore record the interaction between the ancient lithospheric mantle, a Palaeoproterozoic mantle plume and juvenile lithosphere in the form of asthenosphere frozen onto the base of the lithosphere.

The Kimban Orogeny took place between 1750-1700 Ma, and was responsible for deformation of all of the lithologies described above. Metamorphism was distributed asymmetrically about the Kalinjala Shear Zone, suggesting the overall orogenic environment may have been transpressional. Strain and metamorphism was partitioned into distinct zones within the Lincoln Batholith, resulting in enrichment of SiO_2, Na, K, Rb, Th, La and Ce and depletion of Ba, Sr, P, and Ti in felsic lithologies in high strain zones. The geochemical subgroups of the Tournefort dykes display changes in absolute trace element concentrations with increasing deformation, however overall trace element patterns within a geochemical subgroup tend to be preserved, regardless of mineralogy.

The Kimban Orogeny was also accompanied by Moody Suite magmatism west of the Kalinjala Shear Zone. This dominantly felsic magmatic event evolved from early S-type granitoids through I- to A-type granites and intermediate intrusives, terminating in post orogenic small volume mafic-ultramafic magmatism. An increasing mantle input to magmatism during the orogen is implied.

Lincoln Batholith magmatism is similar in age and chemistry to magmatic suites of northern Australia. Further, corresponding isotopic, chemical and terrain scale geophysical signatures suggest a possible correlation between the Lincoln Batholith and the Ewen and Kalkadoon Batholiths of the Mount Isa Inlier. Such a correlation is further strengthened by similarities in timing and style of magmatism in the adjoining eastern terrains; the Moonta subdomain and Eastern Foldbelt respectively. Nd isotope signatures and geochemistry of basement granodiorites at Roxby Downs, and geochronology of magmatism in the Peake and Denison Inliers support correlations by providing a geographic link between the two terrains.

Palaeoproterozoic magmatism in general falls into two distinct classes; those containing primitive isotopic signatures, coincident magmatism and deformation and displaying calc-alkaline affinities. Such magmatic provinces are analogous to Andean and Cordilleran style continental margin settings on the modern Earth, and as such represent a mechanism for Proterozoic crustal growth. However, Palaeoproterozoic provinces such as the Lincoln Batholith and the Ewen-Kalkadoon Belt in Mount Isa record homogeneous magmatic systems with elevated K, LREE, and Y enrichment with respect to modern plate margins. They also occur in intraplate settings with little or no synchronous deformation and contain evolved Nd isotopic ratios. Such magmatic events represent discrete, large volume crustal growth events. In the case of the Kimban Mobile Belt, orogenesis was in part driven by the processes responsible for Lincoln Batholith magmatism. Processes associated with crustal growth and tectonism in such settings are not immediately reconcilable with modern plate tectonic models, and represent a mode of Proterozoic crustal growth competing with uniformitarian processes.

Acknowledgments

A work of this order has involved contributions from a large number of people over the last four or so years. Firstly has been the role played by my supervisors, John Foden and Mike Sandiford. They gave me enough rope to investigate the inevitable tangents, but reeled me back when necessary. The relaxed, but enthusiastic learning environment that resulted is something I'll always be grateful for. Thanks Mike and John!

Two other people played a major role in this project, particularly in field work. Martin Hand arrived just as I was beginning, and the numerous field trips and stimulating discussions about "the Linc" served to keep me on my toes. Hans Hoek has been a revelation regarding matters involving mafic dykes. His unflagging enthusiasm and probing questions have lead to the Tournefort and Jussieu being more than a mere add-on to the southern Eyre Peninsula story. A big thankyou for support above and beyond the call of duty goes to Hans and Martin.

My peers in the department have all in some way contributed to the ongoing enjoyment and support one requires for a project like this. I owe Jon Teasdale a great deal for his ideas, friendship and fantastic field trips out west. To Eike and Betina for help in the field; Kathy for innumerable discussions on the rest of the Gawler Craton; Jon DP for matters Kober related, Bunge, Pete, Marlina, Jerry, Rob, Scotty, Thomas, Haggis, Garry, Paul, Trev, Narelle, Sandra, Simon, Soph and Andy, Jo, Mandy and any I've unwittingly omitted, thanks for various Friday nights and sharing the highs with the lows.

The technical staff at Adelaide have been indispensable to my efforts; David Bruce for being patient with the only person to blow up a bomb, John Stanley for tireless XRF support, Geoff Trevelyan for thin sections and Sherry Proferes for drafting assistance. However, Gerald Buttfield is specifically thanked for his tireless "can do" attitude, even when the request seems too hard and he'd rather be going home!

Thanks must also go to those outside the immediate geology department who have helped at some stage along the way; Colin Rothnie during my time at North and John Parker at Geosurveys spring to mind. So too those "non-geo" friends such as Suse, Tan and Simon; and thanks Nic for wading through a number of drafts of the first four chapters on a subject you weren't really interested in!

Finally, I've been fortunate enough to have a family that has backed me 100% from day one. To Kate and Trent who I've basically shared a house with throughout the PhD, thanks for your patience and being constantly there throughout. To Mum and Dad, a big thankyou for everything; for supporting me when I intermitted for the n^{th} time to go on "yet another trip", for having faith that it would get done (eventually) and for offering a haven at Melaleuca where I could retreat when I needed to recharge my batteries. I don't think I can ever adequately express my thanks to you.

CHAPTER ONE

Thesis Overview

1.1 General introduction

The Proterozoic represents a crucial period in the evolution of the Earth, marking the transition from the youthful, hot Earth of the Archaean to the senescent plate tectonic modern Earth. The record of this transition is to be found in the structure and chemistry of the Proterozoic crust, and considerable effort has been expended on detailing the key aspects of this evolution. Studies investigating the origin and nature of Proterozoic continental crust (Allegre and Othman, 1980; Dewey and Windley, 1991, Condie, 1993; McCulloch and Bennett, 1994; Taylor and McLennan, 1995), mechanisms driving Proterozoic tectonism and orogenesis (Baer, 1983; Etheridge et al., 1987; Hill, 1993), interaction between the crust and lithospheric mantle (Goldstein, 1988; Davies, 1992) and the thermal structure of Proterozoic crust (Davies, 1993) have all served to highlight enigmatic features of this period of Earths history (eg, Moores, 1986).

Such features have proved difficult to decipher, in part due to the polymetamorphic and deformational history of Proterozoic terrains. Increasingly sophisticated geochronological techniques, such as SHRIMP U-Pb zircon analysis, have allowed the construction of accurate temporal frameworks of geological events (eg, Page, 1998). When combined with precise isotopic and geochemical parameterisation of igneous suites such a framework can constrain petrogenetic processes, temporal magmatic evolution and ultimately offer insights into tectonic styles and their driving processes (eg, Allegre and Othman, 1980; Anderson, 1991; Taylor and McLennan, 1995). Further information regarding the nature of tectonism and geodynamics may be derived from integrating structural and metamorphic observations of a given terrain with geochemical data (eg, O'Dea et al., 1997).

This thesis approaches understanding the evolution of Proterozoic terrains and processes from the perspective of geochemistry and crustal evolution, using the Palaeoproterozoic of the southern Eyre Peninsula, South Australia, as a case history.

Eyre Peninsula is well suited to such a study due to; (1) semi-continuous exposure of a large igneous province over a large area allowing evaluation of styles and volumes of the growth of continental crust, (2) extensive mafic dyke magmatism, potentially allowing insights into contemporary mantle chemistry and (3) a well preserved relationship between magmatism and deformation, offering constraints on tectonic setting. Additionally, the nature of contemporary crust can be constrained by proximal basement lithologies, limiting potential crustal contaminantion models. Therefore, the interplay between magmatism, deformation and the lithospheric evolution, and hence crustal growth and Proterozoic tectonism is accessible in such terrains.

The exposed Late Archaean - Palaeoproterozoic supra- and infracrustal rock sequences of the southern Gawler Craton are generally well constrained temporally. These sequences are geochemically and isotopically evaluated from a crustal growth and tectonic perspective, and placed in a global context to determine the validity of regional scale tectonic models to global scale problems associated with the Precambrian.

With this in mind, in order to investigate Proterozoic crustal evolution and growth, the primary aims of this thesis are:

i) documenting the geology of southern Eyre Peninsula, particularly with respect to intrusive rocks, in order to elucidate a model for tectonism and crustal evolution for this setting, and

ii) comparison of geochemical, structual and metamorphic features of the southern Eyre Peninsula with terrains of similar age and/or chemistry in order evaluate secular global variations in tectonism and crustal growth.

To achieve the first of these aims, definition of the primary magmatic relationships, chemistry and petrogenesis of Palaeoproterozoic intrusives of southern Eyre Peninsula and characterisation of the chemical and isotopic evolution of the Palaeoproterozoic lithosphere on the southern Eyre Peninsula by regional scale analysis of older rock suites was conducted. This produced a geodynamic model for the isotopic and structural evolution of the intrusives and their basement during the Kimban Orogen.

The second primary aim involved a review of existing models for Proterozoic tectonism and crustal growth and collection of data from terrains potentially analagous to southern Eyre Peninsula. This allowed the chemistry of Palaeoproterozoic intrusive suites on southern Eyre Peninsula (specifically the Lincoln Batholith and Tournefort Dykes), and the geodynamic model developed from the regional study, to be interpreted in a global geodynamic context.

In order to set the scene for this thesis, the remainder of this chapter briefly outlines some of the prevailing views on Proterozoic tectonics and crustal growth. This is followed by a description of how this thesis is set out to address problems relating to crustal growth and tectonics from the perspective of southern Eyre Peninsula.

1.2 Proterozoic crustal growth

Precambrian terrains contain many features that are not immediately explicable within the modern plate tectonic paradigm (eg, Taylor and McLennan, 1983; Kröner, 1984; Etheridge et al, 1987; Park, 1997). Regional high temperature-low pressure metamorphism (figure 1.1), bimodal magmatism (Etheridge et al., 1987) and an absence of ophiolites (Moores, 1986) and paired metamorphic belts has led to speculation on the relationship between Proterozoic tectonism, continental crustal growth and potential modern analogues (eg, Fyfe, 1978; Etheridge et al., 1987; Moores, 1993; Ellis, 1992; Taylor and McLennan, 1995).

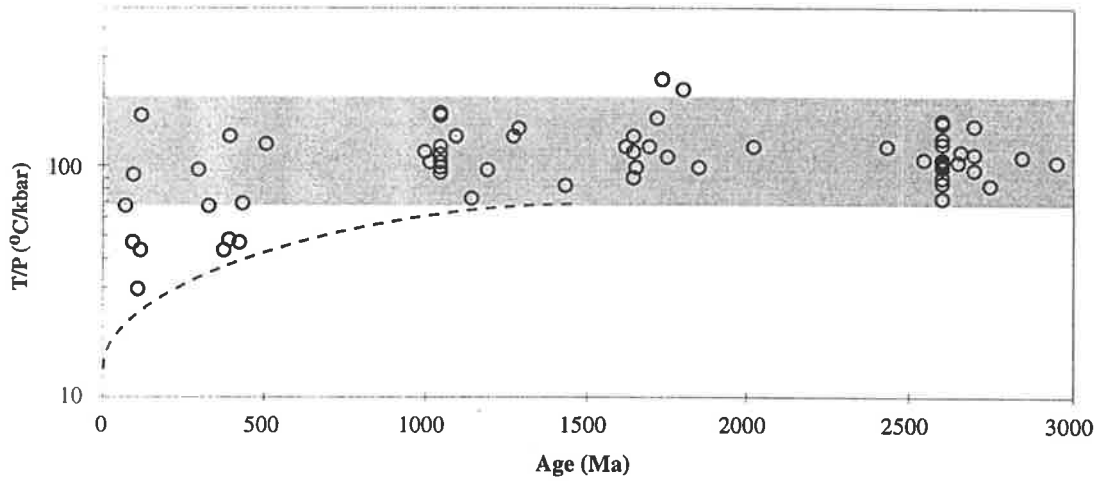

Figure 1.1: An example of non-uniformitarian phenomena. Average values for regional scale metamorphism over the history of the Earth, expressed as a ratio of peak temperature and pressure. A gradual trend towards higher pressure orogens in the Phanerozoic from high temperature/low pressure Proterozoic terrains is observable. Data summarised in Appendix 4.

That features exist in the Precambrian geologic record which do not have immediate modern analogues is undisputed; komatiites and Tonalite-Trondjhemite-Granodiorite's (TTG's) are classic examples of this. The crux of the issue is whether such features are driven by essentially modern processes acting in different conditions, or if they reflect a fundamentally unique tectonic mode and hence geodynamic driving force. One example of such a feature is illustrated in figure 1.1, where peak P-T regional metamorphic conditions are summarised as a function of

the age of the Earth. What is immediately noticeable is that only in the last ~1 Ga has the crust of the Earth preserved low T/high P metamorphism. Moores (1986) notes a distinct change in the nature of ophiolitic and related complexes at about the same time, suggesting that some change in the strength of the lithosphere has occurred during the history of the Earth.

Many other features of the Precambrian show similar temporal patterns, with the apparent age of changing from one distinct characteristic to that of the modern day varying significantly from as early as the Archaean-Proterozoic boundary (eg, changes in the chemistry of sediments; Taylor and McLennan, 1995), to as late as ~1 Ga (as in the example above).

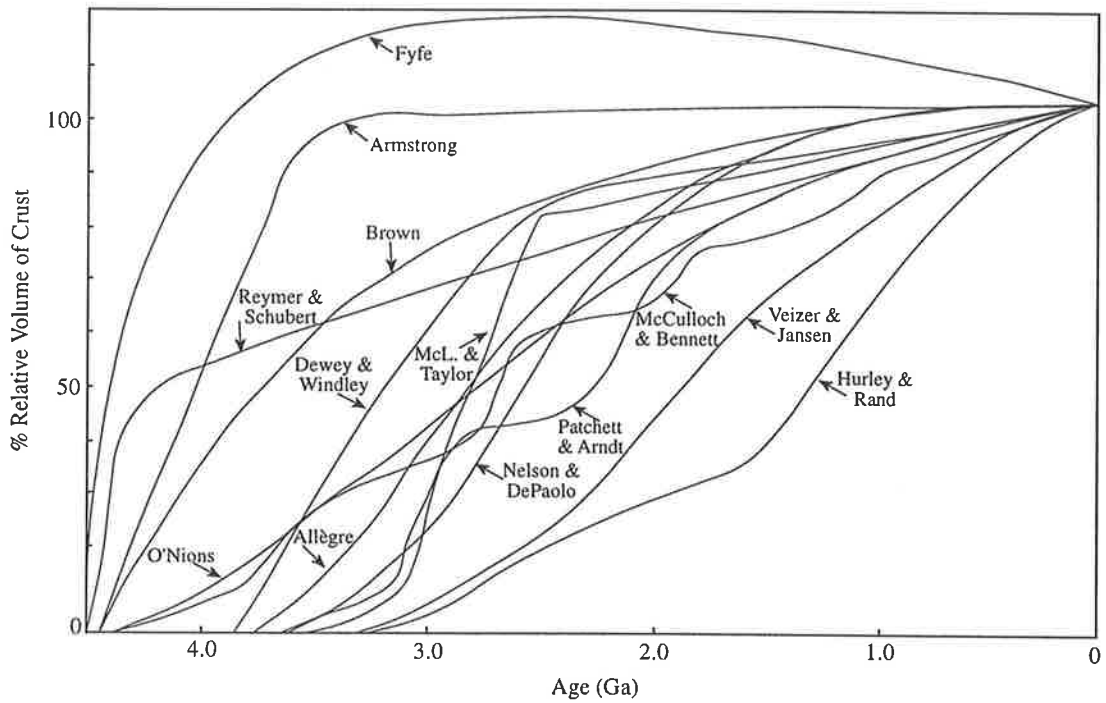

Figure 1.2: Cumulative crustal growth curves from various workers. Note models involving steadily increasing volumes of crust, episodic growth, decreasing and steady state. Curves from Hurley and Rand, 1969; Fyfe 1978; Dewey and Windley, 1981; McLennan and Taylor, 1982; Allégre and Rosseau, 1984; Nelson and DePaolo, 1985; Veizer and Jansen, 1985; Patchett and Arndt, 1986; Reymer and Schubert, 1986; O'Nions and McKenzie, 1988; Armstrong, 1991; McCulloch and Bennett, 1994. Summarised in Tarney and Jones, 1994.

Regardless, there is still no clear understanding of whether the tectonic regime of the Earth has changed over time (a non uniformitarian view, eg, Fyfe, 1978; Kröner, 1983 ,1984; Etheridge et al., 1987), or merely experienced variations within a single tectonic mode (a uniformitarian approach, eg Windley, 1993; Armstrong, 1991). The development of a unifying tectonic theory for the ancient Earth remains of fundamental importance to geoscientists, as tectonics influences setting and duration

of sedimentation, orogenesis and tectonism, as well as style and size of ore deposits (eg, Barley and Groves, 1992).

Central to the notion of a unifying tectonic theory is the concept of crustal growth. Crustal growth in general involves understanding whether the total mass of continental crust has grown, remained constant, or even decreased over time. On the modern Erath, the bulk of continental addition is thought to take place via the lateral accretion of arcs at plate margins (eg, O'Nions et al., 1979; Reymer and Schubert, 1987), with comparatively small (but disputed) masses of continental material being reycled into the mantle at subduction zones. Hence, the growth of continental crust is related directly to the driving tectonic regime on the modern Earth.

Methods for estimating the growth of continental crust vary widely. Arguments involving continental freeboard (eg, Windley, 1977; McLennan and Taylor, 1983; Armstrong, 1991) all agree that greater continental emergence will result in greater deposition of continentally derived sediment in ocean basins, however the net effect of this on crustal growth is unclear (eg, Gurnis and Davies, 1986). Armstrong (1991) interprets greater sedimentation to imply greater rates of sediment subduction. It also appears that continental freeboard is greater on the modern Earth, suggesting greater levels of erosion, however no calculations involving the effect of biota (particularly the emergence of land plants) which may inhibit erosion, have been carried out. Hence, crustal growth curves calculated on freeboard arguments can appear different to those calulated from the age distribution of preserved continental crust (eg, McCulloch and Wasserburg, 1978; Nelson and DePaolo, 1985). Other estimates for crustal growth come from investigating the role granitic magmatism and AFC processes (eg, DePaolo et al., 1991, 1992) in adding new material to the continental crust and those derived from sedimentary residence times and fluxes through various reservoirs (eg Veizer and Jansen, 1985; Condie, 1993). Curves derived by each of these methods are summarised in figure 1.2.

Precambrian crustal growth can be broadly discussed in terms of those models involving an uniformitarian approach, and those requiring secular changes in tectonism and mechanisms of crustal growth during Earth history. Preceding discussion has assumed continental growth, however a model advocated by Armstrong (1991, and references therein), suggests that the mass of the continental crust has remained constant. Armstrong (1991) proposed rapid development of crustal volumes similar to those of the modern Earth, very early in the Earths history. This large crustal volume has been maintained throughout time by balancing crustal growth via volvanic arc related processes with recycling of crustal sediments through the mantle via subduction. Such a model results in a steady state, no net continental crustal growth scenario driven by essentially modern Earth plate tectonic processes (figure 1.2).

In a similar vein, Windley (1993) argued that processes driving orogenesis and tectonism "...since the early Archaean have not been fundamentally different from those that operate today...", resulting in subtly different features forming in response to modern processes. Most notable amongst these are chemical variations in magmatism, both within plates and at plate margins. Modern arcs. for example, commonly (but not exclusively) contain calc-alkaline affinities and intermediate compositions, whereas the reverse appears to be the case for the Proterozoic.

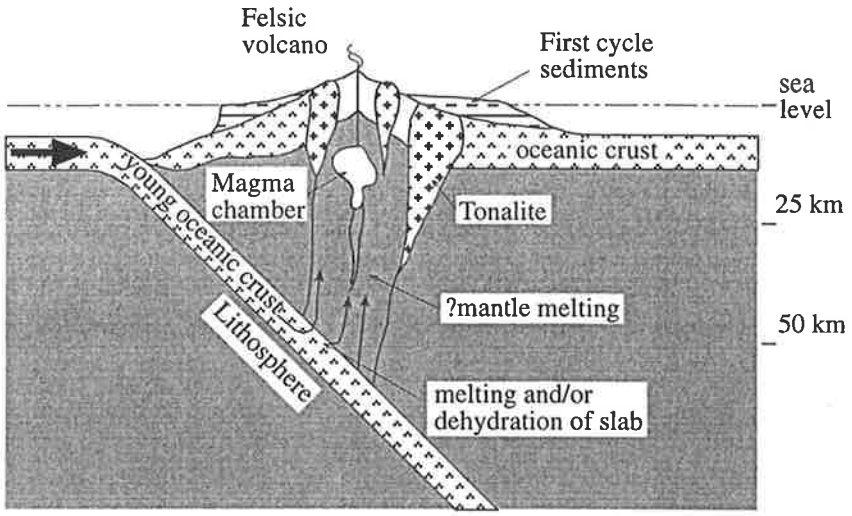

Figure 1.3: Example of Precambrian crustal growth using essentially uniformitarian processes to produce nonuniformitarian features (after Taylor and McLennan, 1995). Subduction of young, hot oceanic crust results in melting reactions taking place prior to complete slab dehydration, with melting occurring not only in the mantle wedge, but in the slab itself. This style of melting produces distinctly bimodal magmatism and sodic felsic intrusives.

Many other uniformitarian models suggest only small volumes of continental crust developed during the early stages of Earth formation, which has been added to subsequently, either by steady state accretion of material from the mantle (eg, O'Nions et al., 1979; Gurnis and Davies, 1986), or punctuated periods of crustal growth in episodic pulses (figure 1.2) within a plate tectonic setting (eg, Taylor and McLennan, 1981, 1995). The main distinctions between models within this latter class is the timing of onset of plate tectonics (or analogous regimes), and whether crustal growth is episodic (Moorbath, 1977) or continuous in nature (eg, Hurley and Rand, 1969; Gurnis and Davies, 1986). All such models assume crustal growth takes place in settings analogous to modern arc settings (eg, figure 1.3), with secular variations in magma chemistry (and hence composition of accreted crust) due to the changing thermal budget of the Earth (Windley, 1993; Taylor and McLennan, 1995). The most commonly cited estimate for the timing of the onset of modern style plate

tectonics is the late Archaean, as reflected by a major pulse of crustal growth (McCulloch and Bennett, 1994), a major change in the REE signatures of sediments at the time, reflecting a change in source areas available for such sediments (Taylor and McLennan, 1985) and possible climate changes (eg, Young, 1991).

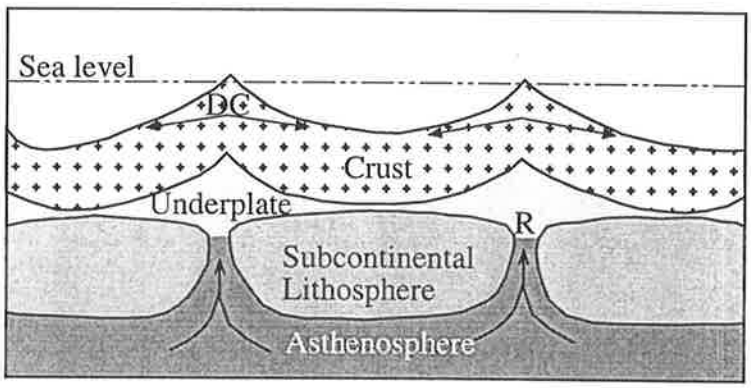

Figure 1.4: "Hot Spot " tectonics of Fyfe, 1978. Mafic magma rises from the asthenosphere over a length scale of hundreds of kilometres, with the majority underplating a layer cake crust of submarine felsic and mafic volcanics. Rising magma domes the crust (DC), creating a gravitational potential resulting in lateral movement of crustal material along thrust planes, overthickening crust between upwelling zones. Cessation of mantle upwelling results in cooling and finally return of overthickened material to the mantle at sites labelled R. Such a scenario would be applicable for Archaean plate motions, setting the scene for a transition towards modern style plate tectonics during the Proterozoic with the generation of increasing volumes of oceanic crust (Fyfe, 1978).

Alternatively, workers have argued for distinctly unique geodynamic processes driving Precambrian tectonism and crustal growth. A comparatively recent (post Palaeoproterozoic) onset of modern style plate tectonics is implied by such models. For example, Fyfe (1978), suggested an early segregation of large volumes of sialic crust, followed by small scale convective tectonics (figure 1.4) after freezing of continental crust to the mantle (ie formation of the subcontinental lithosphere). Proterozoic tectonics was, he argued, dominated by the progressive segregation of the sial and hydrosphere to form continental and oceanic crust, and ultimately lithospheric plates able to be driven by large scale mantle convection. The onset of modern (Wilson cycle) plate tectonics took place at the start of the Phanerozoic, and crustal growth has been maintained essentially in a steady state since this time.

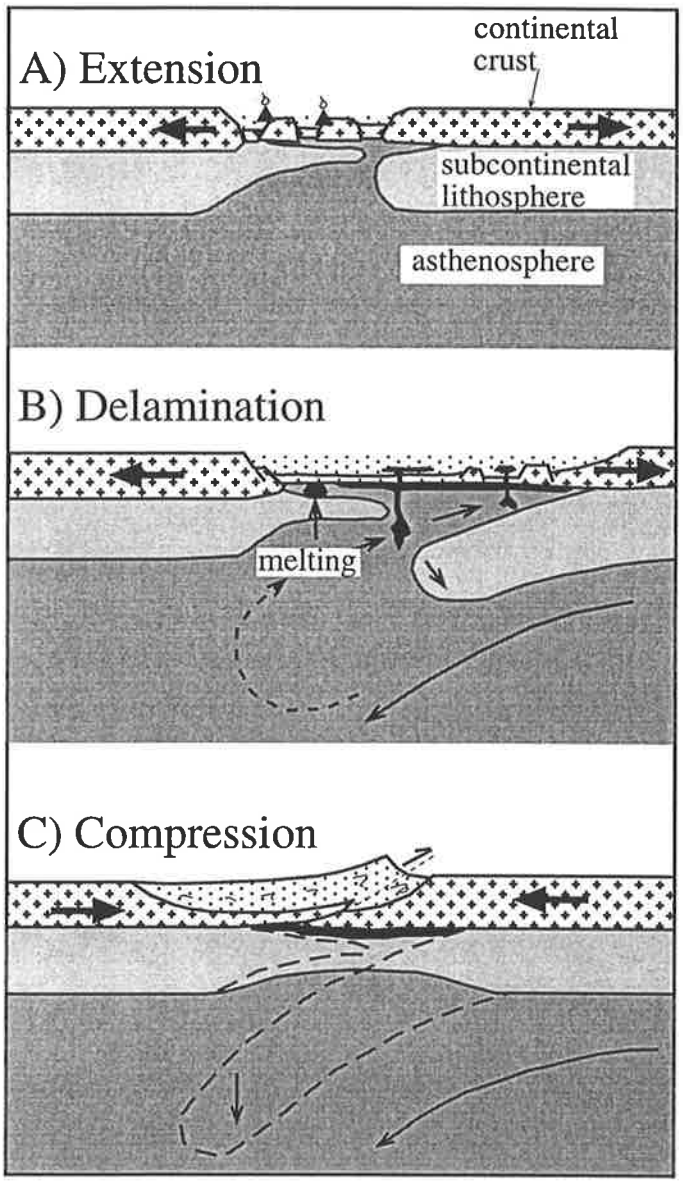

Figure 1.5: Cartoon of ensialic foldbelt evolution involving A-subduction as proposed by Kröner (1983). Lithospheric extension due to transmission of far field stresses results in rifting with small volume extensional magmatism. Decompression melting results in underplating of thinned continental crust, and delamination of subcontinental lithosphere is initiated. Subsequent compression in response to delamination results in crustal interstacking and orogenesis. A variation on this model was proposed for northern Australia by Etheridge et al. (1987). Adapted from Kröner (1984).

Other nonuniformitarian models include that of Etheridge et al. (1987), in which (Palaeo)Proterozoic tectonism and orogenesis is attributed to intracratonic ("ensialic") processes driven by delamination of underplated subcrustal mantle lithosphere ("A-type" subduction of Kröner, 1983, 1984; figure 1.5). Crustal growth in such a scenario is envisaged to take place in an essentially vertical sense, with additions of material to the crust from partial melts derived from both the

underplated layer and upwelling mantle. Vertical crustal accretion is a marked contrast to the essentially lateral continental growth of modern arc related settings. Again, the onset of plate tectonics is held back until the Neoproterozoic, consistent with the Proterozoic being a period of transition from a nonuniformitarian Archaean tectonic regime, to a Phanerozoic plate tectonic regime.

The majority of tectonic models for the duration of the history of the Earth suggest that Wilson style plate tectonics was in operation, but the resulting products were significantly different from their modern analogues due to secular changes in heat flow over Earth history (eg, Ellis, 1992; Windley, 1993). Such models attribute the apparent ensialic nature of orogenesis described by Etheridge et al, (1987) to the transmission of far field stresses from actively convergent plate margins driven by modern geodynamic processes (ie, analagous to the Tien Shan in China).

A final possibility involves the concept of contemporaneous competing tectonic regimes. Therefore, in the Archaean Earth, plate tectonic features were either unable to develop or were effectively swamped by more vigorous, non-uniformitarian processes, with the converse holding for the modern Earth.

Therefore, Proterozoic terrains contain some features which remain unresolved in the geological lterature. By integrating the geochemical features of modern style tectonic regimes and comparing them with ancient orogens, it is possible to place constraints on the nature of processes driving tectonism. Chemically and isotopically evaluating source regions of magmatism and their evolution prior to, during and immediately after tectonism allows insights into the nature of mantle reservoirs, their endurability, and the manner in which they interact with contemporary crust. All such observations result in building a terrain scale picture, linking magmatism with crustal growth, tectonism and in many cases, fundamental geodynamic driving mechanisms.

One of the primary aims of this thesis is to develop such a terrain scale picture for the southern Gawler Craton, and on the basis of broad scale comparative criteria, comment on the driving geodynamic mechanisms of Proterozoic crustal growth and tectonism.

1.3 Organisation of this thesis

This thesis is laid out in a manner which systematically investigates the key elements of the southern Eyre Peninsula in order to gain insights into timing, nature, sources and volumes of crustal growth. Elucidation of such growth mechanisms place constraints on possible tectonic regimes responsible for the generation of the continental crust.

Chapter 2 is a summary of current understanding of the geology of southern Eyre Peninsula, and acts as a reference guide to terminology and nomenclature of

lithologies and events. The derivation of, and changes in usage of various terms pertaining to the geology of Eyre Peninsula is also discussed. Chapter 3 summarises the key chemical and petrological features of the Lincoln Batholith, and integrates field observations with new Sr and Nd isotopic data. A model for petrogenesis for such a homogeneous, large volume magmatic event is developed. Chapter 4 employs a similar approach to investigate the younger Tournefort Dykes. The Tournefort Dykes contain isotopic evidence regarding the nature of the subcontinental lithospheric mantle. Chapter 5 deals briefly with the isotopic nature of the crust within which the Lincoln Batholith and Tournefort Dykes were emplaced. These observations constrain potential sources for crustal contamination, and act as a crucial independent test on petrogenetic models developed in Chapters 3 and 4. The chemical evolution of the syn-Kimban Orogenic Moody Suite Granitoids is also briefly touched upon. The nature of the Kimban Orogeny is further developed in Chapter 6, which summarises prevailing metamorphic conditions within the Lincoln Batholith, and how these relate to the adjacent Hutchison Group Metasediments. The style of deformation and metamorphism within the Kimban Orogeny has significant implications for contemporary geodynamics. A brief investigation into the potential geochemical effects of Kimban overprinting on Lincoln Batholith lithologies is also conducted. Chapter 7 presents a comparative chemical study with other magmatic terrains. Data from terrains of well constrained geodynamic settings (eg, the Andes) is evaluated in terms of the Lincoln Batholith, which is in turn compared with terrains of similar age (eg, Mt Isa). Such comparisons allow the validity of crustal growth models on both the ancient and modern Earth to be discussed. Chapter 8 summarises the key aspects from preceding chapters regarding Proterozoic tectonics, and evaluates the applicability of integrated, geochemical based studies in crustal growth problems.

Some publications have arisen as a consequence of this work. In particular:

Schaefer, B.F., Foden, J., Sandiford, M. and Hoek, J.D., in prep. The Jussieu and Tournefort Dykes of the Gawler Craton, South Australia. (based on chapter 4 and parts of chapters 3 and 6). A copy of this manuscript is included in appendix 5.

Hoek, J.D. and Schaefer, B.F., 1998. The Palaeoproterozoic Kimban mobile belt, Eyre Peninsula: Timing and significance of felsic and mafic magmatism and deformation. *Australian Journal of Earth Sciences.* **45**, p. 305-313 (based on chapter 6 and parts of chapters 3 and 4). A complete version of this paper is in appendix 6.

Conference abstracts derived from this study are included in appendix 7.

CHAPTER TWO

The southern Eyre Peninsula

This chapter summarises the working stratigraphy used within the thesis. A brief historical review of previously applied terminology and nomenclature is also conducted to allow integration of this study with previous work.

2.1 Regional Geology

The Gawler Craton is the largest Precambrian tectonic element in South Australia, and records a significantly different geological history to the dominantly older Western Australian Cratons and many of the cratons and basement inliers of northern Australia. Comprised dominantly of Late Archaean to Mesoproterozoic rocks, this stable crystalline basement province extends from clearly defined southern and eastern margins, the edge of the southern continental shelf and the Torrens Hinge Zone (marking the edge of Delamerian effects) respectively. Recent high resolution aeromagnetic data collected by Mines and Energy, South Australia (MESA) has allowed more precise definition of the western and northern boundaries of the craton, which are obscured by Neoproterozoic and Phanerozoic cover. At present, these margins are placed beneath Officer Basin sediments, and are defined by large scale shear zones (figure 2.1) identifiable as distinct aeromagnetic features.

The Gawler Craton has been further subdivided into discrete subdomains on the basis of geophysical and lithological, structural and metamorphic character, each containing a relatively homogeneous combination of magmatism, deformation and metamorphism, but differing from adjacent regions in several significant aspects (Parker, 1990). Figure 2.1 shows the tectonic subdomains on the Gawler Craton. This differs significantly from those initially defined by Parker (1990) due to the advent of regional scale, high resolution aeromagnetic data. Of primary interest to this thesis are the Coulta and Cleve subdomains, essentially comprising the western and eastern halves of Eyre Peninsula respectively (figure 2.1). The Kalinjala Shear Zone is a major crustal feature within the Cleve subdomain, to a large degree responsible for the

current exhumation level of the lithologies exposed in the southern portion of the domain.

In terms of large scale geological architecture, the Gawler Craton has been considered, by Fanning et al. (1995, 1996) to represent a continuation of lithologies observed across the Southern Ocean, and hence a part of the East Antarctic Shield. The term Mawson Block has been proposed by Fanning et al. (1995, 1996) to incorporate the Gawler Craton, George V Land, Terre Adélie and the Central Transantarctic Mountains. In this context, the proximity of the southern Eyre Peninsula to the southern margin of the Gawler Craton provides a basis for potential correlation of both lithological units and tectonism into the East Antarctic Shield.

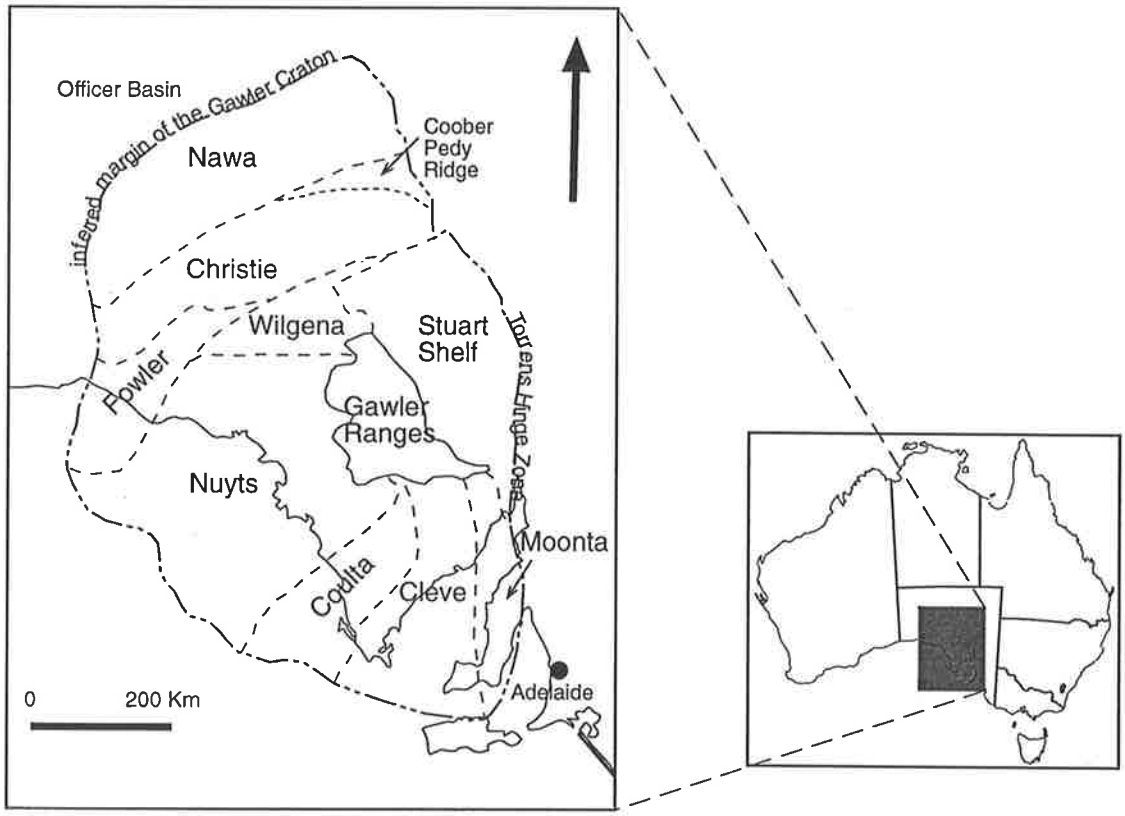

Figure 2.1: Extent of the Gawler Craton, and distribution of tectonic subdomains. Modified from Parker (1990).

The current understanding of the geology of southern Eyre Peninsula, based on a U-Pb zircon geochronology framework, may be summarised as follows (unless otherwise noted, all data and source references are in Drexel et al., 1993):

The Sleaford Complex

The oldest sequence of rocks on southern Eyre Peninsula is the late Archaean Sleaford Complex, which is composed of the dominantly paragneissic granulite facies Carnot Gneisses (Fanning, 1975) and variably deformed Dutton Suite intrusives (Parker et al., 1985). The Sleafordian Orogeny was responsible for high

grade deformation and metamorphism of the Carnot Gneisses, possibly beginning as early as 2631±21 Ma, with peak conditions between ~2440-2400 Ma (Fanning, 1997.). Amphibolite facies metasediments of the Wangary Gneiss (Parker et al., 1985) have been interpreted as lower grade equivalents of the Carnot Gneisses, and metamorphic zircon ages in the Wangary Gneiss of 2479±8 Ma (Fanning, 1997) are consistent with this (figure 2.2). The Dutton Suite, interpreted as a syn-Sleafordian magmatic event, contains the Coulta Granodiorite (2514±9 Ma (Dougherty-Page, unpublished data), 2517±14 Ma (Fanning, 1997)), the Kiana Granite (2459±15 Ma, Fanning, 1997) and the Whidbey Granite, the last of which outcrops only offshore, (2558±27 Ma, Fanning, 1997). The Sleaford Complex covers the western half of Eyre Peninsula, and is correlated with the Mulgathing Complex in the northwestern Gawler Craton.

Post Sleafordian Palaeoproterozoic sequences

The Miltalie Gneiss and equivalents, outcrops of which west of Tumby Bay have been dated at 2003±13 Ma (Fanning, 1997), post date the Sleaford Complex but unconformably underlie younger sediments of the Hutchison Group. The Miltalie Gneiss is typically orthogneissic in character and occurs in a limited areal extent on southern Eyre Peninsula.

Mortimer (1984), recognised a series of pre- D1 ortho- and paragneisses on the eastern side of the Kalinjala Shear Zone, to which he assigned the name Massena Bay Gneisses (figure 2.2). The most distinctive lithologies of this group are metasediments of various metamorphic grade present as enclaves within the younger Lincoln Batholith, and are likely to be either Sleaford Complex or Hutchison Group metasediments. The orthogneissic portions of this sequence are either early phases of the Lincoln Batholith that preserve features of extended D1 (pre-Kimban) deformation during emplacement or Miltalie Gneiss equivalents. For the remainder of this contribution, the term Massena Bay Gneisses will be used for that material that is clearly basement to the Lincoln Batholith, usually lithologies which are metasedimentary in origin.

The Hutchison Group

Unconformably overlying the Miltalie Gneiss and Sleaford Complex is a sequence of shallow to deeper water basinal sediments of the Hutchison Group (figure 2.2). This sequence comprises the basal massive Warrow Quartzite, which is conglomeritic in part and a lateral facies of, and grades into the Middleback subgroup. This subgroup consists of a series of mixed chemical semipelitic metasediments, which are essentially composed of carbonate, sulphide, silicate and oxide facies Banded Iron Formations, grading into deeper water semipelitic sediments of the Cook Gap Schist. The upper portions of the Hutchison Group are locally composed of another deeper water semipelitic sequence, the Yadnarie Schist,

which is considered to be laterally equivalent with a mixed acid volcanic and calcsilicate unit, the Bosanquet Formation.

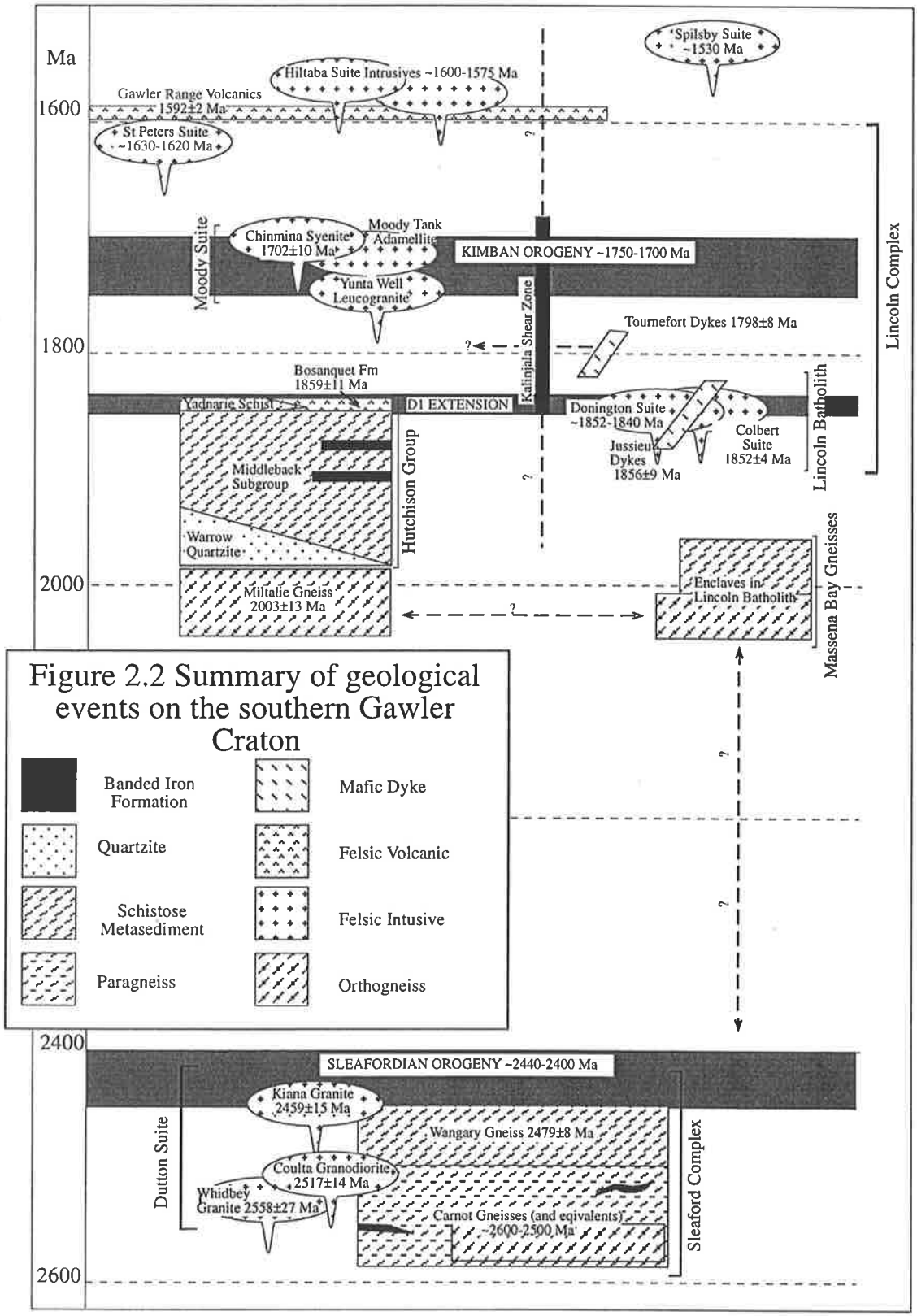

Figure 2.2 Summary of geological events on the southern Gawler Craton

The Bosanquet Formation is the topmost preserved unit of the Hutchison Group (figure 2.2), and a U-Pb zircon age from rhyodacite in the volcanics of 1859±11 Ma presently defines the cessation of sedimentation on the Hutchison Group.

Palaeoproterozoic felsic intrusives

As discussed below, the term Lincoln Complex as defined by Thomson (1980), encompasses all magmatism in the period ~1850 Ma (cessation of Hutchison Group sedimentation) to Gawler Range Volcanics magmatism, at 1592±2 Ma. Within this time frame there are three major suites of dominantly felsic magmatism (figure 2.2), the Lincoln Batholith (~1852-1843 Ma), Moody Suite(~1750-?1700, possibly as late as ~1670 Ma) and St Peters Suite (1630-1620 Ma). Other smaller volume plutons of differing ages and/or uncertain stratigraphic position have been assigned to the Lincoln Complex, which may represent unrecognised correlatives of the suites described above, or an entirely independent magmatic event (eg, the Carappee Granite, on central Eyre Peninsula at 1689±59 Ma). At present, there is no reason to genetically link any of the Lincoln Batholith, Moody Suite or St Peters Suite.

Since recognition of the St Peters Suite (Flint et al., 1990), there has been a trend to define the Kimban Orogeny to encompass the period ~1850-~1700 Ma (see Drexel et al., 1993; Fanning, 1997; Daly et al., in prep), effectively removing the St Peters Suite from the Lincoln Complex *ss*. Furthermore, Hoek and Schaefer (1998) have argued that the Kimban Orogeny should strictly encompass ~1750-1700 Ma, making the Moody Suite the only true Lincoln Complex magmas due to their syn-Kimban nature. They suggested the term Lincoln Batholith (see below) for the ensemble of igneous rocks that predate the Tournefort Dykes (and hence the onset of the Kimban) (figure 2.3).

The Donington Suite is a major component of the Lincoln Batholith, and, along with the Colbert Suite and Jussieu Dykes, comprises a major magmatic event from 1849.8±1.1-1846±14 Ma (Fanning and Mortimer, in prep.) (figure 2.3). Although these two suites were previously considered to be discrete magmatic events (eg, Mortimer et al., 1988a), recent geochemical and geochronological work (Fanning and Mortimer, in prep.) suggests the Colbert Suite is part of the evolving Lincoln Batholith.

The Moody Suite is a series of syn-post Kimban Orogenic granitoids (figure 2.3) ranging in composition from the variably deformed S-type Yunta Well Leucogranite, which is intrusive into, and intimately related with the Hutchison Group in the Tumby Hills, through the weakly deformed Moody Tank Adamellite (1709±14 Ma, Rb-Sr) to the undeformed I-type Chinmina Syenite (1702±10 Ma) and Mooreenia Adamellite (1692±10 Ma, Fanning, 1997). Possible Moody Suite equivalents further north include the Middle Camp Granite (1731±7 Ma, Fanning, 1997), intrusive into the Hutchison Group in the Cleve Hills, and the Burkitt Granite.

The clustering of ages between the period ~1750-~1700 Ma corresponds with gt-whole rock Nd data for peak metamorphism in Tournefort Dykes of ~1740-1710 Ma obtained by Bendall (1994) and Hand et al. (in prep), and suggests a link between peak metamorphism and syn-orogenic granitic magmatism.

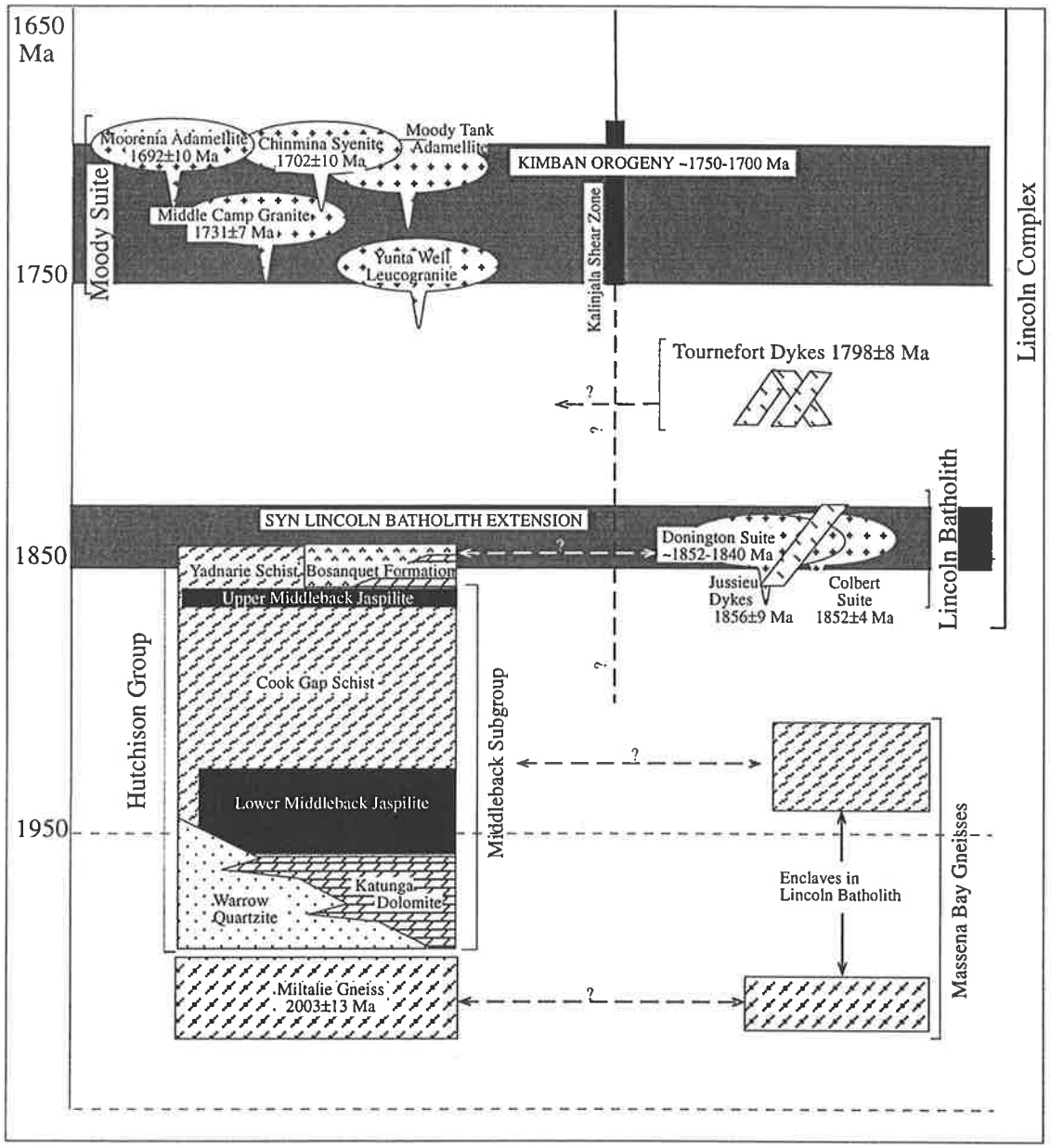

Figure 2.3: Detail of southern Eyre Peninsula geological events during the late Palaeoproterozoic. Symbols as for figure 2.2.

Numerous Rb-Sr studies on southern Eyre Peninsula have also produced isochrons in the range 1750-1700 Ma on lithologies that have subsequently been shown to be older by U-Pb zircon studies (eg, the Colbert Suite; Rb-Sr isochron = 1757±14 Ma, (Mortimer et al. 1986a), whole rock Rb-Sr isochrons on lithologies within the Donington Suite (Mortimer, 1984; this study)), suggesting resetting of the

Rb-Sr system during post crystallisation high grade metamorphism; ie, peak Kimban Orogeny.

The St Peters Suite consists of deformed comagmatic granitoids in the Streaky Bay region and is not currently known to extend significantly further south; however, it is likely to comprise a considerable portion of the western Gawler Craton. These intrusives are typically in the range of ~1630-1620 Ma and have A-type affinities, with small volumes of associated felsic volcanics.

The Tournefort Dykes

A prominent feature on southern Eyre Peninsula is the presence of mafic dykes belonging to the Tournefort Dykes (the term "swarm" has been omitted due to the implicit cogenetic connotations) which are composed of dolerite to gabbronorite dykes, and range from virtually undeformed to highly folded, lineated and amphibolitised mafic boudins, particularly in, and adjacent, high strain zones. The Tournefort Dykes clearly intrude the Donington Suite, and are deformed by all phases of the Kimban Orogeny, effectively restricting their emplacement age to between 1843 and ~1700 Ma (figure 2.3). They also crosscut contacts between the Donington and Colbert Suites (eg, fig 1.3 of Mortimer, 1984), acting as a minimum age constraint on the Colbert Suite. Rb-Sr geochronology by Fanning (1984a) places a minimum age of 1710 Ma on the dykes, with Sm-Nd isochrons on peak metamorphic mineral assemblages by Bendall (1994), further constraining the minimum age of the Tournefort Dykes to between 1740-1710 Ma. The Tournefort Dykes are discussed in Chapter 4.

The Kalinjala Shear Zone and the Kimban Orogeny

Possibly the most distinctive feature associated with the Kimban Orogeny on southern Eyre Peninsula is the Kalinjala Shear Zone (KSZ). The KSZ is a NNE-SSW trending, crustal scale, dominantly ductile feature separating Sleaford Complex and Hutchison Group metasediments in the west from the Lincoln Batholith and Tournefort Dykes to the east. Hand et al. (1995, 1996) noted a distinct asymmetry in baric gradient across the KSZ from west to east, resulting in the juxtaposition of comparatively low pressure rocks of the Hutchison Group, with high pressure Lincoln Batholith and Tournefort Dyke rocks in the shear zone. Regional metamorphism in the Lincoln Batholith stabilises at ~4kbar ~12km away from the shear zone, whereas regional amphibolite facies metamorphism of the order of 3-4kbar may be observed within 2 km of the KSZ to the west. Hand et al. (1995, 1996) considered such a baric gradient to be the result of oblique convergence and the resulting differential exhumation during the Kimban Orogeny.

Gawler Range Volcanics and the Hiltaba Suite

Subsequent to the Kimban Orogeny, voluminous felsic volcanism with A-type affinities of the Gawler Range Volcanics (1592±2) took place in the central Gawler

Craton. Associated with this magmatism was extensive A-type plutonism of the Hiltaba Suite (~1600-1575 Ma), with subordinate mafic intrusives. There are no correlatives of this volcano-plutonic episode on southern Eyre Peninsula, however Ar-Ar geochronology by Foster and Ehlers (1995, 1998) record cooling ages below ~500°C in on southern Eyre Peninsula in the range of ~1600 -1541 Ma, suggesting either activity along the Kalinjala Shear Zone during this period, or widespread denudation of the terrain due to uplift associated with magmatism to the north. The presence of a general trend of decreasing Ar-Ar ages from west to east across the southern Eyre Peninsula may suggest the denudation was in some way controlled by the Kalinjala Shear Zone.

Spilsby Suite

The final event recorded in the basement geology of southern Eyre Peninsula was the emplacement of small volume A-type magmas of the Spilsby Suite which intrude the Donington Suite and amphibolites of the Tournefort Dykes at ~1530 Ma. Outcrop is restricted to the Sir Joseph Banks Group of islands in southern Spencer Gulf.

2.2 Terminology and nomenclature

Workers familiar with the Gawler Craton will note that some of the terminology and nomeclature used in section 2.1 differs from that of previous contributions. This is because as geological understanding of the Eyre Peninsula has improved, the nomenclature applied to the lithologies present has evolved, sometimes in something of a haphazard manner. In order to place the working stratigraphy into context, changing interpretations of the regional geology of southern Eyre Peninsula are summarised below.

The first geological studies of the Eyre Peninsula were carried out by Tilley (1920, 1921a, b, c) who maintained the oldest rocks exposed were a sequence of metasediments (the Hutchison Series) which were intruded by a younger series of granitoids (the Flinders Series). A thick sequence of quartzites on the western Eyre Peninsula he believed to be younger than the Hutchison Series, and these he named the Warrow series, which were in turn intruded by a group of massive granites, the Dutton Series.

This stratigraphy subsequently proved difficult to apply on a regional scale, and simplification by Johns (1961) resulted in the Flinders Group, comprising older gneissic rocks, and the Hutchison Group, composed of younger schistose metasediments. This effectively reversed the relative ages of Tilley's scheme, and implied a metasedimentary origin for all of the Hutchison Group, which now included the Warrow Series.

With the advent of radiometric dating techniques and detailed mapping programs during the late 1960's and 1970's, a more concise description and subdivision of the lithologies on southern Eyre Peninsula was proposed by Thomson in 1980. This scheme has provided the basis for the current working stratigraphy, and incorporates geochronological elements of investigations by Compston and Arriens (1968), Arriens (1975), Fanning (1975), Giddings and Embleton (1976), Webb (1980), Thomson (1980), and metamorphic and geochemical studies by Bradley (1972). The major refinements were the recognition of a granitic and high grade metasedimentary sequence of Late Archaean age (the Sleaford Complex), and the division of the remaining rocks into metasediments of the Hutchison Group and granitic gneisses of the Lincoln Complex (see table 2.1).

This stratigraphy has proved far more durable and widely applicable than those previously proposed, with broad scale correlations possible for the extended Gawler Craton, as in the case of the correlation of the Mulgathing Complex with the Sleaford Complex (Daly et al., 1979). However, the stratigraphy was defined on the basis of distinctive mappable units on the craton scale, with the term Lincoln Complex used to encompass all syn-Kimban Orogenic intrusives. As discussed below, on the craton scale the term Kimban Orogeny implies genetic links between events over an extended period of geological time that may not be wholly appropriate. A result of such a situation is that all "syn-Kimban" orogenic granitoids may not be genetically linked, as the collective term, the Lincoln Complex, implies.

Tilley, 1920, 1921a,b,c	Johns, 1961	Thomson, 1980
DUTTON SERIES Granites intrusive into the Warrow Series	HUTCHISON GROUP Youngest rocks, of sedimentary origin	LINCOLN COMPLEX Granite gneisses
WARROW SERIES Thick quartzite sequence		HUTCHISON GROUP Metasediments that unconformably overlie Sleaford Complex
FLINDERS SERIES Igneous rocks intrusive into the Hutchison Series	FLINDERS GROUP Oldest rocks, metasediments metasomatised to granites	
HUTCHISON SERIES Oldest rocks, of sedimentary origin		SLEAFORD COMPLEX High grade metasediments and granite gneisses

Table 2.1: Summary of previous stratigraphies applied to southern Eyre Peninsula.

The Kimban Orogeny was a term originally coined by Thomson (1969) and Glen et al. (1977) to identify the series of tectonic events recorded in the Hutchison Group. Subsequently the term has been applied on a craton wide basis to encompass any deformation that has taken place between the cessation of deposition of the Hutchison Group (1859±11 Ma; Fanning, 1997), and deposition of the Corunna Conglomerate, thought to be synchronous with eruption of the Gawler Range Volcanics (1592±2 Ma, Fanning et al., 1988). Studies on Eyre Peninsula however, have suggested cessation of Kimban Orogenic effects as recorded in the Hutchison Group to have occurred by ~1700 Ma, effectively putting a minimum age on both the Kimban Orogeny and, by definition, the syn-orogenic Lincoln Complex. Subsequent deformation, such as that recorded in the younger St Peters Suite, has been attributed to the Wartakan Event (or deformation), variously attributed on a local scale as a final phase of the Kimban (eg, Parker et al., 1988; Flint et al., 1990), or a separate event (as described by Parker in Drexel et al., 1993). Development of an early, layer parallel schistosity in the Hutchison Group (D1), considered contemporaneous with emplacement of the Lincoln Batholith (Parker, 1978, Parker and Lemon, 1982) at ~1850 Ma is generally regarded as the onset of the Kimban Orogeny, however to date, no clear genetic link between this period of deformation and subsequent peak metamorphic conditions in the Hutchison Group has been made.

The resultant confusion arising from implied common origins for lithologies mapped on the basis of broad collective criteria, prompted Hoek and Schaefer (1998) to attempt to clarify nomenclature used on southern Eyre Peninsula within the context of the extended Gawler Craton. It is clear that the definition of the Lincoln Complex *sensu stricto* is contingent upon the definition of the Kimban Orogeny (as discussed above), with current consensus placing the end of the Kimban Orogeny at ~1700 Ma. Conversely, the onset of the Kimban is dependent on the relationship between early fabrics preserved in the Donington Suite (~1850 Ma), and peak metamorphism associated with true orogenesis (~1750-1700 Ma). Therefore, the terminology applied in the remainder of this contribution is based on the geology of southern Eyre Peninsula, and is summarised below:

- The term *Lincoln Complex* is applied on a craton wide scale as a mappable unit of intrusive igneous rocks emplaced between the cessation of Hutchison Group deposition (at 1859±11 Ma) and deposition of the Corunna Conglomerate, at 1592±2 Ma. This effectively covers the period of time referred to by Thomson (1969) and Glenn et al. (1977) as the Kimban Orogeny, and is consistent with historical use.

- The *Kimban Orogeny* on southern Eyre Peninsula is restricted to those metamorphic and deformational events within the Hutchison Group that have a common genetic origin with preserved peak metamorphic conditions. Sm-Nd geochronology on peak metamorphic mineral assemblages by Bendall (1994) suggest

this occurred at ~1720 Ma. This corresponds with D2 and D3 of the existing literature (eg, Parker, 1978). An earlier event (D1), considered to be coeval with emplacement of the Donington Suite has no clear genetic link with D2/D3 (eg, Hoek and Schaefer, 1998), and is here referred to as an independent, discrete event. Hence, in this context, the Kimban Orogeny on southern Eyre Peninsula spans the period from ~1750 to ~1700 Ma, and records the highest grade metamorphic conditions experienced on the southern Gawler Craton subsequent to the Sleafordian Orogeny. In such a scenario, the only truly syn-Kimban intrusives are the Moody Suite.

• The *Lincoln Batholith* was applied by Hoek and Schaefer (1998) to describe that subset of the Lincoln Complex incorporating the ensemble of igneous rocks spatially and temporally coeval with the Donington Granitoid Suite of Mortimer et al. (1986). This group of rocks is essentially batholithic in nature, and at present their distribution is restricted to the east of the Kalinjala Shear Zone, however possible correlatives may occur on central Eyre Peninsula in the Refuge Rocks area. Magmatism within the Lincoln Batholith is confined to the period ~1852-1843 Ma, and incorporates the Colbert Suite, Jussieu Dykes and Donington Suite, but not the Tournefort Dykes.

Other new terms (such as the *Jussieu Dykes*) or the use of existing terminology which has been slightly modified (eg, the *Colbert Suite*) will be noted and described at the appropriate point in the body of the thesis.

2.3 Relevance of southern Eyre Peninsula to Proterozoic tectonics

The development of a tectonic model incorporating the genesis and subsequent deformation and metamorphism of the Lincoln Batholith and Tournefort Dykes on the southern Eyre Peninsula will effectively constrain the style and processes driving tectonism for a single case study during this period of the Palaeoproterozoic. Ideally however, relating the processes acting on a single terrain with those on the modern Earth and terrains of similar age will offer insights into global scale tectonics and the relevance of modern analogues to the Precambrian.

CHAPTER THREE

Palaeoproterozoic magmatism of southern Eyre Peninsula I: The Lincoln Batholith

This chapter focusses on understanding the broad scale architectural, chemical and isotopic features of the Lincoln Batholith. The emphasis is on constraining timing and nature of magmatic style, crustal growth and tectonic setting in a larger context, in order to form a basis for discussion on tectonic evolution in later chapters. Detailed petrological studies of the Lincoln Batholith and Colbert Suite were conducted by Mortimer (1984), and are not duplicated here.

3.1 The Lincoln Batholith

The Lincoln Batholith (Hoek and Schaefer, 1998) describes the subset of the Lincoln Complex (Thomson, 1980) incorporating igneous rocks spatially and temporally coeval with the Donington Granitoid Suite of Mortimer et al. (1986). It is currently restricted to the eastern side of the Kalinjala Shear Zone on southern Eyre Peninsula, and incorporates the Donington and Colbert Granitoid Suites of Mortimer (1984) and the Jussieu Dykes of Hoek and Schaefer (1998), but not the subsequent Tournefort Dykes, which post date and crosscut all lithologies of the Lincoln Batholith. The Lincoln Batholith essentially consists of small volumes of mafic to intermediate magmas and voluminous felsic, even-grained and rapakivi textured gneisses. Smaller volume members of the Lincoln Batholith include ultrafractionated members and the hydrous Colbert Suite (1852.5±4.4 Ma, Fanning and Mortimer, in prep.). On the batholith scale, retrogression of charnockitic members of the Lincoln Batholith has commonly resulted in the growth of secondary hornblende and biotite at the expense of primary orthopyroxene and/or clinopyroxene.

Possible correlatives of the Lincoln Batholith may be found in the Refuge Rocks area of eastern Eyre Peninsula, where augen gneisses and associated mafics are intrusive into the Warrow Quartzite of the Hutchison Group; and in basement granodiorite gneisses at Roxby Downs (Creaser, 1995).

3.2 Felsic units of the Lincoln Batholith

The Donington Granitoid Suite of Mortimer (1984) and Mortimer *et al.* (1988a) comprises a series of pyroxene and hornblende-biotite granitoids and gneisses. It is confined to the eastern side of the Kalinjala Shear Zone on southern Eyre Peninsula (figure 3.1). In the Cape Donington locality pyroxene-bearing members have been subdivided into a quartz gabbronorite gneiss (QGNG), the Memory Cove Charnockite (MCC), a megacrystic augen gneiss and a late stage alkali feldspar gneiss (Mortimer, 1984). Retrogression and hydration of these units (excluding the quartz gabbronorite gneiss) prompted Mortimer (1984) to define distinct lithologies for these units, viz. a fine grained granite gneiss (GG1), an augen granite gneiss (GG2) and an alkali feldspar granite gneiss (AGG) respectively.

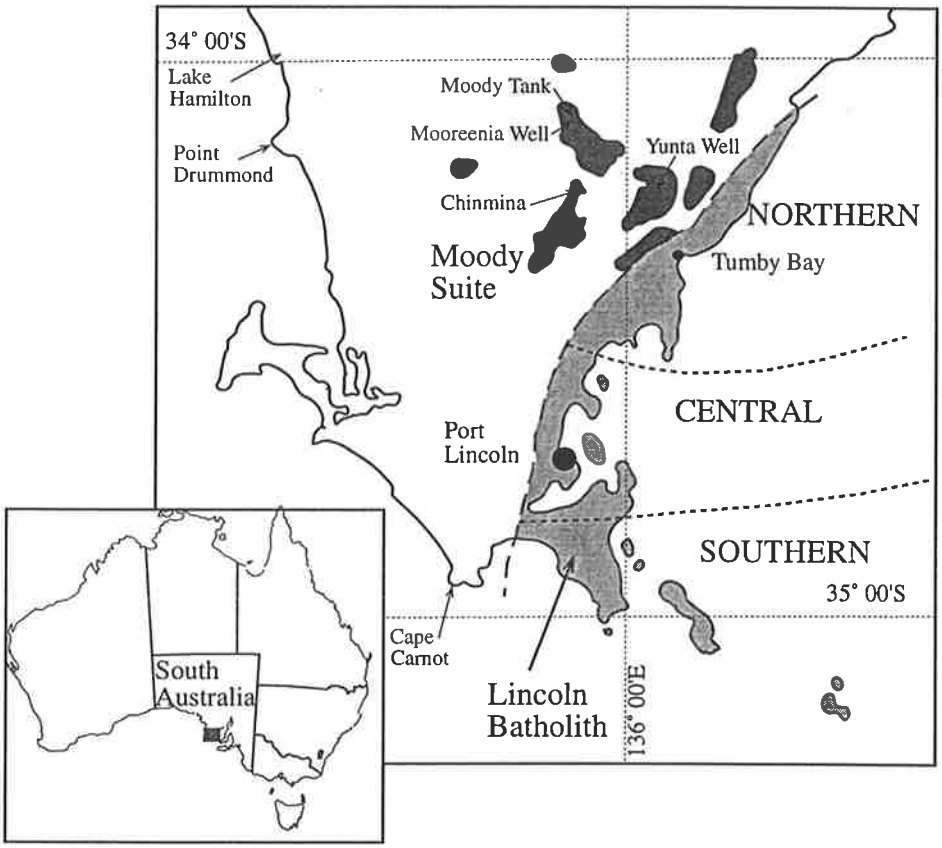

Figure 3.1: Distribution of the Lincoln Batholith on southern Eyre Peninsula, and principal geographic subdivisions within it. Note how distribution is restricted to the eastern side of the Kalinjala Shear Zone (NE-SW trending dash). Also shown are regional isotopic sampling sites (see chapter 5), and the syn-Kimban Moody Suite (see chapter 6).

Such a large number of abbreviations and terms has made application of *sensu stricto* definitions for each of the units in the Cape Donington-McLaren Point region to areas north and south difficult. For the remainder of this thesis, broader terms will be used which encompass, and on the batholith scale are consistent with, the stratigraphy devised by Mortimer (1984). These units are summarised in table 3.1 (along with the Jussieu Dykes, the mafic portion of the Lincoln Batholith), and are described in full below.

	Northern		Central		Southern	
	Primary	Hydrated	Primary	Hydrated	Primary	Hydrated
Jussieu Dykes#	x	?	x	?	5%	
QGNG‡	x	x	5%	x	x	x
Memory Cove Charnockite	5%	35%	FGG1‡ 20%	GG1‡ 15%	<10%	>25%
Megacrystic lithologies	5%	55%	FGG2‡ 15%	GG2‡ 35%	5%	20%
Fractionated liquid	x	x	CRG# 2%	AGG‡ 8%	WIG# 35%	

Table 3.1: Summary of distribution and approximate proportions of distinctive lithologies and correlatives in the Lincoln Batholith. "Primary" refers to charnockitic units, "hydrated" to granitic lithologies. x = not observed, ‡ = term used by Mortimer (1984), # = new term referred to in this thesis. QGNG = Quartz Gabbronorite Gneiss, FGG1 = Ferrohypersthene Granite Gneiss 1, FGG2 = Ferrohypersthene Granite Gneiss 2, EAGG = Eulitic Alkali Granite Gneiss, GG1 = Granite Gneiss 1, GG2 = Granite Gneiss 2, AGG = Alkali Feldspar Granite Gneiss, CRG = Carcase Rock Granite, WIG = Williams Island granite. Note EAGG of Mortimer (1984) is referred to as Carcase Rock Granite (CRG) in this thesis.

3.2.1 Pyroxene bearing felsic gneisses

Quartz Gabbronorite Gneiss: The Quartz Gabbronorite Gneiss (QGNG) of Mortimer (1984) forms one of the oldest recognised intrusive phases in the Lincoln Batholith. Outcrop distribution is limited to the Cape Donington area, and the northern end of the beach at Taylors Landing (figure 3.2), in the central portion of the Lincoln Batholith (figure 3.1). While the two localities preserve similar textural and mineralogical features, significant variations in chemistry may be observed. Both contain mafic enclaves including enclaves of finer grained gabbronorite at Taylors Landing. Primary mineralogy of the Quartz Gabbronorite Gneiss comprises

phenocrystic orthopyroxene + clinopyroxene + plagioclase, with interstitial k-feldspar and quartz. The pyroxenes contain distinctive Fe-Ti oxide exsolution lamellae along cleavage planes (figure 3.3a). Secondary features include partial recrystallisation/exsolution of orthopyroxene and/or clinopyroxene; and distinct rims of hornblende around the pyroxenes (figure 3.3b). The progressive late magmatic or high grade sub-solidus replacement of pyroxene by hornblende (Mortimer, 1984) is demonstrated in the sequence of pictures (figure 3.3a-c), taken from samples in low strain zones. In zones of higher strain, the hornblende defines a prominent foliation, and distinguishing the initial lithology from the Megacrystic Augen Gneiss (see below) becomes difficult. Two generations of biotite are generally present in the Quartz Gabbronorite Gneiss; a late, coarse-grained chocolate coloured variety which is likely to be metamorphic, while a paler, yellow-brown generation is commonly associated with pyroxene grains, and possibly represents a primary igneous phase (Mortimer, 1984).

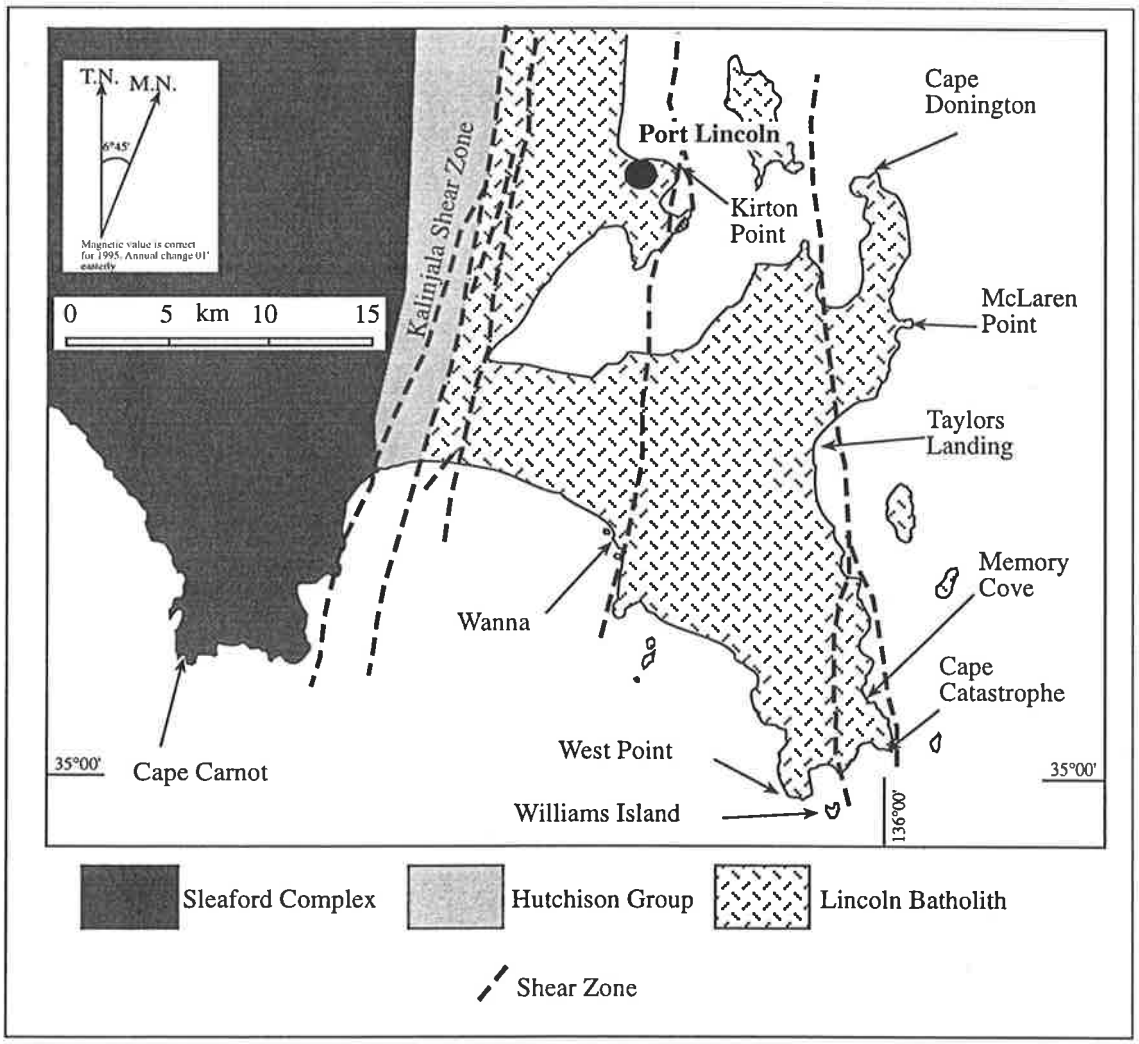

Figure 3.2: Key locality map for portions of the central and southern Lincoln Batholith.

West Point Charnockite (WPC) (New Name): West Point, in the southern portion of the Lincoln Batholith (figure 3.2), contains a small volume of distinctive charnockitic gneisses. In hand specimen these appear similar to the Quartz Gabbronorite Gneiss, but are significantly more chemically evolved (SiO_2 > 62.5 weight %, cf SiO_2 < 59.5 weight % for the Quartz Gabbronorite Gneiss). Petrographically these rocks differ from the Quartz Gabbronorite Gneiss in the dominance of orthopyroxene, and a typically smaller grain size for the ferromagnesian phases. Quartz, plagioclase and k-feldspar (both microcline and orthoclase) are coarser in grain size, and show evidence of recrystallisation in the form of inclusion trails crossing grain boundaries and resorption blebs. This unit is volumetrically minor, and is probably closely related in its genesis to the Memory Cove Charnockite and Megacrystic Charnockite.

Memory Cove Charnockite (MCC): The Memory Cove Charnockite (Parker et al., 1988) is an informal name for FGG1 of Mortimer (1984). It is a prominent lithology which, along with its retrogressed equivalents, can be observed throughout the Lincoln Batholith. It is distinctive by virtue of its even, medium to fine grained nature. Petrographically the MCC preserves a distinctive texture of zoned plagioclase, orthoclase, orthopyroxene and quartz aggregate phenocrysts in a matrix of quartz + plagioclase ± orthoclase ± microcline. Rare clinopyroxene grains may be observed in some samples. The orthopyroxene grains are typically smaller than in the Quartz Gabbronorite Gneiss, and commonly more corroded, often completely replaced by hornblende-biotite aggregates. Exsolution of opaques in MCC pyroxenes is absent. The presence of orthoclase and the relative absence of clinopyroxene in the MCC is a distinct contrast to the Quartz Gabbronorite Gneiss, but very similar to the West Point Charnockite. Phenocrystic feldspars are commonly zoned and may have corroded cores.

Hornblende and biotite commonly occur as intergrown aggregates, and preserve a range of progressive features (figure 3.3d-g) implying they have formed at the expense of pyroxene. The most retrogressed equivalents of the MCC (Granite Gneiss 1), contain pyroxene that has been entirely replaced.

Megacrystic Charnockite: Much of the outcrop of the Lincoln Batholith is composed of megacrystic augen gneisses, although pyroxene bearing members of this group are observed only at a small number of localities. Mortimer (1984) described occurrences at Cape Donington and Point Bolingbroke in the central and northern portions of the Lincoln Batholith respectively, with outcrops in the southern portion of the batholith at Wanna, Williams Island and West Point. The distinctive feature of this lithology is ovoid megacrystic feldspars, and many samples show rapakivi-like textures.

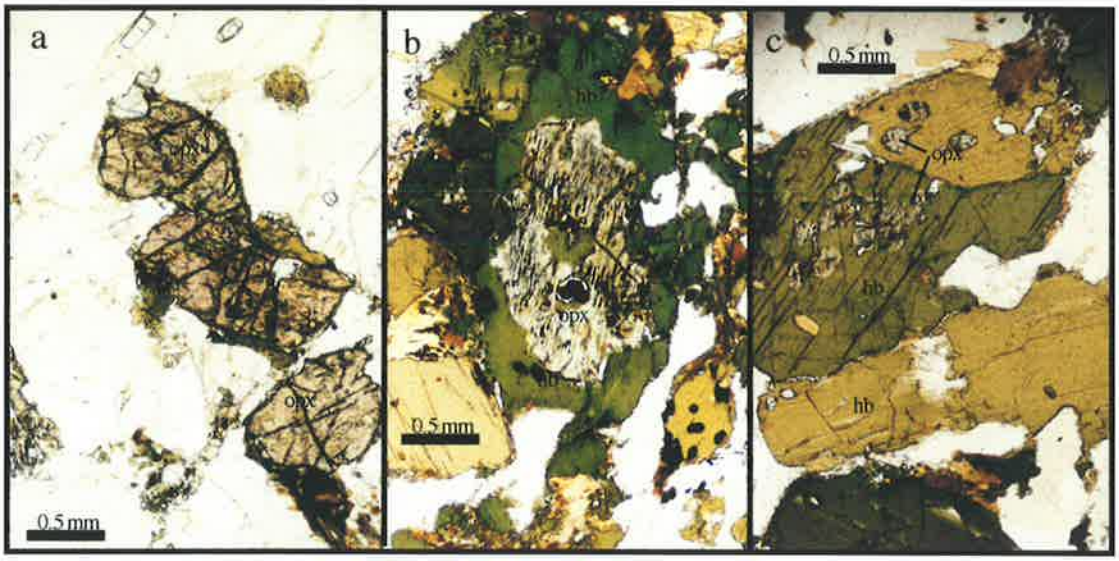

Figure 3.3: Photomicrographs of Quartz Gabbronorite Gneiss (QGNG) and Memory Cove Charnockite (MCC) a) Undeformed and relatively unmetamorphosed QGNG, Cape Donington. Large orthopyroxene (opx) grains contain distinct Fe-Ti oxide exsolution lamellae along cleavage planes. Note minimal hornblende (hb) growth (Sample SEP-086). b) Replacement of primary pyroxenes by hornblende forming mantles of amphibole around pyroxene cores at Taylors Landing. Opaque oxides are involved in this reaction as evidenced by the lack of continuity of exsolution lamellae into hornblende grains (Sample SEP-239). c) Almost complete replacement of pyroxene resulting in even grained amphibolite gneiss, Taylors Landing (Sample SEP-239). d) and e) MCC with pyroxene rimmed by hornblende ± bitotite (bt) (Samples SEP-169, Surfleet Pt and SEP-203, Billy Lights Pt respectively). f) Static replacement of pyroxene by hb+bt to form a granite gneiss (Sample SEP-020, Pt Bolingbroke). g) Granite Gneiss 1, a result of complete replacement of primary pyroxene by hb+bt in a low strain environment; Sample SEP-138 (Cape Euler).

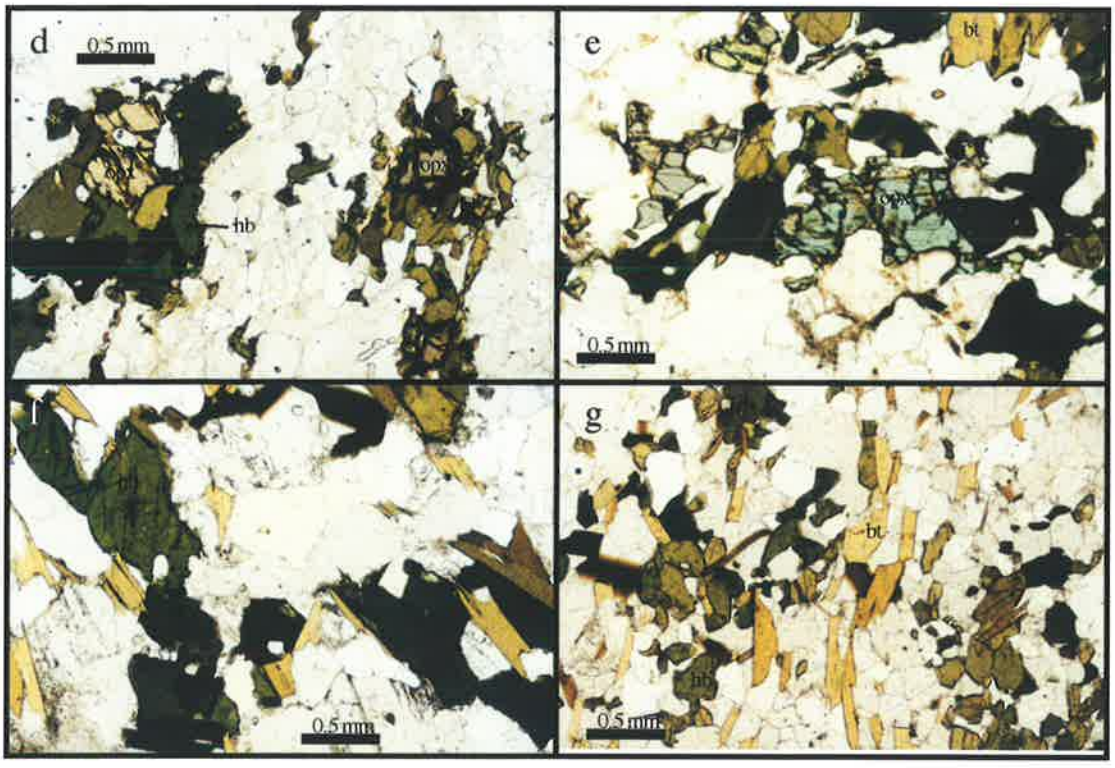

Feldspar megacrysts are either plagioclase aggregates or microcline crystals, occasionally with rims of plagioclase and containing inclusions of plagioclase in optical continuity with the rims. A quartz-plagioclase-microcline-orthopyroxene matrix surrounds the megacrysts. Hornblende and biotite show the same relationship with pyroxenes as in the MCC. The West Point Charnockite contains distinctly lower SiO_2 values (62.5-63.5 wt% and 67.5-70 wt % respectively) than the Megacrystic Charnockite, implying that these are not simply textural variations of a liquid of the same bulk composition.

Carcase Rock Granite (CRG) (New name): The term Carcase Rock Granite is applied to small volume, highly fractionated felsic magmatic phases occurring throughout the Lincoln Batholith. While no fresh pyroxene is observed, the undeformed variety in low strain zones contains relict pyroxene pseudomorphs. This rock type (CRG), is composed of an equigranular groundmass of quartz and alkali feldspar, with volumetrically minor amounts of biotite and hornblende. The CRG typically occurs as small volume veins and pods in the central and northern portions of the Lincoln Batholith, being best exposed at Carcase Rock and McLaren Point.

3.2.2 Granitic Gneisses

Whilst the pyroxene bearing members of the Lincoln Batholith preserve the greatest amount of information about its petrogenesis, by far the majority of the batholith is composed of retrogressed granitic gneiss equivalents of the pyroxene granitoids. Often it is difficult to distinguish between the pyroxene bearing and retrogressed gneisses in the field, and for the purposes of further discussion they are treated as cogenetic equivalents.

Granite Gneiss (MCC equivalent) is widespread around the Tumby Bay-Point Bolingbroke area, where it is composed of a medium, even grained hornblende granite gneiss. Along the coast near Thuruna, the MCC equivalent granite gneiss contains large numbers of enclaves, of a range of lithologies. These include several different types of mafic enclaves, (possible equivalents of the Jussieu Dykes), and a range of metasedimentary lithologies, interpreted as part of the Massena Bay Gneisses (Mortimer, 1984). The MCC equivalent granite gneiss is composed of dominantly quartz-plagioclase-hornblende-biotite±microcline.

Megacrystic Augen Gneiss (Megacrystic Charnockite equivalent): This granitic gneiss forms a distinctive lithology, particularly in highly deformed areas such as Lipson Cove, Port Neill and Mine Creek (figure 3.4) where it consists of megacrystic plagioclase±K-feldspar aggregates in a quartz-biotite±hornblende matrix. In zones of intense local metasomatism, coarse grained garnet may be observed, usually associated with the development of leucosomes in adjacent mafics (eg, Louth Bay,

West Point). Rarely, fine grained garnet is dispersed through the matrix of the megacrystic gneiss.

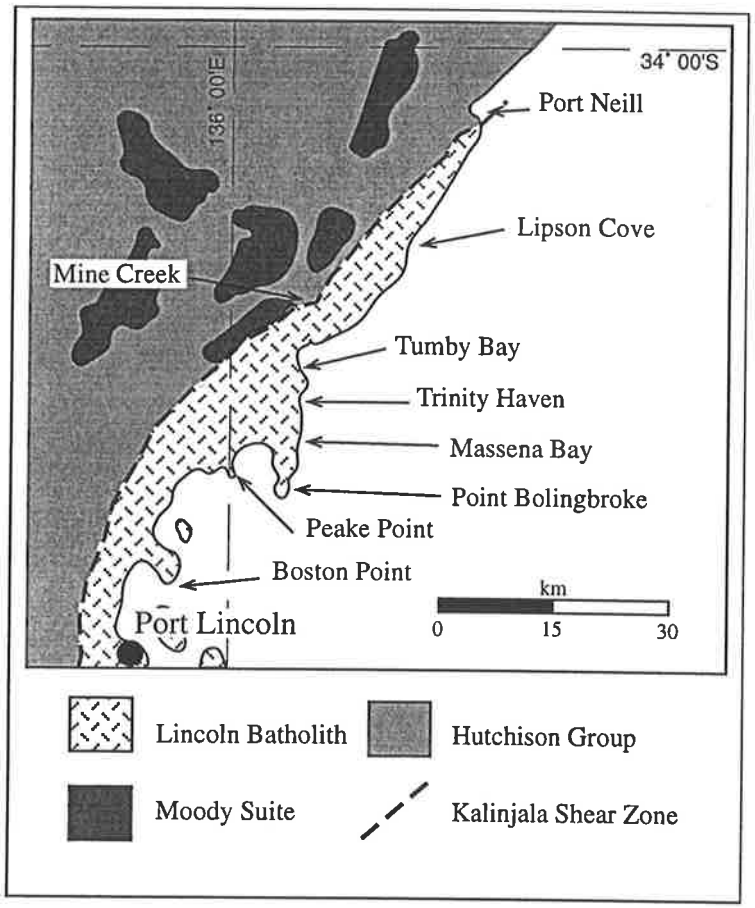

Figure 3.4: Locality map for central and northern portions of the Lincoln Batholith

The *Alkali Feldspar Gneiss (CRG equivalent)* is essentially a late-stage fractionate, composed of quartz, plagioclase and microcline with rare flakes of muscovite. It is leoucocratic, but often weathering to a pale pink colour. The main feature for distinguishing this from the CRG is the absence of pseudomorphs that may have been a ferromagnesian phase, and the pervasive recrystallisation of all samples observed in thin section. Like the CRG, the Alkali Feldspar Gneiss comprises only a small volume of the batholith.

Williams Island Granite (WIG): In the southern Lincoln Batholith, a large volume leucogranite forming large veins, sills and dykes intrusive into (figure 3.5a) and comagmatic with less evolved members of the batholith is observed. This lithology occupies the same relative position in the magmatic crystallisation sequence and SiO_2 wt% as the CRG and AFGG. The Williams Island Granite tends to contain significant proportions of microcline, with hornblende the dominant ferromagnesian phase. Despite occupying a similar position in the sequence as the CRG, some geochemical indicators, such as Rb/Sr ratio, vary considerably between the two (highly variable for the Williams Island Granite, >25 for CRG), suggesting a difference between the southern and central/northern portions of the batholith during late stage fractionation.

Figure 3.5: Intrusive features of the Lincoln Batholith
a) Williams Island Granite (WIG) intruding dark Megacrystic Charnockite. Cliff face ~25 m high, facing north on the west coast of West Point

b) Entrainment of basement orthogneissic enclaves (pale white) into Donington Suite units. Note apparent selvedge of Megacrystic Charnockite separating enclaves from fine grained Memory Cove Charnockite. Large block in centre of view ~0.5m in height.

c) Tesselated pavement of orthogneissic basement blocks, rimmed by partial melts. Continued invasion by the Donington Suite results in rafting of basement blocks (figure 3.5b) and ultimately assimilation into the magma chamber. Southern West Point, pen is ~14cm long.

d) Margin of Jussieu Dyke displaying backveining by selvage. Note the formation of both rounded and subangular enclaves. Chisel ~15cm long. West coast of Williams Island.

The Colbert Suite of Mortimer (1984) and Mortimer *et al.* (1988a) is here considered to be coeval with, and a subordinate part of, the Donington Suite. U-Pb zircon studies by Fanning and Mortimer (in prep) show crystallisation of the Colbert Suite at 1852.5±3.4 Ma, within error of Donington Suite magmatism. Tournefort Dykes crosscutting Colbert / Donington Suite contacts place a minimum age constraint on Colbert Suite magmatism consistent with the U-Pb zircon controls. Mortimer (1984), and Mortimer et al. (1988a) described two members of the Colbert Suite, a hornblende granite gneiss and an alkali feldspar granite gneiss. Petrographic re-examination, coupled with new geochronological constraints (Fanning and Mortimer, in prep), suggests the alkali feldspar member is essentially indistinguishable from the CRG equivalents elsewhere in the Lincoln Batholith. The hornblende bearing gneiss however, appears to be a primary magmatic hornblende liquid, in contrast to the remainder of the Lincoln Batholith.

3.3 Mafic units of the Lincoln Batholith

Identification of syn-plutonic mafic dykes within the Lincoln Batholith has lead to the definition of the *Jussieu Dykes*, a distinctive pre- Tournefort mafic suite (see Hoek and Schaefer, 1998). Known outcrop of the Jussieu Dykes is limited to Williams Island, West Point and north of Taylors Landing, with the bulk of localities on the extreme southern portion of Eyre Peninsula. They comprise <5% of Lincoln Batholith magmatism, however their distribution on offshore islands to the south of Eyre Peninsula is unknown.

The Jussieu Dykes are typically surrounded by a felsic selvage formed by melting and backveining attributed to emplacement of mafic material into relatively hot country rock. Disaggregation and ultimately dissemination of (commonly angular) mafic enclaves into curvilinear trains is observed along strike (figure 3.6a), which, coupled with the frequent association of felsic selvages along dyke margins (figure 3.5d) act as criteria for distinguishing the Jussieu Dykes from the younger Tournefort Dykes in the field. Such features are diagnostic of comagmatism of mafic material with the crystallising felsic magma (Pitcher, 1991; Hoek and Schaefer, 1998) The Tournefort Dykes always crosscut the Jussieu Dykes where such relationships are preserved.

The Jussieu dykes are generally less than ~1m wide, however they may vary in thickness considerably along strike length in response to differing degrees of deformation and to the relative proportion of felsic material comprising vein networks within the dyke and the surrounding selvage. There is no obvious preferred orientation of Jussieu dykes preserved in the field. Most dykes contain aphyric textures of relict plagioclase + clinopyroxene ± orthopyroxene, with subsequent hornblende + quartz ± biotite static retrogression in areas of low strain.

Figure 3.6: Features of the Jussieu Dykes: a) Planar Jussieu Dyke backveined by felsic selvages along margins, northwestern Williams Island, facing south. Hammer is ~1m long. b) Disaggregated and rafted Jussieu Dykes on southern West Point. Field of view ~2m across.

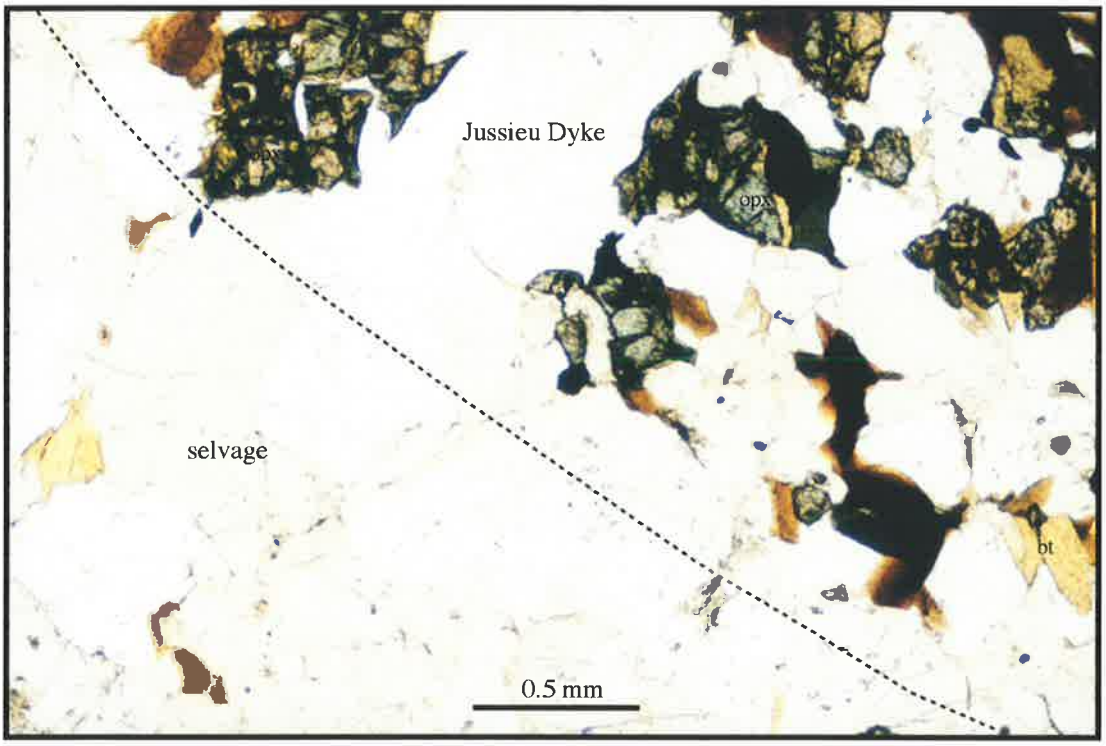

c) Photomicrograph of contact between Jussieu Dyke (upper right corner) and felsic selvage. Sample SEP-250, southern tip of West Point.

In high strain regions Jussieu dykes are indistinguishable from the Tournefort Dykes due to obliteration of diagnostic features, along with accompanying retrogression and amphibolitisation of the mafics.

Contacts between the mafic enclaves comprising Jussieu Dykes and the selvages surrounding them, tend to be distinct, and are often angular (figure 3.5d). A plagioclase + quartz ± orthopyroxene (± secondary hornblende) transition zone up to 1-2mm thick is common around the margins of Jussieu Dykes, while the bulk of the selvage material is composed of quartz + plagioclase + biotite ± hornblende ± orthopyroxene. Large plagioclase crystals in the selvages typically contain distinct rims of hornblende inclusions, suggesting overgrowth of magmatic plagioclase during selvage formation.

3.4 Enclaves within the Lincoln Batholith

The Lincoln Batholith contains several distinct populations of enclaves, both xeno- and autolithic.

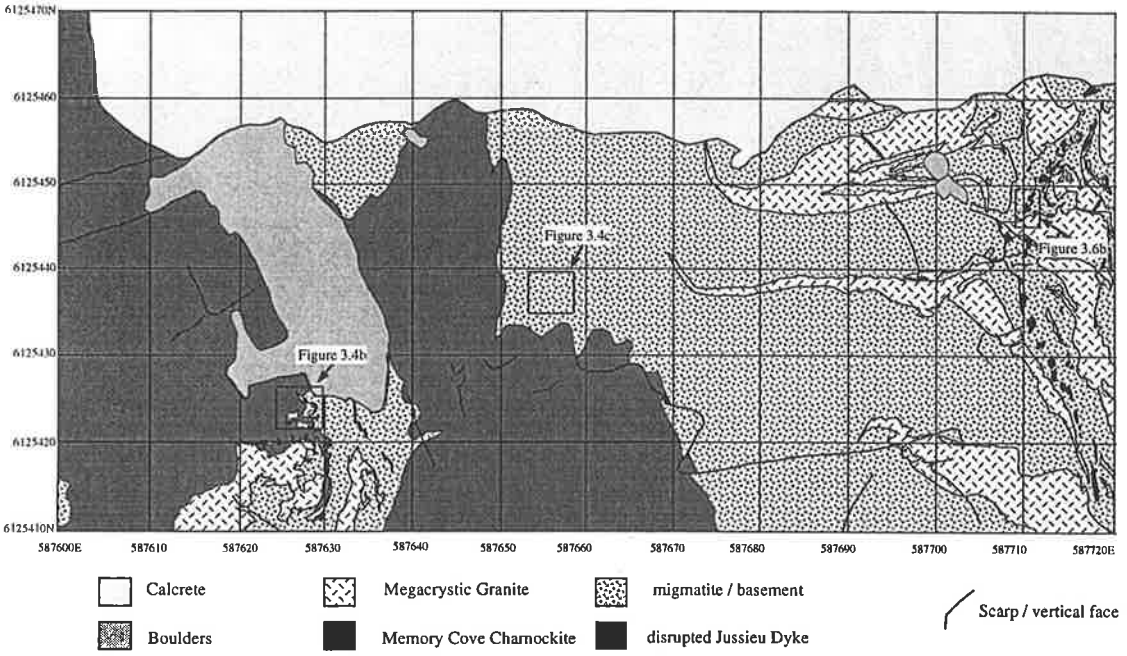

Figure 3.7: Grid map of southern West Point. Note disaggregated Jussieu Dyke and parallel nature of Megacrystic Granite dykes. The irregular contact between Memory Cove Charnockite and migmatised basement reflects partial digestion of the basement by the charnockite. Locations for figures 3.5b, 3.5c and 3.6b are also indicated. Grid co-ordinates are in AMG, zone 53. Mapping conducted in conjunction with J.D. Hoek.

Mafic enclaves observed in the Lincoln Batholith include probable basement xenoliths with distinct tectonic fabrics (eg, Trinity Haven, Kirton Point). Other prominent mafic enclaves can be observed on the southern coast of Williams Island, and along the coast between Lookout Point and Cape Catastrophe. These range in

size from ~15-150cm, and are distinctive by virtue of the ovoid feldspar phenocrysts they contain. Enclave margins are typically diffuse, and irregular in nature. Some of these enclaves are likely to be comagmatic (eg, small enclave in figure 3.5b) with the Lincoln Batholith, and hence coeval with the Jussieu Dykes.

Felsic/basement enclaves; One population of enclaves found in the southern part of the batholith comprise felsic basement lithologies (figure 3.5b,c). Whilst superficially reminiscent of MCC rafts within megacrystic members of the batholith, they are generally rimmed by fine grained felsic melts containing phenocrysts, suggesting incorporation of this material into the megacrystic units. Such basement felsic enclaves are leucocratic quartz-plagioclase-hornblende-biotite gneisses, and contain a fabric which is occasionally discordant to Lincoln Batholith lithologies. These are likely to represent orthogneisses of either Sleaford Complex or Miltalie Gneiss equivalents.

Metasedimentary enclaves comprise calc-silicate, pelitic and quartzo-feldspathic lithologies incorporated into the batholith from the country rock. Examples of the enclaves can be observed along the coast between Massena Bay and Trinity Haven, as well as at Cape Donington and West Point. All such lithologies are found in the metasedimentary portion of the Massena Bay Gneisses (Mortimer, 1984). Isotopic and geochemical features of basement enclaves are described in chapter 5.

3.5 Geochemistry of the Lincoln Batholith

Major and trace element characteristics

Magmas that comprise the Lincoln Batholith range from 48.8 wt % SiO_2 (the Jussieu Dykes) to 78.8 wt % SiO_2 (in the CRG equivalent alkali feldspar gneiss, (figure 3.9)).

Calculated CIPW norms for all felsic units of the Lincoln Batholith are summarised in figure 3.8, which shows a wide range in composition within the batholith from cumulates (Quartz Gabbronorite Gneiss) through to evolved granites (CRG, alkali feldspar gneiss and Williams Island Granite). Some scatter is observed within the Granite Gneiss 1 (MCC equivalents) and Granite Gneiss 2 (Megacrystic / Augen Gneisses) groups, due to Na and K mobility during the Kimban Orogeny (see chapter 6). Trends on figures 3.8 and 3.9 define systematic covariance of trace elements with silica content, consistent with fractionation within a comagmatic sequence of magmas. The Colbert Suite tends to more potassic compositions than the fractionation trend defined by the majority of the batholith.

The trace element signature of the Jussieu Dykes is the flattest primitive mantle normalised pattern within the batholith (figures 3.9, 3.10), consistent with their mafic nature (48.8-51.6 wt % SiO_2),. They typically contain a small negative Ti

anomaly, smooth REE pattern and a conspicuously small negative Sr, P anomaly (figure 3.10). Only a small negative Eu anomaly is present (figure 3.11).

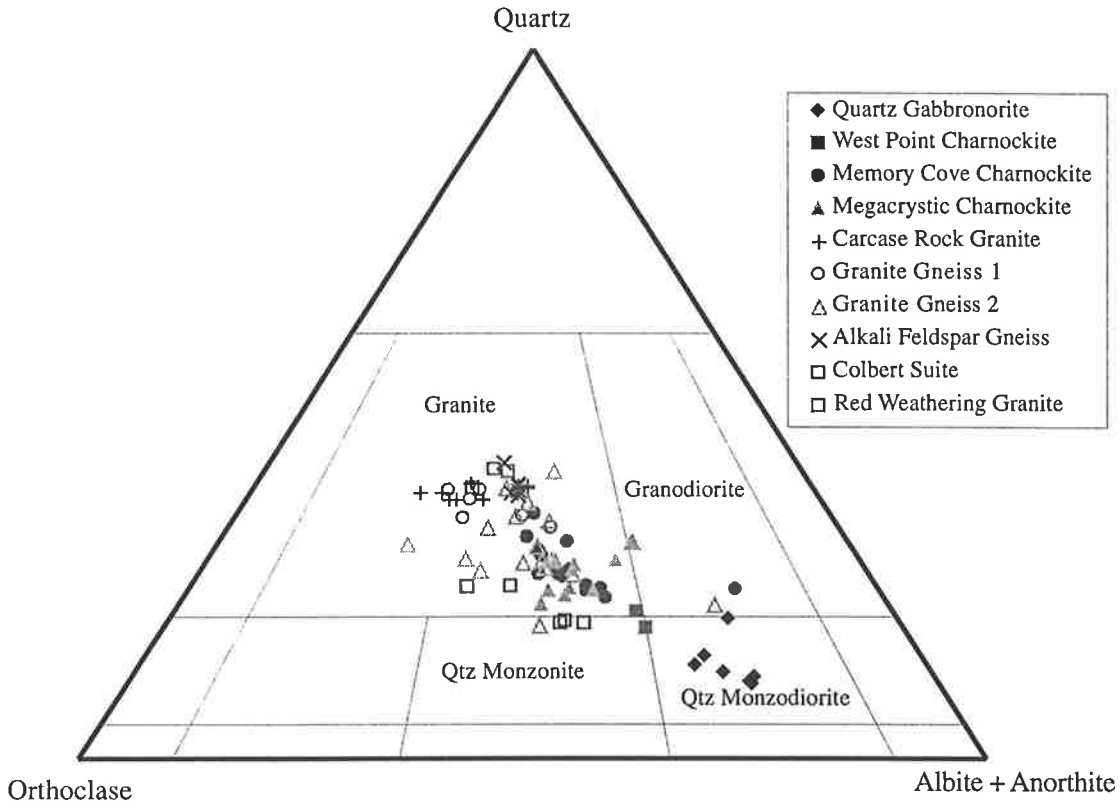

Figure 3.8: Normative ternary plot showing compositional variation for felsic units of the Lincoln Batholith. The Jussieu Dykes are not quartz normative, and as such do not plot.

The Quartz Gabbronorite Gneiss spans a range of intermediate silica compositions (55.5-59.5 wt % SiO_2), however trace elements show a strong locality dependent character. At Taylors Landing, it is more siliceous (59.5 cf 55.5-57.6 wt % SiO_2), and possesses higher trace element abundances than at Cape Donington (figure 3.9). Most notably, the Taylors Landing outcrop has elevated LREE values and distinct negative Zr, Ti, Sr, P and Eu anomalies, which are either non existent or poorly developed at Cape Donington. This suggests that Taylors Landing experienced a slightly longer fractionation history involving accessories such as zircon and apatite, than Cape Donington. As is typical throughout the batholith, a high degree of scatter in U and Th is observed, reflecting either post crystallisation sub-solidus mobility, or accessory controlled local scale fractionation effects. Erratic U and Th concentrations are also observed in the West Point Charnockite, which contains no Zr anomaly, but possesses negative Ti, Sr and P anomalies of similar size to the Quartz Gabbronorite Gneiss. The WPC also has elevated Pb/LREE ratios and higher K values, consistent with a relatively higher degree of fractionation.

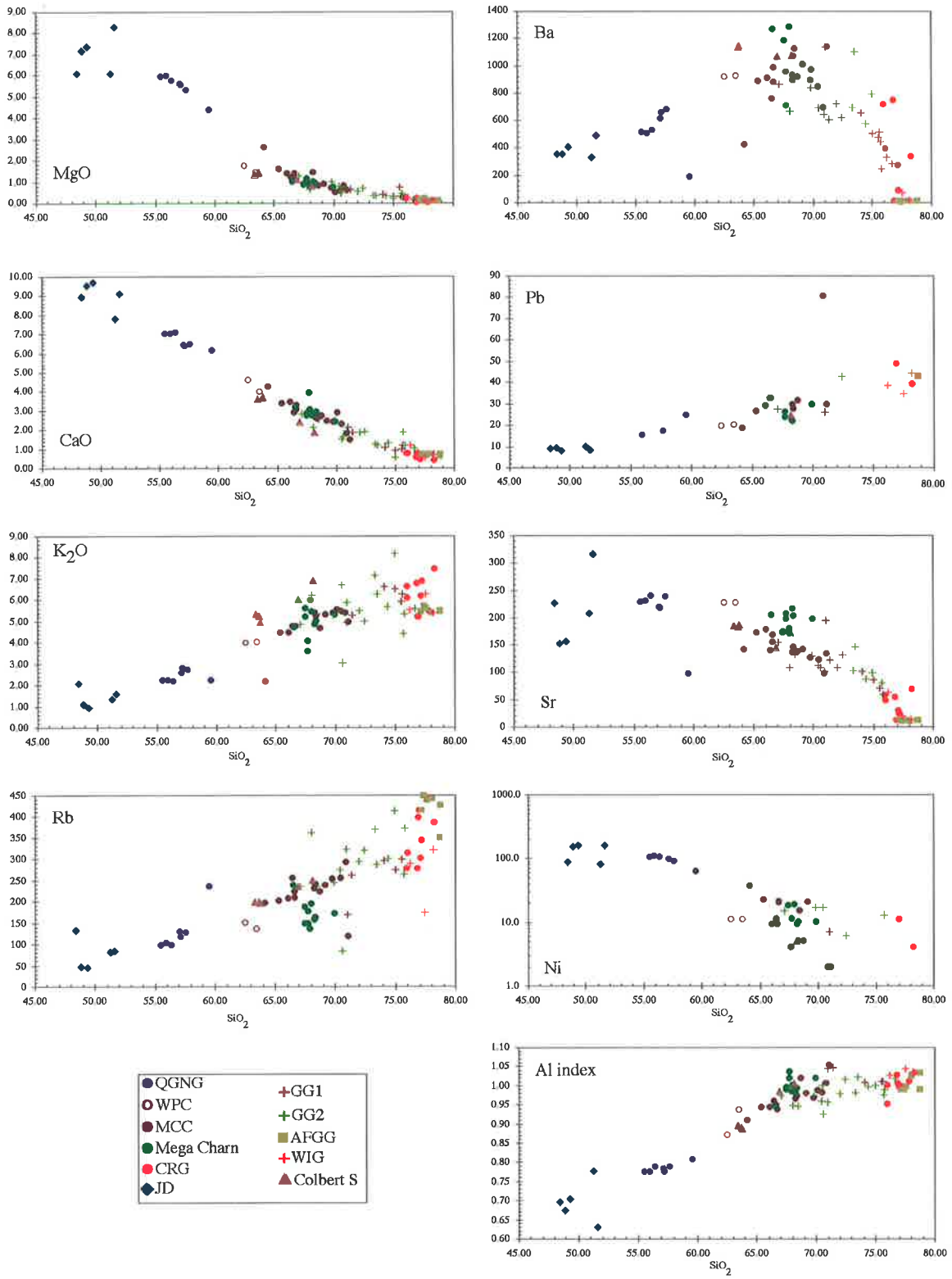

Figure 3.9: Harker variation diagrams for the Lincoln Batholith. Note generally linear trends for variation with increasing silica content. QGNG = Quartz Gabbronorite Gneiss, WPC = West Point Charnockite, MCC = Memory Cove Charnockite, Mega Charn = Megacrystic Charnockite, CRG = Carcase Rock Granite, JD = Jussieu Dykes, GG1 = Granite Gneiss 1 (MCC equivalent), GG2 = Granite Gneiss 2 (Megacrystic Charnockite equivalent), AFGG = Alkali Feldspar Granite Gneiss (Carcase Rock Granite equivalent), WIG = Williams Island Granite, Colbert S = Colbert Suite.

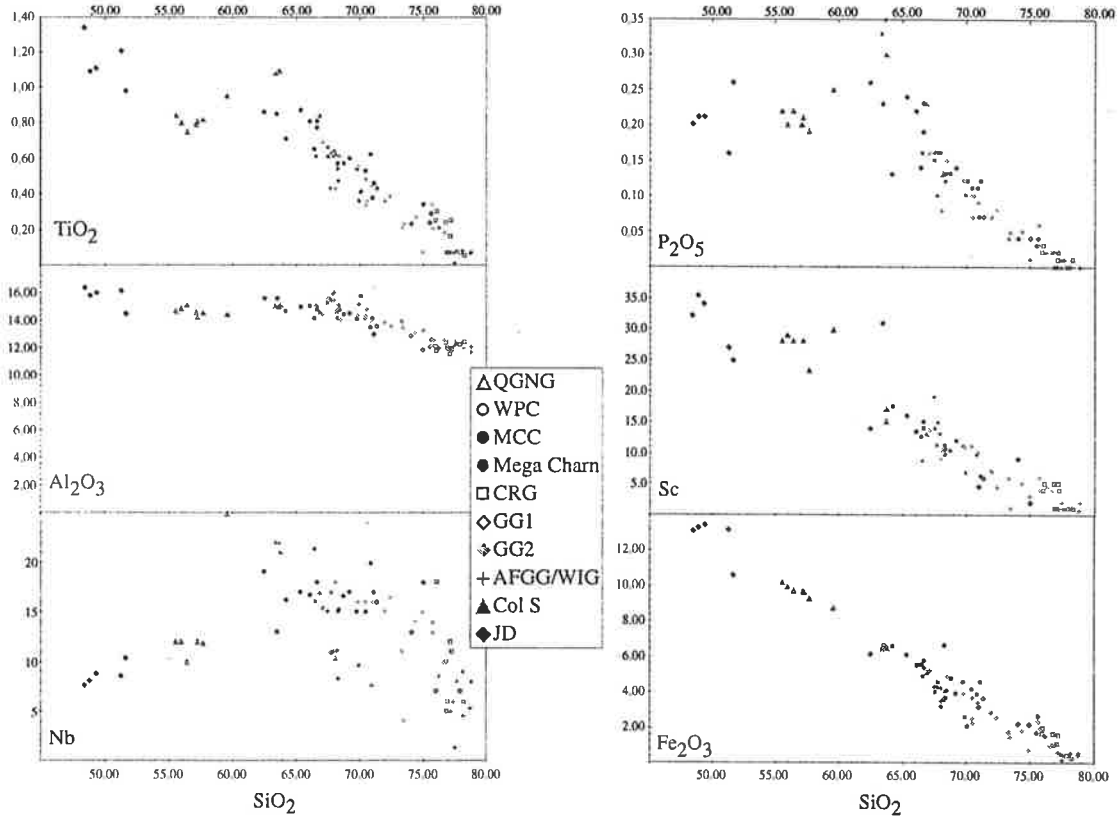

Figure 3.9 (cont): Supplementary Harker variation diagrams for the Lincoln Batholith. Abbreviations as for previous page. Note low (<16 wt%) Al_2O_3 and Fe_2O_3 enriched compositions in the 62-70 wt% SiO_2 range.

The Memory Cove Charnockite (and its retrogressed equivalent, GG1), is the most chemically and isotopically homogeneous unit in the Lincoln Batholith. From localities on Cape Catastrophe to Tumby Bay, it is characterised by a narrow range of Nb, K, LREE, Zr, Ti and Y values, with pronounced negative Ti, Sr, P and Nb anomalies (figure 3.11). U and Th show the least scatter for any lithology in the Lincoln Batholith. A gently decreasing REE element trend with a small negative Eu anomaly is characteristic of both the MCC and GG1. The hornblende granite gneiss of the Colbert Suite is also indistinguishable from the MCC on trace element characteristics, despite being less siliceous. This may indicate that mineralogy in the Colbert Suite is a reflection of crystallisation conditions rather than being an intrinsically chemically distinct magmatic event. The similarity between the two is clearly apparent on the REE plot (figure 3.11), where the Colbert Suite has a slightly more enriched pattern.

The Megacrystic Charnockite is chemically very similar to the MCC, with the only differences being a slightly more negative Nb anomaly, a relatively discrete SiO_2 range (66.5-69.9 wt%), and a slightly less evolved REE pattern (figure 3.10, 3.11).

The pyroxene bearing members of the Lincoln Batholith contain low values of MgO and Ni for a given weight % SiO_2. Non-cumulate portions of the batholith generally have <1.5% MgO, with the bulk of the batholith being <1%. Such low concentrations of compatible elements in the least evolved portions of the batholith are likely to reflect the nature of the source region, rather than secondary processes.

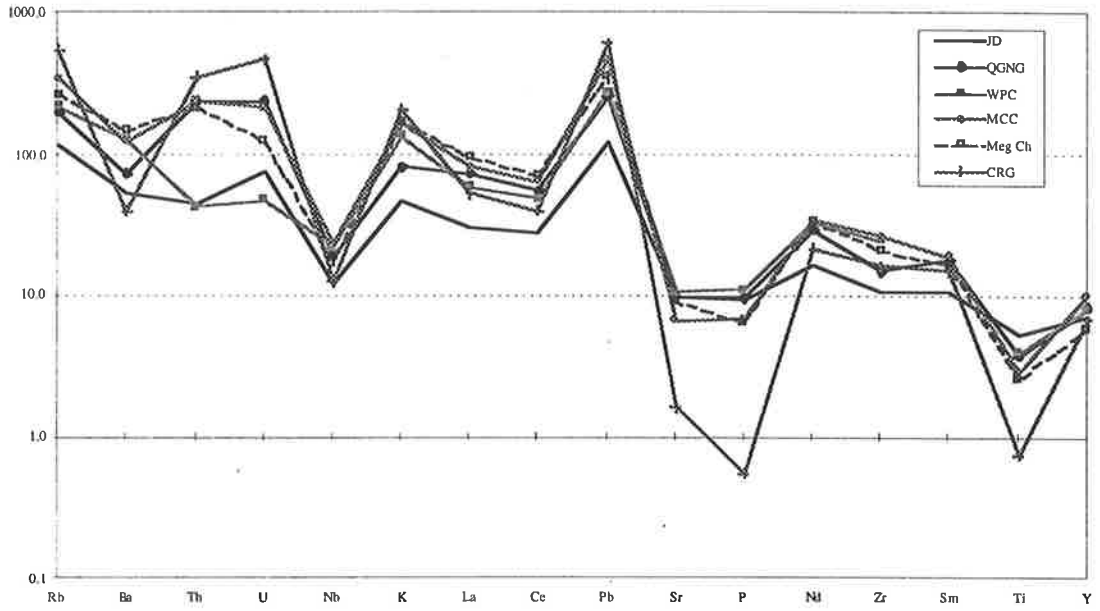

Figure 3.10: Primitive mantle normalised trace element variation diagram for pyroxene bearing members of the Lincoln Batholith. QGNG = Quartz Gabbronorite Gneiss, WPC = West Pt Charnockite, MCC = Memory Cove Charnockite, Meg Ch = Megacrystic Charnockite, CRG = Carcase Rock Granite and JD = Jussieu Dykes.

The Alkali feldspar gneiss, (a retrogressed CRG equivalent), has essentially the same trace element characteristics as the CRG, although with more scatter. Extreme Ba, Sr, P and Ti depletion (figure 3.12) is coupled with LREE depletion, and relatively high Zr levels. This unit contains the most distinctive REE pattern of the batholith, a prominent U-shape of depleted elements centred around Eu, resulting in low La*/Eu* ratios (figure 3.11).

The Williams Island Granite has features in common with both the CRG and the alkali feldspar gneiss. Most notably, extreme Ti depletion and variable degrees of REE depletion, and a distinct Ba depletion. The negative Nb anomaly is the greatest for any unit in the Lincoln Batholith.

While other units of the Lincoln Batholith generally contain trace element concentrations that vary systematically with silica content, the high silica fractionates commonly show asymptotic changes in incompatible elements with covarying silica. This indicates that the environment governing formation of small-volume, late stage melts was one in which the remaining liquid was able to rapidly

and efficiently fractionate, a stark contrast to the larger, apparently internally buffered situation governing the bulk of Lincoln Batholith crystallisation.

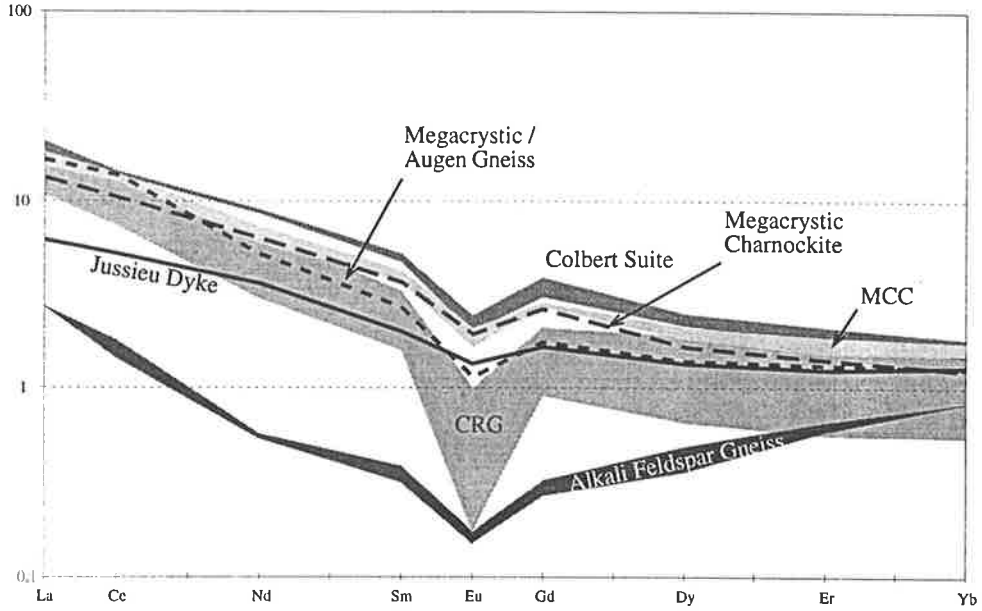

Figure 3.11: Primitive mantle normalised REE variation diagram for the Lincoln Batholith. Shaded areas (in order of decreasing Eu), Colbert Suite, Memory Cove Charnockite (MCC), Carcase Rock Granite (CRG) and Alkali feldspar Gneiss. Solid line = Jussieu Dyke, long dashed line = megacrystic charnockite and short dash = megacrystic gneiss. Data compiled from Mortimer (1984: Colbert Suite, CRG and Alkali Feldspar Gneiss) and this study. Normalisation factors from McDonough et al., 1991.

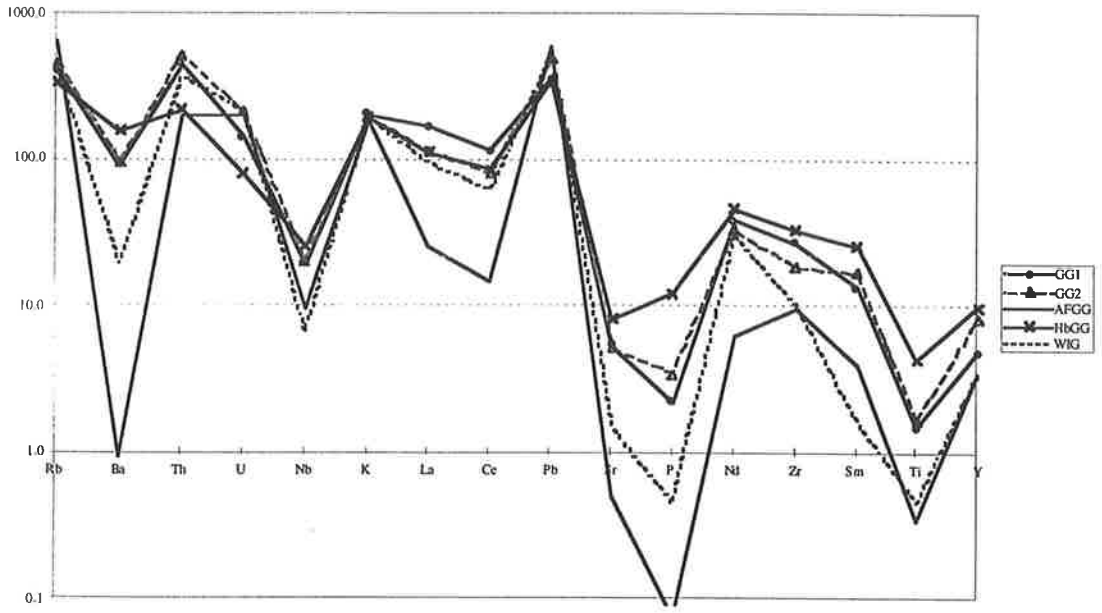

Figure 3.12: Primitive mantle normalised trace element variation diagram for granite gneisses of the Lincoln Batholith. GG1 and GG2 = Granite Gneisses 1 and 2, AFGG = Alkali Feldspar Granite Gneiss, HbGG = Hornblende Granite Gneiss of the Colbert Suite, and WIG = Williams Island Granite.

Isotopic characteristics of the Lincoln Batholith

One of the more remarkable features within the felsic portions of the Lincoln Batholith is the homogeneity of Nd isotopic signatures. $\varepsilon_{Nd(1850)}$ values for felsic units span two epsilon units, ranging from -2.1 to -4.2 (table 3.2). This is the total variation observed from the cumulate Quartz Gabbronorite Gneiss, through the charnockites and including the granitic gneisses, (as indicated by the shaded area in figure 3.13). The Carcase Rock Granite and Williams Island Granite display anomalous Sr and Nd isotopic signatures, due to the extreme levels of fractionation (eg, Rb/Sr ratios ~30, table 3.2), and are omitted from petrogenetic discussion as age corrected calculations on lithologies with such extreme parent/daughter elemental ratios exaggerate observational uncertainties.

The Jussieu Dykes contain a broad range in initial $\varepsilon_{(Nd)}$ values, from +1.5 to -4.0 (table 3.2). Sr isotopes for the Jussieu Dykes form a covarying array with Nd isotopes (figure 3.13) suggestive of mixing between contemporary mantle and continental crust. By contrast, initial Sr isotopic values for the Donington Suite range from 0.70180 to 0.71182, forming an array straddling, but broader in range, than mixing curves between the contemporary mantle and continental crust.

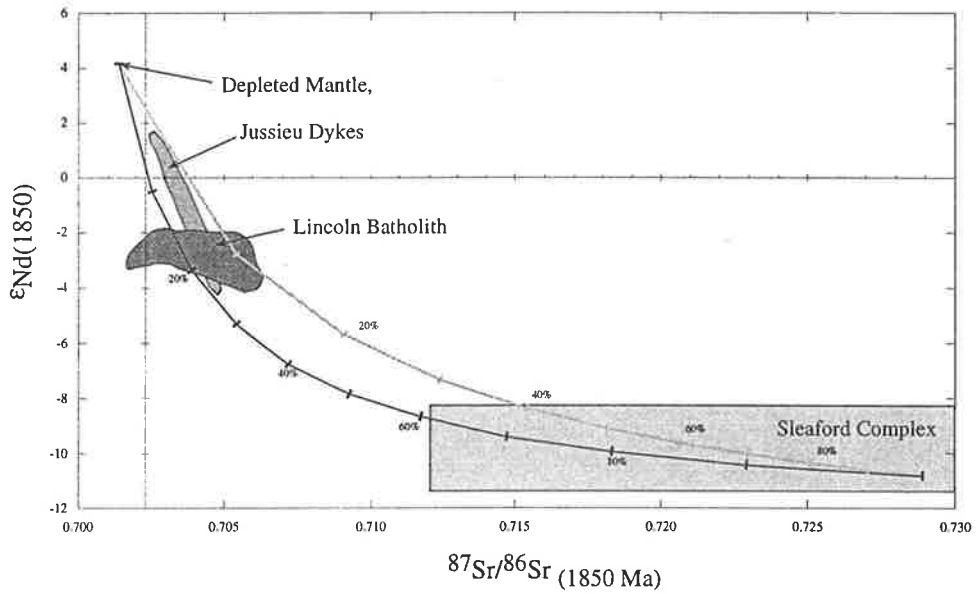

Figure 3.13: Mixing relationships between the Lincoln Batholith and contemporary mantle. Upper and lower curves are models for $(Sr/Nd)_{mantle}/(Sr/Nd)_{crust}$ values of 5 and 10 respectively. Sleaford Complex end member is held constant by an augen gneiss from Cape Carnot as a representative sample of the suite. Depleted mantle chemistry from Sun and McDonough (1989), isotopic compositions of Taylor and McLennan (1985). Tick intervals are 10%.

	Locality	Age, (t)	$^{143}Nd/^{144}Nd$	2 σ	$^{147}Sm/^{144}Nd$	$T_{(DM)}$	$\varepsilon_{Nd(t)}$	$^{87}Sr/^{86}Sr$	2 σ	$^{87}Rb/^{86}Sr$	$^{87}Sr/^{86}Sr_{(t)}$
Jussieu Dyke	SEP-241 *Nth Taylors Ldg*	1850	0.511765	0.000062	0.1418	2.94	-4.0	0.725881	0.000100	0.79443	0.70473
Jussieu Dyke	SEP-250 *West Pt*	1850	0.511825	0.000052	0.1237	2.25	1.5	0.747921	0.000088	1.70038	0.70266
Jussieu Dyke	SEP-261 *Williams Is*	1850	0.511876	0.000048	0.1382	2.58	-1.0	0.733507	0.000128	1.11859	0.70373
Jussieu Dyke	SEP-293 *Williams Is*	1850	0.511700	0.000062	0.1227	2.43	-0.8	0.723656	0.000074	0.76271	0.70335
Quartz Gabbronorite	SEP-239 *Nth Taylors Ldg*	1850	0.511431	0.000064	0.1104	2.54	-3.1	0.900624	0.000034	7.09300	0.71182
Memory Cove Charnockite	SEP-154 *C Catastrophe*	1850	0.511477	0.000042	0.1102	2.47	-2.1	0.792497	0.000032	3.40722	0.70180
Memory Cove Charnockite	SEP-074 *Trinity Haven*	1850	0.511510	0.000058	0.1214	2.71	-4.2	0.838135	0.000030	4.97391	0.70574
Memory Cove Charnockite	SEP-147 *C Catastrophe*	1850	0.511483	0.000036	0.1116	2.49	-2.4	0.830676	0.000032	4.86991	0.70105
Memory Cove Charnockite	SEP-073 *Trinity Haven*	1850	0.511439	0.000018	0.1152	2.65	-4.1	0.832662	0.000040	4.75658	0.70605
Megacrystic Charnockite	SEP-282 *Williams Is*	1850	0.511479	0.000032	0.1112	2.49	-2.3	0.792940	0.000032	3.39523	0.70257
Megacrystic Granite	SEP-249 *West Pt*	1850	0.511168	0.000030	0.0843	2.34	-2.0	0.769390	0.000050	2.49799	0.70290
Megacrystic Charnockite	SEP-265 *Williams Is*	1850	0.511162	0.000024	0.0889	2.43	-3.2	0.760319	0.000068	2.11158	0.70411
Megacrystic Charnockite	SEP-295 *Williams Is*	1850	0.511205	0.000062	0.0944	2.49	-3.7	0.768279	0.000060	2.32823	0.70631
Megacrystic Granite	SEP-264 *Williams Is*	1850	0.511029	0.000039	0.0737	2.31	-2.2	0.773451	0.000418	2.54520	0.70570
Granite Gneiss	SEP-252 *West Pt*	1850	0.510942	0.000038	0.0687	2.32	-2.7	0.773248	0.000054	2.53854	0.70568
Augen Gneiss	SEP-142 *Peake Pt*	1850	0.511477	0.000034	0.1138	2.55	-3.0	0.822241	0.000042	4.46154	0.70348
Williams Island Granite	SEP-283 *Williams Is*	1850	0.511182	0.000034	0.0870	2.37	-2.4	1.431453	0.000056	29.44537	0.64767

Table 3.2: Summary of new isotopic data for the Lincoln Batholith. Data normalised to $^{146}Nd/^{144}Nd=0.7219$, $^{88}Sr/^{86}Sr=8.3752$. Nd model parameters based on Goldstein et al. (1984): $^{143}Nd/^{144}Nd_{DM(0)}=0.51316$, $^{147}Sm/^{144}Nd_{DM(0)}=0.2137$; $^{143}Nd/^{144}Nd_{CHUR}=0.512638$, $^{147}Sm/^{144}Nd_{CHUR}=0.1966$.

While the significant range in Nd isotopes of the Jussieu Dykes appear to indicate interaction of contemporary mantle and crust, the felsic portions of the batholith must reflect processes resulting in remarkably homogeneous Nd and trace element signatures. One scenario consistent with this would require a comparatively small input of contemporary mantle interacting with a large volume lithospheric mantle which has remained isolated for a significant time prior to Lincoln Batholith magmatism. Estimates of the duration for which this reservoir has been isolated are provided by the depleted mantle model ages (T_{DM}) of 2.31-2.71 Ga, substantially older than the emplacement age of the batholith. Alternatively, such ages may reflect interaction with contemporary crust, and will be discussed in the section on petrogenesis below.

3.6 Geochronology of the Lincoln Batholith

Previous geochronology of the Lincoln Batholith has largely centred on samples collected from the Cape Donington locality. Fanning (1997) summarises conventional ID-TIMS and SHRIMP U-Pb zircon geochronology for the Quartz Gabbronorite Gneiss, MCC and Colbert Suite. The best estimates for crystallisation ages cited by Fanning (1997) are: Quartz Gabbronorite Gneiss 1849.8±1.1 Ma, MCC 1850.0±6.5 Ma and 1852.5±4.4 Ma for the Colbert Suite. Therefore, U-Pb zircon studies suggest the bulk of magmatism at Cape Donington took place at ~1850 Ma.

Previous Rb-Sr geochronology has met with mixed success in elucidating emplacement ages. Mortimer (1984) and Mortimer et al. (1986, 1988a) report ages for the pyroxene bearing granitoids similar to U-Pb zircon geochronology, however Rb-Sr data for the Colbert Suite was significantly younger, at 1757±14 Ma.

In an attempt to better define the age variation within the Lincoln Batholith, Pb-Pb zircon geochronology was carried out on samples from Wanna and Trinity Haven in the south and north of the batholith, respectively. Sr whole rock geochronology was also conducted at the latter locality. These samples were selected to test the effect of geographic spread and variation in lithology on the emplacement age of the batholith.

Pb-Pb zircon geochronology

The Pb-Pb zircon evaporation technique as carried out in this study was developed by Kober (1986), with the method applied at Adelaide University outlined in Dougherty-Page and Foden (1996). The technique involves sequentially evaporating layers of zircon and analysing the Pb isotopic composition in a stepwise manner towards the core of the zircon. Ratios of $^{207}Pb/^{206}Pb$, $^{208}Pb/^{206}Pb$ and $^{204}Pb/^{206}Pb$ are thus obtained for each heating step, allowing calculation of a

zircon age from the $^{207}Pb/^{206}Pb$ ratio which has been corrected for common Pb calculated from the $^{204}Pb/^{206}Pb$ ratio (Dougherty-Page and Foden, 1996). Coupled with the age determination is the ability to back calculate Th/U ratios for each analysis (Bartlett et al., in press), using the $^{208}Pb/^{206}Pb$ ratio. This $(Th/U)_t$ value is useful for discriminating separate zircon populations.

The limitation of the evaporation technique is that of demonstrating concordancy. However, using data obtained from many small sequential heating increments, and using only data plateaus in the sequence, discordance is minimised. That is, if a sequence of analyses were discordant, then successive heating steps would produce different measured ratios, and the data would not plateau. Age determinations are thus conducted only on the plateaus of data sets. Multiple analyses of zircons from within a single sample reproducing plateaus of corresponding $^{207}Pb/^{206}Pb$ and $(Th/U)_t$ ratios therefore imply a strong degree of concordance for the population in question.

Two felsic units were selected for Pb-Pb analysis. SEP-194D is from Wanna, a megacrystic augen gneiss of interest because no zircon geochronology has previously been attempted on this unit, its location in the southern portion of the Lincoln Batholith, and the relative styles of deformation between the mafics and felsics at this locality (Bales, 1996). SEP-074 is a Memory Cove Charnockite equivalent from Trinity Haven, near Tumby Bay, and was chosen for analysis due to its location in the north of the batholith, and its proximity to metasedimentary enclaves, effectively acting as a potential source for zircon inheritance.

The Pb-Pb zircon analyses obtained identical ages, and the zircon populations defining such ages contained the same $(U/Th)_t$ ratios. The Megacrystic Augen Gneiss in the south of the batholith gave an age of 1841±9 Ma ($(U/Th)_t$ = 0.40), and the Memory Cove Charnockite equivalent from Trinity Haven gave 1841±8 Ma ($(U/Th)_t$=0.41). No inheritance was observed in the Trinity Haven sample, however the core of one zircon from the Augen Gneiss at Wanna returned an age of 1907±12 Ma, with $(U/Th)_t$=0.32; significantly distinct from the main population and is considered inherited from an older source. The homogeneity of both ages and $(U/Th)_t$ ratios obtained for the two different lithologies from localities ~50km apart suggests the main period of zircon crystallisation took place under stable conditions in a batholith that was homogenous on a very broad scale.

Finally, despite the apparent homogeneity of ages and U/Th ratios from zircons within the Lincoln Batholith, it must be noted that the Pb-Pb ages, even though within error, are slightly younger than the SHRIMP U-Pb zircon ages. This was also noted in multi grain ID TIMS work by Mortimer et al. (1986, 1843±2 Ma), whereas single grain abraded ID TIMS by Fanning and Mortimer (in prep) have

produced ages ~1849 Ma. This suggests the presence of younger rims which are unresolvable by the Pb-Pb evaporation technique. Such overgrowths are likely to reflect Kimban age tectonothermal activity. Indeed, Fanning (1997) reports high U overgrowths and internal structural complexity in zircons from the Memory Cove Charnockite, which are attributed to zircon growth at ~1700 Ma.

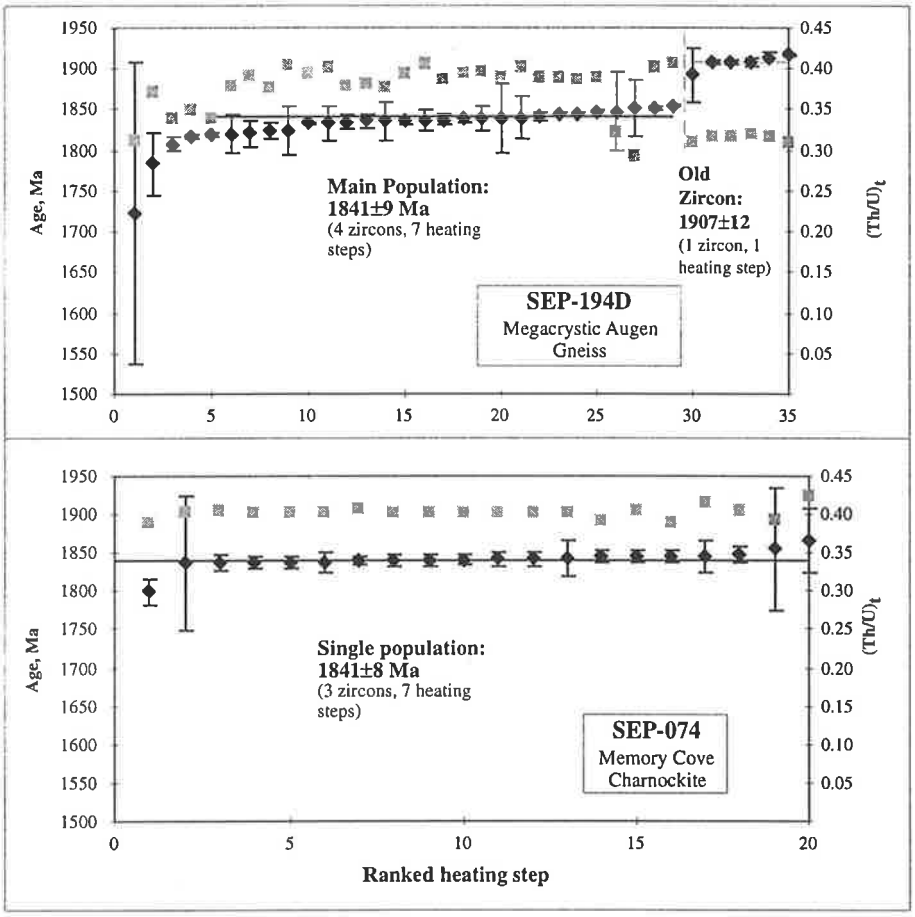

Figure 3.14: Summary of Pb-Pb evaporation data for the Lincoln Batholith. Diamonds with error bars (2σ) are calculated age for a given heating step, square symbols are $(U/Th)_t$ values for the same step.

Rb-Sr whole rock geochronology

Whilst not the primary focus of this study, the measurement of whole rock Rb-Sr data offers an opportunity to further constrain the emplacement of the Lincoln Batholith. Mortimer (1984) reports isochrons in the range of ~1818-1890 Ma for pyroxene bearing members of the Donington Suite. These ages are generally within error of the U-Pb zircon data of subsequent studies.

Figure 3.15a,b presents new data for the Megacrystic Charnockite and MCC from a range of localities within the batholith (summarised in table 3.2), effectively representing Sr isotope variations on the scale of the batholith. By contrast, figure 3.15f are samples from within a 2 m^2 area at Trinity Haven, and reflect

homogenisation of Sr isotopes between both the intruding charnockite and a metasedimentary enclave of the Massena Bay Gneisses on the small scale. Both ages are within error of themselves and of zircon geochronology for the batholith. Sample SEP-074, which returned a Pb-Pb zircon age of 1841±8 Ma, is one of the charnockites defining the 1852±14 Ma (2σ) isochron (figure 3.15f). Sample SEP-147 was omitted from the regression in figure 3.15b due to its location on the margin of a Kimban shear zone at Cape Catastrophe, and resultant Sr disturbance.

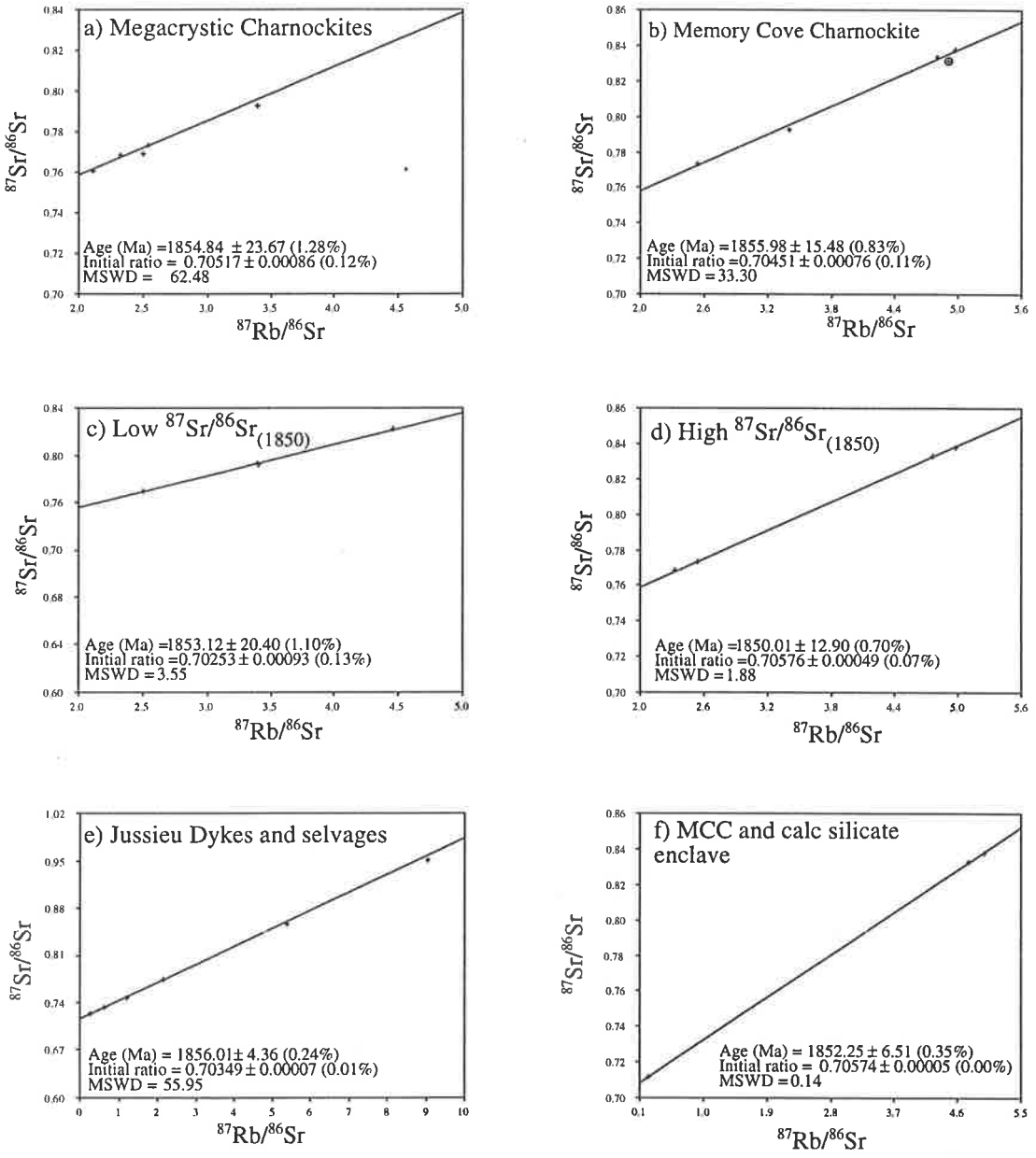

Figure 3.15 Selected Rb-Sr whole rock isochrons for felsic units of the Lincoln Batholith. Errors quoted adjacent age determination are 1σ, those cited in the text are 2σ. Regression after method of York (1969).

Table 3.2 shows two distinct subsets of felsics in the Sr isotopic data at the time of Lincoln Batholith emplacement. These subsets are represented by low

$^{87}Sr/^{86}Sr_{(t)}$, and high $^{87}Sr/^{86}Sr_{(t)}$. Sample locations suggest variations reflect proximity of sampling site to basement (whether para- or orthogneissic) enclaves. Significantly, both subsets yield isochrons of 1853±40 Ma (2σ, figure 3.15c) and 1850±26 (2σ, figure 3.15d) respectively, within error of both zircon geochronology and Rb-Sr whole rock geochronology on both the regional scale (figure 3.15a,b) and small scale (figure 3.15f).

Analysis of three Jussieu Dykes and their surrounding selvages produce a six point isochron which, despite some excess scatter (MSWD = 56), confine the emplacement age of the Jussieu Dykes at 1856±8 Ma (2σ, figure 3.15e), again within error of the Lincoln Batholith (figure 3.15).

3.7 Petrogenesis and tectonic setting

3.7.1 Tectonic discrimination diagrams

The Lincoln Batholith has a chemical signature which, on tectonic discrimination diagrams (Pearce et al., 1984) plots across the boundaries between within plate granites and syn-collisional and volcanic arc granites. With increasing silica content, the position on the discrimination diagram moves from the within plate field into the syn-collisional/volcanic arc fields (figure 3.16a, figure 3.16b). The lowest silica members of the pyroxene bearing granitoids are interpreted to represent the least fractionated and metamorphosed members of the batholith, and are likely to be the most representative lithologies for tectonic discrimination. Hence, the application of the discrimination diagram approach (figure 3.16) support a within plate environment.

The Lincoln Batholith also displays A-type affinities (figure 3.17), with only cumulate and highly fractionated lithologies plotting in the M-, I- and S-type granite field of Whalen et al. (1987). While A-type magmas are not necessarily indicative of a single tectonic environment, the Proterozoic of South Australia contains many examples of within plate A-type magmatism (eg, the Hiltaba (~1592 Ma) and Spilsby (~1530 Ma) Suites of the Gawler Craton, the Moolawatana Suite (~1575 Ma) of the Mount Painter and Babbage Inliers).

3.7.2 Discussion

Any petrogenetic model for the Lincoln Batholith must account for its trace element homogeneity and evolved Nd isotopic signature over a large area (at least ~5000 km^2, possibly more); coexisting mafic and felsic magmas; an environment capable of sustaining protracted large scale fractionation and homogenisation; and the generation of I- to slightly A-type magmas. A further constraint on magmatic setting is provided by P-T data from metapelitic enclaves within the MCC (Bendall, 1994), which suggest equilibration with the surrounding crust occurred at

~5.5 kbar, placing a minimum constraint on the depth of emplacement of ~20 km. The tectonic implications of exposing rocks emplaced at such depths at the surface of normal thickness crust is investigated in chapters 6 and 8.

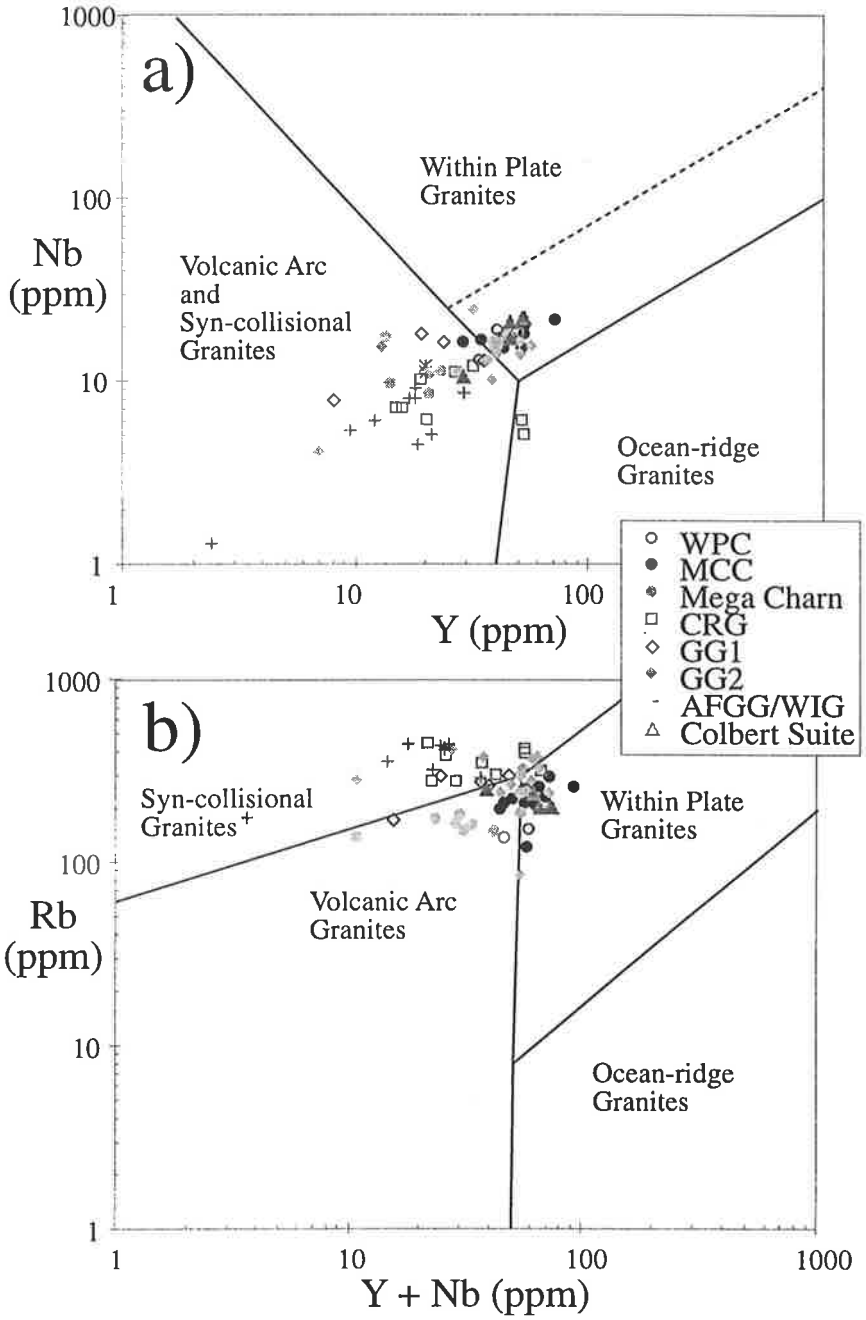

Figure 3.16: Tectonic discrimination diagrams after Pearce et al. (1984) for non-cumulate felsic portions of the Lincoln Batholith. Lowest silica pyroxene members start in the within plate fields on both diagrams, moving progressively towards the syn-collisional and volcanic arc fields with increasing weight % SiO_2.

Various models have been may be applied to the generation of magmas with chemical features broadly similar to the Lincoln Batholith, including:

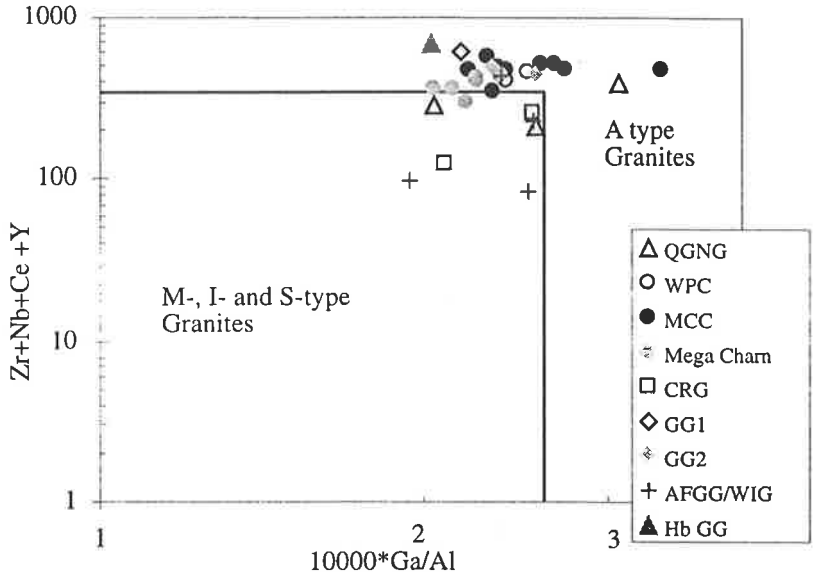

Figure 3.17: A-type discrimination diagram for felsic portions of the Lincoln Batholith. Adapted from Whalen et al. (1987).

a) subduction at (continental) plate margins (eg, Hildebrand et al., 1987; Windley, 1993)

b) fractionation from mantle melts (eg, Turner et al., 1992)

c) derivation from and reworking of Archaean crust (eg, McLennan and Taylor, 1982)

d) mixing between contemporary (1850 Ma) mantle and (Archaean) continental crust (eg, Patchett and Arndt, 1986)

e) two stage derivation from a Palaeoproterozoic underplate (eg, Wyborn, 1988).

Outlined below are diagnostic geochemical, structural and isotopic features for each of the models described above.

a) Continental plate margin related subduction regimes embrace a wide range in magma chemistry, a response to variations in relative crustal and mantle inputs. However, features often observed along modern continental arcs include the amalgamation of outboard terrains and juvenile crustal blocks, hydration melting of the mantle wedge above the subducting slab and intermediate, commonly calc-alkalic magmatism. Magmatism often persists for tens of millions of years, and may be accompanied by syn-emplacement deformation. Depleted mantle model ages are generally close to emplacement ages, as reflected by high initial ε_{Nd} values (eg, figure 3.18b) due to extraction of material from the mantle wedge. Discrete plutons and heterogeneous chemical features on the tens of kilometres scale are common in plate margin settings (eg, Sierra Nevada Batholith).

b) Turner et al. (1992) demonstrated the viability of generating A-type felsic magmas by fractionation of mafic melts. Felsic magmas thus generated would be

expected to preserve initial ε_{Nd} values comparatively close to the contemporary mantle source from which they were derived. Such melts will also reflect a relatively homogeneous source region, but show evidence of a source which is clearly mafic in composition.

c) Intracrustal partial melting (eg, McLennan and Taylor, 1982) should produce magmas with highly evolved Nd isotopic signatures which reflect protracted crustal residence, and highly siliceous compositions due to derivation from an average continental crustal composition. Archaean model ages, very low initial ε_{Nd} values and recycled/inherited zircons are all characteristic of such processes. Additionally, large scale crustal melting would inevitably produce magmas containing low compatible element abundances due to the scarcity of these elements in the continental crust. Additionally, magmas of S-type affinities due to interaction with metasediments during either generation and/or emplacement of the magma may also be observed.

d) Alternatively, mixing of contemporary depleted mantle and Archaean crust has been suggested as a mechanism for the generation of large volumes of 1.9-1.7 Ga continental crust by Patchett and Arndt (1986). From the assumption that the "...depleted mantle was the only type of type of mantle able to participate in large scale crustal genesis...", they argue that crustal growth during this period of the Proterozoic is driven by depleted mantle-continental crust mixing. Magmas generated from such a process are likely to show strong crustal signatures, and preserve high levels of crustally derived phases (eg, zircon inheritance) and crustal trace element signatures such as negative Nb and Ti anomalies, but also reflect contemporary mantle chemistry. Model ages are likely to be substantially older than emplacement ages due to the input of Archaean crust. Hence, distinct isotopic and chemical mixing arrays between crustal and depleted mantle end-members are predicted by this model.

e) Wyborn (1988) appealed to a two stage model involving underplating of the crust with Proterozoic mantle hundreds of millions of years prior to magma generation. Such a two stage model effectively introduces a third source region beyond the continental crust and contemporary mantle described by Patchett and Arndt (1986). The advantage of such a source for magmatism is that of generating a large volume, chemically homogeneous mafic source region with a more evolved isotopic signature than the contemporary depleted mantle. Magma generation in the plagioclase stability field would produce distinctive negative Sr anomalies, and be intermediate to felsic in composition and homogeneous in both isotopic signature and trace element patterns. Evidence of the underplating event would be preserved in zircon inheritance and depleted mantle model ages, which are not simply mixtures of pre-existing crustal sources. The latter would approximate the

time of underplating , which is also manifested as thermal events within the crust, such as mafic magmatism.

Interpretation of the Lincoln Batholith

The aim of the following discussion is to evaluate potential source regions for the Lincoln Batholith in the context of the models described above.

Windley (1991, 1993 and references therein) interprets elongate terrains such as the Ketilidian (in south Greenland) in terms of a plate tectonic paradigm. Rapakivi granites in such settings post date peak metamorphism and deformation by 60 Ma (Windley, 1993), clearly not the case in the Lincoln Batholith where voluminous rapakivi granites predate metamorphism by ~100 Ma. The Lincoln Batholith displays low Al_2O_3 and high Fe_2O_3 at intermediate compositions (figure 3.9), inconsistent with calc-alkaline affinities. Calc-alkaline trends are often cited (Etheridge et al., 1987; Wyborn, 1988) as typical (but not necessarily diagnostic) of subduction related settings. The Lincoln Batholith also shows a volumetric paucity of intermediate magmatism which typifies Andean style tectonic settings, and contains elevated K_2O and Y values with respect to subduction settings. Those subduction related settings on the modern Earth which tend towards relatively high K_2O values at comparable silica levels are continental margins, such as the aforementioned Andean setting and the western US (see chapter 7). A feature of the Lincoln Batholith reminiscent of Cordilleran settings is the presence of co-existing and mingling felsic and mafic magmas, similar to the Sierra Nevada Batholith in California.

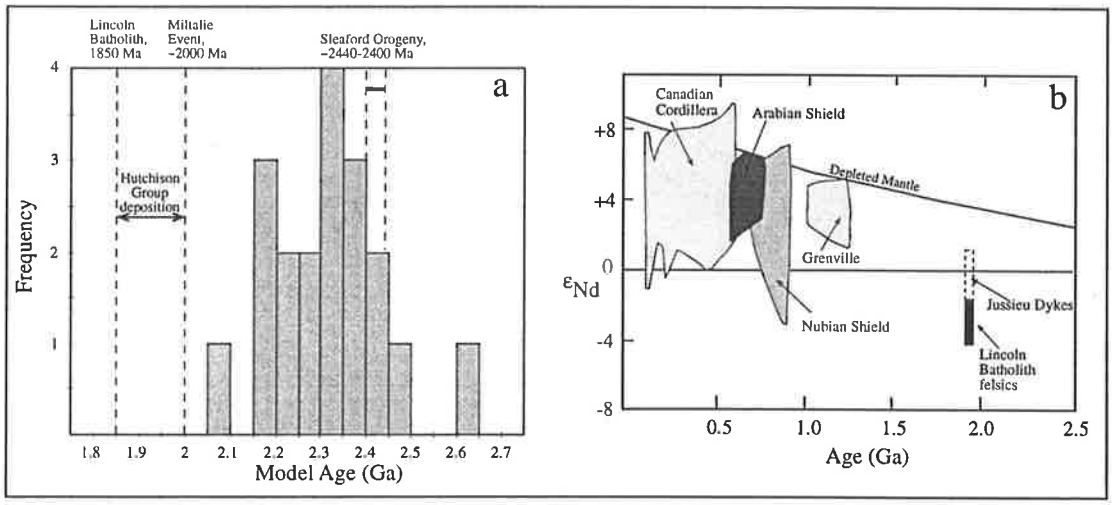

Figure 3.18: Nd isotopic features of the Lincoln Batholith. a) The Lincoln Batholith preserves model ages substantially older than emplacement age. b) Intial ε_{Nd} values for the Lincoln Batholith are significantly lower than for plate margin tectonic settings, such as the Cordilleran and Grenvillian (adapted from Samson and Patchett, 1991).

The most significant distinction between the Lincoln Batholith and Phanerozoic plate margin settings is in terms of their relative Nd isotopic signatures. Figure 3.18 highlights the difference between juvenile crust produced in Grenvillian and Cordilleran settings, as opposed to the more evolved signature preserved in the Lincoln Batholith. This results in distinctly older model ages for the Lincoln Batholith than its magmatic age (figure 3.18a). For reasons elaborated below, this evolved isotopic signature within the Lincoln Batholith is unlikely to be derived wholly by continental crustal contamination, implying that a modern plate margin analogue is unlikely. Structural evidence (eg, Hoek and Schaefer, 1998) suggests Lincoln Batholith emplacement may have occurred in an intracontinental anorogenic to extensional setting.

Therefore, whilst individual features of the Lincoln Batholith taken in isolation may be interpreted in terms of a subduction related accretionary margin, the overall geometric and magmatic system is not readily reconcilable with a subduction related setting. Further discussion on comparisons between plate margin processes and Proterozoic magmatism can be found in chapter 7.

Derivation wholly from depleted mantle derived mafic melts is an unlikely scenario for the Lincoln Batholith due to the evolved Nd and Sr isotopic character of the batholith ($\varepsilon_{Nd(t)}$ values are in the range of ~-2.2 to -4.1 (table 3.2)). Such strongly negative values are inappropriate for complete extraction of the felsics from the depleted mantle at ~1850 Ma. Some Jussieu Dykes contain more positive$\varepsilon_{Nd(i)}$ values (up to +1.5, table 3.2), hinting at a primitive isotopic reservoir, however the volume of such material in the batholith as a whole is relatively minor (<5% of exposed outcrop). Additionally, the high concentrations of Rb, Th, U and LREE at comparatively low SiO_2 levels suggests a source region containing initially elevated concentrations of these elements (figure 3.10), a feature inconsistent with a depleted mantle source. In order to generate the volumes of felsic magmatism observed in the Lincoln Batholith by mafic fractionation requires large volumes of accompanying mafic magmatism (Turner et al., 1992), which, despite exposure of a significant crustal section of the batholith adjacent the Kalinjala Shear Zone (at least ~5 km thick; Bendall, 1994), is not observed. While interaction of small volumes of contemporary mantle with continental crust may account for the mixing array observed in the Jussieu Dykes, a more isotopically evolved and chemically enriched reservoir appears necessary for generation of the Lincoln Batholith felsic magmatism.

Figures 3.13 and 3.18 could imply derivation of the Lincoln Batholith from an Archaean source due the evolved Nd isotopic signature observed. However, wholly sourcing the batholith from contemporary crust is considered unlikely since the model ages for the batholith (and intitial ε_{Nd} values) are younger than the crust from which it would have been derived. Additionally, potential source rocks for the Lincoln Batholith (ie, the Sleaford Complex) are heterogeneous in nature and

had previously experienced pervasive granulite facies metamorphism (~700-800°C and ~7-9kbar during the Sleafordian; Bradley (1979)) during which partial melting would already have been expected to take place. Hence, reworking and partial melting of the Sleaford Complex at ~1850 Ma to generate the (homogeneous) Lincoln Batholith would be expected to leave a substantial geochronological record on the Sleaford Complex, which is markedly absent (see Fanning, 1997). Therefore, the Archaean crust at the current exposure level on southern Eyre Peninsula is an unlikely candidate for a Lincoln Batholith source. Metasedimentary and orthogneissic enclaves within the Lincoln Batholith are also unlikely to source the Lincoln Batholith as they are too felsic to generate the intermediate members of the batholith. The isotopic and geochemical characteristics of these enclaves is discussed further in chapter 5, and their role in the crustal evolution of the southern Eyre Peninsula outlined in chapter 8.

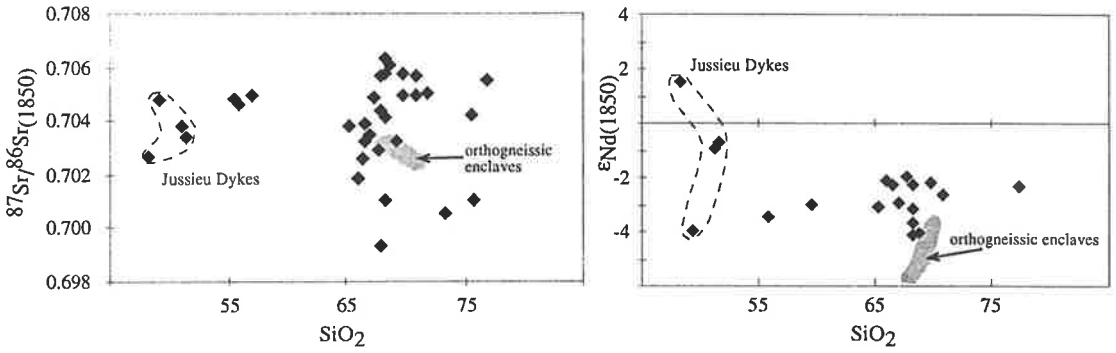

Figure 3.19: Lincoln Batholith isotopic variation as a function of silica content. No real trends between the felsic, non-cumulate portions of the Lincoln Batholith and potential crustal assimilants, in the form of orthogneissic basement enclaves, are observed

Whilst complete derivation of the Lincoln Batholith from contemporary continental crust is considered unlikely, it does preserve evidence of interaction with the crust. Features such as (rare) zircon inheritance (see section 3.6; Fanning, 1997), negative Ti and Nb anomalies, comparatively evolved Nd isotopic signatures and field relationships (figures 3.5, 3.7), suggest some degree of crustal contamination, at least at emplacement level. The mixing model of Patchett and Arndt (1986) is entirely feasible in the case of the Jussieu Dykes as they define a distinct mixing array between contemporary crust (the Sleaford Complex) and the depleted mantle (figure 3.13). However, these comprise a volumetrically minor portion of the Lincoln Batholith (<5%, table 3.1), with the majority of magmatism constrained to a narrow Nd isotopic band at the time of emplacement. This band does not show the distinct array-like geometry of the Jussieu Dykes, displaying only a slight tendency to a mixing curve (figure 3.13). A maximum of ~30% crustal input is suggested by simple mixing calculations (figure 3.13). Initial isotopic ratios also suggest large scale crustal assimilation was unlikely (figure 3.19), with no

systematic isotopic changes with fractionation for non-cumulate lithologies.

The mechanism invoked by Patchett and Arndt (1986) may be valid if one assumes the depleted mantle was not the sole reservoir able to participate in large scale crustal genesis. Trace element chemistry of the large volume members of the Lincoln Batholith (ie, Memory Cove Charnockite, Megacrystic Charnockite and retrogressed equivalents), suggest that the source region for the magmatism was itself voluminous and homogeneous. Generally low MgO and Ni values in non-cumulate members of the Donington Suite (figure 3.9), coupled with elevated REE concentrations relative to Palaeozoic I-type granitoids suggest the source region for the Lincoln Batholith was itself fractionated. Nd isotopes require the source to have been isolated from the depleted mantle for a substantial period of time (figure 3.18) prior to generation of the Lincoln Batholith. A fractionated source region would also account for enriched Rb, La, Ce, Th and U, with even cumulate portions of the batholith (such as the Quartz Gabbronorite Gneiss) containing relatively high concentrations of such elements. This effectively acts as a minimum constraint on source concentration for such elements. Furthermore, the apparent silica gap between the cumulate Quartz Gabbronorite Gneiss (55.5-57.5 weight % SiO_2 at Cape Donington) and the least evolved fractionates of the MCC (~64.2%) place bounding silica compositions on the postulated source region of the Lincoln Batholith, suggesting an intermediate composition. This conclusion is consistent with that of Mortimer (1984).

Wyborn (1988) suggests the presence of such an evolved reservoir for many northern Australian terrains, and attributes its formation to a mafic underplating event hundreds of millions of years prior to felsic magma generation. Such a two stage model effectively accounts for evolved Nd isotopic signatures as well as incorporating negative Sr anomalies due to magma generation in the plagioclase stability field. Such magmas, once generated, are able to interact with contemporary crust to varying degrees to produce the inherited zircon and negative Nb and Ti anomalies observed in the Lincoln Batholith.

It must be pointed out that underplating is by no means the only method available for generating enriched subcontinental lithospheric mantle, with other, passive mechanisms such as freezing on of upwelling asthenosphere during extension a viable alternative. Subsequent enrichment by the movement of small melt fractions from the asthenosphere (eg, McKenzie, 1989; Turner and Hawkesworth, 1995) after generation of new lithosphere are also plausible.

The clustering of Nd depleted mantle model ages between ~2.3-2.5 Ga for the Donington Suite (figure 3.18) suggests such ages are not merely mixtures of old lithosphere with lithosphere formed at the time of Lincoln emplacement. Such a narrow range suggests an isotopic source with its own unique Nd isotopic

signature. This implies an extended isotopic evolution of the Donington Suite source independent of the depleted mantle prior to Lincoln Batholith formation, consistent with either an underplate or enriched subcontinental lithospheric mantle.

Finally, Lincoln Batholith generation was initiated ~150 Ma after extension associated with Hutchison Group sedimentation began. Combined decompression and thermal input associated with asthenospheric upwelling acting upon an enriched subcontinental lithosphere may well have provided the mechanism for Lincoln Batholith magmatism. The source of lithospheric enrichment is not clear; either underplating as described by Etheridge et al. (1987) (which also provides a mechanism for extension) or a steady state continuum of small melt fraction percolation into lithosphere formed during a discrete time in the past (eg, Turner and Hawkesworth, 1995) may be appropriate.

3.8 Conclusions

The Lincoln Batholith represents a large volume, dominantly felsic, intrusive complex emplaced to a maximum of 15km depth over a comparatively short time period around 1850 Ma. There are three distinct portions of the Lincoln Batholith, the syn-plutonic mafic Jussieu Dykes, the (initially) anhydrous Donington Suite and the hydrous Colbert Suite. The majority of magmatism within the batholith is composed of Donington Suite lithologies, which are isotopically homogeneous throughout the batholith.

The batholith as a whole is characterised by negative Nb, Sr, P and Ti anomalies, with a narrow range of initial Nd isotopic signatures (within two ε units). The chemistry and geometry of the batholith is not typical of a Phanerozoic subduction related setting, nor do Sr and Nd isotopes suggest complete derivation from pre-existing continental crust. The key trace element features, including elevated incompatible element concentrations at low silica levels, and evolved isotopic signatures, are consistent with derivation of the Lincoln Batholith from a lithospheric source which had been isolated from the depleted mantle for a substantial period of time previously. Such a source was itself likely to be relatively enriched in incompatible elements, and intermediate in composition, with subsequent trace element variation within the Lincoln Batholith imposed by fractionation upon these source attributes. The role of contemporary mantle during Lincoln Batholith generation was minimal but not trivial, giving rise to the comagmatic Jussieu Dykes; mixing products between depleted mantle and contemporary crust. The presence of the Jussieu Dykes suggest that the depleted mantle was either anomalously hot or close to the surface at the time of Lincoln Batholith generation, implying a thermal link between melting of the depleted mantle and the enriched lithospheric source at ~1850 Ma.

CHAPTER FOUR[1]

Palaeoproterozoic magmatism of southern Eyre Peninsula II: The Tournefort Dykes

4.1 Introduction

Mafic dyke swarms are common in Precambrian terrains (eg, Kuehner, 1989; Zhao and McCulloch, 1993a, b; Mazzucchelli et al., 1995; Condie, 1997; Cadman et al., 1995, 1997; Hageskov, 1997). They have received considerable attention because their lateral continuity and geologically short time scale of emplacement (LeCheminant and Heaman, 1989; Hoek and Seitz, 1995) makes them invaluable time markers. They also offer insights into the stress field and thermal state of the lithosphere into which they are emplaced (Hoek and Seitz, 1995). Additionally, they can provide geochemical information of deeper mantle reservoirs and processes (eg, Hergt et al., 1988; Sun and McDonough, 1989; Zhao and McCulloch, 1993a; Turner and Hawkesworth, 1994).

Many Proterozoic dyke swarms may be related to distinct geological features by virtue of their geometry, for example, the MacKenzie swarm in Canada radiates from a single point, believed to indicate a plume source (LeCheminant and Heaman, 1989). Other swarms of parallel dykes have been ascribed to lithospheric extensional events, such as rifting. In both cases, mafic dyke swarms may well represent the plumbing system of associated continental flood basalt magmatism (Fahrig, 1987). Distinguishing between mafic dyke swarms originating in

[1] The contents of Chapter 4 comprise a manuscript entitled "The Jussieu and Tournefort Dykes of the southern Gawler Craton, South Australia" by Schaefer, B.F., Foden, J.D., Sandiford, M. and Hoek, J.D., for submission to Precambrian Research. In the interests of style and to avoid repetition, this chapter represents a modified form of the manuscript. A complete copy can be found in appendix 5.

subcontinental lithospheric mantle and those of mantle plume origin remains central to understanding the origin and persistence of geochemical reservoirs in the lithospheric mantle. However, identification of the source of mafic dykes is complicated by distinguishing between enriched lithospheric mantle sources and contamination with continental crust. Despite this, mafic dyke swarms rarely show geochemical evidence of such contamination (eg, Weaver and Tarney, 1981; Hergt et al., 1989; Tarney, 1992; Zhao and McCulloch, 1993a; Condie, 1997). Consequently such swarms provide excellent opportunities for identifying the geochemical signatures of mantle reservoirs and their evolution through time (Condie, 1997).

The following chapter uses the geometric, isotopic and geochemical attributes of the Palaeoproterozoic Tournefort Dykes of the southern Gawler Craton, to assess the level of crustal contamination, source region characteristics and place constraints on the nature of subcontinental lithospheric reservoirs for Palaeoproterozoic continental mafic magmatism.

4.2 The Tournefort Dykes

The Tournefort Dykes form a suite of gabbro to gabbronorite dykes and retrogressed equivalents, observed to crosscut all units of the Lincoln Batholith (including the Jussieu Dykes) were deformed and partly metamorphosed during the Kimban Orogeny, and in places (eg, West Point, Kirton Point) contain peak metamorphic assemblages. The timing of the Tournefort Dykes is thus bracketed by Lincoln Batholith magmatism (~1850 Ma) and peak Kimban metamorphism (~1730 Ma, Bendall, 1994; Hand et al., in prep.).

As noted by previous workers, such as Mortimer (1984) and Mortimer et al. (1988b), two distinct types of mafic rocks occur on the southern Eyre Peninsula. These include gabbroic and picritic rocks with a clearly dyke like geometry preserving primary igneous textures as distinct from tectonically concordant boudins of amphibolite with appreciable or complete metamorphic recrystallisation. Detailed mapping has demonstrated that these amphibolites in the Lincoln Batholith preserve the same geometric relationships and are in a broad geochemical sense analogous to the Tournefort Dykes, but are generally found in zones of higher strain and metasomatism. Thus, in this contribution the amphibolites are considered to be retrogressed equivalents of the Tournefort Dykes. However, the bulk of discussion will focus on relatively pristine dykes from regions of low strain and deformation since such areas preserve the most information regarding petrogenesis and magmatic chemistry

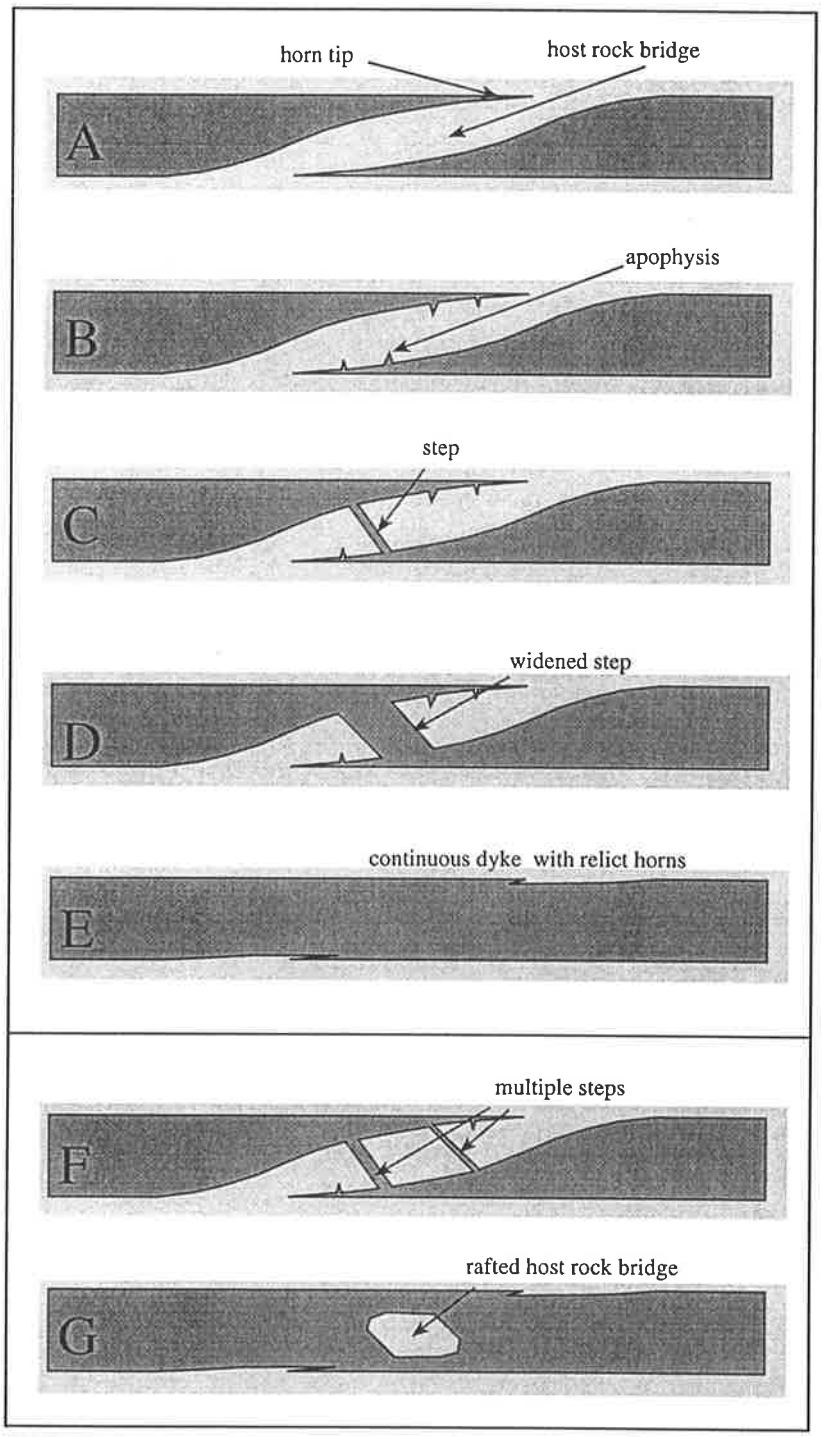

Figure 4.1: Evolution of dyke propagation features observed in low strain zones on southern Eyre Peninsula. Dyke tips propagate either vertically or laterally (A). Extension on the inner surfaces of the tips causes the formation of apophyses (B), which may ultimately breach the bridge of intervening country rock , forming a step (C). Continued passage of material through the step can cause it to widen (D), ultimately resulting in a dyke of original thickness, containing parallel margins with relict horn tips (E). In some cases, multiple steps may be formed (F), forming a raft of host rock material within the body of the dyke (G). Scale: from millimetres to tens of metres.

Figure 4.2: The Tournefort Dykes a)Dyke propagation features on thenorthwestern tip of Williams Island. Apophyses on dyke horn at left of picture are propagating towards broad horn on right of picture. See figure 4.1b for a schematic representation. Notebook is ~15cm long.

b)Effect of deformation on initially planar mafic bodies. Continued deformation has resulted in discontinuous bodies after failure in boudin necks. Broad dyke in centre is ~1m wide.

c) Competence contrasts between a Tournefort Dyke, a relict horn (figure 4.1e) and host Lincoln Batholith augen gneiss. In this example the host gneiss is behaving more rigidly than the surrounding mafic. Kirton Point boat ramp, pen ~14cm long.

Regions of low strain, particularly Williams Island, West Point and McLaren Point preserve a plethora of dyke propagation features, allowing distinction of two dyke emplacement events, characterised by NNW-SSE (~330-350°T) and NE-SW (~25-60°T) trending orientations (Hoek and Schaefer, 1998). Crosscutting relationships on Williams Island suggest the NE trending set to be younger than the NNW trending dykes. Features such as arrested dyke tips, horns, steps, bridges and rafted bridge material (figures 4.1, 4.2a) are typical of dyke propagation (Hoek, 1994). While a range of other dyke and amphibolite orientations are observed along the coast of southern Eyre Peninsula (Giddings and Embleton, 1976; Hoek and Schaefer, 1998), these often reflect rotation due to Kimban deformation. Hence, while the orientation data is considered a useful tool in demonstrating the existence of several dyke emplacement events, it is by no means considered grounds for a definitive classification on the outcrop scale.

Localities such as Kirton Point (figure 4.2c) have been interpreted by some (eg, Tilley, 1921c) to contain amphibolite gneiss which was engulfed and orientated by the intruding felsic gneiss. However, outcrops at Wanna demonstrate how discontinuous mafic bodies can be formed by deformation of initially planar dykes (figure 4.2b; Bales, 1996).

4.3 Geochemistry

The Tournefort dykes are composed of four geochemical groups, reflecting both initial magmatic variation and variable subsequent metasomatic alteration associated with deformation and metamorphism during the Kimban Orogeny. However, all geochemical groupings possess (to varying degrees) negative Nb, Sr and Ti anomalies, along with depleted Y values.

High Mg Tholeiites (HMgT)

Dykes of this group range from picritic to gabbronorite in composition, with variable degrees of secondary amphibolitisation. Their chemistry is distinctive by virtue of very high MgO contents (12.1-24.1%) at low SiO_2 (46.2-53.3%) and CaO (3.9-11.0%). The HMgT also contain comparatively low levels of LILE and pronounced Nb, Sr and P depletions. They contain the lowest levels of LREE of any Tournefort Dykes (figure 4.3) and the highest Ni (382-1228 ppm) and Cr (1027-4166 ppm). Primitive mantle normalised patterns for elements more compatible than Sr tend to be fairly flat (figure 4.3), and in some samples the absolute abundances of Sm, Ti and Y is less than both N- and E- type MORB's.

Lithology	HMgT	HMgT Amphib.	HBaT Amphib.	FeRT	FeRT	Dolerite	Dolerite	Dolerite Amphib.
Sample #	SEP-148	SEP-024	1028-99	SEP-270	SEP-081	SEP-220	SEP-260	1028-110
Location	Memory Cove	Pt. Boling	West Pt	Williams Island	West Pt	West Pt	Williams Island	Tumby Hills
Est Age (Ma)	*1812*	*1812*	*1812*	*1812*	*1812*	*1812*	*1812*	*1812*
SiO_2%	49.07	47.39	51.00	48.07	49.79	53.33	47.70	56.71
Al_2O_3%	8.99	12.96	14.40	13.19	13.63	17.65	14.48	14.84
Fe_2O_3%	11.95	12.10	18.02	17.93	16.75	11.03	15.35	11.73
MnO%	0.19	0.19	0.22	0.26	0.24	0.15	0.22	0.17
MgO%	21.39	12.06	4.62	6.42	5.29	4.40	7.24	3.89
CaO%	6.74	10.96	8.80	9.61	9.43	9.49	9.96	7.06
Na_2O%	0.78	1.97	2.29	2.38	2.61	3.05	2.69	0.65
K_2O%	0.50	0.81	1.73	0.51	1.13	1.21	0.69	1.57
TiO_2%	0.55	0.58	1.76	2.11	2.17	1.12	1.58	1.40
P_2O5%	0.08	0.09	0.35	0.20	0.27	0.20	0.17	0.19
SO_3%	0.01	0.00	0.02	0.04	0.01	0.00	0.03	0.02
LOI%	-0.24	1.10	-2.94	0.06	-0.51	-0.20	0.16	1.91
TOTAL	100.01	100.21	100.26	100.78	100.81	101.43	100.27	100.14
Rb	18.512	47.731	56.898	17.230	55.383	38.169	23.106	95.620
Ba	154.0	118.0	671.0	165	301.0	432	194	234
Th	2.6	0.9	3.9	3.0	6.0	5.2	3.1	9.1
U	0.9	1.8	1.9	0.1	2.3	2.6	1.2	4.2
Nb	4.4	3.1	11.0	9.7	12.7	11.4	7.4	10.1
La	12	3	34	15	21	33	15	19
Ce	14	12	79	41	59	61	37	54
Pb	2.2	4.1	10.6	4.9	8.5	9.4	7.1	5.5
Sr	86.487	80.243	208.945	164.702	135.544	248.553	177.105	150.898
Nd	9.889	6.240	31.912	18.875	26.338	24.300	18.952	25.016
Zr	74.7	38.5	167.1	130.4	203.4	152.8	112.0	169.3
Sm	2.151	1.654	6.999	5.040	6.626	4.890	4.594	5.782
Y	14.6	16.8	42.2	37.3	49.0	28.5	27.5	32.8
V	186	254.5	307.5	466	410.3	215	363	295.8
Sc	25.7	36.8	39.5	44.9	38.3	23.2	37.7	35.8
Cr	3009	1262	67	91	154	86	192	25
Ga	9.6	13.7	22.1	22.2	22.3	22.0	22.3	21.2
Eu	0.588							
Gd	2.310							
Dy	2.287							
Er	1.382							
Yb	1.373							
$^{143}Nd/^{144}Nd$	0.511570	0.512063	0.511627	0.512313	0.512167	0.511436	0.512085	0.511876
2σ	0.000050	0.000064	0.000059	0.000036	0.000056	0.000024	0.000032	0.000059
$^{147}Sm/^{144}Nd$	0.1316	0.1603	0.1327	0.1615	0.1522	0.1217	0.1466	0.1398
$T_{(DM)}$ Nd	**2.67**	**2.70**	**2.60**	**2.13**	**2.16**	**2.61**	**2.16**	**2.37**
$\varepsilon_{Nd(t)}$	-5.72	-2.77	-4.85	1.85	1.17	-6.04	0.86	-1.64
$^{87}Sr/^{86}Sr$	0.722115	0.740074	0.726084	0.710167	0.733129	0.717462	0.712885	0.751932
2σ	0.000048	0.000165	0.000049	0.000040	0.000120	0.000026	0.000036	0.000049
$^{87}Rb/^{86}Sr$	0.6202	1.7265	0.7893	0.3027	1.1851	0.4447	0.3777	1.8413
$^{87}Sr/^{86}Sr_{(t)}$	0.70595	0.69508	0.70551	0.70228	0.70224	0.70587	0.70304	0.70394

Table 4.1: Geochemical data for Tournefort Dykes with new isotopic data.

Iron (Fe) Rich Tholeiites (FeRT)

The Fe rich tholeiites are a series of variously amphibolitised dykes with $Fe_2O_3^T$ > 16%, and elevated (up to 3.6%) TiO_2. They are slightly LREE enriched, and contain widely varying LIL element concentrations (eg, Ba = 56-502 ppm), a reflection in part of element mobility during amphibolitisation. FeRT dykes tend to high V concentrations with respect to the rest of the Tournefort Dykes, as well as containing elevated Rb, Ba, and Zr.

High Ba Tholeiites (HBaT)

This group of mafics typically outcrops as planar arrays of amphibolite rafts and boudins, commonly with partial melts and leucosomes generated in boudin necks and on raft margins (eg, centre of field in lower mafic in figure 4.2c, on tip of bottom portion of central dyke in figure 4.2b). Individual dykes are not as prevalent in this group as in the remainder of the Tournefort Dykes. The distinguishing character of these mafics is their high (>600 ppm) Ba, (figure 4.3). SiO_2 (49.3-58.3%), K_2O and Na_2O levels. They also contain high Rb, Th, Sr, Pb and LREE concentrations (table 4.1). Although it is tempting to attribute many of these features to amphibolitisation, figure 4.3 compares the effects of different metamorphic assemblages on bulk composition for the main dyke groups. While there is some variation in chemistry within groups with increasing degrees of amphibolitisation, it is clear that overall trace element patterns broadly reflect initial compositions. The implications of what such initial compositions may mean are discussed below.

Unassigned Tholeiites

By far the bulk of the Tournefort Dykes fall into this category. A range of tholeiitic dolerites are observed, including plagioclase- and orthopyroxene-phyric dolerites, variably amphibolitised equivalents, and unaltered even grained dolerites. Due to both initial compositional variation and subsequent amphibolitisation, the tholeiite dykes possess a broad range of chemical compositions. SiO_2 values range from 47.0-53.1%, with moderate levels of MgO (5.1-9.7%) and the highest values of CaO (8.6-12.5%) for the Tournefort Dykes. The bulk of unassigned tholeiites are Sr depleted with weakly developed negative Ti and Y anomalies, however absolute trace element abundances trend to higher values than for the HMgT. A wide spread in LILE (K, Rb, Ba) concentrations possibly reflects varying degrees of amphibolitisation and metasomatism during the Kimban Orogeny.

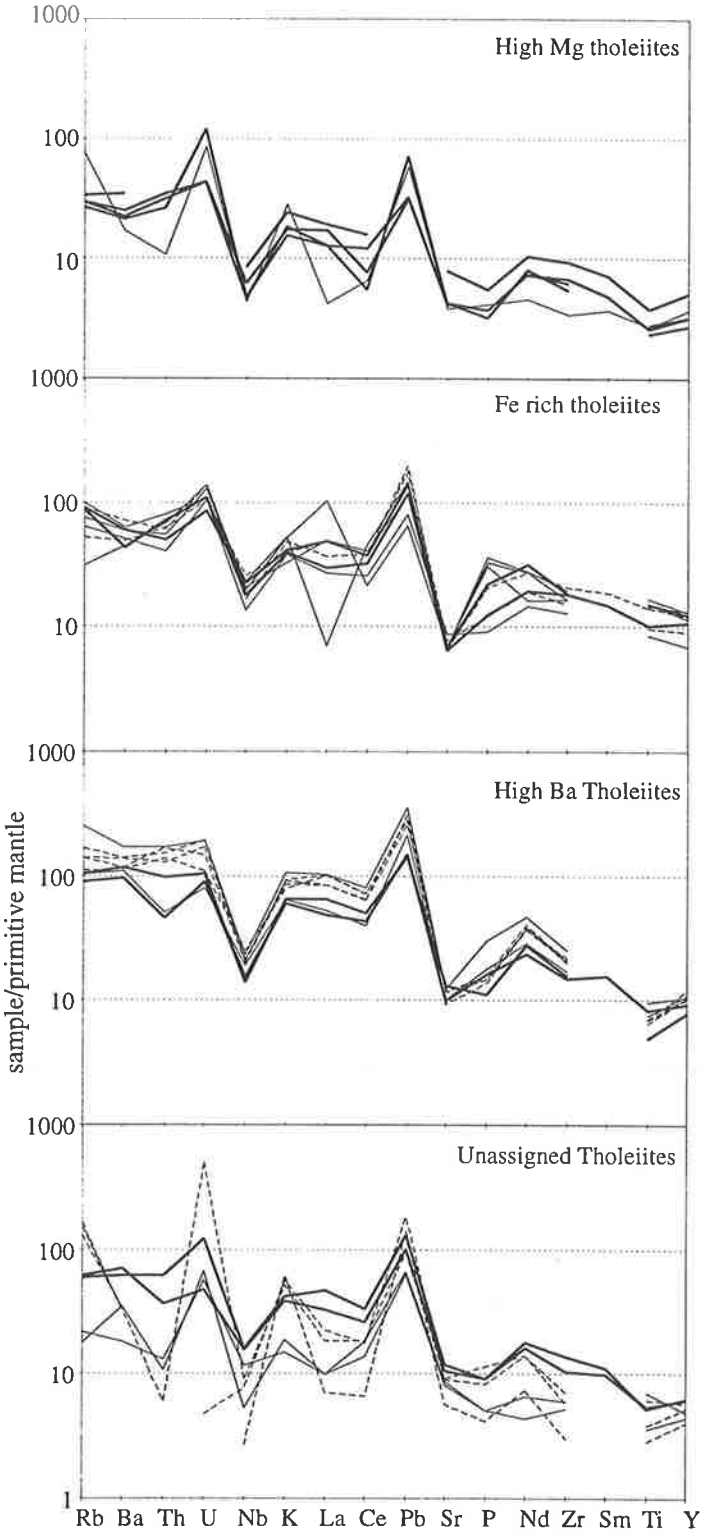

Figure 4.3: Comparative trace element variation diagrams displaying initial compositions and the effects of amphibolitisation of the Tournefort Dykes. Broad solid lines = undeformed dykes, narrow solid lines = hb+bt amphibolites and dashed lines = gt bearing amphibolites.

4.4 Isotopic characteristics

Nd isotopes define two distinct groups within the Tournefort Dykes. One group contains dykes with high $\varepsilon_{Nd(1812)}$ values (+1.9 to -1.6), with the other group containing $\varepsilon_{Nd(1812)}$ values in the range -2.8 to -6.0. This subdivision is independent of the previously described geochemical groups, an effect mirrored in their Sr isotopes. $^{87}Sr/^{86}Sr_{(i)}$ ratios show similar ranges for each geochemical group, ranging from 0.70304-0.70582 for the Unassigned Tholeiites through 0.70385-0.70551 for the HBaT. Only the FeRT show a narrow range (0.70224-0.70228) which probably reflect a sampling bias due to the small number (two) of analyses. Sample SEP-024 shows evidence of strong Rb enrichment during amphibolitisation of the HMgT (see below), resulting in anomalously low $^{87}Sr/^{86}Sr_{(t)}$ ratios. The two Nd isotopic groups are also present in the Sr isotope data, with samples containing low $\varepsilon_{Nd(i)}$ values also containing correspondingly radiogenic $^{87}Sr/^{86}Sr_{(i)}$ signatures (>0.7045). Samples with high $\varepsilon_{Nd(i)}$ values typically have $^{87}Sr/^{86}Sr_{(i)}$ <0.7045 (table 4.1). Therefore, while the isotopic data contains little information within individual geochemical groups, the apparent coupling of the Nd and Sr isotope systems suggests the data reflects an important petrogenetic process.

4.5 Geochronology

Mafic dykes are valuable geochronological markers due to their lateral continuity and their short period of emplacement (eg, Zhao and McCulloch, 1993b). Historically, however, precise age determinations of mafic lithologies has been fraught with difficulty. For example, the relatively low total concentrations of radioactive elements and minimal compositional variation result in a narrow range of parent/daughter ratios, producing large errors in fitting whole rock isochrons. Low levels of accessory phases (such as zircon) amenable to geochronology means mafic dykes pose problematic geochronological targets compared to more commonly studied felsic suites. Internal mineral isochrons have been used to constrain emplacement ages on comparatively unaltered and undeformed dyke suites (eg, Zhao and McCulloch, 1993b), however such an approach is complicated in the Tournefort Dykes due to the effects of the Kimban Orogeny (as observed in Hand et al., in prep).

Previous studies (eg Black et al., 1991; Lanyon et al., 1993) have made use of comagmatic felsic segregations within dykes as sources of radiogenic element bearing phases. Such segregations represent late stage fractionates of the mafic magmas emplaced in veins oriented perpendicular to, but not progressing beyond, dyke margins due to contraction during cooling. Their chemistry is often sufficiently siliceous to allow crystallisation of accessory phases such as zircon which are able

siliceous to allow crystallisation of accessory phases such as zircon which are able to be dated by conventional techniques. Of utmost importance in such studies is the demonstration of the comagmatic nature of the felsic segregations with the dykes (as opposed to later generations of crosscutting veins), and the discrimination between populations of inherited phases (eg Black et al., 1991) from those associated with fractionation and crystallisation of the felsic segregation in question (eg, Lanyon et al., 1993).

4.5.1 Pb-Pb zircon evaporation geochronology

A zircon bearing felsic segregation from a dyke in the low strain zone at McLaren Point (sample GC-99) was identified as a potential geochronological target. This sample preserved diffuse margins with the host dyke, does not continue beyond the dyke margins into the host Lincoln Batholith lithologies and is less siliceous than later (Kimban) felsic veins which crosscut both the dyke and host gneisses. This segregation therefore places a minimum age constraint on the host dyke containing it.

Only a small number of zircons (~20) were retrieved from ~10 kg of sample GC-99, upon which Pb-Pb evaporation geochronology was attempted. Details of this technique are outlined in section 3.6, with further information in Appendix 1. Only 5 of the zircons analysed contained sufficient Pb to form a stable beam enabling data collection.

On the basis of $(U/Th)_t$, age and running criteria, two populations of zircon were identified in GC-99 (figure 4.4) neither of which are observed in the host Lincoln Batholith lithologies (see section 3.6). The populations comprise a younger, high $(U/Th)_t$ population at 1798±8 Ma ($(U/Th)_t$ ~0.45), and a slightly older, low $(U/Th)_t$ population ($(Th/U)_t$ ~0.37) at 1812±5 Ma. Both populations are a marked contrast to magmatic Lincoln Batholith zircons from Tumby Bay and Wanna (1841±8 and 1841±9 Ma respectively, $(Th/U)_t$ ~0.40). U-Pb zircon analyses on the Quartz Gabbronorite Gneiss at Cape Donington and the Memory Cove Charnockite at Memory Cove by Fanning (1997) and Fanning and Mortimer (in prep) also show no evidence of zircon growth at 1798 -1812 Ma.

The reproduction of the age populations in multiple zircons and the marked absence of a Lincoln Batholith component in the zircons analysed, coupled with higher $(Th/U)_t$ ratios measured in GC-99, suggests the ages record reflect periods of new zircon growth. Thus, the youngest age obtained from the felsic segregation places a minimum age constraint on the mafic dyke. Both ages obtained are consistent with the lithological and structural controls on Tournefort Dyke emplacement.

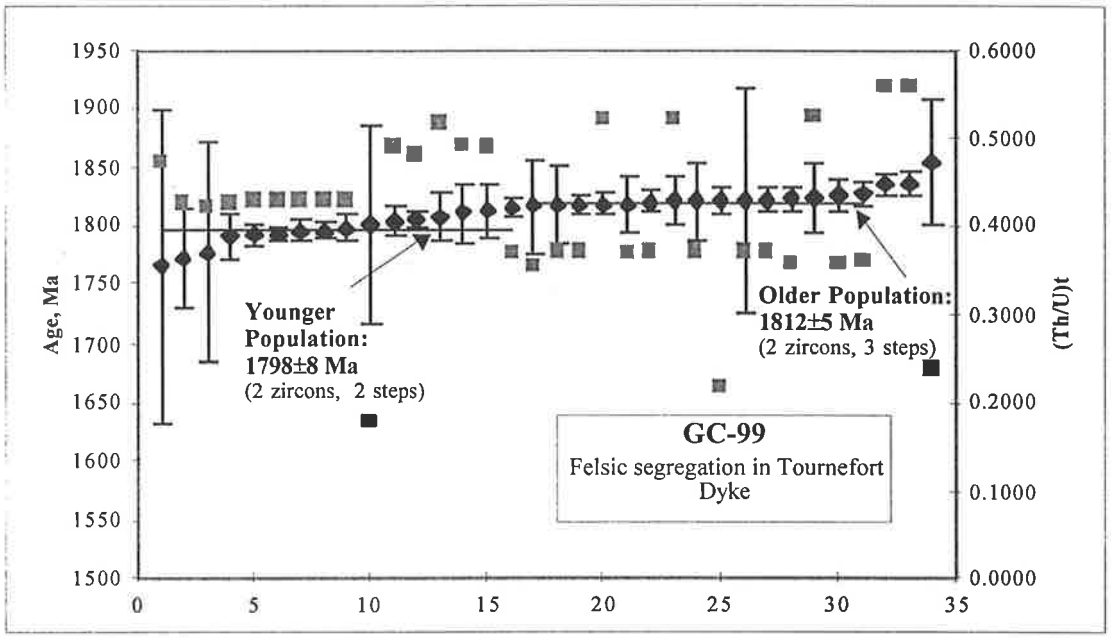

Figure 4.4: Summary of Pb-Pb zircon evaporation data from 4 zircons in sample GC-99 by block. Horizontal lines indicate mean values for the older and younger populations, error bars are 2σ. Solid squares are back calculated $U/Th_{(t)}$ ratios for corresponding blocks. The data is arranged in ranked order of age calculated for each block analysed.

Several scenarios can be envisaged for the presence of two unique zircon populations, including the younger age representing the time of dyke emplacement and the older component a mixing age beyond resolution of the evaporation technique with inherited zircons from the Lincoln Batholith. This is consistent with Lanyon et al. (1993) who noted a large component of inheritance in zircon studies from the Vestfold Hills. Alternatively, the younger age may be a mixing age formed by Kimban overgrowths with the magmatic emplacement age at 1812±5 Ma. At the time of writing it is difficult to distinguish between the two alternatives, except to note in passing that the high $(U/Th)_t$ ratio of the rims is consistent with metamorphic growth. Whilst there is evidence for this elsewhere in the Lincoln Batholith during the Kimban, the McLaren Point locality is a low strain area preserving fine scale magmatic relationships and typical bulk rock chemical and isotopic signatures. Also, as discussed above, the Tournefort Dykes have proved suprisingly robust to large scale metasomatism during amphibolitisation. In conclusion it would appear that the Tournefort Dykes can be no older than 1812±5 Ma, and no younger than 1798±8 Ma, both ages which are consistent with the regional geological constraints.

4.5.2 Rb-Sr whole rock geochronology

Previous attempts at whole rock Rb-Sr geochronology on the Tournefort Dykes have been inconclusive (Giddings and Embleton, 1976; Mortimer, 1984;

Mortimer et al., 1988b). As an adjunct to an extensive palaeomagnetic survey of the Tournefort Dykes on Eyre and Yorke Peninsulas, Giddings and Embleton (1976) cite ages of 1500±200 Ma and 1700±100 Ma for the two palaeomagnetic groupings of dykes observed, however no data is presented. Mortimer (1984) calculated an age of 1539±251 Ma for his Group A mafics, and Mortimer et al. (1988b) reported ~1600 Ma for a number of regressions on the mafics in the Port Lincoln area.

Whole rock studies of mafic dykes are inevitably constrained by the narrow range of bulk compositional variation within a suite, the implicit assumption of cogenesis of parallel mafic dykes and subsequent mobility of Rb and Sr during metamorphism. The net result is that while whole rock Rb-Sr data may place broad constraints on the age of the Tournefort Dykes, detailed whole rock studies are unlikely to provide new insights.

In the course of petrogenetic sampling in this project, seven new whole rock analyses were generated, which, coupled with two previously unpublished analyses of Bendall (1994) and the existing data set of Mortimer (1984), prompted a re-evaluation of the status of whole rock Rb-Sr geochronology of the Tournefort Dykes.

Isochrons generated for each of the major geochemical groupings described above invariably returned a range of ages, some older than the Lincoln Batholith they were intruding (and obviously not of geological significance) and some of post-Kimban Orogeny age (table 4.2).

Geochemical Group	Number of samples	Age (2σ error)	MSWD	Initial Ratio
HMgT	3#	1796±28	135	0.70559
HBaT	2*	~1976	-	0.70362
FeRT	2*	~1809	-	0.70229
Dolerite Dykes	10	1646±33	58	0.70475
All Tournefort	17#	1817±43	38	0.70365

Table 4.2: Summary of whole rock isochron ages for geochemical groupings in the Tournefort Dykes. * = two point "errorchron", #= discarding metasomatised sample SEP-024 from regression.

The seventeen least deformed members of the dataset viewed as a whole, define an isochron of 1817±43 Ma (2σ) with a MSWD of 38 and initial ratio of 0.70365. Whilst the error is clearly large and covers a range of geologically feasible events, including Lincoln Batholith emplacement and initiation of the Kimban, the low initial ratio and large spatial diversity of samples used in construction of the

isochron suggests cogenesis. Significantly, the isochron age is within error of the 1812±5 Ma age determined by Pb-Pb zircon evaporation for Tournefort Dyke emplacement. While taken in isolation, little emphasis would be placed on the Rb-Sr whole rock isochron, however coupled with the Pb-Pb data, it would appear to corroborate the emplacement age of the Tournefort Dykes.

4.5.3 Sm-Nd whole rock geochronology

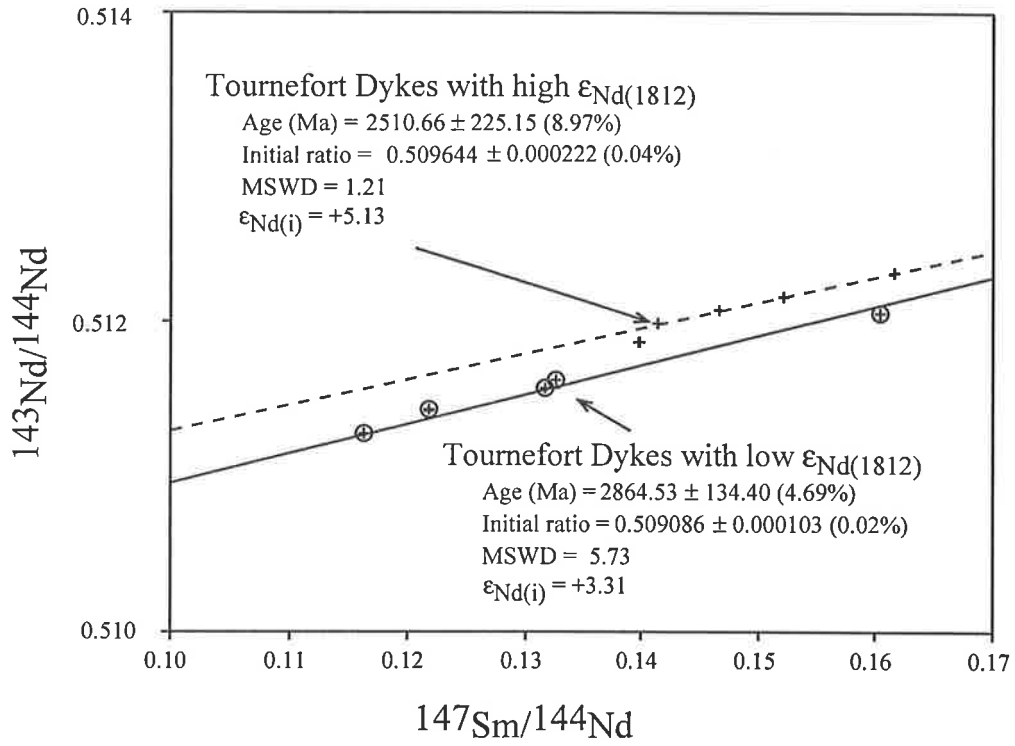

Figure 4.5: Isochrons generated for the two Nd isotopic groups of the Tournefort Dykes.

The Tournefort Dykes form two groups of distinct isotopic signature. One group contains dykes with higher $\varepsilon_{Nd(1812)}$ values (~-2 to +1), with the other group containing $\varepsilon_{Nd(1812)}$ values in the range ~-3 to -6. These two groupings are also reflected in the depleted mantle model ages of the dykes, with the higher $\varepsilon_{Nd(1812)}$ group containing T_{DM} values of ~2.1-2.4 Ga, and the remainder containing older T_{DM}'s at ~2.6-2.7 Ga. While the absolute values of T_{DM} "ages" are strictly model dependent, and may have little strict geological relevance, they do place broad constraints on the crustal prehistory for a set of magmatic rocks. It must be stressed that in the case of the Tournefort Dykes, the two Nd isotopic groupings observed are independent of any of the previously discussed geochemical or orientation groupings, suggesting calculated model ages are artefacts of processes involved in both source and dyke generation.

Using the isotopic subdivision described above, two isochrons are generated from the available dataset. Those dykes with higher $\varepsilon_{Nd(1812)}$ values

produce an array with an age of 2510±225 Ma (1σ), and comprise samples with a generally lower radiogenic component (figure 4.5), whereas the more evolved dykes define an older array (2864±134 Ma (1σ)) with lower $^{143}Nd/^{144}Nd$ components (figure 4.5).

While both ages are clearly too old to reflect emplacement ages, they are broadly equivalent to model ages within the more evolved portions of the Tournefort Dykes. Such features have been observed previously (eg, Zhao and McCulloch, 1993a), potentially offering insights into the petrogenesis of the Tournefort Dykes, and will be discussed in this context below.

4.5.4 Tournefort Dyke geochronology summary

Pb-Pb zircon evaporation data from a felsic segregation interpreted to be comagmatic with Tournefort Dyke emplacement impose a minimum age of 1798±8 Ma and a likely emplacement age of 1812±5 Ma. Whole rock Rb-Sr data on the least deformed and metamorphosed samples of the suite as a whole define an isochron at 1817±43 Ma, of the same order as the Pb-Pb data. While the Pb-Pb age is likely to record crystallisation of a single dyke, the Rb-Sr data suggests this age is applicable to dykes within the larger Tournefort system. The coincidence of ages by independent isotopic systems on different rock samples suggests 1812±5 Ma is a best emplacement age estimate for the Tournefort Dykes, with a minimum age of 1798±8 Ma defined by a younger zircon population.

Sm-Nd whole rock data record no information of Tournefort emplacement. However, "isochrons" defined by the two isotopic groupings observed within the dykes may reflect a long lived enriched mantle source for the Tournefort Dykes.

4.6 Petrogenesis

The Tournefort Dykes show trace element patterns similar to that of the continental crust. They are LILE and LREE enriched, and distinctive by virtue of negative Nb and Sr anomalies, and also have depleted Ti and Y values (figure 4.3). One subdivision on the basis of isotopes preserves crustal signatures in the form of unusually negative initial ε_{Nd} with correspondingly higher $^{87}Sr/^{86}Sr_{(i)}$ values for mafic dykes. At the time of emplacement, ε_{Nd} values of such Tournefort Dykes are more negative than the host gneisses of the Lincoln Batholith they intrude, and only slightly more evolved than the Sleaford Complex regional basement (figure 4.6), effectively ruling out emplacement level contamination. Therefore, elevated $^{87}Sr/^{86}Sr_{(i)}$ ratios coupled with evolved Nd isotopic signatures requires magma production from an environment that has an extended history of enrichment in incompatible elements, which is not preserved at the current erosion level.

With these constraints in mind, there is in essence two options for the generation of basaltic magmas with crust-like signatures; 1) mantle derived magmas contaminated during ascent through (and/or ponding in) the lower crust to a degree that essentially swamps source trace element characteristics; or 2) derivation from a portion of the mantle that has essentially crust-like isotopic and LILE signatures. The further option of emplacement level contamination seems limited in effect due to the extreme isotopic signatures, as noted above.

4.5.1 Constraints on crustal contamination

Samples most likely to have suffered crustal contamination are clearly those with strongly negative $\varepsilon_{Nd(i)}$ values. Samples from the HMgT, HBaT and Dolerite dykes are in this group, with FeRT restricted to more primitive $\varepsilon_{Nd(i)}$ values. In order to evaluate the amount of crustal interaction, the following discussion will centre on those dykes most likely to exhibit contamination, ie, those with more evolved Nd isotopic signatures (see table 4.1).

The absolute Nd concentrations in the least siliceous non cumulate members of the Dolerites and HMgT tend to low values (<19ppm, HMgT = 6-10 ppm). Typical oceanic and continental tholeiites contain ~7-10 ppm, compared to values typically >30 ppm in southern Gawler Craton crust. Therefore, in order to maintain low Nd concentrations in the melt, any potential crustal contaminant would need to be LREE depleted (ie, contain low Nd concentrations), or be mixed in small enough quantities to prevent significant perturbation of the Nd concentration. Since both the Sleaford Complex and Lincoln Batholith are comparatively Nd enriched (Nd ~30-70 ppm for large volume lithologies), the former seems untenable. Dykes containing evolved Nd signatures are distributed widely within the Lincoln Batholith, and comprise approximately half of the total dykes analysed for Nd isotopes. Such widespread and large scale variations in signature coupled with close proximity of dykes with more primitive Nd signatures at localities such as West Point argue against small volume mixing.

The Tournefort Dykes also maintain linear arrays on $\varepsilon_{Nd(1812)}$ vs Sm/Nd, 1/Nd and La/Sm plots (not shown). Such correlations are indicative of simple two component mixing. Situations involving more than two components, or more complex mixing processes (such as AFC) are likely to result in non-linear relationships (Zhao and McCulloch, 1993a). Furthermore, if simple two component mixing did take place, the linearity requires mixing with a crustal contaminant of unique composition. However, the most likely contaminant (the Sleaford Complex) displays a very heterogeneous nature, in both isotopic and trace element geochemical terms. Therefore, such trends would require contamination to have taken place within a specific (homogeneous) portion of the Sleaford Complex

(figure 4.6), which seems unlikely given the spatial distribution of dykes defining the trends.

Contamination by silicic crust also fails to account for the low SiO_2 and high *mg#* of non-cumulate dykes in both the HMgT and Unassigned Tholeiite groups. So too, low $\varepsilon_{Nd(i)}$, HMgT samples display primitive mantle normalised patterns with values similar to or less than N-MORB sources for elements more compatible than Sr. This makes generating the required compositions by bulk mixing of crust with tholeiitic magmas difficult, particularly when trying to maintain a balance with incompatible elements, which are strongly depleted in N-MORB. Additionally, a number of key trace element ratios lie outside of N-MORB-crust mixing trends; eg Ti/V and Zr/Y for example are too low, and Sc/Y too high, to be a result of simple mixing. Therefore, while only comparatively small amounts of contamination are necessary for the LILE and some LREE, compatible elements such as Sm, Ti and Y require large proportions of contaminant to produce signatures observed in the HMgT.

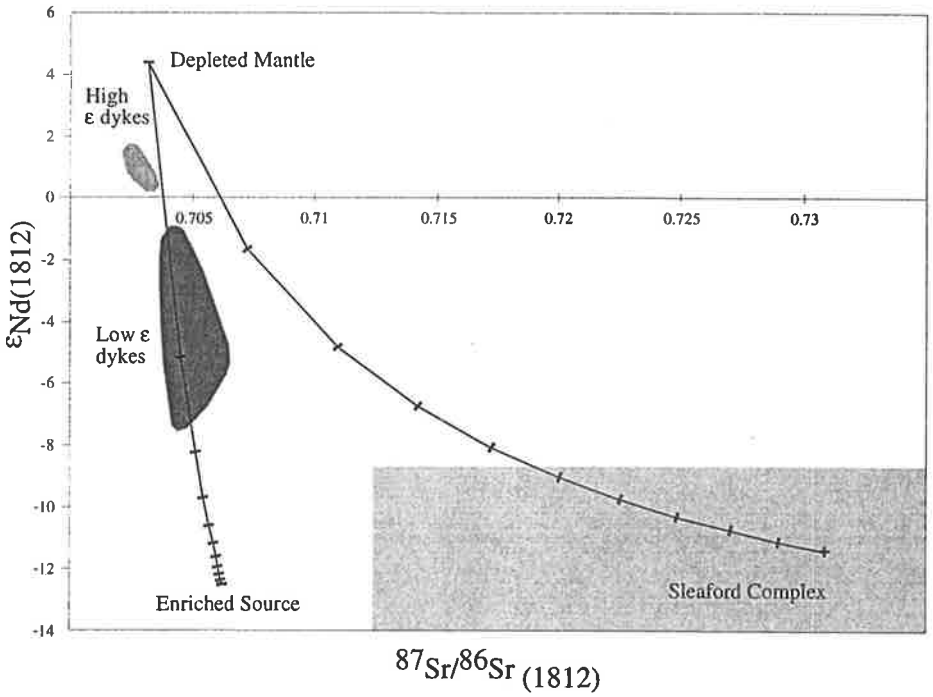

Figure 4.6: Nd-Sr isotope mixing curves between the depleted mantle, contemporary crust (ie, Sleaford Complex) and an enriched mantle source at the time of Tournefort emplacement. Mantle values from Sun and McDonough (1989), enriched (kimberlitic) source from Wedepohl and Muramatsu (1979). Tick marks at 10% intervals.

This effectively leaves two possibilities; 1) the Tournefort Dykes have been contaminated by crust of a very specific composition, which is not exposed on the southern Gawler Craton or 2) the trace element and isotopic signatures reflect mantle source processes and have seen negligible crustal contamination. Regarding

former, given that the top of the Lincoln Batholith was at ~15 km during emplacement, and the structural level of the batholith exposed in the Kalinjala Shear zone is a minimum of several kilobars deeper (Oussa, 1993; Bendall, 1994; Hand et al., 1995; Hand et al., in prep), the Lincoln Batholith occupies a portion of the middle to lower crust with exposed vertical relief of some 5-6 kilometres. With extension taking place during Lincoln Batholith emplacement, and again during Tournefort emplacement, only a comparatively thin and attenuated section of lower crust would have been available to act as a contaminant to the Tournefort Dykes. The composition of such lower crust is inaccessible by direct means, as the only enclaves observed within the Tournefort Dykes are locally derived Lincoln Batholith felsic gneisses. However Nd isotopes suggest that the only crustal contaminant available to the Lincoln Batholith was the Sleaford Complex (see chapter 3). Hence, the only observable crustal contaminant available to the Tournefort Dykes either directly or indirectly (via a two stage process involving the Lincoln Batholith) was the Sleaford Complex. Since neither of the isotopic groupings within the Tournefort Dykes define mixing arrays with Sleafordian crust (figure 4.6), another source for this signature is required. Such a conclusion is consistent with the geochemical constraints discussed above.

Therefore, it would seem the apparent crustal signature of the Tournefort Dykes is a reflection of mantle source characteristics. The presence of enriched lithospheric mantle reservoirs beneath continental crust has been documented in many parts of the world, (eg, Menzies et al., 1987; O'Reilly and Griffin, 1988; Griffin et al., 1988 and references therein), and have been appealed to as sources for mafic magmatic events which preserve similar trace element and isotopic characteristics to the Tournefort Dykes (eg. Hergt et al., 1989; Zhao and McCulloch, 1993a). Enriched lithospheric mantle beneath the Gawler Craton is an appropriate chemical reservoir for the derivation of the Tournefort Dykes, as it is likely to be relatively enriched in incompatible elements, yet still relatively depleted in compatible elements. Isotopically however, samples of the subcontinental lithosphere from beneath the Gawler Craton in the form of xenoliths from kimberlites (Song, 1994), are not evolved enough to produce the signatures observed in the Tournefort Dykes. Instead, while the primitive Tournefort Dykes define mixing trends between the depleted mantle and lithospheric mantle (figure 4.7), the low $\varepsilon_{Nd(i)}$ dykes trend towards an isotopically enriched source, such as that observed in the EM 1 ocean island basalts (OIB's). EM-1 is associated with plume magmatism at the Pitcairn and Tristan hotspots on the modern Earth (Hofmann, 1997), suggesting a role for plume related magmatism in Tournefort Dyke genesis.

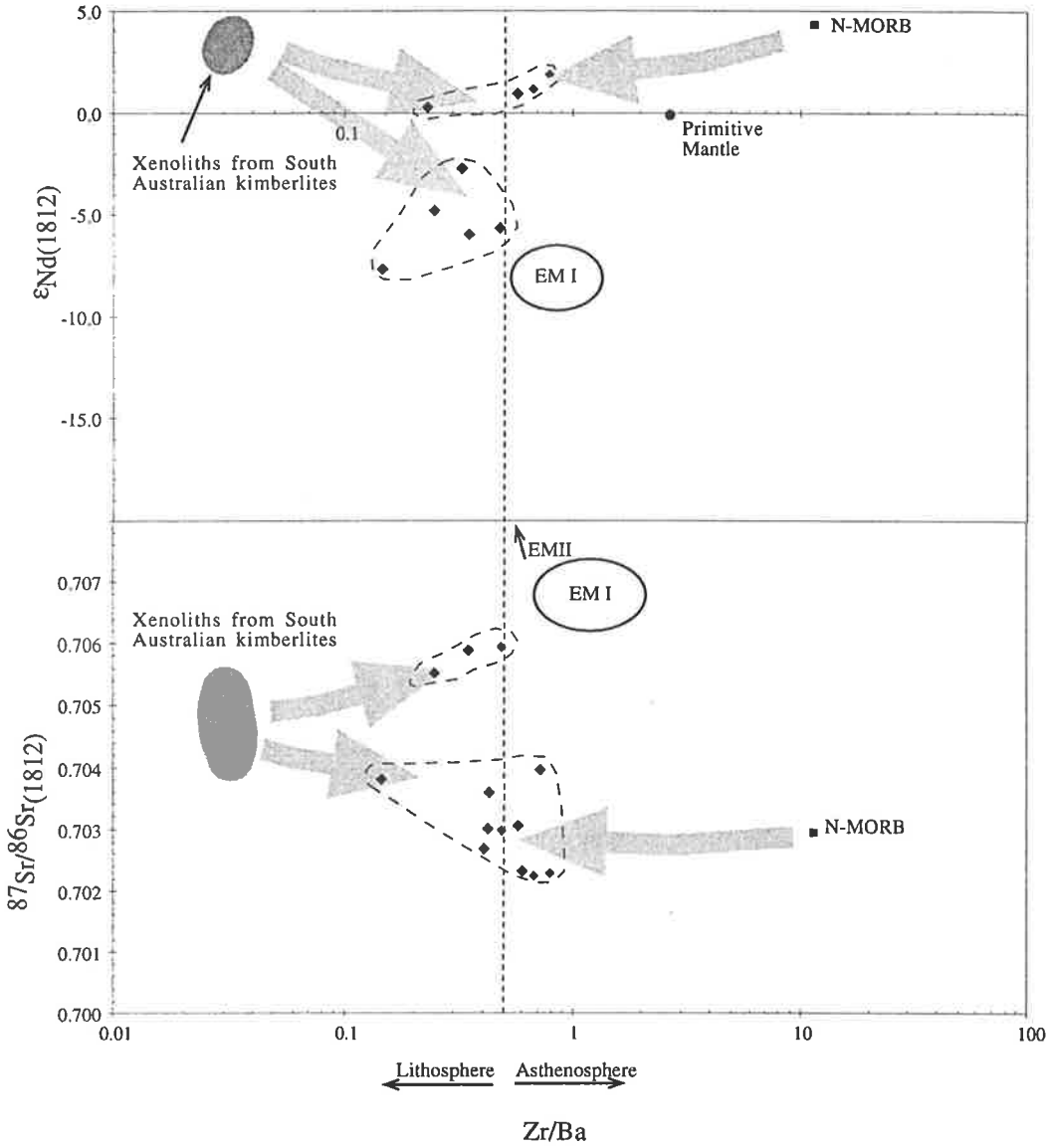

Figure 4.7: Isotopic variations with HFS/LILE ratio (Zr/Ba) with potential mantle reservoirs highlighted for the Tournefort Dykes. Note the tendency to scatter between an asthenospheric and subcontinental lithospheric source. Note also a trend for a subset of the Tournefort Dykes towards an OIB or plume related source. Cutoff Zr/Ba ratio = 0.5 arbitrarily derived from Hawkesworth and Gallagher (1993); Xenolith data from Song (1994). EM I = Enriched Mantle reservoir I, EM II = Enriched Mantle reservoir II, both subsets of OIB's (Ocean Island Basalts). N-MORB = "Normal" Mid Ocean Ridge Basalt.

4.7 Discussion

The origin of enriched mantle remains equivocal. However, only a comparatively small number of mechanisms may be envisaged which result in the formation and continued isolation of such reservoirs. There are essentially three general groups, viz:

1) subduction of continental crust into the upper mantle resulting in enriched lithospheric mantle (Hergt et al., 1989; Zhao and McCulloch, 1993a)
2) Plume driven, OIB type sources; some of which (eg HIMU) are not observed in mafic dyke swarms until the Neoproterozoic (Condie, 1997),
and 3) progressive enrichment of previously depleted subcontinental lithospheric mantle, either by continuous melt percolation from the asthenosphere (Erlank et al., 1987; McKenzie, 1989; Turner and Hawkesworth, 1995) or specific enrichment events.

The features outlined in the preceding section suggest that the Tournefort Dykes reflect the interplay between potentially three mantle sources; that of depleted mantle characteristics, one with a plume derived component and an enriched subcontinental lithospheric mantle.

A mechanism for generation of new continental lithosphere exists on southern Eyre Peninsula. Freezing of asthenosphere to the base of the lithosphere during sedimentation would allow the generation of a relatively primitive reservoir with MORB-like characteristics. However, the shallow nature of the Hutchison Basin (~3.5 km, N. Lemon, pers comm.), requires that the total volumes involved be relatively small, suggesting derivation of primitive Tournefort Dykes wholly from such a source is unlikely. The mixing arrays of the primitive dykes could therefore reflect interaction between relatively juvenile lithosphere with depleted mantle signatures, and the enriched subcontinental lithospheric mantle.

Additionally, the source of both heat and material for Tournefort magmatism may be derived independently of the local geology. Enriched asthenospheric sources for plume related magmatism may offer an alternative origin, (figure 4.7) however this merely moves the initial source of the enrichment one step further back, implying an effective mechanism existed for enriching, and more importantly, preserving chemical heterogeneities in the convective asthenosphere. Sun et al. (1989) note problems with returning (subducting) sufficient volumes of Archaean crustal material to establish large reservoirs early enough in the history of the Earth to source such magmatism. Despite this, portions of the Tournefort Dykes display trace element characteristics, such as flat compatible trace element patterns and arrays trending towards OIB (Ocean Island Basalt) sources (figure 4.7), consistent with derivation, at least in part, from a plume related source.

The origin and nature of a subcontinental lithospheric mantle reservoir remains equivocal. The Tournefort Dykes preserve a long history of enrichment prior to emplacement (~0.4 Ga); with the most evolved portions containing T_{DM} ages older than the those in the Lincoln Batholith they intrude (figure 4.8). As Zhao and McCulloch (1993a) note, subduction modified continental lithospheric mantle

is likely to be readily extracted, particularly in regimes undergoing active extension and/or anomalous thermal activity. On southern Eyre Peninsula, the 150 million years prior to Tournefort emplacement was characterised by extension to allow deposition of the Hutchison Group from ~2000 Ma, and emplacement of the Lincoln Batholith, again probably in an extensional environment at ~1850 Ma. It is only ~20-30 Ma *after* these protracted extensional and magmatic events that Tournefort Dyke magmatism from an enriched source took place. Therefore, the preservation of an ancient subduction modified enriched continental lithosphere for the duration of this tectonic activity seems unlikely.

Another view is that of enrichment of previously depleted peridotite beneath areas of stable continental crust. Turner and Hawkesworth (1995) argue for the establishment of large depleted reservoirs by crustal formation events, which are subsequently hydrated and enriched in incompatible elements. The ultimate source of incompatible elements and hydrous fluids has been suggested to be either the deep mantle (Erlank et al., 1992), or underplated oceanic crust (Tarney, 1992). In either case, lithospheric mantle thus developed is likely to remain isolated from the convecting mantle in the steady state due to its strength and buoyancy, features of its depleted nature.

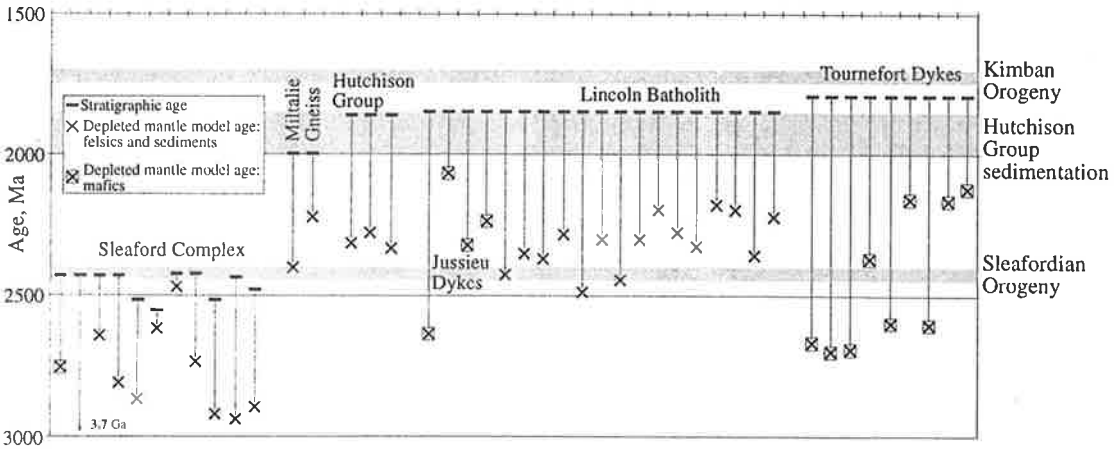

Figure 4.8: Summary of depleted mantle model ages as a function of stratigraphic age and lithotype for the southern Eyre Peninsula. Major geological events are shaded.

O'Reilly and Griffin (1988) point out that once such a chemical reservoir is established, essentially primitive melts generated at depth beneath it are able to take on characteristics of the lithosphere it passes through. This "wall rock reaction" process may be analogous to crustal contamination processes, however the chemical signature is likely to be indistinguishable from the lithospheric mantle the melt transits. This scenario may work well if the initial melt is particularly depleted in incompatible elements, but will retain its initial compatible element distribution. The resulting isotopic signature however, is likely to reflect that of its primary primitive or depleted mantle source.

In the case of the Tournefort Dykes, the active regional prehistory of the terrain argues against the long term evolution of a single stage enriched mantle. T_{DM} values of the Tournefort Dykes fall neatly into two groups (eg, figures 4.6, 4.8, table 4.1), an older group, which is indistinguishable from T_{DM} values of the Sleaford Complex (figure 4.8), and those younger at 2.1 to 2.2 Ga. This suggests the presence and persistence of an old lithospheric component, either formed or completely reset during the Sleafordian Orogeny (2.6-2.7 Ga), which sourced the HMgT, HBaT and parts of the Dolerite Dykes. The younger, more primitive lithospheric source is observed in the FeRT and remaining Dolerite Dykes (table 4.1, figure 4.7). Such a source is likely to be a relatively juvenile asthenospheric underplate formed during extension associated with Hutchison Group sedimentation. Additionally, trends suggesting interaction between enriched subcontinental lithospheric mantle and plume-type sources are observed on isotope vs HFS/LIL element plots such as figure 4.7. Hence, the older, more evolved (low ε_{Nd} dykes) source is partially attributed to a plume component, which also provided the necessary thermal input to drive remelting of the older lithospheric keel. Such a melting mechanism is necessary as decompression melting during continued extension is considered unlikely after removal of hydrous phases and volatiles from the lithospheric mantle during Lincoln Batholith generation. Since only ~20-30 Ma elapsed after Lincoln Batholith magmatism prior to Tournefort Dyke emplacement, it appears unlikely that the lithospheric mantle could become sufficiently enriched in hydrous phases and incompatible elements to generate the Tournefort Dykes in this time.

Therefore, the diversity of chemistry within the Tournefort Dykes can be attributed to entrainment of both ancient and juvenile lithospheric mantle in an ascending plume, emplaced at ~1815 Ma.

In conclusion, the Tournefort Dykes place some constraints on the nature of the continental lithospheric mantle. They argue for the development and persistence of large volumes of ancient lithospheric mantle beneath stable cratonic regions, able to be sampled repeatedly during crustal evolution (eg, Miltalie Gneiss and Lincoln Batholith magmatism prior to Tournefort Dyke extraction). Their longevity also implies the existence of a mechanism capable of replenishing volatiles and incompatible elements in the lithospheric mantle. Mechanisms involving percolation of fluids from the lower mantle such as those invoked by Erlank et al., (1987); McKenzie (1989) and Hawkesworth and Turner (1995) are likely to be appropriate. Since the Tournefort Dykes were emplaced *after* protracted extension and thermal perturbations associated with Lincoln Batholith magmatism, a mechanism other than continued extensional melting is required. A mantle plume able to interact with the subcontinental lithospheric mantle provides the necessary of thermal energy to the lithospheric mantle and continental crust.

CHAPTER FIVE

Basement and syn-orogenic Palaeoproterozoic lithologies

5.1 Introduction

In order to gain an appreciation for the evolution of the crust on southern Eyre Peninsula, regional scale geochemical and isotopic sampling of lithologies which are basement to, and subsequently developed upon, the Lincoln Batholith/Tournefort Dyke association was conducted. It was anticipated that an isotopic study would provide constraints on the nature and composition of the contemporary continental crust during Lincoln Batholith emplacement, as well as provide insights into secular evolution of supracrustal sequences. Additionally, the temporal evolution of syn-Kimban orogenic granitoids (the Moody Suite) is evaluated in the context of the evolving Kimban Orogeny, placing constraints on the thermal nature of the orogen.

Such information, coupled with regional scale structural and metamorphic information outlined in Chapter 6, provides a basis from which to reconstruct the complete tectonic evolution of the Lincoln Batholith, from its genesis, through emplacement and subsequent deformation, effectively establishing comprehensive comparative criteria for contemporaneous magmatic belts.

5.2 Basement lithologies

Samples were collected from the Archaean Sleaford Complex, the most likely candidate for contemporary continental crust. Due to the heterogeneous nature of the Sleaford Complex, samples were collected from a range of localities, and included the full range of lithologies readily accessible. These included high grade para- and orthogneisses of the Carnot Gneisses at Cape Carnot, relatively undeformed Dutton Suite intrusives (the Coulta Granodiorite and Kiana Granite) from Cape Drummond and the amphibolite grade Wangary Gneiss, a low grade metasedimentary equivalent of the Carnot paragneisses (see figure 3.1 for localities). Other lithologies that

effectively acted as basement to the Lincoln Batholith are represented by those enclaves preserved within it. Metasedimentary enclaves from Trinity Haven were sampled, along with orthogneissic basement rafts from West Point.

The database thus generated was combined with other Sm-Nd isotopic data publicly available. A dataset within Turner et al. (1993) contains analyses from southern Eyre Peninsula, and additional data for the Hutchison Group may be found in Simpson (1994). Table 5.1 summarises data generated from this study, however further discussion and plots will involve data from all publicly available sources.

The Sleaford Complex contains a wide range of lithologies, which is reflected in the chemistry and isotopic signatures observed. Mafic granulites from within the Sleaford Complex contain $\varepsilon_{(Nd(i)}$ values of-0.5 and -7.1, however one of these (sample 446/F30) is chemically and isotopically indistinguishable from the Tournefort Dykes, providing evidence for correlation across the Kalinjala Shear Zone. Therefore, the only truly Sleafordian mafic granulite with isotopic data available has an $\varepsilon_{Nd(t)}$ value of -7.1 at 2430 Ma. Orthogneisses at Cape Carnot have $\varepsilon_{Nd(2430)}$ values of -1.3 to -3.7, which are slightly lower than less deformed, higher crustal level members of the Dutton Suite (+0.9 to -2.3 at emplacement age appropriate for each sample). The paragneissic Carnot Gneisses comprise samples from central and northern Eyre Peninsula as well as Cape Carnot, and range in $\varepsilon_{Nd(i)}$ from +2.7 to -4.3. The Cape Carnot value of -4.2 is comparable to -3.9 for their lower grade equivalent, the Wangary Gneiss.

Orthogneissic enclaves within the Lincoln Batholith were also analysed in an attempt to establish a genetic link with the Sleaford Complex. Significantly, the orthogneisses returned $\varepsilon_{Nd(2430)}$ values substantially higher (+2.7 and +5.9) than orthogneisses within the Sleaford Complex, suggesting they represent either a previously unsampled (primitive) portion of the Sleaford Complex or constitute part of a rock sequence previously unidentified east of the Kalinjala Shear Zone. They are unlikely to be part of the Lincoln Batholith itself, as their ε_{Nd} values at Lincoln Batholith emplacement are more negative, and they tend to be slightly more LREE enriched than comparable lithologies in the Donington Suite.

Correlation of the orthogneissic enclaves with the Miltalie Gneiss is suggested on the basis of temporal constraints, lithological similarity and predicted Nd isotopic signatures. In this scenario, $\varepsilon_{Nd(1999)}$ values for the orthogneisses range from -0.18 to -3.6 (table 5.1).

Lithology	Coulta Granod.	Kiana Granite	Metapelite	Wangary Gneiss	Felsic Gneiss	Felsic Gneiss	Metapelite
Sample #	SEP-184	SEP-179	SEP-188	SEP-181	SEP-160	SEP-263	SEP-117
Locality	Pt Drummond	Pt Drummond	C Carnot	L Hamilton	West Pt	Williams Is	Trinity Haven
Est Age (Ma)	*2517*	*2557*	*2440*	*2479*	*1999*	*1999*	*1865*
SiO_2%	67.89	71.10	61.15	70.94	68.09	70.97	53.46
Al_2O_3%	14.21	14.24	16.35	14.99	15.08	14.53	20.81
Fe_2O_3%	5.11	2.95	11.57	2.40	3.10	2.35	10.30
MnO%	0.07	0.03	0.13	0.03	0.05	0.02	0.10
MgO%	1.38	1.01	4.69	2.59	0.98	0.29	4.18
CaO%	3.43	1.50	0.93	0.44	2.27	1.52	3.03
Na_2O%	3.88	3.55	1.14	2.39	2.69	2.66	2.98
K_2O%	2.60	4.11	2.31	3.99	5.94	6.51	3.03
TiO_2%	0.57	0.42	1.03	0.41	0.67	0.21	1.05
P_2O_5%	0.13	0.17	0.03	0.05	0.18	0.03	0.10
SO_3%	0.00	0.00	0.02	0.00	0.01	0.00	0.01
LOI%	0.71	0.55	0.61	1.37	0.34	0.23	0.78
Total	99.98	99.63	99.96	99.60	99.40	99.32	99.83
Rb	86.915	230.162	117.728	164.062	244.958	196.689	173.443
Ba	462	576	391	565	1161	1586	861
Th	13.9	36.5	13.6	36.2	34.1	13.4	39.6
U	4.2	4.2	0.8	5.9	1.3	1.3	8.1
Nb	9.4	13.3	8.3	13.7	20	1.7	19.9
La	37	57	22	46	165	60	85
Ce	79	122	42	105	300	111	168
Pb	14.4	29.8	15.7	14.3	30.3	31.4	22.4
Sr	143.287	114.425	55.774	138.662	199.428	201.019	259.945
Nd	31.052	49.400	29.338	53.157	96.579	37.170	92.960
Zr	222.1	193.6	166.5	212.5	382.6	254.9	326.1
Sm	6.503	8.553	5.940	9.867	13.313	5.393	15.481
Y	41.5	15.6	35.8	22.3	28.7	9.0	40.2
V	54	42	201	38	24	6	188
Sc	12.5	5.7	14.7	9.5	8.8	4.7	22.1
Cr	17	21	265	26	5	*	174
Ga	18	21.5	26.9	19.7	16.3	16.1	30.8
$^{143}Nd/^{144}Nd$	0.511356	0.511134	0.511229	0.511062	0.510964	0.511196	0.511312
2σ	0.000026	0.000040	0.00005	0.000086	0.000074	0.000082	0.000028
$^{147}Sm/^{144}Nd$	0.1267	0.1047	0.1225	0.1123	0.0834	0.0878	0.1007
$T_{(DM)}$	**3.14**	**2.82**	**3.20**	**3.13**	**2.56**	**2.37**	**2.48**
$\varepsilon_{Nd(t)}$	-2.39	0.89	-4.25	-3.88	-3.61	-0.19	-2.93
$^{87}Sr/^{86}Sr$	0.762447	0.911695	0.887256	0.813547	0.798519	0.778371	0.760362
2σ	0.000018	0.000028	0.000048	0.000038	0.000044	0.000030	0.000052
$^{87}Rb/^{86}Sr$	1.7644	5.9358	6.2143	3.4587	3.5854	2.8505	1.9404
$^{87}Sr/^{86}Sr_{(t)}$	0.69824	0.69221	0.66817	0.68963	0.69529	0.69630	0.70829

Table 5.1 Summary of basement isotopic and chemical data generated in the course of this study. Model parameters as for table 3.2. * = below detection. Localities on figure 3.1. Further regional isotopic data can be found in appendix 3.

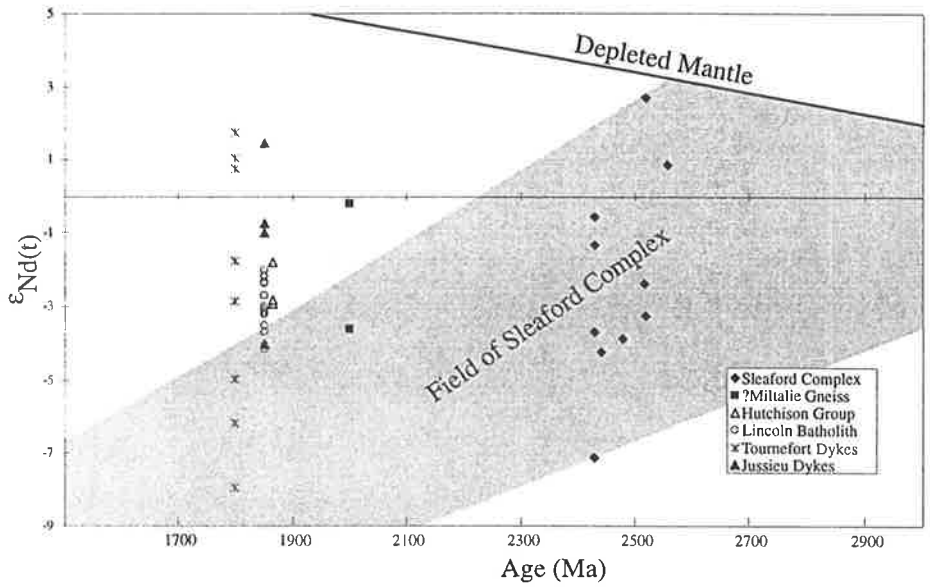

Figure 5.1: Palaeoproterozoic Nd isotopic evolution of southern Eyre Peninsula. Samples for Miltalie Gneiss are enclaves from within the Lincoln Batholith, one of the Hutchison Group samples is a metapelite enclave from within the Lincoln Batholith.

The Hutchison Group constitutes a major portion of the upper crust on southern Eyre Peninsula. The Yadnarie and Cook Gap Schists, both deep water pelites from near the top of the sequence, contain comparable $\varepsilon_{Nd(i)}$ values of -1.9 and -2.8 respectively. The metapelitic enclave within the Lincoln Batholith (sample SEP-117) has an indistinguishable $\varepsilon_{Nd(t)}$ value of -2.9, forming a basis for correlation between the Massena Bay Gneisses and the Hutchison Group. The presence of metasedimentary enclaves also acts as a minimum emplacement depth constraint on the Lincoln Batholith.

Therefore, the Nd isotopic nature of basement lithologies to the Lincoln Batholith is both distinctive and well defined. Despite heterogeneities within the Sleaford Complex, the volumetrically dominant lithologies cluster in the range of ε_{Nd} from -7.6 to -10.8 at 1850 Ma, this range including the majority of paragneissic lithologies, as well as all orthogneissic and felsic intrusive units. By contrast, those units actually observed as enclaves within the Lincoln Batholith have higher ε values at the time of Lincoln Batholith emplacement; ie, ~-5.8 to -2.5 for the interpreted Miltalie Gneiss equivalents, and ~-2 to -3 for the Hutchison Group Metasediments and Massena Bay Gneisses. Finally, the Nd isotopic data generated in this study provides the first direct evidence for across Kalinjala correlation of lithologies, suggesting the two terrains were adjacent at least as early as Hutchison Group sedimentation. This is provided in the form of a mafic granulite from Fishery Bay (446/F30 of Turner et al., (1993)) containing features indistinguishable from the Tournefort Dykes to the east, and a metapelitic enclave in the Lincoln Batholith at

Trinity Haven preserving isotopic characteristics indistinguishable from the Cook Gap Schist to the west.

5.3 The Moody Suite

There are no published Nd isotopic data for the Moody Suite, however, several broad scale features relevant to the evolution of the Kimban Orogeny are worthy of note.

The Moody Suite consists of syn-Kimban intrusives, emplaced dominantly between ~1750-1700 Ma, although some younger granitoids, such as the Carappee Granite have been associated with this suite. For the purposes of this discussion however, the Moody Suite is confined to those intrusives within the Hutchison Group in the Tumby (see figure 3.1 for localities) and Cleve Hills.

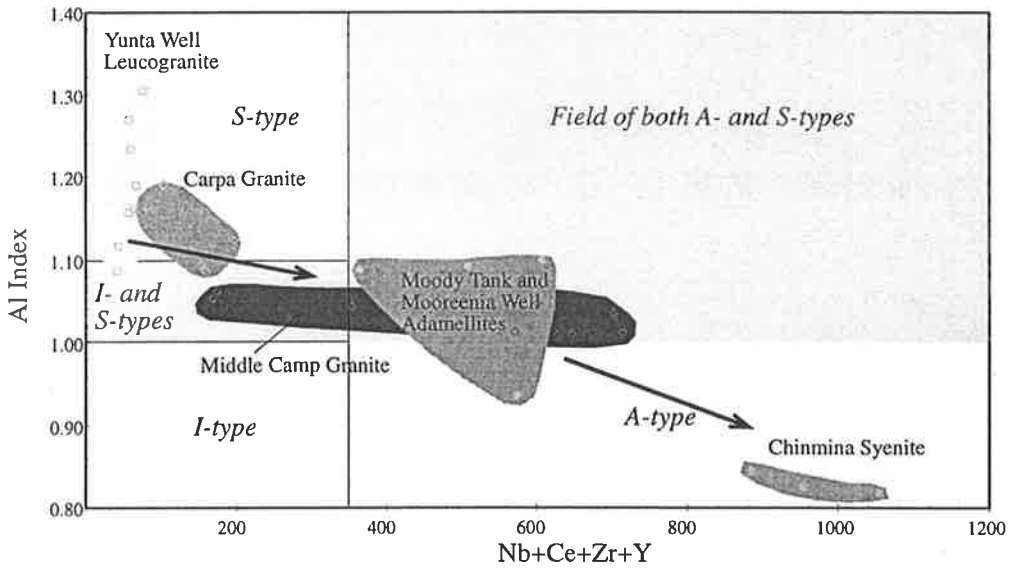

Figure 5.2: Broad scale variations in chemistry of the Moody Suite. Data from Coin (1976), Mortimer (1984), N. Neumann (unpublished data) and this study. Diagram is constructed on the basis of I- S- type classification after Chappell and White (1992) and A-type classification of Whalen et al., (1987). Arrows indicate general age progression in Moody Suite magmatism.

Coin (1976) and Mortimer (1984) subdivided the Moody Suite into a number of lithologies, the key elements of which are outlined in Chapter 2. One of the most interesting features of the Moody Suite is the apparent trend from early, voluminous, dominantly S-type magmatism (eg, Yunta Well Leucogranite in the Tumby Hills (Mortimer, 1984)), through increasingly I-type (Middle Camp Granite in the Cleve Hills, 1731±7 Ma (Parker, 1978; Fanning, 1997)) and intermediate (Chinmina Syenite, 1702±10 Ma (Fanning, 1997)) to mafic and ultramafic (Coonta Gabbro of Schwarz, 1998) compositions.

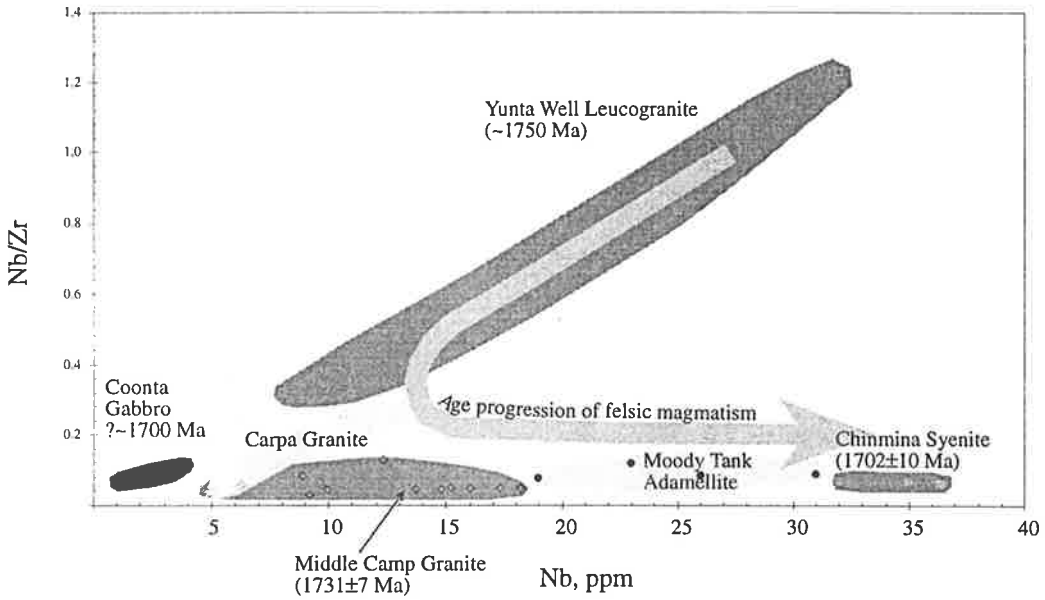

Figure 5.3: Temporal evolution of Nb and Zr within the Moody Suite. Early, S-type magmas such as the Yunta Well Leucogranite and Carpa Granite show constant Zr levels with changing Nb, whereas later intrusives display covarying Nb and Zr levels, resulting in a constant Nb/Zr ratio. Data sources as for figure 5.2 with unpublished Coonta Gabbro data supplied by PIRSA.

An independent chemical observation consistent with the notion of Moody Suite magmatism evolving from comparatively low temperature anatexis of supracrustal sequences through progressively higher temperature melts is suggested by figure 5.3. Early S-type melts appear to have Zr levels held constant during melt generation, indicating retention of Zr in an accessory phase such as zircon. Only later in the magmatic evolution of the orogen do ambient temperatures become great enough to cause zircon breakdown and covarying Nb and Zr behaviour. Such observations are collaborated by the large population of inherited zircons in the Carpa Granite (Fanning, 1997). Inherited zircons appear less frequently in the Middle Camp Granite (Fanning, 1997) and are virtually non-existent in the Chinmina Syenite. Such observations are consistent with the whole rock chemistry of the intrusives involved and indicate changes in magma chemistry over time that may be a function of both magma temperature and degree of interaction with emplacement level crust.

Slightly younger granitoids on central Eyre Peninsula, such as the Carappee Granite (1689±59 Ma, Flint et al. (1988)) have A-type affinities, suggesting a broad temporal trend culminating in syn-post orogenic I- and A-type magmatism. Clearly, further geochronological data is required to constrain this trend, however, the presence of (small volume) late orogenic mafic to ultramafic magmatism suggests an increasing mantle chemical (and by inference, thermal) input during orogenesis. An alternative hypothesis that the Coonta Gabbro is actually a pre-Kimban equivalent of

the Tournefort Dykes is considered unlikely due to its outcrop relationships with the Kalinjala Shear Zone (Schwarz, 1998).

Hence, on the basis of broad geochemical and geochronological criteria, the Moody Suite appear to reflect a temporal change from crustal to increasingly (but not exclusively) mantle derived magmatism during and immediately after the Kimban Orogeny.

5.4 Conclusions

Although not the primary focus of this study, other Palaeoproterozoic lithologies of the southern and central Eyre Peninsula contain important information on the evolution of the crust prior to Lincoln Batholith magmatism and immediately after the Kimban Orogeny. Three basement crustal sequences have been recognised and characterised on the basis of isotopic and geochronological criteria.

The voluminous portions of the Sleaford Complex which are likely to have comprised a large amount of the contemporary crust into which the Lincoln Batholith was emplaced contain ε_{Nd} values in the range of -7.6 to -10.8 at 1850 Ma. Orthogneissic enclaves within the batholith however, have ε_{Nd} signatures significantly less evolved, in the range of -5.8 to -2.5 at 1850 Ma, and are tentatively correlated with the Miltalie Gneiss, outcrops of which occur in the Tumby Hills adjacent the Kalinjala Shear Zone. Metapelites of the Hutchison Group and Massena Bay Gneisses preserve $\varepsilon_{Nd(1850)}$ signatures that are virtually indistinguishable, and range from ~-2 to -3 during Lincoln Batholith emplacement.

Therefore, each source of potential crustal contamination in the Lincoln Batholith may be readily characterised on the basis of Nd isotopes.

The syn-Kimban Moody Suite granitoids reflect a temporal change in chemistry from S-type to I- and A-type during the evolution of the orogen. The presence of late stage intermediate and mafic to ultramafic units suggests an increasing proportion of potentially mantle derived magmatism during the Kimban. Such compositional evolution is consistent with changing thermal conditions within the orogen, the consequences of which are evaluated in chapters 7 and 8.

CHAPTER SIX

Palaeoproterozoic deformation and metamorphism on southern Eyre Peninsula

6.1 Introduction

The main thrust of this project has been to evaluate the magmatic evolution of the southern Eyre Peninsula from a geochemical and isotopic perspective. However the ongoing magmatic evolution must also be seen in light of the ongoing tectonic regime in which magma generation and emplacement took place. To this end, a summary of the current understanding of the timing, style and duration of deformation and metamorphism on southern Eyre Peninsula is presented. The focus is on the regional scale, with observations derived from both the literature and fieldwork conducted during this study.

This section will summarise deformation and metamorphism postdating the Sleafordian Orogeny, and so incorporates the Miltalie "event" of Fanning (1997) and the three phases of deformation ascribed to the Kimban Orogeny by Parker et al. (1988) and Parker (1993). Further discussion on the nature of deformation in the Kimban Orogeny in the Lincoln Batholith is summarised in section 2.2 and in Hoek and Schaefer (1998).

6.2 Pre- syn Lincoln Batholith deformation

As noted in chapter 3, and discussed further in chapter 5, enclaves of felsic basement material within the southern Lincoln Batholith contain Nd isotopic signatures attributable to Miltalie Gneiss sources. Such gneisses post-date the Sleaford Complex (and hence Sleafordian deformation). A hornblende-biotite tectonic foliation slightly discordant to, but not continuing into or crosscutting, units of the Lincoln

Batholith (Hoek and Schaefer, 1998) is observed in these enclaves. Enclaves at West Point also preserve apparent retrogression of the hornblende fabric to a biotite fabric, however the relative timing of such an event cannot be deduced. Thus the orthogneissic basement enclaves preserve a tectonic fabric that clearly predates the Lincoln Batholith, but is likely to postdate Sleafordian deformation. This is the only known example of pre-Donington deformation observed on the east side of the Kalinjala Shear Zone.

Syn-Donington Suite deformation is preserved only rarely in low (Kimban) strain zones. These include migmatitic shears, boudinage and (rare) local development of a hornblende+biotite foliation (Hoek and Schaefer, 1998). This fabric is equated with S1 of Parker and Lemon (1982); an originally flat lying, layer parallel fabric in the Hutchison Group, subsequently folded during D2. Indeed, the relative scarcity of a pervasive fabric associated with this event was considered by Hoek and Schaefer (1998) to reflect deformation in the presence of a partial melt fraction. No folds have been recognised with syn-Donington Suite deformation, which is here considered to be extensional in nature. This is due to its association with continued sedimentation in the Hutchison Group (in the form of the Yadnarie Schist and Bosanquet Formation), its subtle nature (ie, lack of pervasiveness and preserved only in or adjacent rigid country rocks) and the basic necessity of accommodating a large volume of felsic magma in the crust.

This deformation has previously been considered (Parker et al., 1988) to mark the onset of the Kimban Orogeny, however, as indicated in chapter 2 and discussed below, there is no clear genetic link between this phase of deformation and subsequent peak deformation and metamorphism between ~1750-1700 Ma.

6.3 Peak metamorphism and deformation: The Kimban Orogeny

Kimban deformation and metamorphism on the western side of the Kalinjala Shear Zone is well documented in the Hutchison Group (Parker and Lemon, 1982; Parker et al., 1988; Parker 1993 and references therein), allowing a concise picture to be built up on a number of scales. In the Lincoln Batholith, Kimban deformation is heterogeneous over a range of scales. Due to the variation in lithologies being deformed and the style of deformation preserved in each terrain, simple interpolation and correlation of structural styles between the two terrains is not straightforward.

High grade metamorphism and deformation to the west of the Kalinjala is succinctly described in Parker and Lemon (1982) and summarised in Drexel et al. (1993). In the interests of consistency, the structural terminology of Parker and Lemon (1982) is maintained, where D1 is the early phase of deformation associated with Donington Suite emplacement (see 6.2 above) and D2 and D3 are ascribed to high grade Kimban metamorphism between ~1750 and 1700 Ma (Hoek and Schaefer,

1998). D2 is characterised by tight to isoclinal folding with pervasive axial planar schistosities (S2). Upper amphibolite facies metamorphism prevailed throughout the Cleve and Tumby Hills during this time. F2 folds were originally shallowly inclined or recumbent and overturned to the west (Parker and Lemon, 1982; Parker in Drexel et al., 1993). Parker (in Drexel et al, 1993) attributes the formation of regional folds and major mylonitic shear zones to D3, a pervasive retrogressive event. F3 folds are typically open and upright in character. Parker and Lemon (1982) note a distinct decrease in strain associated with D3 structures away from the Kalinjala Shear Zone from east to west.

As previously noted, such a distinct subdivision of structural features is not readily observable in the Lincoln Batholith due to the heterogeneous distribution of strain. Much of the apparent complexity on the outcrop scale can be attributed to rheological contrasts between mafic dykes and felsics of the Donington Suite (eg, figure 4.2c). Moderate intensity strain localities such as Wanna produce complex deformation geometries due to strain partitioning and localisation (figure 4.2b; Bales, 1996) controlled by the high density of mafic dykes. Conversely, moderate to high strain zones with relatively few dykes, such as Cape Catastrophe, preserve more homogeneous deformation patterns on the hundred-metre scale. In areas of low overall strain, regardless of the presence of dykes (eg, Memory Cove, Williams Island), strain is generally localised into shear zones or brittle features along rheological discontinuities such as dyke margins or intrusive contacts. Fault features in such regions include shear zones with minimal grain size reduction, mylonites, cataclasites and breccias (Hoek and Schaefer, 1998).

While the regional gneissic foliation approximates the strike of the Kalinjala Shear Zone (ie, trending N to NNE), the detailed evolution of individual shear zones (such as Lookout and smaller features on Williams Island) shows evidence of a prolonged history and possibly reactivation under variable metamorphic conditions during the Kimban Orogeny (Hoek and Schaefer, 1998).

Hand et al. (1995, in prep) reported peak metamorphic assemblages within Tournefort Dykes dated between ~1750-1715 Ma using garnet-hornblende-whole rock Sm-Nd data (Bendall, 1994; Hand et al., 1995; Hand et al. in prep.). All metamorphic assemblages dated by such means define a distinct baric gradient within the Lincoln Batholith, with pressures increasing from ~5 kbar at ~25 km east of the Kalinjala Shear Zone to ~10 kbar within the shear zone at Port Neill. Hence, an age of 1728±41 Ma (MSWD=0.84) from within the Kalinjala is within error of isochrons at 1748±25 (MSWD=0.48) and 1717±65 Ma (MSWD=0.58) for ~5 kbar garnet granulite assemblages at West Point, ~20 km across strike from the Kalinjala (Hand et al., in prep.). Immediately to the west of the Kalinjala, peak metamorphic conditions appear to rapidly stabilise at ~4-5 kbar within 3 km of the shear zone (figure 6.1). Such a

regional baric gradient is clearly a reflection of large scale processes active during the Kimban Orogen. Bearing in mind that the Kalinjala is dominated by subhorizontal kinematics (Parker, 1980), Hand et al. (1995; in prep) suggested a regime of oblique convergence (ie, transpression) could account for the differential exhumation about the Kalinjala Shear Zone. Peak metamorphic conditions in the Lincoln Batholith therefore correspond to the period of syn-orogenic magmatism of the Moody Suite (~1750-1700 Ma, see chapter 5) within the Hutchison Group.

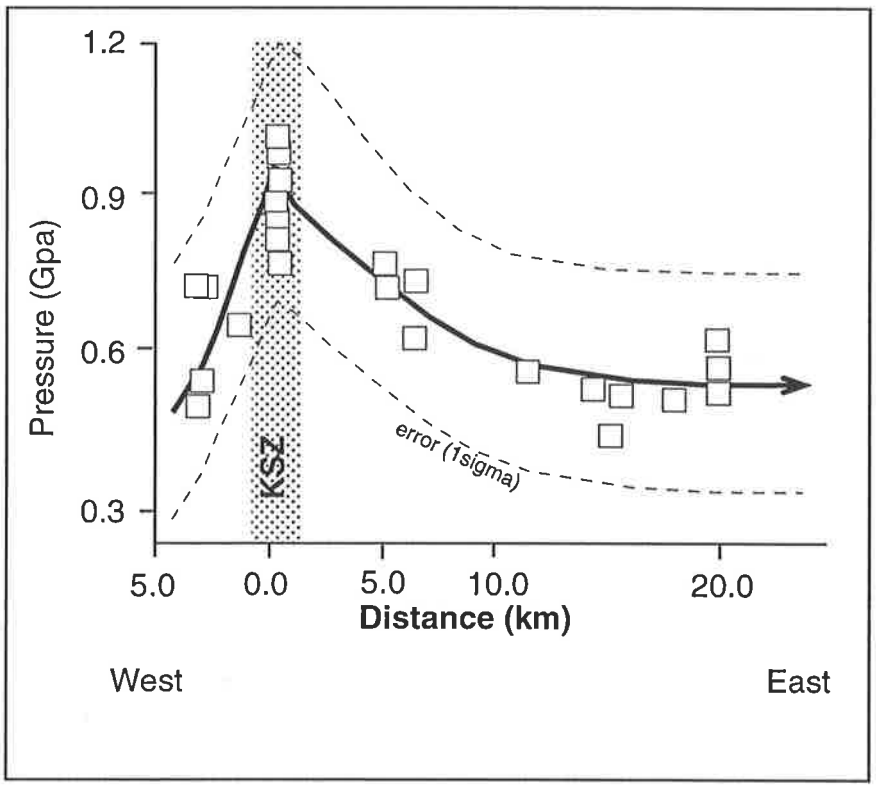

Figure 6.1: Summary of asymmetric baric gradient across the Kalinjala Shear Zone, from Hutchison Group metasediments in the west to the Lincoln Batholith in the east. 1σ error envelope extrapolated from measured uncertainties on pressure calculation. From Hand et al. (1995).

All peak-Kimban deformation postdates Tournefort Dyke emplacement, effectively placing an upper age limit on the onset of the Kimban Orogeny. From geochronological constraints imposed in chapters 3 and 4, a period of at least 50 million years is required between deformation associated with the Lincoln Batholith and emplacement of the Tournefort Dykes, with a further 50 Ma prior to the development of the earliest Kimban features. The presence of the Tournefort Dykes between high grade metamorphic events suggests that D1 (ie, syn-Lincoln Batholith) features are independent of the Kimban Orogeny proper (ie, D2 and D3 features). It therefore seems appropriate to use the term "Kimban Orogeny" to describe the period

of clearly demonstrated convergent/transpressional orogenesis (ie, ~1750-1700 Ma) and consider D1 to be part of a discrete deformational (extensional) episode (at ~1850 Ma). This effectively shortens the Kimban Orogeny from an protracted orogen (~150 Ma), to a shorter lived tectonothermal event (~50 Ma).

6.4 Geochemical effects of Kimban overprinting on intrusive lithologies

6.4.1 Felsic units

While this study has focussed primarily on the pyroxene bearing members of the Donington Suite, it is constructive to review the effects of hydration and pyroxene replacement reactions on bulk rock chemistry.

The major distinction between the charnockites and granite gneisses is the relative ranges in silica composition, with the granite gneisses being substantially more siliceous than their pyroxene bearing precursors (eg, MCC = 64.21-71.14%, average =68.18% SiO_2, Granite Gneiss = 70.97-75.62%, average = 73.76% SiO_2; see table 6.1). Correspondingly, all major elements with the exception of Na and K show depletions with alteration (table 6.1).

	MCC	Mega Charn	Granite Gneiss	Augen Gneiss
n	*15*	*10*	*6*	*17*
SiO_2	68.18	67.97	73.76	72.04
Al_2O_3	14.39	15.32	12.81	13.72
Fe_2O_3	4.91	3.97	2.62	2.72
MnO	0.07	0.05	0.03	0.04
MgO	1.09	0.91	0.49	0.56
CaO	2.76	2.94	1.36	1.74
Na_2O	2.81	2.85	2.24	2.90
K_2O	4.83	4.97	5.92	5.63
TiO_2	0.64	0.56	0.32	0.36
P_2O_5	0.15	0.14	0.05	0.08

Table 6.1: Average major element compositions for pyroxene bearing members of the Lincoln Batholith and their hydrated granite gneiss equivalents, n = number of analyses.

The trend towards increasingly SiO_2 rich compositions is also reflected by trace element variations in figure 6.2. The comparison between average trace element composition of the Memory Cove and Megacrystic Charnockites and their gneissic equivalents (figure 6.2) has several notable features, including systematic enrichment

in Rb, K, Th, La and Ce, with depletions in Ba, Sr and P. Ti also shows depletion, however other HFSE, such as Nb and Zr, appear unaffected by retrogression.

On a regional scale, these features are highlighted by proximity to the Kalinjala Shear Zone. Localities which are comparatively close to the KSZ, such as Kirton Point, are comprised exclusively of Augen Gneiss, whereas those more distant, such as Cape Donington, tend to contain Megacrystic Charnockites. Such trends are further complicated by shear zones outcropping at a range of scales in the Lincoln Batholith, from hundreds of metres wide adjacent Lookout, through tens of metres on Williams Island down to centimetres at Memory Cove, with corresponding variations in metamorphic grade in and adjacent these shear zones.

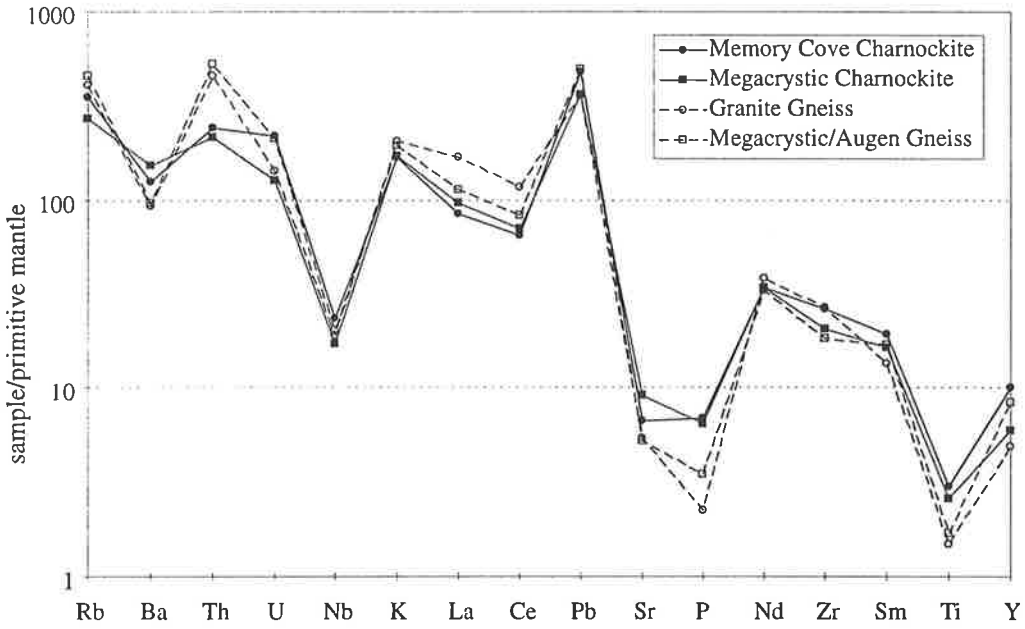

Figure 6.2: Trace element variation diagrams for pyroxene bearing felsic lithologies of the Lincoln Batholith (solid lines and filled symbols) and their retrogressed equivalents (dashed lines, open symbols).

6.4.2 Tournefort Dykes

Variations in whole rock chemistry within groupings of the Tournefort Dykes may be a result of post emplacement metasomatism and amphibolitisation associated with the Kimban Orogeny. This section investigates both regional and outcrop scale whole rock geochemical variation with increasing deformation and amphibolitisation in the Tournefort Dykes.

Figure 6.3 compares trace element chemistry of amphibolites and relatively unmetamorphosed dykes of the HBaT (high Ba tholeiites), FeRT (Iron rich tholeiites) and Unassigned Tholeiite groups. In all cases, the amphibolites are hornblende-biotite gneisses, whereas the unaltered samples preserve primary pyroxenes and magmatic

textures. One of the most striking characteristics of the HBaT and FeRT suites is the relatively minor changes in trace element chemistry observed during amphibole growth. Variations that are observed, particularly amongst the LILE, are usually systematic within a group, however no across group systematic variations are observed. Hence, amphibolitisation of HBaT appears to increase Th, U, Nb, K, Pb, LREE and Ti, whereas little variation in these elements from unaltered compositions is observed in the FeRT. By contrast, the Unassigned Tholeiites preserve distinct decreases in Rb, Ba, Th, Nb, LREE and Ti, suggesting that compositional variation due to metasomatism is controlled in part by initial dyke composition, rather than systematically driven by the individual trace elements considered.

Dykes containing metamorphic garnet occur in the same three groups, and no systematic variation in bulk rock chemistry is involved with garnet growth (figure 6.3). In each group, garnet bearing mafics display bulk compositions that mirror those of unaltered samples, with limited non-systematic erratic element behaviour (eg U in the Unassigned Tholeiites). This indicates garnet growth is not a response to pervasive metasomatism, but driven by ambient pressure and temperature conditions for a given bulk composition.

In an attempt to quantify smaller scale trace element variation with metamorphism, a series of samples across a boudin neck were collected at Kirton Point. The dyke consisted of a recrystallised core mantled by leucosome bearing amphibolites. On approaching the boudin neck, the core and leucosomes became increasingly tectonised Figure 6.4a-e is a summary series of photomicrographs of the effects of continued tectonism on HBaT dykes.

Samples were collected in a transect across the boudin neck of the leucosome bearing amphibolites, and the central portion of the dyke in both the boudin neck and from a low strain zone 10m along strike. The amount of trace element variation is depicted in the amphibolite samples for the HBaT in figure 6.3a, and can be observed to vary little from the relatively undeformed central portion of the dyke, and indeed from the rest of the undeformed dykes of the same geochemical group.

A garnet-bearing mafic from the same locality possesses a primitive mantle normalised trace element pattern that is indistinguishable from the amphibolites (figure 6.3a). Hence, trace element variations on the metre scale appear to be small, despite distinct changes in hand specimen appearance and total strain. It is therefore reasonable to conclude either that metasomatism took place on a large scale such the rocks sampled were essentially homogenised during amphibolitisation, or that amphibolitisation (at Kirton Point at least) resulted in little chemical variation in the mafics, even with moderate variations in strain. The latter hypothesis is favoured for the Kirton Point study as there is no evidence in the surrounding felsic gneisses for metasomatic processes acting on the scales required. However, whilst the observed

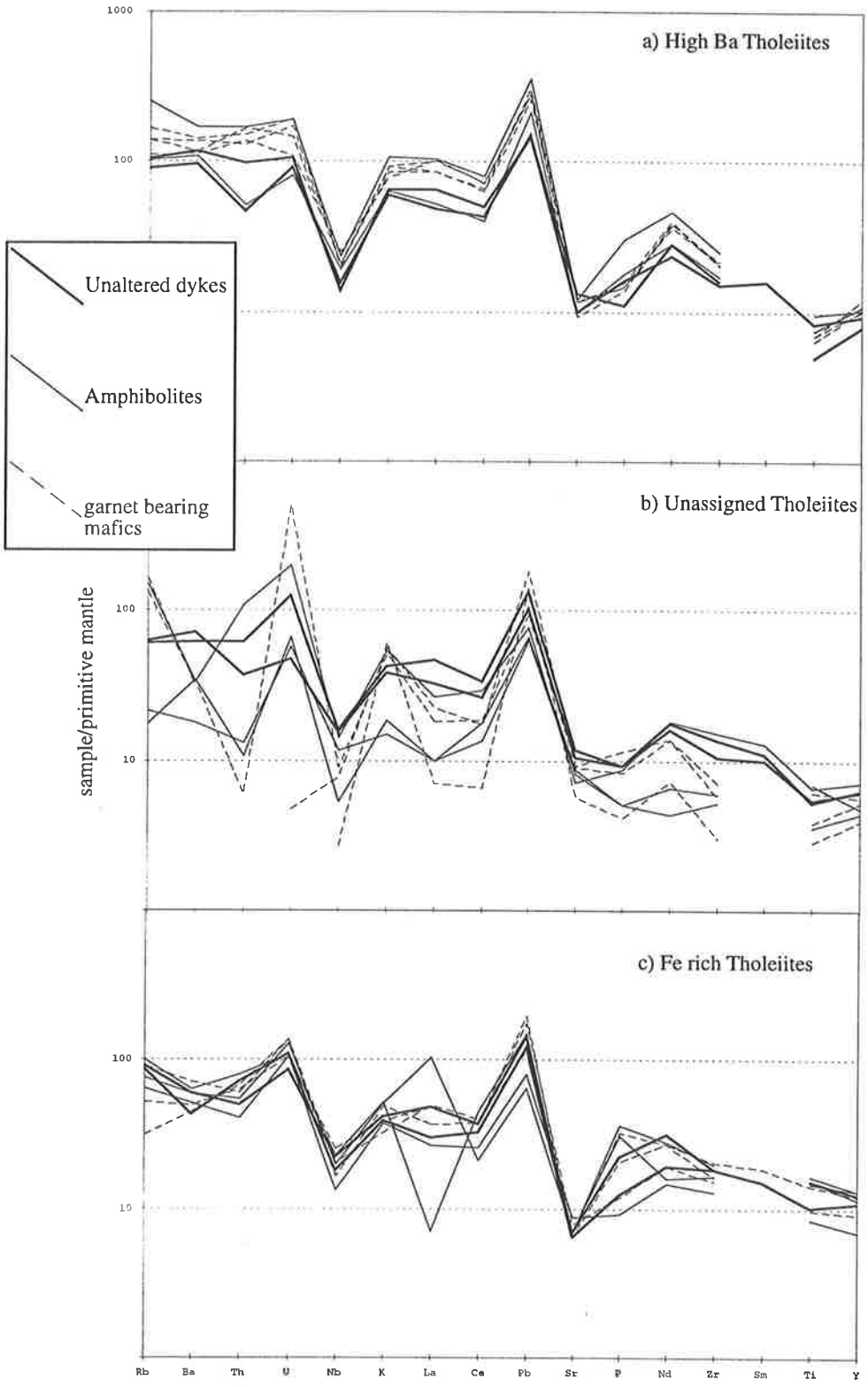

Figure 6.3: Comparative trace element variation diagrams for amphibolitisation of the Tournefort Dykes. Broad solid lines = undeformed dykes, narrow solid lines = hornblende + biotite amphibolites and dashed lines = garnet bearing amphibolites.

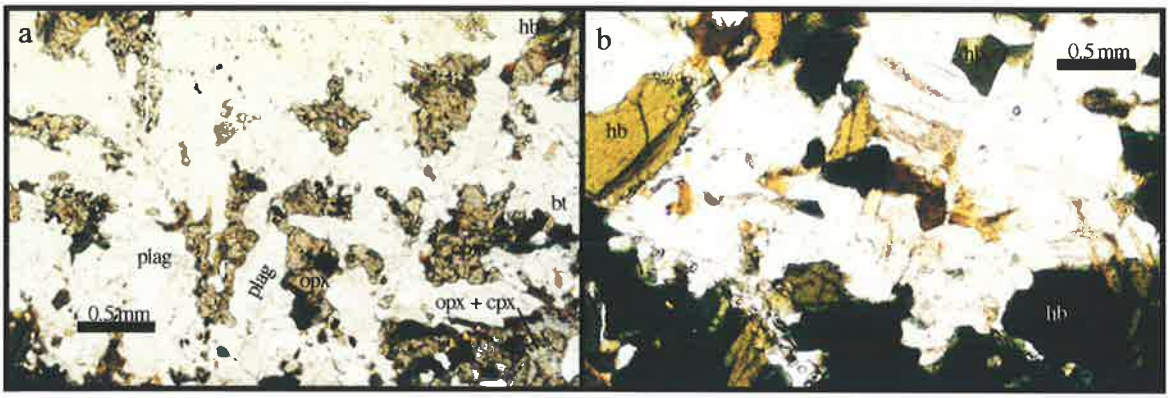

Figure 6.4: Photomicrographs of progressive deformation in High Barium Tholeiites (HBaT): a) Undeformed HBaT from a low strain zone at Wanna (Sample SEP-198). Both ortho- and clinopyroxene (opx and cpx respectively) are present amongst medium to coarse grained plagioclase (plag) laths. Hornblende (hb) and biotite (bt) growth is minimal. b) Growth of medium grained hornblende and minor biotite at the expense of pyroxene. Random orientation of amphiboles indicates a low strain environment during and after hornblende growth. (Sample SEP-196A, Wanna).

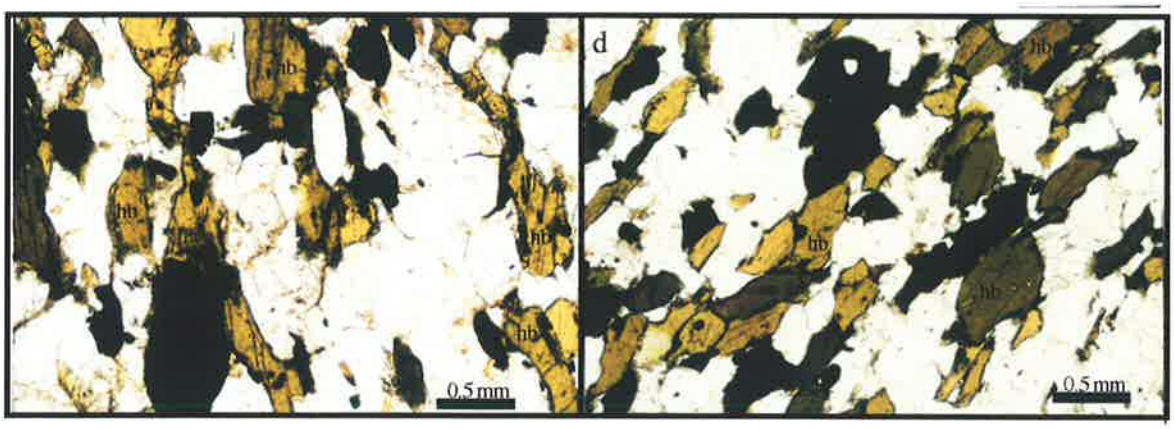

c) Higher strain results in alignment of hornblende grains as one approaches the neck of a boudin. Sample SEP-199B, Kirton Point. d) Sample collected from boudin neck at Kirton Point (Sample SEP-199C). Locally intense strain produces amphibolite gneiss; however all samples depicted (6.4a-d) have indistinguishable bulk rock chemistry.

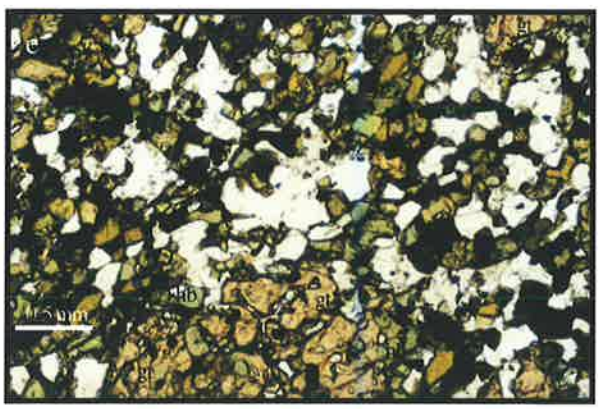

e) Garnet bearing HBaT from the west coast of West Point. Garnet rich bands are observed on the outcrop scale, however inclusion rich garnet (gt) + hornblende (hb) aggregates are observed in thin section. Sample SEP-111.

variations are small, they are not trivial, and clearly with increasing strain (such as within the Kalinjala Shear Zone, or high strain zones such as Lookout), masking of initial trace element patterns would be expected. Since such samples are not routinely collected in petrogenetic studies, this hypothesis is untestable at the present time.

Therefore, only in the case of the Dolerite dykes does amphibolitisation appear to have radically altered both the pattern and absolute trace element concentrations. On the basis of whole rock trace element geochemistry, it may be concluded that the amphibolites of this study are indeed highly deformed and retrogressed equivalents of the Tournefort Dykes, consistent with petrological observations and field relation inference.

6.4.3 Conclusions

The Kimban Orogeny has been responsible for the observed metamorphic and structural features developed in much of the Lincoln Batholith and Tournefort Dykes, particularly in zones of comparatively high strain. Comparison of whole rock geochemical data from felsic lithologies with dominantly primary igneous textures and mineralogy (ie, the large volume charnockite units of the Lincoln Batholith) with granitic gneisses displaying features consistent with progressive replacement of primary pyroxenes by amphibole and mica (picture series in 3.3d-g in chapter 3) suggests:

a) Metamorphism and deformation has resulted in felsic units becoming more siliceous, with corresponding decreases in all other major elements except Na and K.

b) Rb, Th, La and Ce are enriched during deformation;

c) Ba, Sr, P and Ti are depleted, and

d)Nb and Zr are unaffected.

In the case of the Tournefort Dykes, changes in bulk composition vary in response to the initial composition of the dyke. While retrogressive features within a single geochemical group are systematic, there appears no consistent changes in chemistry for the mafic dykes in general (eg, Th, LREE and Ti are enriched in the HBaT, whereas these same elements are depleted in the Unassigned Tholeiites). However, in all but the most deformed dykes analysed, the total changes to trace element geochemistry is generally quite low, and these elements provide a good reflection of initial composition. The growth of metamorphic garnet in the mafic rocks has little effect on both the FeRT and HBaT, however it does change the composition of the Unassigned Tholeiites. Therefore HMgT, FeRT and HBaT are the most constructive mafic dyke groups to use for petrogenetic studies.

One unanticipated observation for both the mafic and felsic lithologies is the relative mobility of Ti, an element usually considered to be immobile.

6.5 Summary of deformation and metamorphism in the Lincoln Batholith and Tournefort Dykes

The Lincoln Batholith contains syn-emplacement fabrics (D1), which indicate emplacement into a deforming environment. This fabric is tentatively correlated with D1 in the Hutchison Group, a layer parallel, horizontal fabric, probably associated with an extensional environment. Further extension is accommodated by the emplacement of the Tournefort Dykes, however there appears to be no evidence of fabric development associated with this.

Peak metamorphism and deformation (D2) was associated with the Kimban Orogeny in the period ~1750-1700 Ma, with granulite facies conditions recorded in mafic lithologies in high strain zones. Terrain scale rehydration throughout the Lincoln Batholith followed during D3, the waning stages of the Kimban. An asymmetric baric gradient across the Kalinjala Shear Zone is a reflection of the prevailing regional tectonic driving mechanisms during the terminal Kimban. Field evidence of late stage low angle transport directions along the Kalinjala suggest a strike slip component was prevalent late in the history of the shear zone. However, the greatest amount of exhumation is also recorded in the centre of the shear zone, with 10 kbar assemblages indicating significant vertical transport during the Kimban. A pronounced baric gradient reaches a regional equilibrium of ~5 kbar 20 km from the Kalinjala to the east, and ~4.5 kbar 3 km west of the Kalinjala. Therefore, the combination of large scale strike- and dip-slip components suggests an overall transpressional regime, possible analogous to the Alpine fault on the South Island of New Zealand. Peak metamorphism in the adjacent Hutchison Group was never greater than mid amphibolite facies, emphasising the asymmetry across the shear zone, with Kimban structures dominantly being west verging folds and local thrusts.

The southern Eyre Peninsula therefore records a history of continued extension from the onset of Hutchison sedimentation (at ~2000 Ma), through Lincoln Batholith (D1) and Tournefort emplacement. At ~1750 Ma, the orogenesis in a transpressive regime resulted in substantial crustal thickening and cycling of Lincoln Batholith material through the crust to at least 30 km (as is currently exposed in the heart of the Kalinjala) and regional amphibolite facies metamorphism with two phases of west verging folds in the Hutchison Group.

The Kimban Orogeny was also responsible for rehydration of the Lincoln Batholith, particularly in zones of dynamic recrystallisation (ie, high strain zones). The effects of such rehydration are most pronounced in the major element compositions of felsic lithologies, with trace elements of both mafics and felsics maintaining similar trace element patterns (if not absolute abundances) until reasonable levels of strain. However, low strain areas provide samples that appear both petrographically and chemically to have suffered little alteration.

CHAPTER SEVEN

Comparison of modern and ancient magmatism with southern Eyre Peninsula

7.1 Introduction

In order to place the magmatism of the Lincoln Batholith and Tournefort Dykes into context on the global scale, this section sets out to compare the southern Eyre Peninsula with terrains of various ages and tectonic settings.

The southern Eyre Peninsula is considered firstly in an Australian context, in order to gain an appreciation for timing and styles of magmatism and orogenesis during the Australian Palaeoproterozoic. One unanticipated outcome of this work, a potential correlation of the Lincoln Batholith with parts of the Mount Isa Inlier, is then investigated in detail, before the discussion is broadened to incorporate chemical and magmatic features of the Torngat Orogen, Svecofennian Shield and the Wopmay Orogen. These terrains are investigated as they contain tectonothermal events of essentially the same age as the Lincoln Batholith. The features of a potential modern analogue of the Lincoln Batholith, such as Andean style, continental margin magmatism, are also investigated in detail. Other potential Phanerozoic analogues are also touched upon in order to gain an appreciation for the range of chemical and spatial features observed in magmatic belts in a temporal sense. Finally, a comparison of the record of crustal growth in several Australian Proterozoic terrains with modern sites of crustal growth is conducted in order to evaluate how Palaeoproterozoic terrains relate to the modern Earth.

First however, it is constructive to review the key features of the Lincoln Batholith on the local scale. These are dominated by a small number of important observations: 1) The Lincoln Batholith is part of a short lived (~10 Ma), large

elongate magmatic zone ~100 x 50 km in size; 2) Within this body are few individual plutons; 3) The system is remarkable for its overall chemical and isotopic homogeneity; 4) Key chemical features include elevated K, Y and LREE levels with negative Nb, Sr, P and Ti anomalies. Incompatible element concentrations are elevated at low SiO_2 levels; 5) Depleted mantle model ages in the Lincoln Batholith cluster between 2.3-2.5 Ga, substantially predating the magmatic event at 1.85 Ga. Finally, 6) the Lincoln Batholith contains evidence of syn-plutonic mafic magmatism in the form of the Jussieu Dykes.

7.2 Comparison of the Lincoln Batholith with ancient tectonic settings

The Proterozoic contains an enormous volume and variety of felsic magmatism. This discussion will initially focus on magmatic terrains of similar age to the Lincoln Batholith, and touch briefly upon some of the tectonic models which have been applied for those most appropriate. An investigation into how typical such magmatism is for the Proterozoic will form the basis for discussion in chapter 8, and the relevance of modern analogues to Precambrian terrains will also be discussed.

7.2.1 The southern Eyre Peninsula in an Australian context

Proterozoic crustal evolution in Australia has long been held to have taken place in essentially stable crustal blocks with intracratonic tectonic and magmatic activity dominating vertical crustal growth processes (eg, Etheridge et al., 1987; Wyborn , 1988). By contrast, the work of Hoffman (1988) and Windley (1993) on North America and Europe, who interpret aggregation of Proterozoic terrains by processes analogous to modern day plate tectonics, led Myers et al. (1996) to consider the development of Precambrian Australia in terms of lateral accretion of smaller crustal fragments. This section outlines the broad scale geological events of the Australian continent during the Palaeoproterozoic, placing the southern Eyre Peninsula into an appropriate continental context for further discussion.

Of primary interest here are events within the Australian continent taking place during the period ~2000-1700 Ma, effectively spanning the interval from cessation of the Miltalie event to the end of the Kimban Orogeny on southern Eyre Peninsula. This incorporates Hutchison Group sedimentation as well as Lincoln Batholith, Tournefort Dyke and Moody Suite magmatism. Much of the data for the following discussion is derived from Myers et al. (1996), unless otherwise specified.

Very little ~2000 Ma activity is recorded in Australia, with sedimentation dominating the record on the margin of the Western Australian Archaean cratons. McDonald et al. (1997) infer magmatic activity at ~2.0-1.97 Ga from zircon rims in basement gneisses in the Mount Isa Inlier, which appears to be the only other record of tectonothermal activity in Australia during this period.

The period from ~2000-1850 Ma involved Hutchison Group sedimentation on the Gawler Craton. Sedimentation appeared to dominate elsewhere in Australia, with the latter part of this period reflecting the onset of voluminous magmatism throughout northern Australia from ~1880 Ma. Deformation is preserved in rocks from the Hooper Orogen (subsequently reworked in the King Leopold Orogen) and Yaringa Metamorphics (the Barramundi Orogeny) in the Mount Isa Inlier. An inherited zircon core in the megacrystic augen gneiss from Wanna (1907±12 Ma) may record the presence of crust of this age on southern Eyre Peninsula.

Figure 7.1: Archaean cratons (light shading) and dominantly Palaeoproterozoic inliers and orogenic belts (dark shading) of Australia.

The ~1880-1840 Ma magmatic event of Wyborn (1988) incorporates the Lincoln Batholith, as well as magmatism in the Mount Isa, Pine Creek, King Leopold, Granites-Tanami, Arunta and Tennant Creek Blocks (see figure 7.1). Significantly, many of these intrusives contain similar chemical characteristics, particularly in the form of elevated LREE and Sr depletion. The nature of these features is expanded in section 7.2.1.1 below. The Capricorn Orogeny, incorporating collision between the Yilgarn and Pilbara cratons also took place during this period.

By the time of extension on the southern Gawler Carton to allow Tournefort Dyke emplacement at ~1815 Ma, sedimentation and mafic volcanism was occurring in the Mount Isa Inlier, as well as the Kimberly Basin. The Halls Creek Orogeny took place from ~1830-1800 Ma.

The period of quiescence on southern Eyre Peninsula from ~1800-1750 Ma contrasts with magmatic and volcano-sedimentary activity to the east on the Moonta

subdomain of the Gawler Craton. The Strangways Orogeny and accompanying magmatism in the Arunta Inlier took place during this time, whilst deposition continued in the Mount Isa Inlier.

The onset of the Kimban Orogeny at ~1750 Ma, and continuing until ~1700 Ma involved the emplacement of the Moody Suite on Eyre Peninsula. Further magmatism took place in the Moonta subdomain, however the record of northern Australia at this time appears dominated by sedimentation, particularly in the McArthur Basin and Mount Isa Inlier.

Therefore, the geological record of southern Eyre Peninsula broadly contains some similarities (chiefly in terms of timing of magmatism and magmatic chemistry) with portions of other Australian terrains, as well distinct differences (mainly in timing of orogenic events and sedimentation). One unexpected observation of such broad scale correlative work was some remarkable similarities between the evolution of the southern Eyre Peninsula and Moonta subdomain of the Gawler Craton with the central (Kalkadoon-Leichardt) and Eastern Belts of the Mount Isa Inlier. The detail of these similarities is investigated below.

7.2.1.1 A correlation between the Lincoln Batholith and the Mount Isa Inlier?

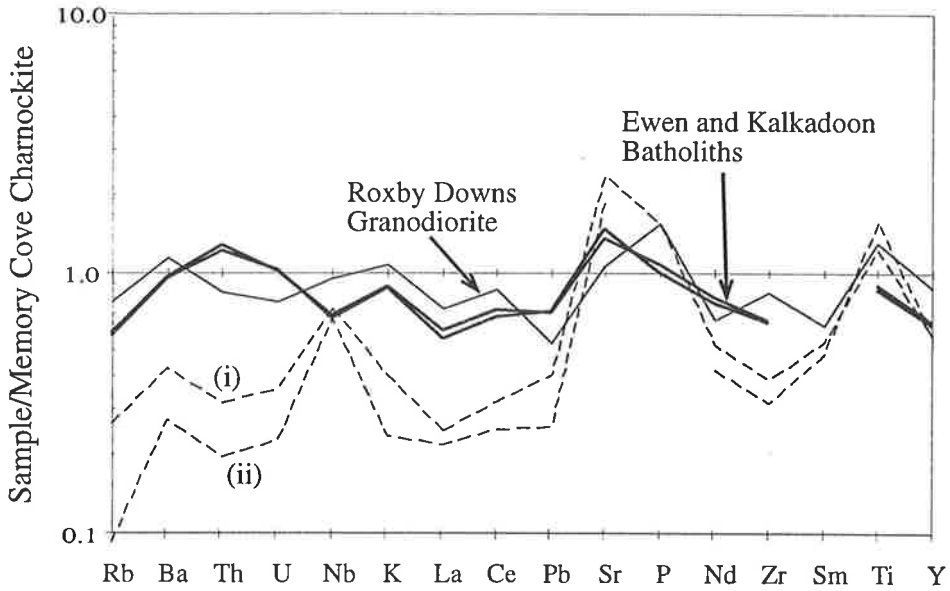

Figure 7.2: Comparison of representative analyses from the Roxby Downs Granodiorite and Ewen and Kalkadoon Batholiths of the Mt Isa Inlier. Data are normalised to a typical Memory Cove Charnockite, sample SEP-074. Included for reference are two estimates of average crustal composition: (i) Taylor and McLennan (1985), and (ii) Rudnick and Fountain (1995). Ewen and Kalkadoon data from Wyborn and Page (1983), Roxby Downs data from Creaser (1989).

The abrupt truncation of magnetic and structural features at the southern margin of the Mount Isa Inlier have lead to speculation as to where (if at all) its

potentially metallogenic southern continuation is (eg, Wilson, 1987; Connors and Page, 1995; O'Dea et al., 1997; Teasdale, 1997). The following discussion presents one possible explanation for this conundrum.

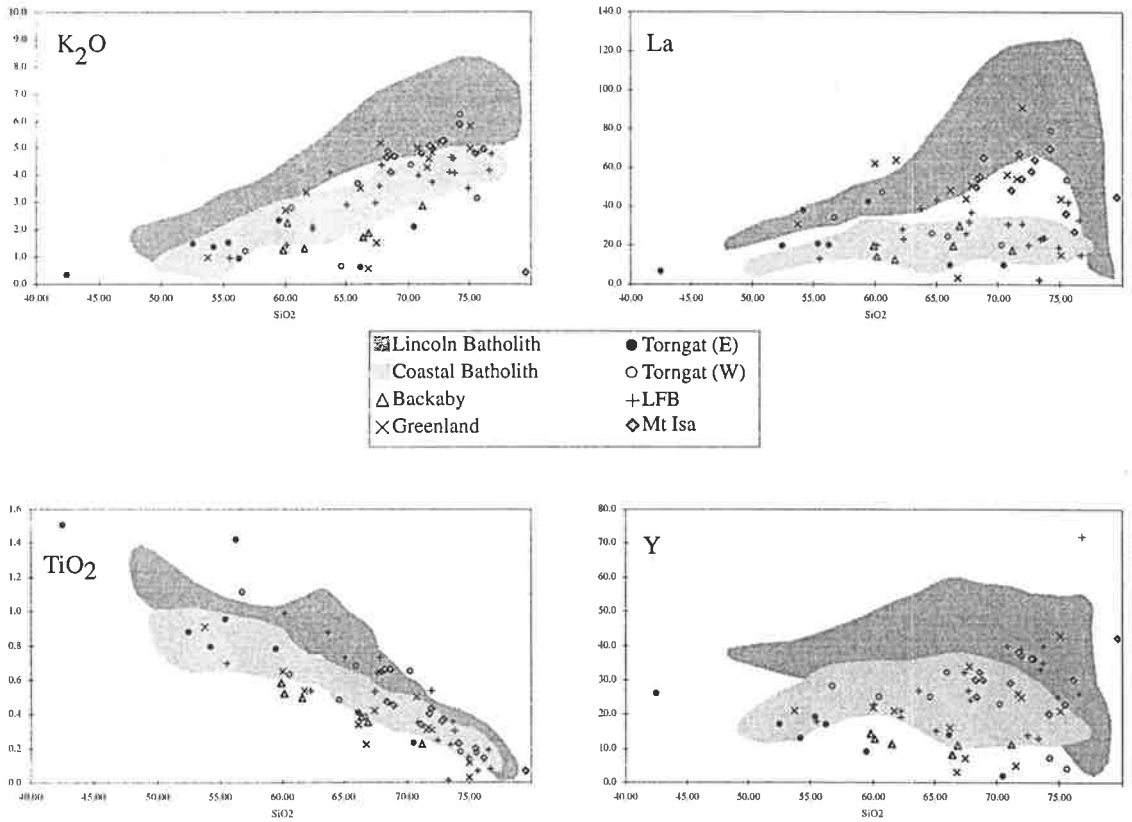

Figure 7.3: Harker variation diagrams for magmatic suites discussed in the text. Lincoln Batholith magmatism includes Jussieu Dykes and Colbert Suite, and ranges from ~1852-1840 Ma. Coastal Batholith data from Pitcher et al. (1985), and are post Cretaceous in age. Bäckaby is 1834±3 Ma (Mansfeld (1996)), Greenland >1750 Ma (Kalsbeek, 1995), Mt Isa data for the Ewen and Kalkadoon Batholiths (~1860-1850 Ma, Wyborn and Page (1983)), Torngat Intrusives = 1877±1 Ma (Theriault and Ermanovics (1997) and Phanerozoic Lachlan Fold Belt data from Chappell and White (1992). Note high K_2O, La and Y values of Australian Proterozoic suites with respect to modern subduction settings (eg, Coastal Batholith).

The key correlative features involved here, the Ewen and Kalkadoon Batholiths, occupy part of the central portion of the Mount Isa Inlier (figure 7.1). With their extrusive equivalents, the Leichardt Volcanics, they comprise a widespread and voluminous magmatic event. Wyborn (1988) outlined grounds for correlation of this event in a genetic sense with other granites of similar age from the Murphy, Pine Creek, Halls Creek, King Leopold, Granites-Tanami, Arunta and Tennant Creek Inliers. However, the following discussion will be restricted purely to the Mount Isa intrusives for structural and temporal reasons. It must be noted that the chemical and isotopic features proposed by Wyborn (1988) may indicate a

common genesis of the Lincoln Batholith with intrusives from other northern Australian inliers. Several features of the Ewen (1843±7 Ma, McDonald and Collerson, 1998) and Kalkadoon (1856±10 Ma, Wyborn and Page, 1983) Batholiths invite comparison with the Lincoln Batholith. The first is the similarity in major and trace element geochemistry (figures 7.2 and 7.3). Both suites of rocks contain elevated K_2O, Ba, and LREE (figure 7.2) (Wyborn and Page, 1983; Wyborn et al., 1992).

Recent Nd work conducted within the Kalkadoon Batholith (McDonald et al., 1997) reveals signatures indistinguishable from the Lincoln Batholith at the time of emplacement. Back calculation of Nd isotopic signatures from both terrains reveal similar evolutionary trajectories (figure 7.4). Nd isotopes for the 1850 Ma basement granodiorites at Roxby Downs (figure 7.5), which are chemically comparable to the Lincoln and Kalkadoon Batholiths (figure 7.2; Creaser, 1989; 1995) are also indistinguishable at the time of Lincoln Batholith magmatism (figure 7.4).

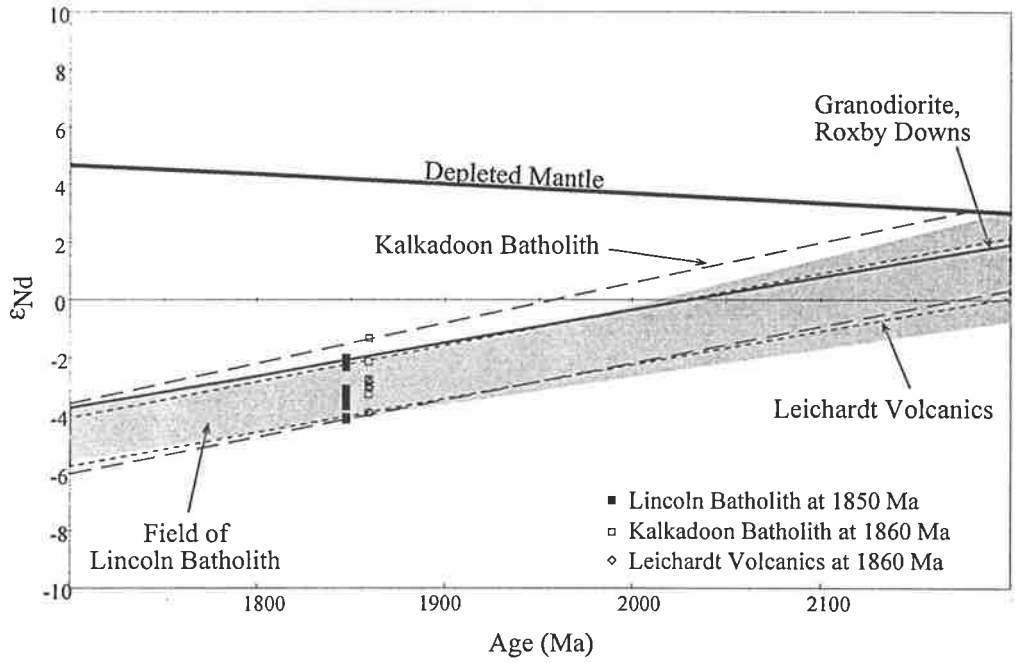

Figure 7.4: Comparison of Nd isotopic signatures between the Kalkadoon-Leichardt association, Lincoln Batholith and granodiorite from Roxby Downs. All suites are indistinguishable at the time of Lincoln Batholith magmatism. Mount Isa data from McDonald et al., 1997; Roxby Downs data from Creaser, 1995.

Several features of the Ewen and Kalkadoon distinguish them from the Lincoln; eg, they preserve no evidence of pyroxene, and contain a number of geographically distinct plutonic events. However, pyroxene growth may merely reflect emplacement conditions (particularly given similarities between the two regions in bulk composition), whilst the presence of discrete plutons is likely to be a function of the thermal state and/or emplacement level of the Ewen and Kalkadoon

Batholiths. Indeed, while there is some variation in chemistry between plutons (particularly in the Kalkadoon Batholith), Wyborn and Page (1983) note that the total range of variation is minimal in a regional context. The total range of chemistry in the Ewen-Kalkadoon association and their contemporaneous volcanics (the Leichardt Volcanics) is comparable to that of the Lincoln Batholith (Wyborn and Page, 1983), as illustrated in figure 7.3.

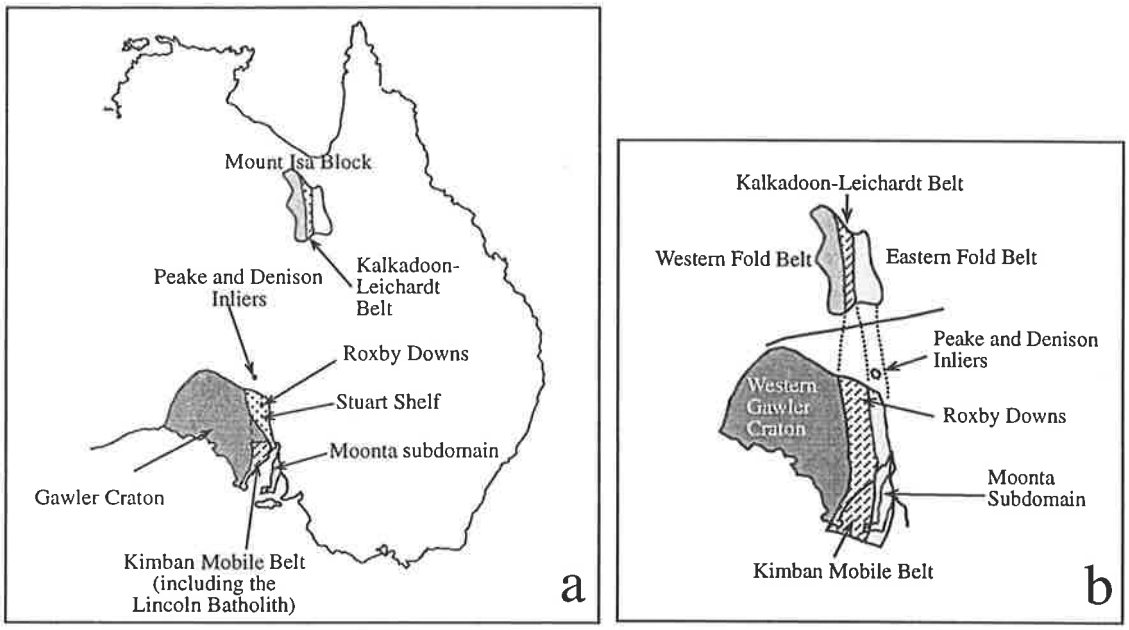

Figure 7.5a: Sketch map of key localities and terrains regarding potential correlation of the Lincoln Batholith with the Kalkadoon-Leichardt Belt of the Mount Isa Block. b: Palaeoproterozoic geology and a possible juxtaposition of the Gawler Craton and Mount Isa Block at ~1700 Ma.

Further, Wyborn and Page (1983) note the uniform age and compositional similarity of rocks of the Ewen-Kalkadoon-Leichardt association over a large area (>5000 km^2), a feature diagnostic of the Lincoln Batholith (over a comparable area of at least 5000 km^2). Indeed such large scale chemical and isotopic homogeneity (figure 7.4) appears to be one of the most defining characteristics of this style of magmatism.

Coincidence of both isotopic and chemical features in magmatic systems of similar age suggest a somewhat closer spatial juxtaposition of the two terrains than at present. Several lines of evidence support the notion of a more or less continuous belt, albeit disrupted by faulting (figure 7.5b). Firstly, granodiorite gneisses from basement sequences at Roxby Downs are indistinguishable chemically and isotopically from the Lincoln and Kalkadoon Batholiths (figure 7.4). The Roxby Downs granodiorites are interpreted to represent a northerly extension of Lincoln

Batholith style magmatism beneath the Stuart Shelf at 1850 Ma (Creaser, 1995; preliminary U-Pb zircon data), and provide a vital link in any terrain scale correlation of 1850 Ma magmatism.

Kimban Mobile Belt	Moonta subdomain and Roxby Downs	Peake and Denison Inliers	Mount Isa Inlier
1500 Ma[1]: Sr isotope resetting in GRV and Hiltaba Suite	1510± 12 Ma: Spilsby Suite		
		1533±6 Ma: Granite Dykes	~1530 Ma: Isan Orogeny
1600-1580 Ma: Gawler Range Volcanics and Hiltaba Suite	1600-1580 Ma: Gawler Range Volcanics and Hiltaba Suite		
~1750-1700 Ma: Moody Suite magmatism, Kimban Orogeny	1737±5 Ma: Moonta Porphyry ~1740 Ma: McGregor Volcanics	1746±6 Ma: Metarhyolite	1745±15 Ma: Wonga Batholith; Burstall Batholith
~1810 Ma: Tournefort Dykes	1791±4 Ma: Myola Volcanics	1780±12 Ma: Metavolcanics 1793±8 Ma: Wirriecurrie Granite	1781±3 Ma: Argylla Formation >1781 Ma: Magna Lynn Basalt 1790±9 Ma: Bottletree Formation
1852-1849 Ma: Lincoln Batholith 1859±11 Ma: Bosanquet Volcanics	~1850 Ma: Granodiorite at Roxby Downs		1856-1843 Ma: Ewen and Kalkadoon-Leichardt association

Table 7.1: Summary of broad geochronological comparisons between the eastern Gawler Craton, Peake and Denison Inliers and portions of the Mount Isa Block. Gawler Craton data from Fanning (1997) and this study, Peake and Denison data from Hopper and Collerson, 1998 and Mt Isa data compiled from Blake, 1986; O'Dea et al., 1997 and Page, 1998. [1]= K. Stewart, University of Adelaide, compilation of unpublished Sr data.

Further correlations involving the subsequent evolution of the two terrains can be made. Geochronology of the Peake and Denison Inliers off the north eastern

margin of the Gawler Craton (Hopper and Collerson, 1998), indicates Palaeoproterozoic sequences in these inliers can be correlated with the Moonta subdomain of the eastern Gawler Craton (table 7.1, figure 7.5b) and also the Eastern Fold Belt of the Mount Isa Inlier (Hopper and Collerson, 1998). The timing of coincident magmatic events in all three terrains at 1790-1780 and 1740 Ma strengthens the chemical and isotopic tie established by ~1850 Ma magmatism. Hence, the Peake and Denison Inliers may represent a fragment, or continuation of, the Moonta subdomain off the northeastern margin of the Gawler Craton (figure 7.5b).

A characteristic of the later Gawler Craton and Mount Isa Inlier evolution is a corresponding variation from west to east in both domains. That is, the oldest sequences are in the west (ie, Kimban Mobile Belt and Kalkadoon-Leichardt Belt respectively) and the younger sequences to the east (Moonta Subdomain and Eastern Fold Belt in their respective terrains; see figure 7.5b), geometrically consistent with a geographic reconstruction.

	Tournefort Dykes			Mt Isa Dolerites		
	Mean HMgT	Mean HBaT	Mean FeRT	?HMgT	?HBaT	?FeRT equiv
SiO_2%	50.02	54.06	48.86	48.59	54.55	51.02
Al_2O_3%	10.35	13.66	13.39	15.13	16.31	13.53
Fe_2O_3%	12.12	14.46	17.55	11.21	13.26	15.52
MnO%	0.19	0.19	0.24	0.26	0.16	0.23
MgO%	16.31	3.66	5.10	10.71	2.31	6.00
CaO%	8.10	7.25	8.79	11.65	7.51	9.85
Na_2O%	1.40	2.66	2.22	1.20	3.52	2.34
K_2O%	0.60	2.31	1.10	1.30	0.64	0.92
TiO_2%	0.58	1.64	2.60	0.81	2.32	1.76
P_2O_5%	0.09	0.43	0.39	0.07	0.56	0.15
SO_3%	0.01	0.01	0.03			
LOI%	-0.05	-0.20	0.02			
TOTAL	99.75	100.19	100.28	100.93	101.14	101.32
Rb	24.4	87.8	44.1	89	23	56
Ba	176	894	332	506	1224	138
K	4952	19198	9117	10792	5313	7637
Pb	3	16	9	42	12	6
Sr	108	250	149	183	211	177
P	393	1870	1687	305	2444	655
Zr	73	218	188	40	296	130
Ti	3500	9844	15562	4856	13908	10551
Y	17	47	49	18	62	27
V	194	258	394	240	100	390
Sc	31	39	42	15	20	20
Cr	2192	64	97	970	5	95
Cu	72	95	194	300	92	224
Zn	81	128	151	240	116	130
Ni	715	36	64	345	30	84

Table 7.2: Comparative geochemistry for mean Tournefort Dykes and selected Basement Dykes from the Mount Isa Inlier. Mount Isa Data from Ellis and Wyborn, 1984.

Further, mafic dykes in the basement of the Mount Isa Inlier display broadly similar geochemical groupings to those of the Tournefort Dykes (Table 7.2). Whether the mafic dykes described by Ellis and Wyborn (1984) are true correlatives of the Tournefort is unclear, however temporal correlation can be assigned on the basis of the preferred age of Tournefort emplacement derived from chapter 4, and the age of mafic magmatism (eg, the Magna Lynn Basalt) in the Mount Isa Inlier (table 7.1).

Finally, the presence of late, large scale sinistral strike-slip faults along the northwestern margin of the Gawler Craton led Teasdale (1997) to suggest that such features extend and correlate with broad scale structures at the southern end of the Mount Isa Inlier, and are of Grenvillian (~1100 Ma) age. Such observations offer a mechanism for juxtaposition and correlation of sequences in the Mount Isa Inlier and Gawler Craton (eg, Wilson, 1987).

Regardless of whether portions of the Mount Isa Inlier and Gawler Craton were ever parts of a contiguous Palaeoproterozoic terrain, the remarkable similarities in chemistry and isotopic character of large volume ~1850 Ma felsic magmatic events highlights a similarity of process in both terrains. Thus the size, homogeneous chemical and isotopic nature and short temporal duration of such magmatic settings contain significant implications for Proterozoic crustal growth. The consequences of this will be discussed in chapter 8.

7.2.2 Other Proterozoic terrains

The Great Bear Magmatic Zone of the Wopmay Orogen

The Great Bear magmatic zone of the Wopmay Orogen contains a magmatic history spanning 1875-1840 Ma (Hildebrand et al., 1987; Bowring and Podosek, 1989). Magmatism in the Great Bear zone extends over a strike length of ~900 km, and is ~100 km wide. Two subgroups, an earlier calc-alkaline succession, and a later, bimodal suite of magmatism may be recognised within the zone. The older (~1875-1860 Ma) sequence is folded and deformed, whereas the younger (~1850-1840 Ma) suite appears to be post deformational (Hildebrand et al., 1987).

Rocks of the older suite define a calc-alkaline trend, both within and between numerous individual compositionally zoned plutons. The younger suite contains plutons that are generally larger and chemically homogeneous, comprising more siliceous and potassic units (Hildebrand et al., 1987). Associated with most magmatic suites are extensive volcanics, typically of intermediate (~53-64 wt% SiO_2) composition (Hildebrand et al., 1987).

Hence, the Great Bear magmatic zone is characterised by calc alkaline magmatism in two discrete phases, separated by a period of convergent deformation (Hildebrand et al., 1987; Bowring and Podosek, 1989; Bowring and Grotzinger, 1992). Numerous plutons are identifiable in both magmatic events, many of which

are zoned from intermediate to felsic compositions. The magmatic zone is itself a large, elongate (~900 x 100 km) belt emplaced in an active tectonic setting.

Intrusives of the Torngat Orogen, Canada

The Torngat Orogen of eastern Canada is a granulite facies belt between the Archaean Nain and Rae provinces of Labrador (Ermanovics and Van Kranendonk, 1990; Theriault and Ermanovics, 1997). Magmatism is divided into an eastern and a western metaplutonic suite, with plutons in the eastern suite tending to more mafic compositions. The bulk of plutonic magmatism took place at 1877±1 Ma (Theriault and Ermanovics, 1997), outcropping intermittently over an area of ~100 x 50 km. In general, magmatism in the Torngat Orogen tends to low K_2O and TiO_2, and intermediate SiO_2 levels (figure 7.3). There is some enrichment in LREE in both the eastern and western suites, despite distinctly different amounts of interaction with continental crust (Theriault and Ermanovics, 1997).

Plutonic magmatism immediately predates convergent orogenesis and crustal thickening at 1860 Ma, which continued until ~1780 Ma with final uplift of the terrain.

In summary, the Torngat intrusives comprise numerous plutons of relatively small volume magmatism over a short period of time. Magmatism displays intermediate chemistry with a considerable range in chemical features both within and between the eastern and western successions. Convergent orogenesis of the Torngat Orogen immediately post-dated plutonic magmatism, suggesting an active tectonic setting, probably on the margins of the adjacent Nain and Rae provinces.

The Bäckaby Intrusion, Sweden

The Bäckaby intrusion of southeast Sweden was emplaced at 1834±3 Ma, and predates the Transscandanavian Igneous Belt at ~1800 Ma, but post-dates the ~1900 Ma granitoids of the Svecofennian Domain (Mansfeld, 1996). Although only a single, relatively small (~22 x 12 km) body is observed, the Bäckaby intrusion is of interest due to its temporal setting between two regionally major events. The Bäckaby intrusion is more primitive than subsequent Transscandinavian Igneous Belt intrusions (Mansfeld 1996), preserving characteristics such as a calc-alkaline trend and flat REE patterns with a small negative Eu anomaly more typical of the older Svecofennian granitoids (~1.9 Ga). Further, the Bäckaby intrusion is syn-kinematic, suggesting an active tectonic setting (Mansfeld, 1996).

The preceding examples of magmatism similar in age to the Lincoln Batholith have been selected to highlight the variation in size, nature, composition and relationship of magmatism to orogenesis. Several observations pertaining to the Palaeoproterozoic intrusives discussed may be made. Firstly is the question of scale. Both the Lincoln Batholith and Mount Isa Batholiths are relatively homogeneous on a

scale appropriate to their individual outcrop boundaries. Further, when considered as part of a contiguous terrain, they represent part of an exceptionally large, homogeneous felsic magmatic linear belt. By contrast, the Torngat, Great Bear and Bäckaby examples show extensive chemical and physical variation from the within pluton (Great Bear, Bäckaby), between pluton (Great Bear, Torngat) and regional scales (Torngat). Significantly, each of these magmatic systems are either syn- or immediately pre- convergent deformation/orogenesis, whereas both the Lincoln and Ewen and Kalkadoon Batholiths preserve evidence for tectonic quiescence both before and after emplacement.

To find chemical analogues of the Lincoln Batholith (aside from the northern Australian examples described above), it is necessary to look at suites of significantly different age within the Proterozoic. Suites broadly similar in composition to the Lincoln Batholith include the Ardery Charnockite (~970 Ma, immediately post orogenic, Young et al., 1996; 1997) and Mount Crofton Granite Complex, ~700 Ma, Goellnicht et al., 1991; Wyborn et al., 1992). However, neither of these suites contains the same broad scale homogeneity observed in the Lincoln and Kalkadoon Batholiths, suggesting that regardless of the tectonic association of these younger suites, they may not be good analogues.

7.3 Comparison of the southern Eyre Peninsula with modern tectonic settings

From the examples outlined above, it is clear that scale is important when discussing the relevance of potentially analogous magmatic systems. The Lincoln-Mount Isa magmatic system defines a linear belt of homogeneous isotopic and chemical features, approaching the thousand kilometre scale. A natural starting point is to investigate magmatic systems on the modern Earth capable of generating such features. Additionally, it is constructive to consider which regimes on the modern Earth may be able to generate Lincoln-style magmatism on a smaller scale, such as that observed on the southern Eyre Peninsula.

With these ends in view, the Coastal Batholith of the Andes is considered, as it is a linear magmatic belt extending ~1600 km along strike and ~60 km wide (of the order of the Lincoln-Mount Isa magmatic system), and represents one of the simplest continental arc settings on the modern Earth. The Coastal Batholith is thought to contain little evidence of "suspect terrains", with Mesozoic arc magmatism superimposed on the Palaeozoic Andean margin (Cobbing, in Pitcher et al., 1985). Therefore, geochemical and structural features observed in the Peruvian Andes are likely to truly reflect processes driven by continent-ocean convergence, with minimal external influences. Additionally, the Coastal Batholith is comprised of a series of segments, each of an order of the individual Lincoln Batholith, allowing a direct comparison between the two settings on a smaller scale.

A continental arc, as opposed to an oceanic arc, is necessary for such a comparison due to the role the adjacent crustal block (the Gawler Craton) played in the evolution of the Lincoln Batholith (see chapter 3).

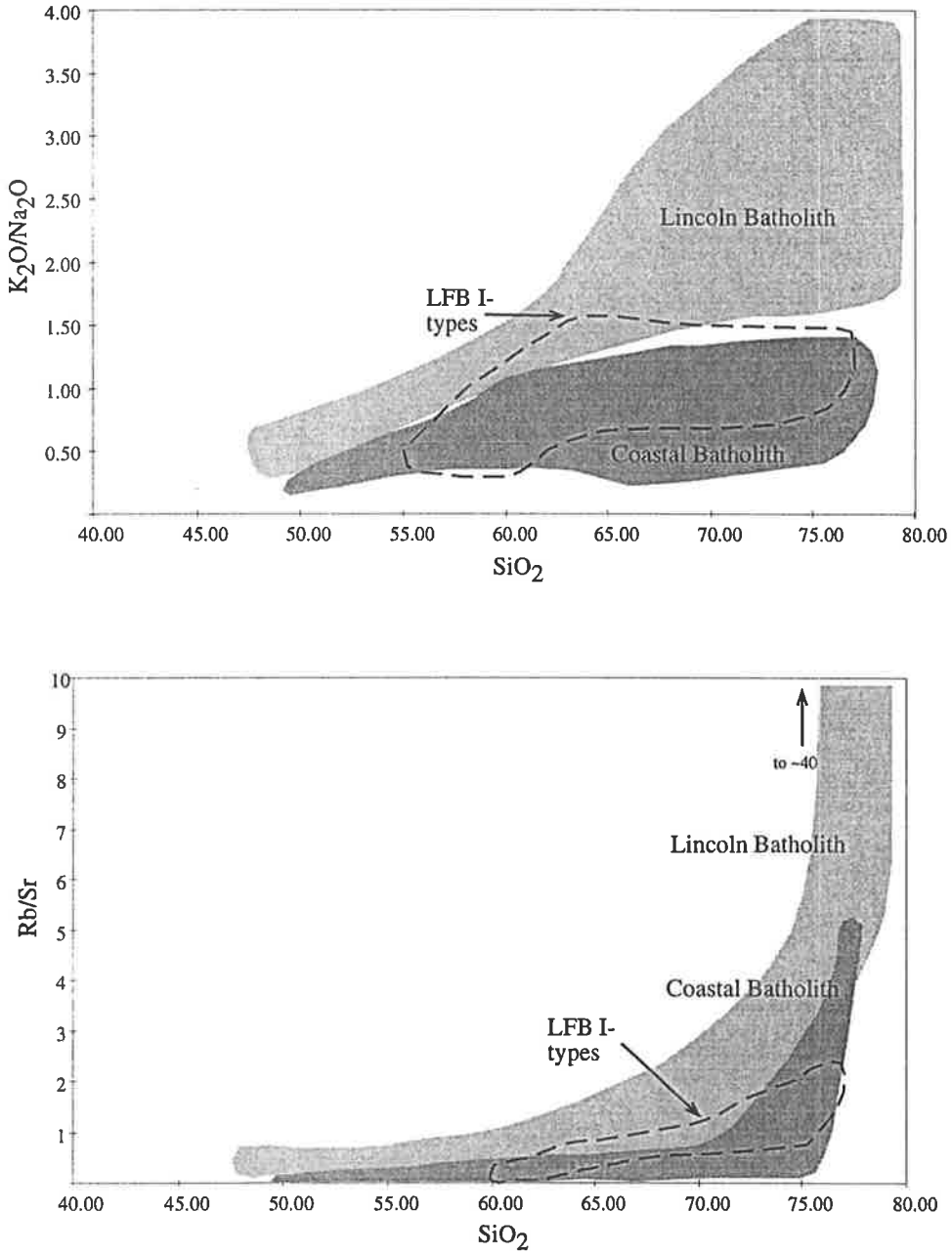

Figure 7.6: Comparison of the Lincoln Batholith with some Phanerozoic analogues: The Coastal Batholith (Peruvian Andes; data from Pitcher et al., 1985) and the Lachlan Fold Belt (LFB I-types, representative samples from Chappell and White, 1992). See also figure 7.3.

The Coastal Batholith can be summarised as containing the following features (from Pitcher et al., 1985 and references therein):

1) Chemically the Trujillo, Lima and Arequipa segments of the Coastal Batholith consistently show low K_2O, LREE, Ti and K_2O/Na_2O values over a range of SiO_2 levels (eg, figures 7.3, 7.6). These differences may be partially inherited from the continental crust into which each magmatic event was intruding, however the general trends from a large number of regions in the Andes (~700 km of strike length) suggest such features reflect large scale processes, and not local plutonic variations. 2) A weak silica bimodality is observed in the Coastal Batholith, however a proportionately significant amount of intermediate magmatism is observed (Pitcher et al., 1985). 3) The Coastal Batholith is dominantly calc-alkaline in character. 4) Considerable chemical and isotopic variation is observed both along the total strike length of the Coastal Batholith (Pitcher et al., 1985), and within the individual segments of the batholith (typically several hundred kilometres long). 5) Individual segments are composed of numerous plutons. 6) Magmatism is composite and commonly episodic over an extended period of time (of the order of ~80 Ma) in each of the batholith segments. 7) Mukasa and Tilton (in Pitcher et al., 1985) note crustal contamination varies discretely along strike length. 8) Magmatism has taken place in an active, generally convergent tectonic setting.

7.4 The record of crustal growth in modern and ancient terrains

One of the underlying themes of the introductory chapters has been that of the relationship between the formation, preservation and ultimately destruction of continental crust and tectonic setting. On geochemical, structural and geochronological grounds outlined in sections 7.2 and 7.3, there is an indication that not all features observed in Proterozoic terrains such as the Lincoln Batholith and its potential correlatives in northern Australia, may be described by a simple uniformitarian/plate tectonic analogue. The following section describes the broad scale crustal evolution of Proterozoic terrains from an isotopic and crustal growth perspective, with a view to investigating whether processes pertaining to crustal growth have varied over time.

The relationship between the depleted mantle model age (T_{DM}) and stratigraphic age for a given lithology gives some indication as to the relative contributions old and new crust to the generation of an intrusive. This becomes particularly powerful on the terrain scale when evaluating the timing of relative contributions to crustal formation in a terrain. Hence, those terrains forming new crust directly from the depleted mantle will have T_{DM}'s close to their magmatic ages, whereas those involving greater amounts of crustal reworking will contain substantially older T_{DM} values. It is important to note that T_{DM} ages in ancient felsic rocks rarely reflect the "true" age of extraction of this material from the mantle.

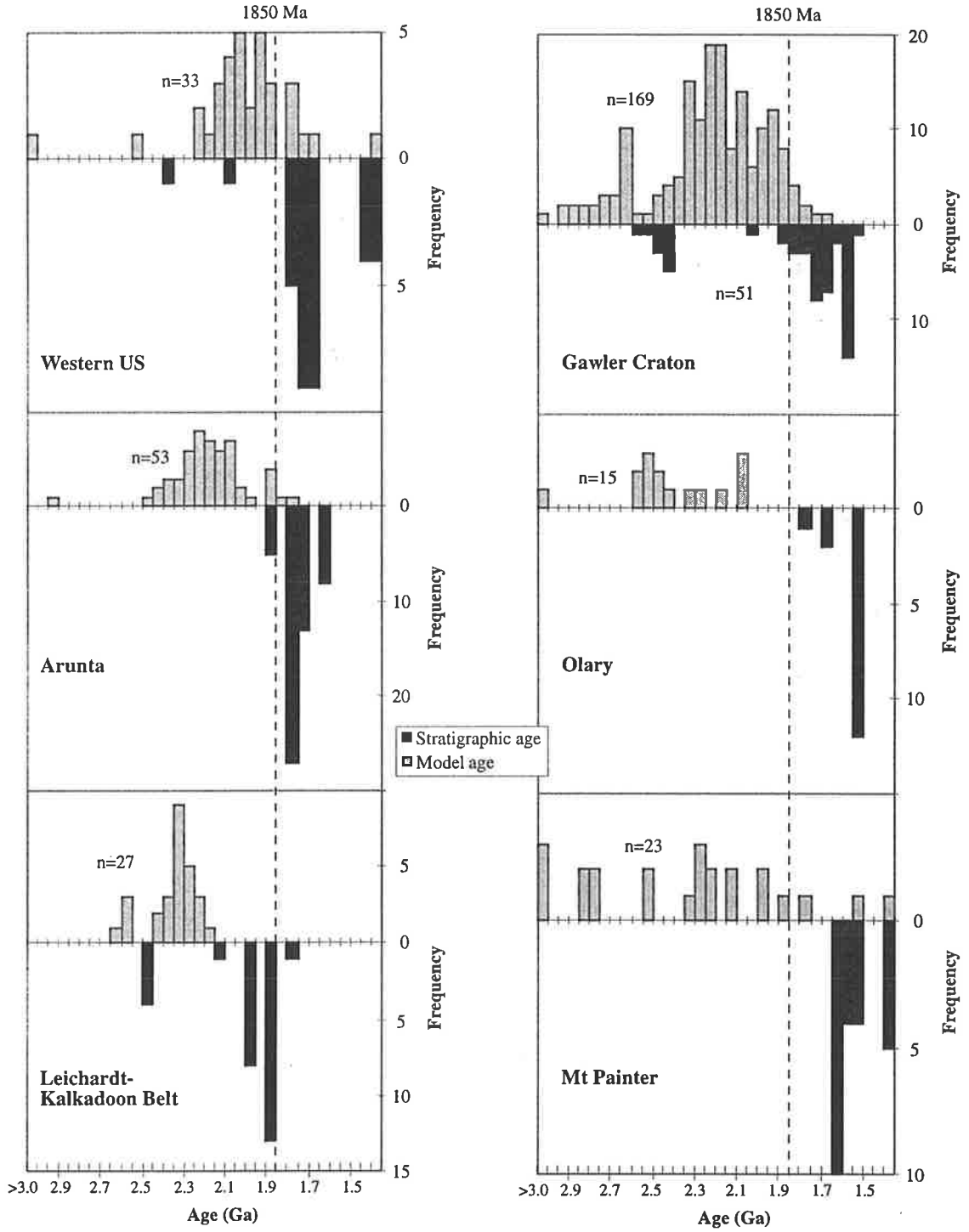

Figure 7.7: Comparison of stratigraphic age distribution and depleted mantle model age for six Proterozoic terrains. Western US data from Bennett and DePaolo (1987, corrected to $^{146}Nd/^{144}Nd = 0.7219$), Arunta data from Zhao (1992) and Foden et al. (1995); Leichardt - Kalkadoon Block data from McDonald et al. (1997). Data for South Australian terrains compiled from Turner et al. (1993), Creaser (1995) and unpublished University of Adelaide theses (Schaefer, 1993; Bendall, 1994; Benton, 1994; Stewart, 1994; Freeman, 1995; Neumann, 1996; Dove, 1997, and Knight, 1997). n= number of analyses. Multiple stratigraphic determinations on repeatedly sampled Gawler Craton lithologies have been excluded.

This is due in part to the dependency of the calculation on which particular depleted mantle is being modelled, but more significantly to the interaction of mantle material with contemporary crust. T_{DM} ages in the following discussion are therefore not regarded as "absolute" ages, but rather as the average time at which material comprising the lithologies in question was extracted from the mantle (eg, see Arndt and Goldstein, 1987).

Notwithstanding, the distribution of T_{DM} values with respect to tectonothermal events within a terrain offers insights into the relative timing of crustal growth in that terrain. Figure 7.7 portrays T_{DM} and stratigraphic age data from six Palaeo-Mesoproterozoic terrains. The most overwhelming feature of figure 7.7 is the trend towards significantly older T_{DM} ages than stratigraphic ages within the same terrain; typically of the order of hundreds of millions of years.

Such features are also expressed in initial Nd isotopic signatures. Figure 7.8 compares initial ε_{Nd} values for various tectonic domains and orogenic belts throughout the history of the Earth. Those terrains with high initial ε_{Nd} values also typically contain T_{DM} values which are correspondingly closer to their stratigraphic ages. Therefore, it becomes immediately apparent that juvenile terrains such as the Grenville, Canadian Cordillera, Nubian Shield and Arabian Shield contain a strong depleted mantle derived component. By contrast, the Himalayas, Hercinides and Caledonides preserve large amounts of crustal recycling, reflecting the role of continental crust in orogenesis in these settings.

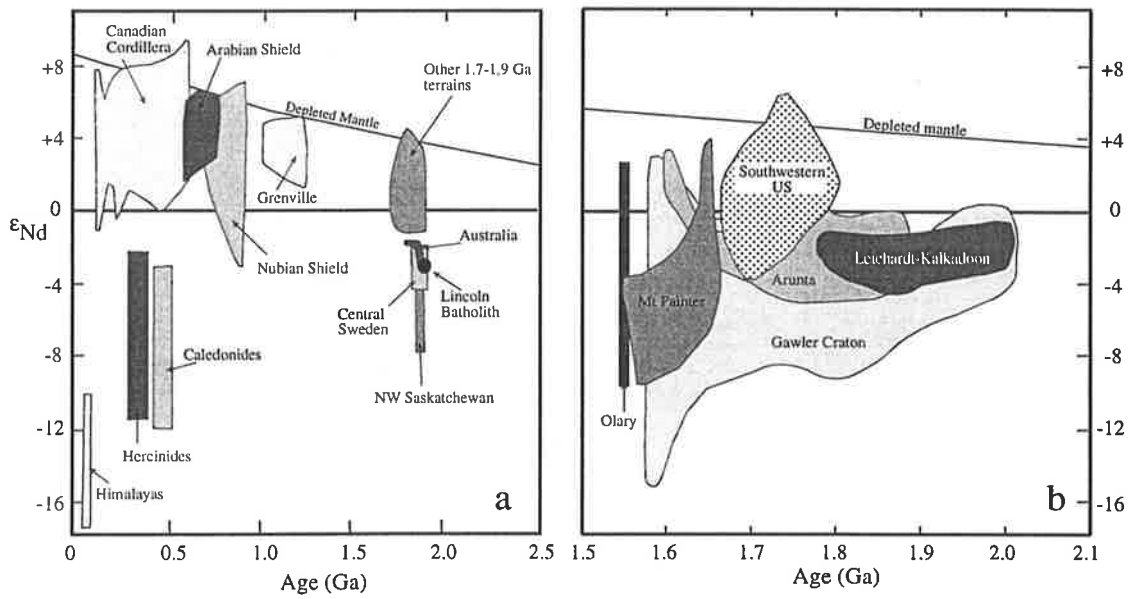

Figure 7.8: Comparison of initial Nd isotopic signatures for modern and ancient orogenies and magmatic events. a) Comparison of ancient and modern terrains (adapted from Samson and Patchett (1991)). b) Enlarged portion of figure 7.8a displaying fields for terrains depicted in figure 7.7.

Such a dichotomy exists for Meso-Palaeoproterozoic terrains as well (figure 7.8b), with the south-western United States tending towards depleted mantle signatures, and Central Sweden, northwest Saskatchewan and Australian Proterozoic terrains preserving more evolved signatures. Samson and Patchett (1991) argued that the presence of high initial ε_{Nd} values implied the accretion of crustal material by the assembly of juvenile crustal blocks, as in the case of the Canadian Cordillera. The presence of comparatively ε_{Nd} negative Proterozoic terrains is ascribed by Samson and Patchett (1991) to proximity of Archaean crust or craton derived sediment, in a manner analogous to the Himalayan Orogen of the modern Earth. However, such an analogy breaks down when considering crustal growth in relatively inactive tectonic settings, such as the Lincoln Batholith, as opposed to active tectonic settings (such as plate margins or orogenic belts). Whereas the Himalayan Orogenic belt (and indeed other ε_{Nd} negative examples illustrated on figure 7.8a for the Phanerozoic) are related to convergent orogenesis, the Gawler Craton at ~1850 and ~1600 Ma experienced minimal orogenic activity, yet was still the site of large volumes of magmatic activity and addition of material to the continental crust (figure 7.7). It therefore seems inappropriate to immediately assume all low ε_{Nd} terrains are of orogenic nature. Their Nd isotopic signature clearly shows involvement of significant volumes of continental crust, however this does not imply convergence, or indeed plate marginal tectonism.

Therefore, the Nd isotopic record of the continental crust contains several important constraints on crustal growth, and associated tectonism. Firstly, there is evidence throughout Earths history for the addition of juvenile material to the continental crust at times of orogenesis. Such processes are typically (but not exclusively) ascribed to lateral continental growth at plate margins (eg, Samson and Patchett, 1991; Myers et al., 1996; McDonald et al., 1997). Additionally, convergent orogenesis on the modern Earth can produce belts of extensively recycled continental crust, such as the Himalayas, and some Proterozoic terrains, such as north-west Saskatchewan and central Sweden. Indeed, the early portions of the syn-Kimban Moody Suite, would be expected to be of this type. However, there are substantial volumes of Proterozoic magmatism, such as the Lincoln Batholith, which show some evidence of crustal recycling, but also contain significant volumes of material derived from the mantle. Such events are responsible for the growth of continental crust by the transfer of material in a vertical sense, and are typically found in anorogenic or weakly extensional settings. This contrasts with high ε_{Nd} Proterozoic provinces, such as the south-western United States, which are likely to be analogues of the Canadian Cordillera and or Coastal Batholith of Peru, located in convergent plate margins.

7.5 Discussion and conclusions

Whether considering the extended Lincoln-Mount Isa magmatic system, or the individual Lincoln Batholith, it is clear that a simple extrapolation of a continental arc setting, such as the Andes or the Canadian Cordillera, to the Lincoln Batholith is inappropriate. Regardless of scale, the homogeneous nature of the Lincoln Batholith (and the Ewen and Kalkadoon in the extended system) is immediately distinctive from modern plate margin settings. Relatively minor amounts of (probably extensional) deformation during and immediately after Lincoln Batholith emplacement contrasts markedly with active convergent tectonism in an Andean setting. So too does the brief timescale over which the whole magmatic event took place (a maximum of ~10 Ma), and the apparently well mixed and evenly distributed crustal contamination in the Lincoln Batholith. Further, isotopic signatures preserved in juvenile, active settings are distinctive from the Nd isotopic evolution of large volume, essentially anorogenic Proterozoic magmatic events. This isotopic signature is effectively a record of crustal growth in a given terrain, and varies significantly with tectonic setting. Therefore, it would seem inappropriate to ascribe large volume linear magmatic belts of the Lincoln Batholith type (and hence analogous Roxby Downs and Mount Isa magmatic events) to modern style continental arc processes.

Other Palaeoproterozoic terrains which display a close temporal association with convergent orogenesis and/or tectonism, such as the Great Bear magmatic zone and Torngat Orogen, display some or all of the characteristics of Andean style plate margins. Additionally, such terrains preserve elevated ε_{Nd} signatures, in keeping with Cordilleran or Andean style crustal growth processes. This clearly indicates an apparent dichotomy in style of magmatism on the Palaeoproterozoic Earth, with both contributing to the net growth of continental crust.

CHAPTER EIGHT

Insights into Proterozoic tectonics from the southern Eyre Peninsula

8.1 Introduction

The purpose of the preceding chapters has been to establish a framework upon which to construct a tectonic evolution for the southern Eyre Peninsula, and investigate the consequences of such a tectonic evolution in terms of global geodynamics. Therefore, this chapter comprises two distinct portions; firstly the regional scale, in which local observations are drawn together into a tectonomagmatic model, and secondly the applicability of such a model to terrains globally. In so doing, it is hoped that an appreciation is gained as to the relevance of regional scale geochemical studies to global geodynamic problems.

8.2 A tectonic model for the Palaeoproterozoic of southern Eyre Peninsula

Figure 8.1 is a cartoon summarising broad tectonic features of the Palaeoproterozoic on southern Eyre Peninsula. In detail, this model involves:

~2000 Ma: The Miltalie event, interpreted by Fanning (1997) to represent the juxtaposition of deeper crustal level Sleaford Complex (the Carnot Gneisses) with their lower grade equivalents (eg, the Wangary Gneiss), culminates in gradual lithospheric extension. Strain rates are generally quite low. This scenario continues throughout Hutchison Group sedimentation, with the Kalinjala Shear Zone forming as an extensional feature and to some extent controlling sedimentation.

Decompressive melting of enriched sub-continental lithospheric mantle at ~1850 Ma produces the Lincoln Batholith. The chemical and isotopic homogeneity of magmatism is a reflection of the extensional regime into which it was emplaced, allowing thorough assimilation of ~20-30% contemporary crust. The remainder of the Batholith represents the addition of new material to the crust from either the

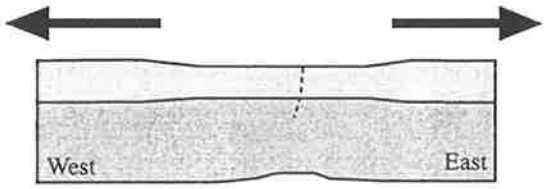

Figure 8.1: Schematic tectonic evolution for the Palaeoproterozoic of southern Eyre Peninsula

~2000 Ma
Slow extension following cessation of Miltalie "event'

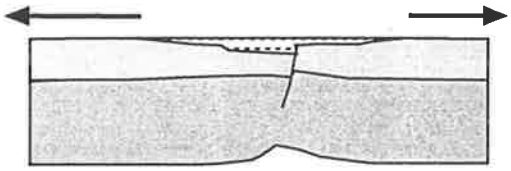

2000-1900 Ma
Hutchison Group sedimentation, thickening of sequence adjacent proto Kalinjala Shear Zone

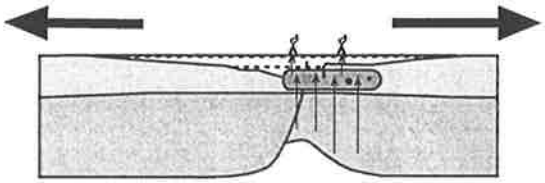

~1850 Ma
Rapid increase in rate of extension drives decompressive melting of the lithospheric mantle producing the Bosanquet Volcanics and Lincoln Batholith. Asthenospheric mantle upwells to accomodate thinned lithospheric mantle

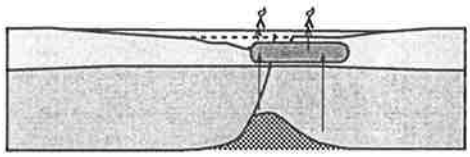

~1845 Ma
Lincoln Batholith magmatism wanes, asthenospheric mantle begins cooling. Extension has ceased.

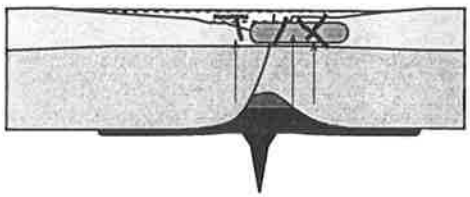

~1815 Ma
Plume impinges upon the base of the lithosphere and is focussed into previously weakened zone of asthenospheric upwelling. Tournefort Dykes generated from both refractory SCLM after Lincoln Batholith generation and asthenospheric sources which have mixed with SCLM.

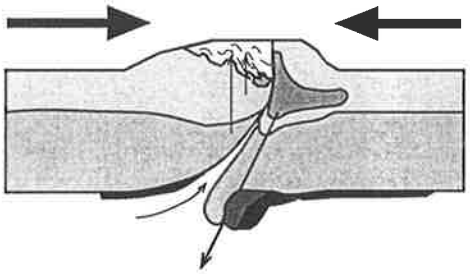

~1750 Ma
Delamination of cold asthenospheric and plume derived material. Compressive orogenesis driven by such removal. Upwelling asthenosphere on the western side of the Kalinjala provides heat source for Moody Suite, which becomes more mafic as the orogeny progresses and asthenosphere rises further. Crust on the eastern side of the Kalinjala is cycled to deeper levels due to attachment with the delaminating lithosphere

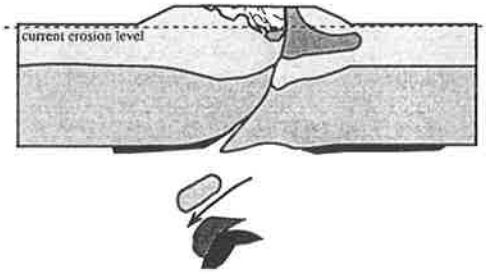

~1700 Ma
Complete removal of asthenospheric block causes remaining lithospheric mantle to rebound, effectively expelling asthenosphere and closing the gap between the two lithospheric blocks.

depleted mantle (eg, the Jussieu Dykes) or the mantle lithosphere. The Bosanquet Formation is the surface expression of this magmatic event, with D1 deformation in the Hutchison Group consisting of an extensional, layer parallel schistosity and sub horizontal fabrics in the Lincoln Batholith. Cooling of upwelling asthenosphere is interrupted at ~1815 Ma by the impingement of a mantle plume. Tournefort Dykes are generated by melting of thermally perturbed lithospheric mantle, and also from asthenospheric melts taking on chemical characteristics of the lithospheric mantle.

Continued cooling of asthenospheric material from both the Tournefort plume and upwelling mantle ultimately produces a gravitationally unstable block which returns to the convecting mantle. Delamination of this material drives compressive orogenesis and brings thermally perturbed asthenosphere beneath the Hutchison Group. Moody Suite magmatism forms in response to increasing thermal perturbation during orogenesis, with early S-type magmatism giving way to increasingly lower crustal and ultimately, mantle derived magmatism (eg, the Coonta Gabbro). Crustal thickening is greatest on the eastern side of the Kalinjala Shear Zone due to the asymmetric distribution of delaminating asthenospheric material. Complete detachment of negatively buoyant frozen asthenosphere results in rapid uplift of remaining lithospheric mantle material, abruptly insulating the thermal source for Moody Suite magmatism. Transpression may be a response to the asymmetric distribution of the delaminating block along the strike length of the orogen.

Post Kimban perturbations along the Kalinjala Shear Zone have been recorded in Ar-Ar work by Foster and Ehlers (1995, 1998). This is likely to be a response to crustal scale accommodation of the Gawler Range Volcanics and Hiltaba Suite Granitoids at ~1600-1575 Ma. The final magmatic event on southern Eyre Peninsula, the A-type Spilsby Suite, has an uncertain petrogenetic source, however in the absence of further deformational events at the time of emplacement, a within plate, anorogenic setting is implied. Sm-Nd isotopic studies would further constrain the origin and evolution of the Spilsby Suite.

Several points pertaining to the model outlined above are worthy of further discussion. Firstly, with the exception of the initiation of extension, the model is largely self contained. All that is required is prolonged extension at low strain rates to act upon an enriched lithospheric mantle in order to ultimately produce Lincoln Batholith style magmatism. The comparatively unusual feature of having volcanic magmatism near the top of the sequence in the Hutchison Group (as opposed to near the base, as is typically the case in rift settings) is a reflection of the low strain rates. Decompressive melting, when it finally took place, was a comparatively subdued event allowing extended magmatic chemical evolution and isotopic mixing within the extensional environment. Indeed, the crystallisation of large volumes of felsic magma

in mid-crustal regions may have acted to slow and ultimately stop extension at this time.

The arrival of a plume ~40 Ma later is entirely coincidental, and need not have been necessary for driving the Kimban Orogeny. However, the combined lithospheric keel of cold asthenosphere and plume material greatly enhanced the potential for delamination and hence the Kimba Orogeny.

Finally, the model outlined above is readily testable. Implicit within it is that the Bosanquet Formation should contain similar Nd isotopic signatures to the Lincoln Batholith (provided further mixing with upper crustal sequences prior to eruption has not taken place), and the Moody Suite magmatism should show a progressive trend towards depleted mantle signatures with younger plutons (particularly the intermediate to mafic members). A combined geochronological and Nd isotopic study would readily constrain this. Additionally, an appreciation for the petrogenesis of the Spilsby Suite would further constrain the evolution of the crust and lithospheric mantle in the immediate post-Palaeoproterozoic on southern Eyre Peninsula. Finally, Tournefort magmatism could be further constrained by Re-Os studies, and the Lincoln Batholith-Moody Suite-lithospheric mantle evolution further constrained by combined Lu-Hf and Sm-Nd studies.

The model presented above is intracratonic, and provides a mechanism for substantial volumes of crustal growth due to vertical transfer of material from the mantle to the crust, rather than lateral growth which dominates modern processes. Additionally, subsequent orogenesis (the Kimban) is driven by processes contained within the regional tectonic setting, and not necessarily by far field stresses.

8.3 Constraints on Proterozoic tectonics from the southern Eyre Peninsula

The tectonic evolution of southern Eyre Peninsula offers some crucial insights into the geodynamic nature of the Earth during the Palaeoproterozoic. Whilst processes involving extension, sedimentation and decompressive melting are clearly uniformitarian, the generation of large volume, homogeneous, LREE enriched magmatism with transitional A-type affinities in an intracontinental setting have no immediate modern Earth analogues. The presence of long lived continental lithospheric mantle reservoirs is attested to by the Nd isotopic signatures of portions of the Tournefort Dykes, while the presence of the dykes themselves indicate extension and plume activity during this period of Earth evolution.

Significantly, the driving mechanism for orogenesis on southern Eyre Peninsula is itself not controlled by far field stresses, but follows as a natural consequence of the interplay between cooling of upwelling asthenosphere and mantle plume material.

All such features form a stark counterpoint to magmatism and deformation of similar age which may be viewed in terms of modern day analogues, such as the

Torngat Orogen. These settings are dominated by plate margin processes, and are considered analogous to Andean style magmatism and tectonism. On the other hand, the Lincoln Batholith is not the sole example of intracratonic nonuniformitarian processes acting during the Proterozoic. Other terrains from northern Australia, such as Mount Isa, contain a similar record of style and chemistry of magmatism to the Lincoln Batholith.

Therefore, the Palaeoproterozoic Earth may be viewed as growing crust in two distinctly different tectonic settings, both plate margin and intracratonic (figure 8.2). However, intracontinental crustal growth from the southern Eyre Peninsula acted in a form unique to modern within-plate settings, and in so doing set the stage for subsequent (Kimban) orogenesis.

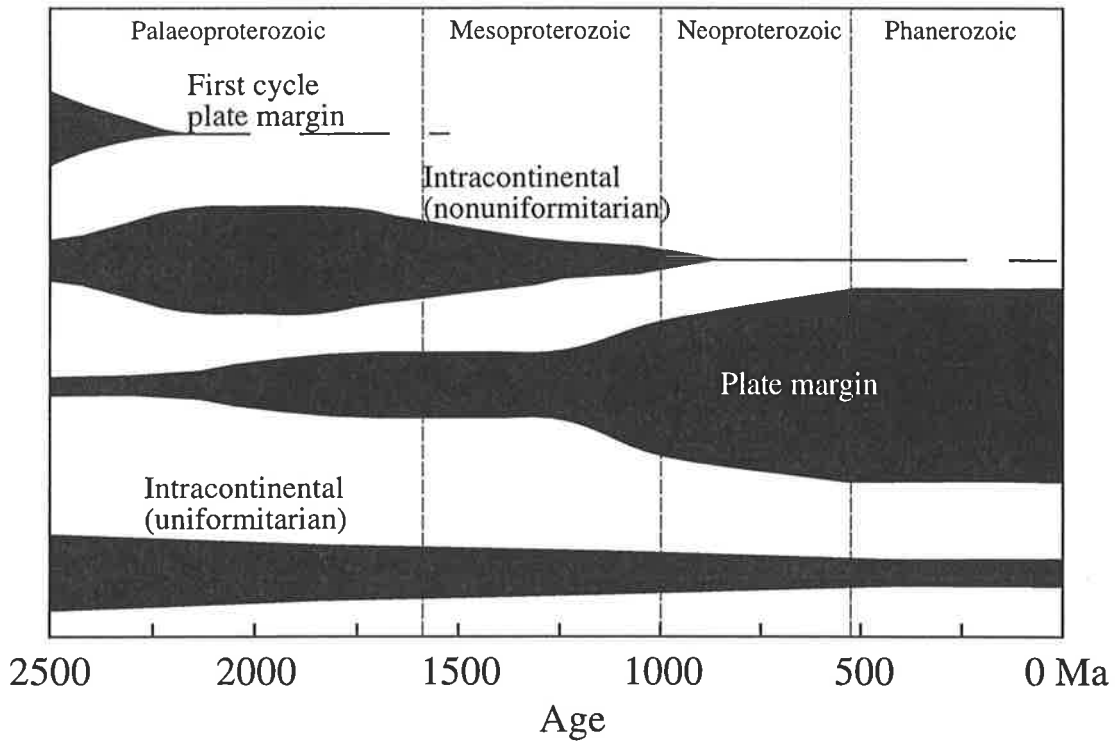

Figure 8.2: Schematic representation of competing modes of crustal growth on the post-Archaean Earth. Plate margin processes are those pertaining to modern plate tectonic analogues; first cycle plate margins are those analogous to Taylor and McLennan (1995) (see figure 1.3), whereby uniformitarian processes produce distinctly different features. Intracontinental (nonuniformitarian) processes are those typified by voluminous Proterozoic ensialic magmatism, such as the Lincoln Batholith, Mt Isa and Hiltaba Suite magmatism, as opposed to those intracratonic processes acting today. Plate margin processes have come to dominate since the Neoproterozoic.

The similarity in large scale chemistry and geometry of terrains such as southern Eyre Peninsula and Mount Isa suggests the existence of Palaeoproterozoic

tectonic processes which are not only unique, but significant in terms of volume and rate of crustal growth. The Palaeoproterozoic record contains evidence of the relative motion of crustal blocks in order to apply far field extensional stresses and juxtapose terrains of different character. This is clearly significant for generating the uniformitarian features observed on the Palaeoproterozoic Earth, however it appears to be superimposed on additional processes which are nonuniformitarian in nature. Therefore, the evolution of tectonism and continental growth has involved the interplay of competing geodynamic modes over the course of the history of the Earth (eg, figure 8.2).

Further, the Palaeoproterozoic crustal evolution of southern Eyre Peninsula suggests that the Earth has been able to develop and maintain long lived heterogeneities in the lithospheric mantle. Additionally, mechanisms of both crustal growth (by melting of enriched lithospheric mantle) and return of crustally contaminated material (through delamination) are conceivable in nonuniformitarian, intracratonic settings. The universal application of plate tectonic paradigms to Proterozoic terrains is therefore inappropriate, and a cautious approach must be adopted when investigating Precambrian terrains.

Therefore, the primary outcome of this study has been that Proterozoic tectonics and crustal growth was dominated by competing processes; those situated on plate margins, and those in intracratonic settings. The Proterozoic Earth differed significantly from the modern Earth in that large volumes of continental growth took place within plates, such as on the southern Eyre Peninsula, and subsequent orogenesis at such sites need not have been driven by far field stresses. Whilst no attempt is made to quantify the relative contributions of such competing processes during the Palaeoproterozoic, it is clear that nonuniformitarian tectonism and crustal growth declined rapidly in significance during the Neoproterozoic, when uniformitarian features came to overwhelmingly dominate the geological record.

References

Allegre, C.J. and Othman, D.B., 1980. Nd-Sr isotopic relationship in granitoid rocks and continental crust development: a chemical approach to orogenesis. *Nature* **286**, p. 335-341.

Allegre, C.J.and Rosseau, D., 1984. The growth of the continents through geological time: studies by Nd analysis of shales. *Earth and Planetary Science Letters.* **67**, p. 19-34.

Anderson, D.L., 1994. Superplumes or supercontinents? *Geology* **22**, p. 39-42.

Armstrong, R.L., 1991. The persistent myth of continental growth. *Australian Journal of Earth Sciences.* **38**, p. 613-630.

Arndt, N.T. and Goldstein, S.L., 1987. The use and abuse of crust-formation ages.*Geology.* 15, p. 893-895.

Arriens, P.A., 1975. Geochronological studies of some Proterozoic rocks in Australia. *In: 1st Australian Geological Convention, Adelaide, 1975. Abstracts. Geological Society of Australia.* p 63.

Baer, A.J., 1983. Proterozoic orogenies and crustal evolution. *Geological Society of America* , **Memoir 161**, p. 47-58.

Bales, 1996. A structural analysis of Wanna, South Australia: The comparative behaviour of mafic dykes and granite during deformation. *Honours Thesis, University of Melbourne. Unpublished.*

Barley, M.E., and Groves, D.I., 1992. Supercontinent cycles and the deposition of metal deposits through time. *Geology,* **20**, p. 291-294.

Bartlett, J.M., Dougherty-Page, J.S., Harris, N.B.W., Hawkesworth, C.J. and Santosh, M., *in press*. The application of zircon evaporation and model Nd ages tp the interpretation of polymetamorphic terranes: an example from the Proterozoic mobile belt of south India. *Contributions to Mineralogy and Petrology.*

Bendall, B.R., 1994. Metamorphic and geochronological constraints on the Kimban Orogeny, southern Eyre Peninsula. *Univ. Adel. Hons. Thesis. Unpubl.*

Bennett, V.C., Nutman, A.P. and McCulloch, M.T., 1993. Nd isotopic evidence for transient, highly depleted mantle reservoirs in the early history of the Earth. *Earth and Planetary Science Letters.* **119**, p. 299-317.

Benton, R.Y., 1994. A petrological, geochemical and isotopic investigation of granitoids from the Olary Province of South Australia - implications for Proterozoic crustal growth. *University of Adelaide. Honours Thesis. Unpublished.*

Black, L.P., Kinny, P.D. and Sheraton, J.W., 1991. The difficulties of dating mafic dykes: an Antarctic example. *Contributions to Mineralogy and Petrology,* **109**, p.183-194.

Blake, D.H., 1986. Middle Proterozoic evolution of the Mt Isa Inlier, north-western Queensland, Australia: a synthesis. *Transactions of the Geological Society of South Africa,* **89**, p. 253-262.

Bowring, S.A. and Podosek, F.A., 1989. Nd isotopic evidence from Wopmay Orogen for 2.0-2.4 Ga crust in western North America. *Earth and Planetary Science Letters,* **94**, p. 217-230.

Bowring, S.A. and Grotzinger, J.P., 1992. Implications of new chronostratigraphy for tectonic evolution of Wopmay Orogen, northwest Canadian Shield. *American Journal of Science*, **292**, p. 1-20.

Bradley, G.N., 1972. The geochemistry of a medium pressure granulite terrain at southern Eyre Peninsula, Australia. *Australian National University Ph. D. Thesis. Unpublished.*

Cadman, A.C., Tarney, J. and Baragar, W.R.A., 1995. Nature of mantle source contributions and the role of contamination and *in situ* crystallisation in the petrogenesis of Proterozoic mafic dykes and flood basalts, Labrador. *Contributions to Mineralogy and Petrology*, **122**, p. 213-219.

Cadman, A.C., Tarney, J. and Hamilton, M.A., 1997. Petrogenetic relationship between Palaeoproterozoic tholeiitic dykes and associated high Mg noritic dykes, Labrador, Canada. *Precambrian Research*, **82**, p. 63-84.

Carter, S.R., Evenson, N.M., Hamilton, P.J. and O'Nions, R.K., 1978. Neodymium and Strontium isotope evidence for crustal contamination of continental volcanics. *Science* **202**, p. 743-746.

Chappell, B.W. and White, A.J.R., 1992. I- and S-type granites in the Lachlan Fold Belt. *Transactions of the Royal Society of Edinburgh: Earth Sciences*, **83**, p. 1-26.

Coin, C.D.A., 1976. A study of the Precambrian rocks in the vicinity of Tumby Bay, South Australia. *University of Adelaide Ph.D. thesis. Unpublished.*

Compston, W., and Arriens, P.A., 1968. The Precambrian geochronology of Australia. *Canadian Journal of Earth Sciences.* **5**, p. 561-583.

Condie, K.C., 1993. Chemical composition and evolution of the upper continental crust: Contrasting results from surface samples and shales. *Chemical Geology.* **104**, p. 1-37.

Condie, K.C., 1997. Sources of Proterozoic mafic dyke swarms: constraints from Th/Ta and La/Yb ratios. *Precambrian Research*, **81**, p. 3-14.

Connors, K.A. and Page, R.W., 1995. Relationships between magmatism, metamorphism and deformation in the western Mount Isa Inlier, Australia. *Precambrian Research*, **71**, p.131-153.

Cooper, J.A. and Ding, P.Q., 1997. Zircon ages constrain the timing of deformation events in The Granites-Tanami region, northwest Australia. *Australian Journal of Earth Sciences*, **44(6)**, p. 777-788.

Creaser, R.A., 1989. The geology and petrology of Middle Proterozoic felsic mgmatism of the Stuart Shelf, South Australia. *PhD. Thesis, LaTrobe University. Unpublished.*

Creaser, R.A., 1995. Neodymium isotopic constraints for the origin of Mesoproterozoic felsic magmatism, Gawler Craton, South Australia. *Canadian Journal of Earth Sciences*, **32**, p. 460-471.

Creaser, R.A.and Fanning, C.M., 1993. A U-Pb zircon study of the Mesoproterozoic Charleston Granite, Gawler Craton, South Australia. *Australian Journal of Earth Sciences.* **40**, p. 519-526.

Daly, S.J., Fanning, C.M. and Fairclough, M.C., in prep. Tectonic evolution and exploration potential of the Gawler Craton.

Daly, S.J., Benbow, M.C. and Blissett, A.H., 1979. Archaean to Early Proterozoic geology of the northwestern Gawler Craton. *In:* Parker, A.J. (compiler), *Symposium on the Gawler Craton, Adelaide, 1979. Extended abstracts.* Geological Society of Australia (SA Division). p. 16-19.

Davies, G.F., 1992. On the emergence of plate tectonics. *Geology* **20**, p. 963-966.

Davies, G.F., 1993. Conjectures on the thermal and tectonic evolution of the Earth. *Lithos*, **30**, p. 281-289.

DePaolo, D.J., 1981. Trace element and isotopic effects of combined wallrock assimilation and fractional crystallisation. *Earth and Planetary Science Letters* **53**, p. 189-202.

DePaolo, D.J., Linn, A.M. and Schubert, G., 1991. The continental crustal age distribution: Methods of determining mantle separation ages from Sm-Nd isotopic data and application to the Southwestern United States. *Journal of Geophysical Research,* **96**, p. 2071-2088.

DePaolo, D.J., Perry, F.V. and Baldridge, W.S., 1992. Crustal versus mantle sources of granitic magmas: a two-parameter model based on Nd isotopic studies. *Transactions of the Royal Society of Edinburgh: Earth Sciences.* **83**, p. 439-446.

Dewey, J.F. and Windley, B.F., 1981. Growth and differentiation of the continental crust. *Philosophical Transactions of the Royal Society of London,* **A301**, p. 189-206.

Dougherty-Page, J.S. and Foden, J., 1996. A Pb-Pb zircon evaporation date for the Charleston Granite: Comparisons with other zircon geochronology techniques. *Australian Journal of Earth Sciences,* **43(2)**, p. 133-137.

Dove, M.B., 1997. The geology, petrology, geochemistry and isotope geology of the eastern St Peter Suite, western Gawler Craton, South Australia. *University of Adelaide. Honours Thesis. Unpublished.*

Drexel, J.F., Preiss, W.V. and Parker, A.J. (eds), 1993. The Geology of South Australia. Vol. 1. The Precambrian. *South Aust. Geol. Surv. Bull.* **54**.

Ellis, D.J., 1992. Precambrian tectonics and the physiochemical evolution of the continental crust. II. Lithosphere delamination and ensialic orogeny. *Precambrian Research.* **55**, p. 507-524.

Ellis, D.J. and Wyborn, L.A.I., 1984. Petrology and geochemistry of Proterozoic dolerites from the Mount Isa Inlier. *BMR Journal of Australian Geology and* Geophysics. **9**, p. 19-32.

Ellis, D.J. and Maboko, M.A.H., 1992. Precambrian tectonics and the physiochemical evolution of the continental crust. I. The gabbro-eclogite transition revisited. *Precambrian Research.* **55**, p. 491-506.

Erlank, A.J., Waters, F.G., Hawkesworth, C.J., Haggerty, S.E., Allsopp, H.L., Rickard, R.S. and Menzies, M.A., 1987. Evidence for mantle metasomatism in preidotite nodules from the Kimberly pipes, South Africa. In: Menzies, M.A. and Hawkesworth, C.J. (eds), *Mantle Metasomatism.* Geological Series, Academic Press, New York. p.221-312.

Ermanovics, I., and Van Kanendonk, 1990. The Torngat Orogen in in the North River-Nutak transect area of Nain and Churchill provinces. *Geoscience Canada,* **17**, p. 279-283.

Etheridge, M.A., Rutland, R.W.R and Wyborn, L.A.I., 1987. Orogenesis and tectonic process in the early to middle Proterozoic of northern Australia. *In*: Proterozoic Lithospheric Evolution, *Am. Geophys. Union Geodyn. Ser.*, **17**, p. 131-147.

Fahrig, W.F., 1987. The tectonic settings of continental mafic dyke swarms: failed arm and passive margin. *Geological Association of Canada, Special Papers*, **34**, 331-348.

Fanning, C.M., 1975. Petrology, structure and geochronolgy of some high grade metamorphic rocks at Fishery Bay and Cape Carnot, southern Eyre Peninsula. *Univ. Adel. Hon. Thesis. Unpublished.*

Fanning, C.M., 1984. Rb-Sr geochronology of a pegmatite intrusive into the Kalinjala Mylonite Zone. *Amdel Report*, GS6102/84. *Unpublished.*

Fanning, C.M., 1997. Geochronological synthesis of southern Australia. Part II. The Gawler Craton. *South Australia. Department of Mines and Energy. Open file envelope, 8918. Unpublished.*

Fanning, C.M., and Mortimer, G.E., *in prep.* SHRIMP and ID TIMS U-Pb zircon dating of the Donington Granitoid Suite, southern Eyre Peninsula, South Australia.

Fanning, C.M., Flint, R.B., Parker, A.J., Ludwig, K.R. and Blissett, A.H., 1988. Refined Proterozoic evolution of the Gawler Craton, South Australia, through U-Pb zircon geochronology. *Precambrian Research.* **40/41**, p. 363-386.

Fanning, C.M., Daly, S.J., Bennett, V.C., Menot, R.P., Peucat, J.J. and Oliver, R.L., 1995. The "Mawson Block": once contiguous Archean to Proterozoic crust in the East Antarctic Shield and Gawler Craton, Australia. *7th International Symposium on Antarctic Earth Scienecs, Siena. Extended Abstracts.*

Fanning, C.M., Moore, D.H., Bennett, V.C. and Daly, S.J., 1996. The "Mawson Continent": Archaean to Proterozoic crust in the East Antarctic Shield and Gawler Craton, Australia. A cornerstone in Rodinia and Gondwanaland.*Geological Society of Australia, Abstracts.* **41**, p. 135.

Flint, R.B.and Rankin, L.R., 1991. The St Francis Granite of the southwestern Gawler Craton. *South Australia Geological Survey. Quarterly Geological Notes.* **119**, p. 17-24.

Flint, R.B., Fanning, C.M. and Rankin, L.R., 1988. Carappee granite of the central Eyre Peninsula. *South Australia. Geological Survey. Quarterly Geological Notes* p. 2-6.

Flint, R.B., Rankin, L.R. and Fanning, C.M., 1990. Definition- the Palaeoproterozoic St Peter Suite of the western Gawler Craton. *South Australia Geological Survey. Quarterly Geological Notes.* **114**, p. 2-8.

Foden, J.D., Buick, I.S. and Mortimer, G.E., 1988. The petrology and geochemistry of granitic gneisses from the east Arunta Inlier, Central Australia: Implications for Proterozoic crustal development. *Precambrian Research.* **40/41**, p. 233-259.

Foster, D.A. and Ehlers, K., 1995. The Mesoproterozoic and Neoproterozoic thermal and tectonic history of the southern Gawler Craton: constraints from $^{40}Ar/^{39}Ar$ geochronology. *Geological Society of Australia. Abstracts.* **Vol 40**, p 48.

Foster, D.A. and Ehlers, K., 1998. ^{40}Ar-^{39}Ar thermochronology of the southern Gawler Craton, Australia: Implications for Mesoproterozoic and Neoproterozoic tectonics of East Gondwana and Rodinia. *Journal of Geophysical Research.* **103, B5**, p. 10177-10193.

Fowler, T.J., 1994. Sheeted and bulbous pluton intrusion mechanisms of a small granitoid from southeastern Australia: implications for dyke-to-pluton transformation during emplacement. *Tectonophysics.* **234**, p. 197-215.

Freeman, H.S.R, 1995. A geochemical and isotopic study of the mafic and intermediate rocks in the Olary Province, South Australia - magma discrimination and geochronological framework. *University of Adelaide. Honours Thesis. Unpublished.*

Fyfe, W.S., 1978. The evolution of the Earth's crust: modern plate tectonics to hot spot tectonics? *Chemical Geology.* **23**, p. 89-114.

Giddings, J.W. and Embleton, B.J.J., 1976. Precambrian palaeomagnetism in Australia II: Basic dykes from the Gawler Block. *Tectonophysics,* **30**, p. 109-118.

Glen, R.A., Laing, W.P., Parker, A.J. and Rutland, W.R., 1977. Tectonic relationships between the Proterozoic Gawler and Willyama orogenic domains, Australia. *Journal of the Geological Society of Australia.* **24, Pt 3.**, p. 125-150.

Glikson, A.Y., 1983. Geochemical, isotopic and palaeomagnetic tests of early sial-sima patterns: The Precambrian crustal enigma revisited. *Geological Society of America* **Memoir 161**, p. 95-117.

Goellnicht, N.M., Groves, D.I. and McNaughton, N.J. 1991. Late Proterozoic fractioanted granitoids of the mineralised Telfer area, Paterson Province, Western Australia. *Precambrian Research,* **51**, p. 375-391.

Goldstein, S.L., 1988. Decoupled evolution of Nd and Sr isotopes in the continental crust and the mantle. *Nature* **336**, p. 733-738.

Goldstein, S.L., O'Nions, R.K. and Hamilton, P.J., 1984. A Sm-Nd study of atmospheric dusts and particulates from major river systems. *Earth and Planetary Science Letters,* **70**, p. 221-236.

Griffin, W.L., O'Reilly, S.Y. and Stabel, A., 1988. Mantle metsomatism beneath western Victoria, Australia: II. Isotopic geochemistry of Cr-diopside lherzolites and Al-augite pyroxenites. *Geochimica et Cosmochimica Acta,* **52**, p. 449-459.

Grocott, J., Brown, M., Dallmeyer, R.D., Taylor, G.K. and Treloar, P.J., 1994. Mechanisms of continental growth in extensional arcs: An example from the Andean plate-boundary zone. *Geology* **22**, p. 391-394.

Gurnis, M. and Davies, G.F., 1986. Apparent episodic crustal growth arising from a smoothly evolving mantle. *Geology* **14**, p. 396-399.

Hageskov, B., 1997. Geochemistry and tectonic significance of late Gothian mafic dykes in the Østfold-Marstrand belt of S.E. Norway and W. Sweden. *Precambrian Research,* **82**, p. 287-309.

Hand, M., Bendall, B. and Sandiford, M., 1995. Metamorphic evidence for Palaeoproterozoic oblique convergence in the eastern Gawler Craton. *Geological Society of Australia. Abstracts.* **Vol 40**, p 59

Hand, M., Bendall, B. and Sandiford, M., 1996. Metamorphic record of strain partitioning during oblique convergence. *Geological Society of Australia. Abstracts.* **Vol 41**, p 178.

Hand, M., Bendall, B. and Sandiford, M., in prep. Metamorphic and geochronological record of oblique convergence in the Kimban Orogen.

Hawkesworth, C.J. and Gallagher., K., 1993. Mantle hotspots, plumes and regional tectonics as causes of intraplate magmatism. *Terra Nova* **5**, p. 552-559.

Hergt, J.M., Chappell, B.W., McCulloch, M.T., McDougall, I. and Chivas, A.R., 1989. Geochemical and isotopic constraints on the origin of the Jurassic Dolerites of Tasmania. *Journal of Petrology*, **30(4)**, p. 841-883.

Hildebrand, R.S., Hoffman, P.F. and Bowring, S.A., 1987. Tectono-magmatic evolution of the 1.9 Ga Great Bear magmatic zone, Wopmay Orogen, northwestern Canada. *Journal of Volcanology and Geothermal Research*, **32**, p. 99-118.

Hill, R.I., 1993. Mantle plumes and continental tectonics. *Lithos*, **30**, p. 193-206.

Hoek, J.D., 1994. Mafic dykes of the Vestfold Hills, East Antarctica. *University of Utrecht. Ph.D. Thesis. Unpublished.*

Hoek, J.D. and Schaefer, B.F. 1998. The Palaeoproterozoic Kimban mobile belt, Eyre Peninsula: Timing and significance of felsic and mafic magmatism and deformation. *Australian Journal of Earth Sciences.* **45**, p. 305-313.

Hofmann, A.W., 1997. Mantle geochemistry: the message from oceanic volcanism. *Nature.* **385 (16 Jan)**, p. 219-229.

Hopper, D.J. and Collerson, K.D., 1998. Crustal evolution of Early to Mid-Proterozoic basement in the Peake and Denison Ranges, northern South Australia. *Geological Society of Australia. Abstracts.* **Vol 49**, p 213.

Hurley, P.M. and Rand, J.R., 1969. Pre-drift continental nucleii. *Science*, **164**, p. 1229-1242.

Johns, R.K., 1961. Geology and mineral resources of southern Eyre Peninsula. *South Australia. Geological Survey. Bulletin*, **37**.

Kalsbeek, F., 1995. Geochemistry, tectonic setting and poly-orogenic history of Palaeoproterozoic basement rocks from the Caledonian fold belt of North-East Greenland. *Precambrian Research*, **72**, p. 301-315.

Kay, R.W., Mahlburg Kay, S., and Arculus, R.J., 1992. Magma genesis and crustal processing. In: Fountain, D.M., Arculus, R.J., and Kay, R.W. *Continental Lower Crust.* **Developments in Geotectonics 23**, p. 423-445.

Kilpatrick, J.A. and Ellis, D.J., 1992. C-type magmas: igneous charnockites and their extrusive equivalents. *Transactions of the Royal Society Edinburgh. Earth Sciences* **83**, p. 155-164.

Knight, J.M., 1997. Petrogensis of the western St Peter Suite, western Gawler Craton, South Australia - a petrological, geochemical and isotopic investigation. *University of Adelaide. Honours Thesis. Unpublished.*

Kober, B., 1986. Whole grain evaporation for $^{207}Pb/^{206}Pb$-age investigations on single zircons using a double-filament thermal ion source. *Contributions to Mineralogy and Petrology.* **93**, p.482-490.

Kröner, A., 1983. Proterozoic mobile belts compatible with the plate tectonic concept. In: Medaris, Jr., G.L. (ed), *Proterozoic Geology: Selected papersfrom an International Proterozoic Symposium. Geological Society of America.* **Memoir 161**, p. 59-74.

Kröner, A., 1984. Evolution, growth and stabilisation of the Precambrian Lithosphere. In: Pollack, H.N. and Murthy, U.H. (Eds.) *Structure and Evolution of the Continental Lithosphere. Physics and Chemistry of the Earth,* **15**, p. 69-106.

Kuehner, S.M., 1989. Petrology and geochemistry of early Proterozoic high Mg dykes from the Vestfold Hills, Antarctica. In: Crawford, A.J. (ed). *Boninites and related rocks.* Unwin Hyman. London. p. 208-231.

Lanyon, R., Black, L.P. and Seitz, H-M., 1993. U-Pb zircon dating of mafic dykes and its application to the Proterozoic geological history of the Vestfold Hills, East Antarctica. *Contributions to Mineralogy and Petrology.* **115**, p. 184-203.

LeCheminant, A.N. and Heaman, L.M., 1989. Mackenzie igneous events, Canada: Middle Proterozoic hotspot magmatism associated with ocean opening. *Earth and Planetary Science Letters,* **96**, p. 38-48.

Mansfeld, J., 1996. Geological, geochemical and geochronological evidence for a new Palaeoproterozoic terrane in southwestern Sweden. *Precambrian Research,* **77**, p. 91-103.

Mazzucchelli, M., Rivalenti, G., Piccrillo, E.M., Girardi, V.A.V., Civetta, L. and Petrini, R., 1995. Petrology of the Proterozoic mafic dyke swarms of Uruguay and constraints on their mantle source composition. *Precambrian Research,* **74**, p. 177-194

McCulloch, M.T.and Wasserburg, G.J., 1978. Sm-Nd and Rb-Sr chronology of continental crust formation. *Science.* **200**, p. 1003-1011.

McCulloch, M.T.and Chappell, B.W., 1982. Nd isotopic characteristics of S- and I-type granites. *Earth and Planetary Science Letters.* **58**, p. 51-64.

McCulloch, M.T. and Bennett, V.C., 1994. Progressive growth of the Earth's continental crust and depleted mantle: Geochemical constraints. *Geochimica et Cosmochimica Acta,* **58**, p. 4717-4738.

McDonald, G., Collerson, K.D. and Kinny, P.D., 1997. Late Archaean and Early Proterozoic crustal evolution of the Mount Isa Block, northwest Queensland, Australia. *Geology.* **25**, p. 1095-1098.

McKenzie, D., 1984. The generation and compaction of partially molten rock. *Journal of Petrology.* **Vol 25, Part 3**, p 713-765.

McKenzie, D., 1989. Some remarks on the movement of small melt fractions in the mantle. *Earth and Planetary Science Letters.* **95**, p. 53-72.

McKenzie, D.and Bickle, M.J., 1988. The volume and composition of melt generated by extension of the lithosphere. *Journal of Petrology.* **29**, p. 625-679.

McLennan, S.M. and Taylor, S.R., 1982. Geochemical constraints on the growth of the continental crust. *Journal of Geology,* **90**, p. 347-361.

Menzies, M.A., Rogers, N., Tindle, A. and Hawkesworth, C., 1987. Metasomatic and enrichment processes in lithospheric peridotites, an effect of asthenosphere-lithosphere interaction. In: Menzies, M. and Hawkesworth, C. (eds), *Mantle Metasomatism,* p. 313-361. Academic Press, UK.

Moorbath, S., 1977. Ages, isotopes and evolution of Precambrian continental crust. *Chemical Geology.* **20**, p. 151-187.

Moores, E.M., 1986. The Proterozoic ophiolite problem, continental emergence and the Venus connection. *Science.* **234**, p. 65-68.

Moores, E.M., 1993. Neoproterozoic oceanic crustal thinning, emergence of continents, and origin of the Phanerozoic ecosystem: A model. *Geology.* **21**, p. 5-8.

Mortimer, G.E., 1984. Early to Middle Proterozoic, basaltic dykes and associated layered rocks of southeastern Eure Peninsula, South Australia. *Univ. Adel. PhD. Thesis. Unpubl.*

Mortimer, G.E., Cooper, J.A. and Oliver, R.L., 1986. The geochronological and geochemical evolution of the Proterozoic Lincoln Complex, Eyre Peninsula, South Australia. *In:* 8th Australian Geological Convention, Adelaide. *Geological Society of Australia. Abstracts,* **15**, p. 140-141.

Mortimer, G.E., Cooper, J.A. and Oliver, R.L., 1988a. The geochemical evolution of Proterozoic granitoids near Port Lincoln in the Gawler Orogenic Domain of South Australia. *Precambrian Research.* **40/41**, p. 387-406.

Mortimer, G.E., Cooper, J.A. and Oliver, R.L., 1988b. Proterozoic mafic dykes near Port Lincoln, South Australia: Composition, age and origin. *Australian Journal of Earth Sciences,* **35**, p. 93-110.

Mueller, P.A.and Wooden, J.L., 1988. Evidence for Archean subduction and crustal recycling, Wyoming province. *Geology* **16**, p. 871-874.

Nance, W.B.and Taylor, S.R., 1976. Rare earth element patterns and crustal evolution- I. Australian post-Archean sedimentary rocks. *Geochimica et Cosmochimica Acta.* **40**, p. 1539-1551.

Nelson, B.K. and DePaolo, D.J., 1985. Rapid production of contiental crust 1.7 to 1.9 b.y. ago: Nd isotopic evidence from the basement of the North American mid-continent. *Geological Society of America Bulletin,* **96**, p. 746-754.

Neumann, N.L., 1996. Isotopic and geochemical characteristics of the British Empire Granite as indicators of magma provenance and processes of melt generation in the Mount Painter Inlier, South Australia. *University of Adelaide. Honours Thesis. Unpublished.*

O'Brien, H.E., Irving, A.J., McCallum, I.S. and Thirlwall, M.F., 1995. Strontium, neodymium and lead isotopic evidence for the interaction of post-subduction asthenospheric potassic magmas of the Highwood Mountains, Montana, USA, with ancient Wyoming craton lithospheric mantle. *Geochimica et Cosmochimica Acta,* **59**, p. 4539- 4556.

O'Dea, M.G., Lister, G.S., Maccready, T., P.G. Betts, N.H.S. Oliver, Pound, K.S., Huang, W. and Valenta, R.K., 1997. Geodynamic evolution of the Proterozoic Mount Isa terrain. *In:* Burg, J.-P, and Ford, M. (eds) *Orogeny through time.* **Geological Society Special Publication 121**, p. 99-122.

Oliver, R.L., Cooper, J.A. and Truelove, A.J., Petrology and zircon geochronology of Herring Island and Commonwealth Bay and evidence for Gondwana reconstruction.

O'Nions, R.K.and McKenzie, D.P., 1988. Melting and continent generation. *Earth and Planetary Science Letters.* **90**, p. 449-456.

O'Nions, R.K., Evensen, N.M. and Hamilton, P.J., 1979. Geochemical modelling of mantle differentiation and crustal growth. *Journal of Geophysical Research,* **84**, p. 6091-6101.

O'Reilly, S.Y. and Griffin, W.L., 1988. Mantle metasomatism beneath western Victoria, Australia: I. Metasomatic processes in Cr-diopside lherzolites. *Geochimica et Cosmochimica Acta,* **52**, p. 433-447.

Oussa, S., 1993. Description of a granultie facies shear zone (Kalinjala Mylonite Zone), and inferred cooling rates following granulite facies metamorphism.*Honours Thesis, University of Melbourne, Unpublished.*

Page, R.W., 1998. Links between Easter and Western Fold Belts in the Mount Isa Inlier, based on SHRIMP U-Pb studies. *Geological Society of Australia. Abstracts.* **Vol 49**, p 349.

Park, R.G., 1997. Early Precambrian plate tectonics. *South African Journal of Geology.* **100(1)**, p. 23-35.

Parker A.J., 1978. Structural, stratigraphic and metamorphic geology of Lower Proterozoic rocks in the Cowell/Cleve district, eastern Eyre Peninsula. *University of Adelaide Ph. D. thesis. Unpublished.*

Parker, A.J., 1980. The Kalinjala Mylonite Zone, eastern Eyre Peninsula.*Geological Survey. South Australia. Quarterly Geological Notes.* **76**, p. 6-11.

Parker, A.J., 1990. Gawler Craton and Stuart Shelf- Regional geology and mineralisation. In: Hughes, F.E. (Ed), *Geology of the mineral deposits of Australia and Papua New Guinea.* The Australasian Institute of Mining and Metallurgy: Melbourne. pp. 999-1008.

Parker, A.J., 1993. Kimban Orogeny. *In:* Drexel, J.F., Preiss, W.V. and Parker, A.J. (eds). The Geology of South Australia. Vol. 1. The Precambrian. *South Australian Geological Survey.* **Bulletin 54**.

Parker, A.J. and Lemon, N.M., 1982. Reconstruction of the Early Proterozoic stratigraphy of the Gawler Craton, South Australia. *Geological Society of Australia. Journal,* **29**, p. 221-238.

Parker, A.J., Fanning, C.M., and Flint, R.B., 1985. Geology. *In:* Twidale, C.R., Tyler, M.J. and Davies, M. (Eds.). Natural history of Eyre Peninsula. *Royal Society of South Australia. Occasional Publications,* **4**, p.21-45.

Parker, A.J., Fanning, C.M., Flint, R.B., Martin, A.R. and Rankin, L.R., 1988. Archaean - Early Proterozoic granitoids, metasediments and mylonites of southern Eyre Peninsula, South Australia. *Specialist Group in Tectonics and Structural Geology Field Guide Series, No 2. Geological Society of Australia.*

Patchett, P.J. and Arndt, N.T., 1986. Nd isotopes and tectonics of 1.9-1.7 Ga crustal genesis. *Earth and Planetary Science Letters,* **78**, p. 329-338.

Pearce, J.A., Harris, N.B.W. and Tindle, A.G., 1984. Trace element discrimination diagrams for tectonic interpretation of granitic rocks. *Journal of Petrology* **25**, p. 956-983.

Pitcher, W., 1991. Synplutonic dykes and mafic enclaves. In: Didier, J. and Babarin, B. (eds), *Enclaves and Granite Petrology.* **Developments in Petrology 13**.

Pitcher, W.S., Atherton, M.P., Cobbing, E.J. and Beckinsale, R.D., 1985. Magmatism at a plate edge: the Peruvian Andes. Blackie, London. 328 pp.

Rankin, L.R., Flint, R.B. and Fanning, C.M., 1988. The Bosanquet Formation of the Gawler Craton.*Geological Survey. South Australia. Quarterly Geological Notes.* p. 12-18.

Reymer, A.P.S., and Schubert, G., 1986. Rapid growth of some major segments of continental crust. *Geology*, **14**, p. 299-302.

Rogers, J.J.W., 1984. Evolution of continents. *Tectonophysics* , **105**, p. 55-69.

Rudnick, R.L. and Fountain, D.M., 1995. Nature and composition of the continental crust; a lower crustal perspective. *Reviews of Geophysics.* **33 (3)**, p. 267-309.

Samson, S.D. and Patchett, P.J., 1991. The Canadian Cordillera as a modern analogue of Proterozoic crustal growth. *Australian Journal of Earth* Sciences, 38, p. 595-611.

Schaefer, B.F., 1993. Isotopic and geochemical constraints on Proterozoic crustal growth from the Mt Painter Inlier. *University of Adelaide. Honours Thesis. Unpublished.*

Schaefer, B.F. 1996. Geochemical evolution of magmatism and deformation in the Palaeoproterozoic Lincoln Complex, South Australia: Insights into orogenesis and tectonism during the Proterozoic. *Geological Society of Australia. Abstracts.* **Vol 41**, p 378.

Schaefer, B.F., Hand, M., Bendall, B., Foden, J. and Sandiford, M. 1995. Chronology of magmatism and deformation in the Lincoln Complex; constraints on the Kimban Orogeny. *Geological Society of Australia. Abstracts.* **Vol 40**, p 149.

Schaefer, B.F. Hoek, J.D. and Foden, J. 1997a. Physical and chemical characteristics of the Lincoln Batholith: Aspects of Palaeoproterozoic magmatism and potential analogues. *Geological Society of Australia. Abstracts.* **Vol 45**, p 82-84.

Schaefer, B.F., Foden, J. and Sandiford, M., 1997b. Palaeoproterozoic crustal evolution of the southern Eyre Peninsula, Gawler Craton, Australia. In *Seventh Annual V.M. Goldschmidt Conference,* p. 185, LPI Contribution **No. 921**, Lunar and Planetary Institute, Houston.

Schwarz, M., 1998. The Coonta Gabbro, southern Gawler Craton. *South Australian Geological Survey. MESA Journal.* **9**, p. 34-35.

Shaw, D.M., 1980. Evolutionary tectonics of the Earth in light of early crustal structure.

Simpson, 1994. Constraints on Proterozoic crustal evolution from an isotopic and geochemical study of clastic sediments of the Gawler Craton, S.S. *University of Adelaide, Honours Thesis. Unpublished.*

Smith, R.B. and Braile, L.W, 1994. The Yellowstone hotspot. *Journal of Vulcanology and Geothermal Research.* **61**, p, 121-187.

Song, S., 1994. Geochemical evolution of Phanerozoic Lithospheric mantle beneath S.E. South Australia. *University of Adelaide PhD. Thesis. Unpublished.*

Stewart, K.P., 1994. High temperature felsic volcanism and the role of mantle magmas in Proterozoic crustal growth, the Gawler Range Volcanic Province. *University of Adelaide. Ph.D. Thesis. Unpublished.*

Sun, S.-s. and McDonough, W.F., 1989. Chemical and isotopic systematics of oceanic basalts: implications for mantle composition and processes. In: Saunders, A.D. and Norry, M.J. (eds), *Magmatism in the ocean basins,* **Geological Society Special Publication 42**, p. 313-345.

Sun, S.-s, Nesbitt, R.W. and McCulloch, M.T., 1989. Geochemistry and petrogenesis of Archaean and early Proterozoic siliceous high-magnesian basalts. In: Crawford, A.J. (ed). *Boninites*. p.148-173. Unwin Hyman.

Tarney, J., 1992. Geochemistry and significance of mafic dyke swarms in the Proterozoic. In: Condie, K.C. (ed), *Proterozoic Crustal Evolution*. Elsevier, Amsterdam. p. 151-179.

Tarney, J. and Jones, C.E., 1994. Trace element geochemistry of orogenic igneous rocks and crustal growth models. *Journal of the Geological Society, London,* **151**, p. 855-868.

Taylor, S.R.and McLennan, S.M., 1983. Geochemistry of Early Proterozoic sedimentary rocks and the Archean/Proterozoic boundary. *Geological Society of America,* **Memoir 161**, p. 119-131.

Taylor, S.R.and McLennan, S.M., 1985. *The Continental Crust: Its composition and Evolution*. Blackwells, Oxford, 312pp.

Taylor, S.R.and McLennan, S.M., 1995. The Geochemical evolution of the Continental Crust. *Reviews of Geophysics,* **33(2)**, p. 241-265.

Teasdale, J.P., 1997. Methods for understanding poorly exposed terrains: The interpretative geology and tectonothermal evolution of the western Gawler Craton. *University of Adelaide Ph D. Thesis. Unpublished.*

Thériault, R.J. and Ermanovics, I., 1997. Sm-Nd isotopic and geochemical characterisation of the Paleoproterozoic Torngat Orogen, Labrador, Canada. *Precambrian Research,* **81**, p. 15-35.

Thompson, R.N.and Gibson, S.A., 1994. Magmatic expression of lithospheric thinning across continental rifts. *Tectonophysics.* **233**, p. 41-68.

Thomson, B.P., 1969. Precambrian crystalline basement. *In:* Parkin, L.W. (Ed.) Handbook of South Australian geology. *Geological Survey of South Australia.* p. 21-48.

Thomson, B.P. (compiler), 1980. Geological map of South Australia. *South Australia. Geological Survey. Maps of South Australia Series, 1:1 000 000.*

Tilley, C.E., 1920. The metamorphism of Precambrian dolomites of Southern Eyre Peninsula, South Australia. *Geological Magazine,* **57**, p. 449-462, 492-500.

Tilley, C.E., 1921a. The graphite rocks of Sleaford Bay, South Australia. *Economic Geology,* **16**, p. 184-198.

Tilley, C.E., 1921b. Precambrian para-gneisses of Southern Eyre Peninsula, South Australia. *Geological Magazine,* **58**, p. 251-259, 305-312.

Tilley, C.E., 1921c.The granite gneisses of Southern Eyre Peninsula (South Australia) and their associated amphibolites. *Quarterly Journal of the Geological Society of London,* **77**, p. 75-134.

Turner, S.P. and Hawkesworth, C.J., 1994. The nature of the sub-continental mantle: constraints from the major-element composition of continental flood basalts. *Chemical Geology,* **120**, p. 295-314.

Turner, S.P., Foden, J.D. and Morrison, R.S., 1992. Derivation of some A-type magmas by fractionation of basaltic magma: An example from the Padthaway Ridge, South Australia. *Lithos* **28**, 151-179.

Turner, S., Foden, J. Sandiford, M. and Bruce, D., 1993. Sm-Nd evidence for the provenance of sediments from the Adelaide Fold Belt and southeastern Australia with implications for episodic crustal addition. *Geochimica et Cosmochimica Acta.* **57**, p. 1837-1856.

Veizer, J.and Jansen, S.I., 1985. Basement and sedimentary recycling - 2: Time dimension to global tectonics. *The Journal of Geology* , **93**, p. 625-643.

Weaver, B.L. and Tarney, J., 1981. The Scourie dyke suite: petrogenesis and geochemical nature of the Proterozoic subcontinental mantle. *Contributions to Mineralogy and Petrology,* **78**, p. 175-188.

Webb, 1980. Geochronology of stratigraphically significant rocks- Amdel progress report 30. *South Australia. Department of Mines and Energy. Open file envelope,* 1689. *Unpublished.*

Webb, A.W., Thomson, B.P., Blissett, A.H., Daly, S.J., Flint, R.B. and Parker, A.J., 1986. Geochronolgy of the Gawler Craton, South Australia. *Australian Journal of Earth Sciences.* **33** p.119-143.

West, G.F., 1980. Formation of continental crust. In: *Continental Crust and its mineral deposits. Geological Association of Canada.* **Special paper 20**, p. 65-73.

Whalen, J.B., Currie, K.L. and Chappell, B.W., 1987. A-type granites: geochemical characteristics, discrimination and petrogenesis. *Contributions to Mineralogy and Petrology,* **95**, p. 407-419.

White, R.and McKenzie, D., 1989. Magmatism at rift zones: The generation of volcanic continental margins and flood basalts. *Journal of Geophysical Research* **94**, p. 7685-7729.

Wilson, I.H., 1987. Geochemistry of Proterozoic volcanics, Mount Isa Inlier, Australia. *In:* Pharoah, T.C., Beckinsale, R.D. and Rickard, D. eds. Geochemistry and mineralisation of Proterozoic Volcanic suites. *Geological Society Special Publication.* **No. 33**, p. 409-423.

Winchester, J.A.and Floyd, P.A., 1977. Geochemical discrimination of different magma series and their differentiation products using immobile elements. *Chemical Geology.* **20**, p. 325-343.

Windley, B.F., 1977. Timing of continental growth and emergence. *Nature (London).* **270** 5636, p. 426-428.

Windley, B.F., 1991. Early Proterozoic collision tectonics, and rapakivi granites as intrusions in an extensional thrust thickened crust: the Ketilidian orogen, south Greenland. *Tectonophysics,* **195**, p. 1-10.

Windley, B.F., 1993. Uniformitarianism today: plate tectonics is the key to the past. *Journal of the Geological Society, London,* **150**, p. 7-19.

Wyborn, L.A.I., 1985. Geochemistry and origin of a major Early Proterozoic felsic igneous event of Northern Australia and evidence for substantial vertical accretion of the crust. From: *Abstracts for the tectonics and geochemistry of Early - Middle Proterozoic fold belts, Darwin. BMR Geology and Geophysics, Record,* **1985/28.**

Wyborn, L.A.I., 1988. Petrology, geochemistry and origin of a major Australian 1880-1840 Ma felsic volcano-plutonic suite: a model for intracontinental felsic magma generation. *Precambrian Research.* **40/41**, p. 37-60.

Wyborn, L.A.I. and Page, R.W., 1983. The Proterozoic Kalkadoon and Ewen Batholiths, Mount Isa Inlier, Queensland: Source, chemistry, age and metamorphism. *Journal of Australian Geology and Geophysics.* **8**, p. 53-69.

Wyborn, L.A.I., Page, R.W. and Parker, A.J., 1987. Geochemical and geochronological signatures in Australian Proterozoic igneous rocks. *In*: Pharoah, T.C., Beckinsale, R.D. and Rickard, D. eds. Geochemistry and mineralisation of Proterozoic Volcanic suites. *Geological Society Special Publication.* **No. 33**, p. 377-394.

Wyborn, L.A.I., Wyborn, D., Warren, R.G. and Drummond B.J., 1992. Proterozoic granite types in Australia: implications for lower crust composition, structure and evolution. *Transactions of the Royal Society of Edinburgh: Earth Sciences,* **83**, p. 201-209.

York, D., 1969. Least squares fitting of a straight line with correlated errors. *Earth and Planetary Science Letters,* **5**, p.320-334.

Young, G.M., 1991. The geologic record of glaciation: Relevance to the climatic history of the Earth. *Geoscience, Canada,* **18**, p. 100-108.

Young, D.N., Ellis, D.J., Zhao, J.X. and McCulloch, M.T., 1996. Petrology of igneous charnockites, Mawson, Antarctica: Granite source provinces as indicators of possible terrain boundaries. *Geological Society of Australia. Abstracts.* **Vol 41**, p. 487.

Young, D.N., Zhao, J.-X., Ellis, D.J. and McCulloch, M.T., 1997. Geochemical and Sr-Nd isotopic mapping of source provinces for the Mawson charnockites, east Antarctica: implications for Proterozoic tectonics and Gondwana reconstruction. *Precambrian research.* **86**, p. 1-19.

Zhao, J.X, 1992. Proterozoic crust-mantle evolution in Central Australia: Geochemical and isotopic constraints. *Australian National University. Ph.D. Thesis. Unpublished.*

Zhao, J.X.and Cooper, J.A., 1992. The Atnarpa Igneous Complex, southeast Arunta Inlier, central Australia: implications for subduction at an Early-Mid Proterozoic continental margin. *Precambrian Research.* **56**, p. 227-253.

Zhao, J.X., and McCulloch, M.T., 1993a. Melting of a subduction modified continental lithospheric mantle: Evidence from Late Proterozoic mafic dike swarms in central Australia. *Geology,* **21**, p. 463-466.

Zhao, J.X. and McCulloch, M.T., 1993b. Sm-Nd isochron ages of Late Proterozoic dyke swarms in Australia: evidence for two distinctive events of mafic magmatism and crustal extension. *Chemical Geology (Isotope Geoscience Section),* **109**, p. 341-354.

Zhao, J.X., McCulloch, M.T. and Bennett, V.C., 1992. Sm-Nd and U-Pb isotopic constraints on the provenance of sediments from the Amadeus basin, central Australia: Evidence for REE fractionation. *Geochimica et Cosmochimica Acta.* **56**, p. 921-940.

Symbols and abbreviations used in text

AFC	Assimilation and fractional crystallisation
AGG/ AFGG	Alkali Feldspar Granite Gneiss
Al	Aluminium
Ar	Argon
Ba	Barium
BIF	Banded Iron Formation
bt	biotite
cpx	clinopyroxene
CRG	Carcase Rock Granite
$\varepsilon_{Nd(i)}$, / $\varepsilon_{Nd(t)}$	Initial epsilon Nd; epsilon Nd at time t
EAGG	Eulitic Alkali Feldspar Granite Gneiss
EM1 & EM2	Enriched asthenospheric mantle reservoirs sampled by plumes
Fe^T & $Fe_2O_3^T$	Total Iron, Total Iron expressed as Ferrous oxide
FeRT	Iron Rich Tholeiite
FGG1	Ferrohypersthene Granite Gneiss 1
FGG2	Ferrohypersthene GraniteGneiss II
Ga	Giga-anna, = 1 billion years
GC-	Prefix of sample supplied by J.D. Hoek
GG1	Granite Gneiss 1
GG2	Granite Gneiss 2
gt	garnet
hb	hornblende
HBaT	High Barium Tholeiite
HFS(E)	High Field Strength (Element)
HMgT	High Magnesium Tholeiite
in prep.	(manuscript) in preparation
JD	Jussieu Dyke(s)
K	Potassium
kbar	kilobar, = 1000x atmospheric pressure
KSZ	Kalinjala Shear Zone
La	Lanthanum
LIL(E)	Large Ion Lithophile (Element)
LREE	Light Rare Earth Element
Mg, mg #	Magnesium, Magnesium number, = (Mg / (Mg+0.8998Fe^T))
MCC	Memory Cove Charnockite
MESA	Mines and Energy, South Australia
Na	Sodium
Nb	Niobium
Nd	Neodymium
Ni	Nickel
N-MORB	"Normal" Mid Ocean Ridge Basalt
OIB	Ocean Island Basalt
opx	orthopyroxene
P	Phosphorus
Pb	Lead
PIRSA	Primary Industries and Resources, South Australia
plag	plagioclase
P-T	Pressure-Temperature conditions of metamorphism
QGNG	Quartz Gabbronorite Gneiss
Rb	Rubidium
REE	Rare Earth Elements
σ	standard deviation
SEP-	Prefix of sample collected by the author
SHRIMP	Sensitive High Resolution Ion Microprobe
Sm	Samarium
Sr	Strontium
ss	sensu stricto
T_{DM}	Depleted mantle model age
Th	Thorium
Ti	Titanium
TTG	Tonalite - Trondjhemite - Granodiorite association
U	Uranium
UT	Unassigned Tholeiites
V	Vanadium
WIG	Williams Island Granite
WPC	West Point Charnockite
Y	Yttrium
Zr	Zirconium

Appendix 1:

Analytical Techniques

Appendix 1: Analytical techniques

Whole Rock chemical analysis:

Samples were trimmed to remove weathered edges and crushed using a jaw crusher. Powders were produced from crushed samples by grinding in a tungsten carbide mill. Major element samples were dried in an oven at 110°C for over two hours to remove the absorbed moisture. They were then weighed into alumina crucibles and ignited overnight in a furnace at 960°, to yield the Loss on Ignition (LOI) values. Nominally 1g of the ignited material was then accurately weighed with nominally 4g of flux (comprising 35.3% lithium tetraborate and 64.7% lithium metaborate). The sample-flux mixture was fused using a propane-oxygen flame, at a temperature of approx. 1150°, using Pt-Au crucibles, and cast into a preheated mould to produce a glass disc suitable for analysis.

The samples were analysed using a Philips PW 1480 Xray Fluorescence Spectrometer, using an analysis program calibrated against several international and local Standard Reference Materials (SRM's). A dual-anode (Sc-Mo) Xray tube was used, operating at 40kV, 75mA.

Iron was analysed as total Fe (combining the ferrous and ferric forms), expressed as Fe_2O_3.

About 5-10g of sample powder (depending on whether Boric Acid is used as a backing) was mixed with nominally 1ml of binder solution (Poly Vinyl Alcohol) and pressed to form a pellet. This was allowed to dry in air and was heated for a further 1 to 2 hours in a 60° oven to ensure that the pellet was completely dry before analysis.

The samples were analysed using a Philips PW 1480 XRF Spectrometer, using several analysis programs covering suites of from 1 to 7 trace elements, with conditions optimised for the elements being analysed. The programs were calibrated against many (30 or more in some cases) local and international SRM's. The dual-anode Sc-Mo tube and a Au tube were used for the analyses. Matrix corrections are made using either the Compton Scatter peak, or mass absorption coefficients calculated from the major element data.

Elements analysed (detection limits [DL] in ppm in brackets - accuracy +/- 5% at 100 x DL):

Sr (1.0), Rb (1.0), Y (1.0), Zr (2.0), Nb (1.5), Pb (2.5), Th (1.5), U (1.5), Ba (3), Sc (2), Ga (2), V (2), Cr (1.5), Ce (5), Nd (3), La (2), Ni (3), Cu (4), Zn (3), Co (2).

Rb-Sr and Sm-Nd isotope analysis:

Approximately 100mg of sample were dissolved in HF by bomb dissolution and converted to chloride using 6M HCl prior to spiking with ^{150}Nd-^{147}Sm tracer. Sr, Nd and Sm were extracted using a two stage cation exchange procedure. Double Ta-Re, Re-Re and single Re filaments were used for the mass spectroscopic analysis of Nd, Sm and Sr respectively, on a Finnigan MAT 261 at the University of Adelaide. Data blocks of ten scans were repetitively collected until acceptable within run statistics were achieved (8-15 blocks for Sr isotopic compositions with a fixed double collector, and 15-25 blocks for Nd isotopic compositions with a single collector). All Sr and Nd isotopic ratios were corrected for mass fractionation by normalisation of $^{88}Sr/^{86}Sr$ to 8.3752 and $^{146}Nd/^{144}Nd$ to 0.7219. All errors are quoted to $2\sigma_{(mean)}$.

The following results were obtained for duplicate samples and standards during the course of this work (numbers in parentheses indicate number of analyses):

Sample	$^{143}Nd/^{144}Nd \pm 2\sigma$	$^{87}Sr/^{86}Sr \pm 2\sigma$
La Jolla	0.511822±16 (3)	
BCR-1	0.512629±39 (3)	0.704976±261 (3)
Tasbas (Adel. Uni internal standard)	0.512923±7 (46)	0.703486±11 (57)
duplicate	0.512920±48	
duplicate	0.512921±32	
Sample SEP-220		0.717462±26
duplicate		0.717420±22

Average total procedural blanks during the course of the analysis were:

Sr 1.7 ng
Nd 600 pg
Sm 745 pg

$^{147}Sm/^{143}Nd$ was calculated from concentrations obtained by isotope dilution on spiked samples run concurrently with isotope composition analyses. $^{87}Rb/^{86}Sr$ was calculated from accurate Rb and Sr analyses obtained by extended XRF routine.

Isotope constants and model parameters used are:

$^{88}Sr/^{86}Sr = 8.3752$

$\lambda_{Rb} = 1.42 \times 10^{-11} y^{-1}$

$^{146}Nd/^{144}Nd = 0.7219$

$\lambda_{Sm} = 6.54 \times 10^{-12} y^{-1}$

$^{147}Sm/^{144}Nd_{CHUR} = 0.1967$

$^{147}Sm/^{144}Nd_{DM} = 0.2137$

$^{143}Nd/^{144}Nd_{CHUR} = 0.512638$

$^{143}Nd/^{144}Nd_{DM} = 0.51316$

Pb-Pb zircon evaporation geochronology:

Zircon analysis conducted in this study broadly followed the technique outlined in Dougherty-Page and Foden, 1996, with advanced data handling techniques outlined in Bartlett et al., in press.

Zircons were extracted from jaw crushed samples by conventional separation techniques, typically involving Wilfley table followed by magnetic and heavy liquid separation. The resulting zircon fraction was then cleaned using double distilled water in an ultrasonic bath. Clear, crack free, whole zircons were then hand picked for analysis.

Selected zircons were loaded by crimping onto Re "evaporation" filament, which was aligned adjacent Re "ionisation" filament. Filaments were then loaded into a Finnigan MAT 261 TIMS at the University of Adelaide. Analysis was conducted by sequentially heating the evaporation filament, causing the embedded zircon to emit Pb and silica, caused by the breakdown of zircon ($ZrSiO_4$) to Baddeleyite (ZrO_2). The silica and Pb are deposited on the opposing (cold) ionisation filament to form an emitter compound. The evaporation filament is then turned off, and the ionisation filament turned up to produce a Pb ion beam. Progressive heating, deposition and measurement steps allows a systematic step-wise extraction of Pb from the rim to core of the zircon in concentric zones.

Prior to analysis, each zircon was conditioned in order to remove surface contamination and metamict (and therefore non-concordant) zircon. Conditioning was conducted by heating the evaporation filament to temperatures just below that which non-metamict zircon breakdown occurs, whilst simultaneously heating the ionisation filament to a high temperature to prevent contamination of unwanted material from the zircon.

Data was collected using the Secondary Electron Multiplier (SEM) by magnetic peak switching from masses in the sequence 206-207-208-207-206-204. Blocks of data comprising 11 complete mass scans per block were collected, of which 10 were used in the age determination. The detection limit of ^{204}Pb was taken to correspond to a $^{206}Pb/^{204}Pb$ ratio of 10^5. All $^{207}Pb/^{206}Pb$ ratios were corrected for common Pb, as measured by $^{204}Pb/^{206}Pb$ ratios during analysis. The resultant common Pb corrected $^{207}Pb/^{206}Pb$ ratios were then used for calculation of the crystallisation age of zircon deposited for that particular heating step. Determinations were conducted only on plateaus in the sequential heating data, implying concordance from one deposition to the next. If successive steps showed significant changes in $^{207}Pb/^{206}Pb$ ratio, they were considered to be discordant and not included in the age determination.

Further resolution of potential populations of zircons is the calculation of a U/Th ratio for a given heating step, using the $^{208}Pb/^{206}Pb$ and the age determined by the process outlined above. This effectively allows zircon populations to be characterised on both their $^{207}Pb/^{206}Pb$ and $^{208}Pb/^{206}Pb$ ratios.

Appendix 2:

Compilation of geochemical data from southern Eyre Peninsula

Lithology	Quartz Gabbronorite Gneiss (QGNG)							West Pt Charnockite		Memory Cove Charnockite (MCC)								
Type	QGNG	QGNG	QGNG	QGNG	QGNG	QGNG	QGNG	charnockite	charnockite	MCC	MCC	MCC	MCC	MCC	MCC	MCC	MCC	MCC
Sample #	B203	B201	B205	B204	B202	SEP-086	SEP-239	SEP-083	SEP-095	SEP-138	B143	SEP-154	SEP-025	B144	B25	SEP-074	SEP-147	SEP-073
Location	*C Donington*	*C Donington*	*C Donington*	*C Donington*	*C Donington*	*C Donington*	*Nth Taylors L*	*W West Point*	*E West Pt*	*Trinity Haven*	*C Colbert*	*CC-Lookout*	*Bolingbroke*	*C Colbert*	*Surfleet Cove*	*Trinity Haven*	*Memory Cove*	*Trinity Haven*
Source	Mortimer, 1984	Mortimer, 1984	Mortimer, 1984	Mortimer, 1984	Mortimer, 1984						Mortimer, 1984			Mortimer, 1984	Mortimer, 1984			
Easting						590750	590640	585800	587460	602450		589500	600700			602205	591020	602205
Northing						6156725	6145380	6127800	6126460	6189889		6127420	6177960			6187005	6129080	6187005
SiO_2%	55.53	55.96	56.41	57.12	57.22	57.67	59.56	62.50	63.50	64.21	65.37	66.11	66.47	66.66	66.68	68.34	68.42	68.78
Al_2O_3%	14.64	14.78	15.09	14.50	14.17	14.49	14.39	15.52	15.53	14.62	14.92	14.96	14.06	14.71	14.90	14.09	14.68	14.35
Fe_2O_3%	10.14	9.93	9.70	9.65	9.63	9.27	8.74	6.14	6.64	6.57	6.09	5.52	5.55	5.38	5.76	6.64	4.08	4.77
MnO%	0.15	0.15	0.15	0.15	0.14	0.13	0.13	0.09	0.08	0.09	0.10	0.07	0.07	0.09	0.08	0.07	0.05	0.07
MgO%	5.91	5.95	5.71	5.58	5.53	5.30	4.34	1.72	1.40	2.59	1.57	1.37	1.19	1.23	1.39	1.40	0.91	0.76
CaO%	6.93	6.94	7.02	6.38	6.29	6.42	6.11	4.58	3.99	4.24	3.37	3.44	2.89	3.06	3.28	2.60	2.57	2.70
Na_2O%	2.38	2.47	2.47	2.55	2.35	2.34	2.66	3.18	3.02	3.68	2.98	2.91	2.60	2.93	2.91	2.47	2.92	2.52
K_2O%	2.20	2.21	2.17	2.52	2.80	2.68	2.20	3.94	4.02	2.15	4.43	4.47	4.75	4.75	4.76	5.38	5.21	4.65
TiO_2%	0.84	0.80	0.75	0.79	0.81	0.82	0.95	0.86	0.85	0.71	0.87	0.81	0.65	0.77	0.81	0.57	0.61	0.57
P_2O_5%	0.22	0.20	0.22	0.20	0.21	0.19	0.25	0.26	0.23	0.13	0.24	0.22	0.14	0.19	0.23	0.13	0.13	0.13
SO_3%						0.01	0.00	0.01	0.01	0.00		0.00	0.01			0.00	0.00	0.01
LOI%	0.33	0.44	0.30	0.33	0.40	0.21	0.30	0.29	0.18	0.38	0.09	-0.06	0.39	0.59	0.30	0.22	0.11	0.25
TOTAL	99.27	99.83	99.99	99.77	99.55	99.52	99.63	99.08	99.44	99.37	100.03	99.82	98.76	100.36	101.10	101.91	99.69	99.55
Rb	97	102	97	130	117	126.4	234.6	148.5	134.5	195.0	201.0	205.9	255.4	223	207	228.7	239.5	221.8
Ba	506	500	522	605	655	680	185	913	919	419	885	902	757	985	878	891	1118	913
Th		8				9.6	43.2	0.5	6.7	24.2	17	16	27.9			11.3	20.2	17.8
U		7.6				2.4	5.4	0.5	1.5	5.5	5	5	5.0			4.2	2.9	4.0
Nb	12	12	10		12	11.9	24.9	19.0	13.0	16.2	17	17	21.3	18		15.1	15.2	16.6
La		38.0	33.1			39	102	46	38	13	58.5	56.0	75			66	55	73
Ce		74.0	67.1			74	197	97	82	33	120.0	117.0	141			131	113	132
Pb		15				17.2	24.4	19.8	20.2	18.8	26	29	32.4			29.4	27.5	31.3
Sr	229	231	240	219	217	238.2	97.5	226.3	226.8	141.0	171	176.3	138.8	155	167	134.7	144.0	136.6
Nd		28.8	28.5			35	70.843	47	46	18	50.9	47.449	67			41.968	46.162	37.950
Zr	138	168	138		380	92	106	295	267	259	288	283	240	316		306	306	317
Sm		5.68	5.64				12.93				9.58	8.65				8.42	8.52	7.23
Y	32	31	30	43	34	31.8	63.4	40.9	34.3	29.3	47	42	72.1	53	47	43.6	41	35.1
V	169	157	157		154	164	164	70	51	89	58	56	69	49	56	30	32	33
Sc	28.0	29.0	28.0		28.0	23.3	29.8	13.9	30.9	17.4	16.0	13.4	12.6	14.0	15.0	11.2	10.6	10.4
Cr		575				329	236	23	16	106	16	23	24	17		11	9	13
Ga		16.0				19.6	23.3	20.6	19.7	18.0	17.4	19.0	20.3			19.3	18.3	20.2
Cu						50	53	36	29	28		32.0	18			17	17	12
Zn						90	113	70	77	76		63.0	80			72	47	69
Ni	107.0	111.0	104.0		99.0	91	61	11	11	36	22.0	9.0	11	20.0	21.0	5	15	5
Co						51	43	68	48.1	51.0		46.0	42.5			43.1	40	34.9
Eu			1.460				1.131				1.770	1.646				1.440		
Gd			5.350				11.856				8.600	8.033				8.333		
Dy			5.13				10.602				7.93	6.881				7.519		
Er			3.03				6.026				4.62	3.757				4.001		
Yb			2.94				6.118				4.32	3.754				4.020		

Lithology	MCC						Megacrystic Charnockite										Carcase Rock Granite	
Type	MCC	MCC	MCC	MCC	MCC	MCC	Megacrystic Charnockite	Megacrystic Charnockite	Megacrystic Charnockite	Megacrystic Charnockite	Megacrystic Charnockite	Megacrystic Charnockite	Megacrystic Charnockite	Megacrystic Charnockite	Megacrystic Charnockite	Megacrystic Charnockite	CRG	CRG
Sample #	**B145**	**D118**	**D111**	**D116**	**SEP-001**	**1031-008**	**SEP-282**	**D108**	**A109B**	**SEP-041**	**SEP-249**	**A109A**	**D107**	**SEP-265**	**SEP-295**	**SEP-264**	**B129B**	**A119**
Location	*C Colbert*	*Trinity Haven*	*Bolingbroke*	*Trinity Haven*	*C Catastrophe*	*Tumby Hills*	*SE Will Is*	*Bolingbroke*	*C Donington*	*Massena Bay*	*S West Pt*	*C Donington*	*Bolingbroke*	*NW Will. Is.*	*NE Will. Is*	*NW Will. Is*		
Source	Mortimer, 1984	Mortimer, 1984	Mortimer, 1984	Mortimer, 1984		Simpson, 1994		Mortimer, 1984	Mortimer, 1984			Mortimer, 1984	Mortimer, 1984				Mortimer, 1984	Mortimer, 1984
Easting					591040		589432			602405	587520			588006	589279	588036		
Northing					6128080		6122718			6182105	6125760			6123978	6124074	6123837		
SiO_2%	69.22	69.80	70.12	70.48	70.88	71.14	66.57	67.50	67.53	67.77	67.78	67.96	68.02	68.31	68.36	69.94	76.01	76.08
Al_2O_3%	14.47	14.01	15.68	14.03	13.43	12.96	14.99	15.23	15.54	15.45	15.40	15.85	15.90	14.73	15.03	15.08	12.06	11.72
Fe_2O_3%	3.92	4.60	2.09	4.20	3.88	4.60	4.87	4.25	3.99	4.25	4.57	4.21	3.16	4.05	3.69	2.61	1.69	1.99
MnO%	0.06	0.07	0.03	0.05	0.05	0.06	0.06	0.04	0.04	0.05	0.05	0.05	0.04	0.05	0.05	0.03	0.02	0.04
MgO%	0.88	0.67	0.48	0.56	0.79	0.60	0.97	0.85	0.90	1.09	1.11	0.90	0.75	0.96	0.85	0.71	0.20	0.25
CaO%	2.44	2.40	2.87	2.27	1.77	1.45	3.13	2.72	2.83	3.91	3.03	2.78	2.73	2.94	2.88	2.41	0.75	0.76
Na_2O%	2.83	2.64	2.87	2.64	2.62	2.65	3.08	2.95	2.70	2.54	3.02	2.81	3.08	2.72	2.77	2.87	2.18	2.67
K_2O%	5.28	5.36	5.53	5.41	5.39	4.92	4.71	5.19	5.60	3.59	4.06	5.96	5.45	4.85	4.97	5.27	6.59	6.06
TiO_2%	0.60	0.54	0.41	0.53	0.62	0.46	0.61	0.66	0.61	0.43	0.63	0.61	0.64	0.54	0.47	0.36	0.25	0.30
P_2O_5%	0.14	0.12	0.12	0.11	0.11	0.12	0.16	0.15	0.16	0.10	0.16	0.16	0.16	0.13	0.12	0.10	0.02	0.03
SO_3%					0.00	0.01	0.04			0.00	0.01			0.01	0.03	0.00		
LOI%	0.20	0.40	0.47	0.20	0.19	0.35	0.29	0.29	0.11	0.32	0.24	0.15	0.57	0.30	0.44	0.28	0.40	0.27
TOTAL	100.04	100.61	100.67	100.48	99.73	99.32	99.48	99.83	100.01	99.50	100.06	101.44	100.50	99.59	99.66	99.66	100.17	100.17
Rb	238	251		255	290.7	118.4	236.6	185	147	147.4	177.0	135	193	156.4	161.2	172.0	277	312
Ba	1004	888		847	695	1137	1263	1176	1178	711	948	1281		1062	927	968	711	387
Th					33.1	15.2	18.0			20.5	27.0			11.8	11.1	20.0		
U					7.7	2.4	8.1			3.1	0.4			1.3	1.4	1.8		
Nb	17	15		15	19.9	17.0	16.1	15		10.9	16.9	11		11.1	8.3	9.6	7	18
La					73	65.0	56	49.3		53	73			80	72	94		
Ce					142	138.0	122	101.0		95	137			145	138	171		
Pb					80.1	29.4	32.3			25.8	23.5			22.7	21.5	29.3		
Sr	140	126		121	96.2	132.7	203.3	171	174	195.3	206.3	174	179	215.5	201.5	196.8	57	48
Nd	47.9				57.0	57.0	49.570	45.4		43	37.185			49.075	41.972	60.805		
Zr	305	307		311	351	265	226	315		166	269	300		229	194	166	235	263
Sm	9.00						9.11	8.56			5.18			7.21	6.55	7.41		
Y	43	44		52	53.1	42.3	39.7	40	43	20.7	13.6			23.5	20.8	14.2	16	50
V	31	27		26	33	6	35		53	47	46	53		37	35	23		
Sc	12.0	11.0		11.0	9.8	6.3	8.7	19.0	14.0	11.2	14.9	13.0		9.7	9.9	6.8	4.0	5.0
Cr	7	10	12	11	11	9	4		16	12	13	19	23	12	14	11	0	
Ga					16.4	23.1	17.8			18.0	19.3			17.5	17.0	16.3		
Cu					40	7	17			10	15			13	36	13		
Zn					86	84	47			54	72			48	40	40		
Ni	20.0				2	2	9	18.0		4	11		19.0	9	10	10		
Co					73	39.7	31			53.6	33			41	33	42		
Eu	1.520							1.700										
Gd	8.020							8.170										
Dy	7.50							6.45										
Er	4.39							3.58										
Yb	4.09							3.14										

Lithology	Carcase Rock Granite							Granite Gneiss 1 (retrogressed MCC)						Granite Gneiss 2 (retrogressed Megacrystic Charnockite)				
Type	CRG	CRG	CRG	CRG	CRG	CRG	CRG	Even Grained Granite Gn.	Even Grained Granite Gn.	Even Grained Granite Gn.	Even Grained Granite Gn.	Even Grained Granite Gn.	Even Grained Granite Gn.	Megacrystic Granite Gn.	Megacrystic Granite Gn.	Megacrystic Granite Gn.	Megacrystic Granite Gn.	Megacrystic Granite Gn.
Sample #	B125A	B153	B152	B130A	A90	B154B	SEP-217	SEP-252	B111	B103	B106	B101	B109	SEP-142	B168	A88	A121	D206
Location		*Carcase R*	*Carcase R*			*Carcase R*	*E C Tournefor*	*S West Pt*	*C Donington*	*C Donington*	*C Donington*	*C Donington*	*C Donington*	*Peake Pt*	*Engine Pt*	*McLaren Pt*	*Kirton Pt*	*Kirton Pt*
Source	Mortimer, 1984	Mortimer, 1984	Mortimer, 1984	Mortimer, 1984	Mortimer, 1984	Mortimer, 1984			Mortimer, 1984	Mortimer, 1984	Mortimer, 1984	Mortimer, 1984	Mortimer, 1984		Mortimer, 1984	Mortimer, 1984	Mortimer, 1984	Mortimer, 1984
Easting							578300	587530						593190				
Northing							6134720	6125760						6180040				
SiO_2%	76.83	76.91	77.01	77.16	77.24	77.93	78.29	70.97	71.35	74.10	74.99	75.52	75.62	67.11	68.04	68.48	69.84	70.44
Al_2O_3%	12.35	11.93	11.88	11.47	11.85	12.17	12.36	14.08	13.50	12.85	11.81	12.03	12.56	14.42	15.46	14.02	14.32	14.10
Fe_2O_3%	1.66	1.03	1.04	1.12	1.62	0.45	0.24	3.20	3.69	2.23	2.21	1.72	2.69	5.23	3.48	4.92	3.94	3.71
MnO%	0.01	0.11	0.03	0.01	0.02	0.00	0.00	0.03	0.05	0.02	0.02	0.02	0.03	0.06	0.04	0.07	0.05	0.05
MgO%	0.07	0.02	0.18	0.07	0.15	0.00	0.12	0.64	0.63	0.37	0.27	0.74	0.30	1.29	0.65	0.83	1.00	0.76
CaO%	0.55	0.76	0.74	0.46	0.58	0.73	0.39	2.10	1.84	1.10	0.91	1.00	1.20	2.85	2.12	2.56	2.50	2.26
Na_2O%	2.25	2.96	3.03	2.42	2.08	2.94	1.97	2.64	2.35	2.20	1.90	2.23	2.10	2.68	3.48	2.69	2.73	2.84
K_2O%	6.77	5.20	5.20	6.17	6.85	5.45	7.42	4.95	5.26	6.58	6.49	5.94	6.28	4.83	6.23	5.33	5.26	5.46
TiO_2%	0.24	0.07	0.07	0.16	0.25	0.07	0.05	0.38	0.43	0.23	0.34	0.24	0.29	0.69	0.43	0.61	0.55	0.48
P_2O_5%	0.02	0.00	0.00	0.01	0.02	0.00	0.01	0.07	0.07	0.04	0.04	0.03	0.04	0.16	0.08	0.15	0.12	0.10
SO_3%							-0.01	0.00						0.02				
LOI%	0.43	0.22	0.22	0.24	0.30	0.06	0.19	0.31	0.63	0.46	0.42		0.41	0.53	0.34	0.40	0.38	0.30
TOTAL	101.18	99.21	99.40	99.29	100.96	99.80	101.04	99.37	99.80	100.18	99.40	99.47	101.52	99.87	100.35	100.06	100.69	100.50
Rb	276	397	413	300	342	442	383.1	168.7	261	296	274	299		233.9	361	235	244	273
Ba	743	5	6	267	84	5	324	1137	610	652	505	474	506	861	670	901	835	689
Th			36				24.6	38.3						25.2				
U			13				6.5	3.0						3.5				
Nb	10	5	6	12	11	7	6.0	7.7	16	13	18			15.4	18		16	16
La	62.3		39.0				12	119						96				
Ce	123		74.0				25	213						179				
Pb			49				38.9	25.7						27.6				
Sr	54	12	12	28	22	11	68.8	193.5	121	101	85	70		153.4	108	131	129	113
Nd	47.7		33.8				9	52.501						47.236				
Zr	226	100	118	173	335	148	71	379	330	222	267			233	231	318	228	227
Sm	7.66		5.74					5.96						8.89				
Y	19	53	52	32	27	15	20.2	8.1	24	36	19	25		58.1	45	45	43	45
V		0	1				4	28						67			38	
Sc	5.0	1.0	1.0	5.0	4.0	1.0	0.9	4.6	6.0	9.0	2.0			13.8	9.0		11.0	11.0
Cr	0		1	0		0	12	13						28	10		12	
Ga			16.0				13.7	16.2						17.8				
Cu							11	11						20				
Zn							1	30						64				
Ni			11.0				4	7						15			17.0	17.0
Co							36.0	28						32				
Eu	0.857		0.163															
Gd	3.900		6.450															
Dy	3.98		7.13															
Er	1.81		4.33															
Yb	1.37		4.02															

Lithology	Granite Gneiss 2 (retrogressed Megacrystic Charnockite)												Alkali Feldspar Granite Gneiss (AFGG)					
Type	Megacrystic Granite Gn.	Megacrystic Granite Gn.	Megacrystic Granite Gn.	Megacrystic Granite Gn.	Megacrystic Granite Gn.	Megacrystic Granite Gn.	Megacrystic Granite Gn.	Megacrystic Granite Gn.	Megacrystic Granite Gn.	Megacrystic Granite Gn.	Megacrystic Granite Gn.	Megacrystic Granite Gn.	AFGG	AFGG	AFGG	AFGG	AFGG	AFGG
Sample #	SEP-194D	KP309	B164D	D21	SEP-218D	B164E	KP300	KP307	B164B	B500	D205	B163	B161A	B22C	B159B	B154A	SEP-088	B22B
Location	*Wanna*	*Kirrton Pt*	*Engine Pt*	*Kirton Pt*	*C Tournefort*	*Engine Pt*	*Kirton Pt*	*Kirton Pt*	*Engine Pt*	*Billy Lights Pt*	*Kirton Pt*	*Carcase R*	*Carcase Rk*	*Carcase R*	*Carcase Rk*	*Carcase R*	*C Donington*	*Carcase R*
Source		Mortimer, 1984	Mortimer, 1984	Mortimer, 1984		Mortimer, 1984	Mortimer, 1984	Mortimer, 1984	Mortimer, 1984	Mortimer, 1984	Mortimer, 1984	Mortimer, 1984	Mortimer, 1984	Mortimer, 1984	Mortimer, 1984	Mortimer, 1984		Mortimer, 1984
Easting	577760				578460												591130	
Northing	6138560				6135100												6156610	
SiO_2%	70.48	70.58	70.94	71.98	72.41	73.34	73.48	74.39	74.98	75.71	75.79	76.65	77.20	77.42	77.64	78.10	78.73	78.81
Al_2O_3%	14.20	14.81	13.93	13.74	13.54	13.90	13.43	13.00	13.25	12.09	12.52	12.45	11.94	12.11	12.24	12.27	11.61	12.05
Fe_2O_3%	2.55	2.27	3.41	2.90	2.58	1.75	1.44	1.89	0.72	2.39	1.97	1.03	0.64	0.50	0.48	0.54	0.47	0.60
MnO%	0.03	0.03	0.05	0.05	0.03	0.02	0.02	0.03	0.01	0.02	0.03	0.01	0.01	0.01	0.01	0.02	0.00	0.01
MgO%	0.58	0.45	0.72	0.52	0.70	0.34	0.36	0.34	0.19	0.44	0.26	0.17	0.15	0.04	0.21	0.09	0.08	0.05
CaO%	1.54	1.64	1.97	1.83	1.88	1.27	1.22	1.33	0.55	1.92	1.18	1.04	0.71	0.73	0.73	0.73	0.59	0.72
Na_2O%	2.52	5.90	2.83	2.91	2.75	2.54	2.52	2.73	2.10	2.52	2.89	2.60	2.97	2.92	3.00	2.92	2.62	3.01
K_2O%	6.72	3.05	5.87	5.50	4.99	7.12	6.26	5.66	8.15	4.41	5.33	5.60	5.44	5.65	5.56	5.40	5.41	5.47
TiO_2%	0.33	0.36	0.44	0.36	0.39	0.21	0.23	0.27	0.07	0.34	0.21	0.18	0.07	0.07	0.08	0.08	0.07	0.07
P_2O_5%	0.07	0.10	0.09	0.07	0.08	0.04	0.05	0.05	0.01	0.06	0.03	0.02	0.00	0.00	0.01	0.00	0.00	0.00
SO_3%	0.00				0.00												0.00	
LOI%	0.34		0.11	0.36	0.34	0.15	0.33	0.39	0.15	0.25	0.25	0.27	0.24	0.30	0.27	0.26	0.17	0.23
TOTAL	99.36	99.19	100.36	100.22	99.69	100.68	99.34	100.08	100.18	100.15	100.46	100.02	99.37	99.75	100.23	100.41	99.75	101.02
Rb		84	323	293	320.0	370	285	301	414	263	371		413	448	437	440	350.7	425
Ba			647	722	627	689	1093	575	788	439	246	279	6	3	9	5	9	8
Th					64.2												17.0	
U					5.4												4.3	
Nb		24	16	15	16.5	11	4	14	15	13	14	10	5	6	8	9	5.3	8
La					84					60.8					9.9	38.8	6	
Ce					149					129.0				17.1	13.8	70.3	5	
Pb					42.6												42.6	
Sr		109	100	109	130.4	103	147	88	99	79	59		11	10	12	10	10.5	11
Nd					51					37.0				4.0	3.9	20.9	6	
Zr		76	217	172	224	300	130	169	316	151	174	140	129	92	114	137	65	122
Sm										6.17				0.73	0.88	3.70		
Y		32	51	41	39.9	28	7	41	13	37	51	39	21	12	17	18	9.5	18
V					25					20							4	
Sc			10.0	7.0	4.5	6.0	1.0	5.0	3.0	6.0	4.0	4.0	1.0	2.0	1.0	1.0	0.7	2.0
Cr			11	10	7				2	6				3		0	2	
Ga					18.3												15.4	
Cu					50												0	
Zn					34												10	
Ni					6						13.0						0	
Co					59												53.0	
Eu	0.858									1.000				0.130	0.150	0.150		
Gd	6.406									5.410				0.818	0.990	2.800		
Dy	5.539									5.30				1.35	1.84	2.50		
Er	2.968									3.31				1.45	1.64	1.40		
Yb	2.801									3.19				2.05	2.05	1.40		

Lithology	Colbert Suite					Williams Island Granite			Moody Suite									
Type	Hornblende Granite	Hornblende Granite	Hornblende Granite	Hornblende Granite	Hornblende Granite				Chinmina Svenite	Moreenia Adamellite	Moody Tank Adamellite	Moody Tank Adamellite	Moody Tank Adamellite	Moody Tank Adamellite	Moody West Adamellite	Yunta Well Leucogranite	Yunta Well Leucogranite	Yunta Well Leucogranite
Sample #	B112B	B112A	B109	B135	SEP-094	SEP-087	SEP-283	SEP-089	829	839	SEP-063	801(4)	241	801(6)	849	419	854	858
Location	*Cape Colbert*	*Cape Colbert*	*Cape Colbert*	*Cape Colbert*	*E West Pt*	*C Donington*	*Williams Is*	*C Donington*			*Moody Tank*							
Source	Mortimer, 1984	Mortimer, 1984	Mortimer, 1984	Mortimer, 1984					Mortimer, 1984	Mortimer, 1984		Mortimer, 1984	Mortimer, 1984	Mortimer, 1984	Mortimer, 1984	Mortimer, 1984	Mortimer, 1984	Mortimer, 1984
Easting					587460	590930	589404	591910										
Northing					6126360	6156820	6122608	6155370										
SiO_2%	63.35	63.66	63.75	66.90	68.17	76.23	77.50	78.18	58.88	66.04	71.93	72.10	72.14	72.57	72.66	72.16	75.39	73.67
Al_2O_3%	14.99	14.95	15.08	14.55	14.61	11.94	12.38	11.93	15.57	13.93	14.22	14.23	14.15	14.07	14.46	14.17	14.60	15.38
Fe_2O_3%	6.43	6.56	6.48	5.12	3.59	1.54	0.13	0.60	7.33	5.68	1.97	3.24	2.53	2.83	3.38	1.26	1.30	1.19
MnO%	0.09	0.08	0.08	0.05	0.03	0.02	0.00	0.01	0.12	0.10	0.02	0.05	0.05	0.04	0.06	0.04	0.12	0.03
MgO%	1.32	1.39	1.43	1.07	0.80	0.26	0.11	0.11	2.31	0.81	0.44	0.37	0.46	0.37	0.48	0.16	0.06	0.19
CaO%	3.56	3.62	3.70	2.41	1.83	1.17	0.54	0.69	4.28	2.26	1.14	1.19	1.29	1.19	1.43	0.50	0.61	0.73
Na_2O%	2.75	2.77	2.97	2.38	2.28	2.16	2.49	2.69	3.27	2.87	2.84	3.31	2.87	3.31	2.91	4.29	3.98	3.30
K_2O%	5.32	5.23	4.94	6.02	6.91	5.51	6.28	5.40	5.28	5.60	5.85	4.94	5.32	4.86	5.42	5.90	5.02	4.66
TiO_2%	1.08	1.10	1.09	0.84	0.62	0.21	0.01	0.08	1.40	0.79	0.29	0.35	0.29	0.35	0.42	0.09	0.03	0.07
P_2O_5%	0.33	0.35	0.30	0.23	0.13	0.02	0.01	0.00	0.63	0.32	0.10	0.08	0.13	0.09	0.63	0.30	0.30	0.34
SO_3%					0.00	0.00	0.00	0.00			0.00							
LOI%	0.41	0.40	0.61	0.38	0.34	0.39	0.36	0.22	1.03	0.51	0.47	0.57	0.34	0.57	0.62	0.92	0.56	0.77
TOTAL	99.63	100.11	100.43	99.95	99.31	99.45	99.81	99.91	100.10	98.91	99.27	100.43	99.57	100.25	102.47	99.79	101.97	100.33
Rb	198	197	196	235	248.9	288.2	172.9	322.0	164	201	278.5	263			206		343	308
Ba		1133	1144	1063	1071	324	68	17	2471	1229	490	340			606		3	28
Th					18.6	59.5	19.2	16.4			42.3							
U					1.7	7.1	2.7	4.1			78.4							
Nb	22	22	21	17	10.4	8.5	1.3	4.5	32	26	23.0	31			19		8	32
La		62.2		75.2	104	123	12	68	236	104	65	102			101			
Ce		136			177	232	21	94	418	212	122	191			204			
Pb					24.6	38.3	34.3	44.1			59.3							
Sr	184	183	187	145	170.9	63.2	18.2	13.7	774	340	104.5	97			132		8	23
Nd		62.8		60.6	67	92	5.158	32	169	90.7	52.0	71.1			70.2			
Zr	333	339	343	411	456	167	73	111	464	311	197	349			247		25	26
Sm		12.00		10.90			0.74		22.90	11.40		13.70			11.30			
Y	52	53	46	46	29.0	28.9	2.4	18.3	40	25	22	37			38		11	18
V					35	7	5	4			14							
Sc		17.0	15.0	13.0	10.5	4.5	1.1	1.3	12.0	10.0	2.4	5.0			5.0		2.0	5.0
Cr	10	4		5	8	2 *		2			4							
Ga					15.7	15.0	12.7	16.0			21.2							
Cu					16	11	6	4			4							
Zn					40	26	5	14			43							
Ni					5	0 *		0			1							
Co					57.4	96.9	80	59.9										
Eu		2.070		1.710					4.030	2.050		0.915			1.140			
Gd		11.800		9.380					14.300	6.950		9.270			7.930			
Dy		9.47		8.11					8.89	4.52		6.20			6.24			
Er		5.24		4.36					4.66	2.00		3.13			3.22			
Yb		4.46		3.66					3.64	1.35		3.35			2.80			

Lithology	Moody Suite						Selvages and leucosomes				Jussieu Dykes					High Mg Tholeiites (HMgT)		
Type	Yunta Well Leucogranite	Yunta Well Leucogranite	Yunta Well Leucogranite	Yunta Well Leucogranite	Yunta Well Leucogranite	Yunta Well Leucogranite	selvage/ charnockite	felsic selvage	felsic selvage	leucosome	Jussieu Dyke	Jussieu Dyke	Jussieu Dyke	Jussieu Dyke	Jussieu Dyke			
Sample #	853	SEP-062	851	857	1031-006	856	SEP-251	SEP-296	SEP-262	SEP-026	SEP-240	SEP-241	SEP-250	SEP-261	SEP-293	785	786	739
Location		*Yunta Well*			*Yunta Well*		*S West Pt*	*NE Will. Is*	*NW Will. Is*	*Bolingbroke*	*N Taylors Ldg*	*S McLaren Pt*	*S West Pt*	*NW Will. Is*	*NE Will. Is*	*Fishery Bay*	*Fishery Bay*	*Memory Cove*
Source	Mortimer, 1984		Mortimer, 1984	Mortimer, 1984	Simpson, 1994	Mortimer, 1984										Bradley, 1972	Bradley, 1972	Bradley, 1972
Easting		596900					587520	589279	588036	600700	590739	590740	587520	588036	589279			
Northing		6207200					6125760	6124074	6123837	6177960	6145455	6145460	6125760	6123837	6124074			
SiO_2%	73.83	73.88	74.12	74.31	74.73	75.73	70.36	71.90	74.64	76.49	48.84	49.33	48.40	51.26	51.62	53.33	52.00	47.19
Al_2O_3%	14.33	14.39	14.53	15.20	14.94	13.76	14.30	13.38	13.38	13.12	15.76	15.99	16.37	16.12	14.45	5.95	5.83	8.19
Fe_2O_3%	0.93	0.87	1.00	0.98	0.27	1.09	2.69	2.29	0.71	0.26	13.25	13.41	13.07	13.14	10.57	16.47	16.52	11.77
MnO%	0.07	0.03	0.06	0.14	0.03	0.08	0.03	0.03	0.03	0.00	0.17	0.18	0.17	0.19	0.16	0.27	0.28	0.18
MgO%	0.06	0.19	0.58	0.63	0.13	0.06	0.74	0.68	0.22	0.11	7.15	7.36	6.08	6.06	8.29	17.62	15.79	23.94
CaO%	0.53	0.48	0.52	0.63	1.75	0.46	2.39	1.17	1.08	1.20	9.49	9.67	8.89	7.75	9.10	3.85	6.32	6.38
Na_2O%	4.32	3.82	4.30	3.99	4.68	3.57	2.50	2.04	2.34	2.31	3.03	2.53	3.16	3.20	2.83	1.16	1.20	0.96
K_2O%	4.00	4.84	3.89	4.28	2.66	3.83	5.43	7.05	6.89	5.80	1.07	0.95	2.04	1.32	1.57	0.67	0.68	0.48
TiO_2%	0.03	0.05	0.03	0.03	0.02	0.03	0.38	0.34	0.02	0.06	1.09	1.11	1.34	1.21	0.98	0.45	0.46	0.48
P_2O_5%	0.30	0.25	0.30	0.19	0.07	0.30	0.08	0.12	0.04	0.01	0.21	0.21	0.20	0.16	0.26	0.11	0.15	0.08
SO_3%		0.00			0.00		0.00	0.00	0.00	0.00	0.00	0.02	0.03	0.02	0.02			
LOI%	0.64	0.56	0.61	0.44	0.23	0.35	0.48	0.51	0.24	0.28	0.38	-0.06	0.26	-0.14	0.35			
TOTAL	99.04	99.36	99.94	100.82	99.51	99.26	99.38	99.51	99.59	99.64	100.44	100.70	100.01	100.29	100.20	99.88	99.23	99.65
Rb	303	394	356	257	63.0	416	190.0	262.6	189.0	256.5	45.8	42.8	132.1	79.8	83.1	37.0	32.0	15.0
Ba	2	66	1	55	215	2	1193	686	167	667	349	400	353	324	489	175	178	128
Th		4.6			1.6		25.1	14.4	11.5	13.1	4.7	6.1	2.1	5.4	0.5			
U		8.7			3.4		1.4	1.5	11.7	3.9	1.5	2.4	1.6	1.4	1.1			
Nb	18	17.2	25	11	0.8	27	8.0	10.7	0.2	3.7	8.1	8.8	7.6	8.6	10.4	5.0	5.0	2.0
La		3			8.0		81	27	9	12	23	24	22	22	18	9	10	8
Ce		3	6	4	16.0		142	57	20	27	50	54	54	50	45	19	26	14
Pb		27			45.2		26.3	35.2	44.8	41.7	9.2	7.6	8.8	10.0	8.4			
Sr	7	27.8	7	15	108.0	8	207.9	131.1	58.6	129.4	151.5	156.2	225.6	206.8	315.8	85	80	77
Nd		3			10.0		37.858	25.529	6.501	6.627	26	22.177	23.282	21.752	19.313			
Zr	33	30	30	35	20	25	316	242	66	157	121	120	149	134	82	84	69	59
Sm							4.30	4.76	1.53	1.21	4.71	5.20	4.76	4.97	3.92			
Y	7	12.4	6	9	4.3	6	6.4	19.3	12.8	7.4	37.5	37.5	36.0	33.3	21.3	12	19	12
V		4			4		19	25	4	9	195	202	173	164	213	108	138	140
Sc	1.0	1.4	1.0	3.0	1	1.0	2.9	4.2	3.6	2.2	35.4	34.0	32.1	27.0	24.9	32.0	31.0	24.0
Cr		2			10.0		9	18	1	3	284	296	104	88	840	1284	1027	3421
Ga		19			11.7		15.9	14.5	13.5	15.7	18.9	19.9	19.9	20.7	16.8			
Cu		7			3.0		9	12	21	0	118	111	84	88	98			
Zn		29			4		36	22	8	6	115	110	115	112	78			
Ni		0			4		8	8	2	1	152	156	86	82	158			
Co		55.2			4		63	60	58	54.3	73	65	66	67	64			
Eu											1.176							
Gd											5.152							
Dy											5.311							
Er											3.206							
Yb											3.232							

Lithology	High Mg Tholeiites (HMgT)										Unassigned Tholeiites							
Type	ultramafic	ultramafic	def mafic	ultramafic	Norite	Norite	Norite	Plag-phyric dolerites	mafic	Norite	Plag-phyric dolerite	Plag-phyric dolerite	Plag-phyric dolerite	Deformed dolerite		Norite	mafic	mafic granulite
Sample #	1028-5	SEP-148	SEP-024	1028-6	B58	B60	B2	F52	1028-71	B69	B52	F38	D102	SEP-121	744	A15	1028-87	SEP-066
Location	*Mem cove*	*Mem Cove*	*Bolingbroke*	*Mem cove*	*C Donington*	*C Donington*	*S McLaren Pt*	*S C Donington*	*Pt Boston*	*C Donington*	*C Donington*	*C Colbert*	*C Colbert*	*Massena Bay*	*Cape Catastro*	*Pt Boston*	*C Donington*	*Mine Road*
Source	Bendall, 1994			Bendall, 1994	Mortimer, 1984	Mortimer, 1984	Mortimer, 1984	Mortimer, 1984	Bendall, 1994	Mortimer, 1984	Mortimer, 1984	Mortimer, 1984	Mortimer, 1984		Bradley, 1972	Mortimer, 1984	Bendall, 1994	
Easting		591020	600740															597160
Northing		6129080	6178020															6200160
SiO_2%	46.16	49.07	47.39	50.68	49.99	51.66	51.17	49.07	51.48	51.10	49.46	49.52	49.16	46.97	49.40	52.84	52.76	49.99
Al_2O_3%	8.11	8.99	12.96	9.54	11.05	11.61	12.12	13.69	12.93	13.63	15.79	16.44	16.08	15.30	16.04	16.12	13.38	16.99
Fe_2O_3%	11.78	11.95	12.10	11.36	11.35	11.20	10.74	11.01	10.62	10.70	11.28	11.47	11.89	11.05	11.94	9.99	10.75	8.52
MnO%	0.18	0.19	0.19	0.18	0.17	0.18	0.18	0.17	0.17	0.17	0.16	0.18	0.18	0.17	0.19	0.15	0.17	0.14
MgO%	24.13	21.39	12.06	18.26	15.86	13.59	13.33	13.34	12.10	10.60	9.68	8.44	8.90	9.74	8.37	6.88	9.81	6.80
CaO%	6.25	6.74	10.96	7.30	9.04	9.01	9.55	9.96	9.86	10.07	11.33	11.00	10.94	10.38	11.60	10.06	10.05	12.59
Na_2O%	1.00	0.78	1.97	1.24	1.29	1.68	1.63	1.46	1.87	2.00	1.65	1.83	1.77	1.87	1.81	2.42	2.02	2.25
K_2O%	0.44	0.50	0.81	0.52	0.53	0.67	0.52	0.68	0.56	0.69	0.51	0.56	0.52	1.78	0.46	0.94	0.86	1.14
TiO_2%	0.50	0.55	0.58	0.59	0.62	0.65	0.64	0.54	0.72	0.81	0.52	0.60	0.60	0.61	0.67	0.74	0.74	0.75
P_2O_5%	0.07	0.08	0.09	0.08	0.08	0.08	0.07	0.06	0.10	0.12	0.08	0.09	0.10	0.09	0.10	0.14	0.10	0.09
SO_3%	0.01	0.01	0.00	0.02	0.00	0.00			0.00	0.00				0.02			0.00	0.00
LOI%	0.44	-0.24	1.10	-0.24	0.14	-0.03			-0.12	-1.42				1.70			-0.21	1.29
TOTAL	99.08	100.01	100.21	99.53	100.12	100.30	99.95	99.98	100.29	98.47	100.46	100.13	100.14	99.68	100.58	100.28	100.44	100.55
Rb	16.8	18.5	47.7	18.6	19.0	25.0	16	32	19.0	21.0	20.0	17	14	104.7	9.0	29	34.8	55.3
Ba	147	154	118	173	151	209	197	198	213	241	160	197	198	224	134	408	245	173
Th	2.2	2.6	0.9	2.9					2.3								5.3	3.1
U	2.5	0.9	1.8	0.9					1.4								1.4	1.6
Nb	3.4	4.4	3.1	3.3	5.0	6.0	4	2	4.9	6.0	8.0	3	3	1.9	10.0	6	6.2	3.3
La	9	12	3	9	12.9	12.3			25	13.5	6			5	5		19	7
Ce	10	14	12	22	23.8	25.5			25	28.5	19			12	16		42	19
Pb	5	2.2	4.1	2.3					3.7					10.0			7.1	4.8
Sr	88.5	86.5	80.2	89.5	112	126	143	119	148.9	165	58	151	154	120.3	148	227	145.4	179.9
Nd	11	9.889	6.240	10	12.1	13.4			14.0	14.1	11.0			10	8.0		14.0	13.0
Zr	60	75	39	69	74	89	79	54	89	104	46	51	53	34	42	104	105	55
Sm		2.15	1.65		2.71	3.19				3.16								
Y	12.3	14.6	16.8	14.5	16	20	18	18	18.4	23	16	21	19	18.2	16	25	20.8	17.7
V	168	186	255	208	231	238			229	235	105			243	205		241	312
Sc	22.0	25.7	36.8	28.1	37.0	31.0	34	35	29.1	32.0	30.0	39	36	35.3	36.0	30	29.4	39.4
Cr	4166	3009	1262	3261	2401	1655			1504	1119	507			494	485		889	389
Ga	9	9.6	13.7	12.2					15.5					15.4			15.7	18.2
Cu	46	68	101	62					82					117			80	81
Zn	84	78	86	82					75					95			75	62
Ni	1228	853	382	724					389					288	156		220	106
Co	105.9	111.0	73.7	92.6					62.7		49			70.0	485		61.2	54.3
Eu		0.588			0.831	1.01				1.06								
Gd		2.310			3.05	3.6				3.44								
Dy		2.287			3.19	3.77				3.51								
Er		1.382			1.98	2.41				2.1								
Yb		1.373			1.96	2.42				1.96								

Lithology	Unassigned Tholeiites																	
Type	mafic	gt mafic	Plag-phyric dolerite		Norite		Norite				hb 2px granu				amphibolite	amphibolite		
Sample #	1028-2	1028-100	B7	742	D104	SEP-039	B16	1028-78	1028-80	SEP-238	1028-28	1028-29	SEP-220	1396	SEP-013	1031-002	SEP-124	1028-49
Location	*E West P*	*W West Pt*	*McClaren Pt*	*Fishery Bay*	*C Colbert*	*Massena Bay*	*Fisherman Pt*	*Pt Boston*	*Pt Boston*	*McL Pt*	*Pt Warna*	*Mine Ck*	*W West Pt*	*Point Warna*	*C Catastrophe*	*Tumby Hills*	*Tumby Bay*	*C Catastrophe*
Source	Bendall, 1994	Bendall, 1994	Mortimer, 1984	Bradley, 1972	Mortimer, 1984		Mortimer, 1984	Bendall, 1994	Bendall, 1994		Bendall, 1994	Bendall, 1994		Bradley, 1972		Simpson, 1994		Bendall, 1994
Easting						602520				592600			585860		591320		602100	
Northing						6182240				6148960			6128024		6128010		6194120	
SiO_2%	48.94	48.71	48.72	48.41	51.88	48.37	51.83	49.26	48.75	50.47	49.47	48.27	53.33	48.26	49.15	50.06	49.07	48.97
Al_2O_3%	16.83	16.90	16.64	15.41	15.01	16.10	14.92	15.95	16.31	15.97	15.63	14.62	17.65	15.01	15.30	14.06	15.68	15.13
Fe_2O_3%	12.49	12.73	12.55	11.64	10.28	11.69	10.69	12.72	10.93	13.91	12.15	12.83	11.03	13.53	13.93	10.71	12.81	14.22
MnO%	0.17	0.18	0.18	0.18	0.18	0.17	0.17	0.18	0.17	0.19	0.18	0.19	0.15	0.21	0.19	0.18	0.17	0.18
MgO%	8.16	7.89	8.24	9.63	8.31	7.54	7.66	8.03	8.69	6.78	8.07	7.67	4.40	8.44	7.62	5.59	7.51	7.21
CaO%	10.74	10.49	10.28	10.84	10.44	10.06	10.31	10.48	12.49	9.83	11.66	10.31	9.49	11.45	9.75	14.85	9.88	9.49
Na_2O%	2.08	2.33	1.96	1.76	2.10	2.35	2.28	2.15	2.03	2.42	1.87	1.79	3.05	1.85	2.30	2.92	3.12	2.47
K_2O%	0.53	0.54	0.69	0.50	0.86	1.63	0.84	0.70	0.24	1.00	0.25	1.65	1.21	0.35	1.11	0.43	0.68	1.18
TiO_2%	0.77	0.77	0.78	0.81	0.82	0.82	0.88	0.92	0.95	0.95	1.04	1.09	1.12	1.15	1.15	1.16	1.17	1.23
P_2O_5%	0.11	0.11	0.13	0.08	0.10	0.18	0.12	0.16	0.08	0.19	0.08	0.08	0.20	0.10	0.20	0.13	0.11	0.20
SO_3%	0.02	0.03				0.01	0.00	0.01	0.01	0.01	0.04	0.02	0.00		0.03	0.03	0.00	0.01
LOI%	-0.08	-0.04				0.91	-1.49	-0.20	-0.29	-0.15	0.06	1.49	-0.20		-0.07	0.34	0.80	-0.20
TOTAL	100.75	100.63	100.17	99.26	99.98	99.83	98.21	100.36	100.34	101.57	100.50	100.01	101.43	100.35	100.66	100.45	101.00	100.08
Rb	11.6	11.3	22	12.0	35	95.9	30.0	21.0	8.6	31.8	8.3	109.6	38.2	9.0	39.6	8.2	24.1	43.3
Ba	239	243	264	99	277	233	273	303	65	415	95	134	432	85	494	187	124	456
Th	1.3	0.9						2.1	1.9	1.3	1.1	17.2	5.2		3.1	0.8	0.6	3.0
U	2.3	1.4				0.1		1.1	0.4	0.7	0.9	1.1	2.6		1.0	2.1	0.8	2.2
Nb	3.9	3.8	4	8.0	5	5.5	6.0	6.1	3.7	6.4	5.3	5.0	11.4	6.0	11.1	3.6	6.2	10.4
La	7	7		6		16	17.5	11	2	21	6	3	33	5	23	3.0	16	54
Ce	21	25		19		32	36.5	35	18	42	24	24	61	19	48	11.0	37	54
Pb	4.4	4.5				13.2		2.3	1.8	7	1.2	3.4	9.4		7.2	2.0	5.6	7.5
Sr	177.6	172	210	58	184	189.5	182	199.7	165.1	198.9	168.9	150.3	248.6	164	221.9	143.5	214.1	204.9
Nd	5.0	6.0		11.0		19.0	17.6	12.0	5.0	22	7.0	7.0	24.300	7.0	22	8.0	18	21
Zr	55	59	60	46	110	78	116	73	46	93	43	51	153	54	116	66	82	119
Sm	4.40						3.83						4.89		4.38			
Y	19.6	20.1	26	16	23	23.7	25	21.2	16.6	27.3	24.2	16	28.5	16	28.2	30.9	20.5	29.2
V	232	239		105		226	256	241	253	257	319	324	215	270	234	41	314	246
Sc	32.1	32.7	38	30.0	33	33.9	35.0	32.4	33.7	30.8	39.8	43.9	23.2	32.0	29.3	91.0	33.6	32.5
Cr	135	113		507		205	568	304	375	73	276	306	86	202	331	351.9	84	330
Ga	17.9	16.3				20.1		17.9	17.1	20.8	15.4	16.9	22.0		20.1	61.1	19.7	18.1
Cu	66	245				93		112	130	99	218	99	108		180	15.4	126	108
Zn	96	98				107		96	73	104	93	89	84		111	100	91	115
Ni	234	221		162		190		206	277	147	239	117	68	163	196	100	193	216
Co	70.9	80.6		49		80		68.3	85.1	68	93.4	16.9	69	202	74	74	65	71.3
Eu							1.17								1.182			
Gd							4.03								4.598			
Dy							4.22								4.650			
Er							2.57								2.738			
Yb							2.46								2.790			

Lithology	Unassigned Toleiites														High Ba Tholeiites (HBaT)			
Type				gt hb mafic	ig tex mafic		gt granulite	2px	Late Dyke	Gabbro norite			dyke centre	ig tex mafic	hb 2px granulite	Norite	Gabbro norite	gt mafic
Sample #	SEP-034	SEP-195F	SEP-233A	1028-110	1028-117	1354	1028-27	1028-79	SEP-260	B36	SEP-068	1374	SEP-006	1028-117B	1028-99	B26	B17	SEP-111
Location	*Massena Bay*	*Wanna*	*W West Pt*	*Mine Ck*	*Peake Pt*	*Fishery Bay*	*Pt Warna*	*Pt Boston*	*NW Will. Is*	*Surfleet Pt*	*S Trinity Hav.*	*Cape Wiles*	*C Catastrophe*	*Peake Pt*	*W West Pt*	*Surfleet Pt*	*C Donington*	*W West Pt*
Source				Bendall, 1994	Bendall, 1994	Bradley, 1972	Bendall, 1994	Bendall, 1994		Mortimer, 1984		Bradley, 1972		Bendall, 1994	Bendall, 1994	Mortimer, 1984	Mortimer, 1984	
Easting	602280	577740	585920						588036		602320		591020					585960
Northing	6183240	6138500	6127050						6123837		6186720		6127940					6126000
SiO_2%	47.01	48.55	53.10	56.71	50.21	52.27	48.84	49.34	47.70	47.33	50.57	49.93	55.36	49.52	51.00	52.89	45.37	49.27
Al_2O_3%	15.97	14.53	14.85	14.84	14.44	15.63	14.56	14.58	14.48	16.16	14.21	13.86	13.42	14.24	14.40	15.13	13.99	13.33
Fe_2O_3%	12.32	13.35	12.23	11.73	14.54	13.39	15.33	15.54	15.35	15.49	13.54	15.10	14.41	14.54	18.02	10.67	19.49	19.88
MnO%	0.18	0.17	0.17	0.17	0.20	0.19	0.21	0.22	0.22	0.21	0.19	0.22	0.19	0.20	0.22	0.17	0.25	0.23
MgO%	8.30	7.93	5.09	3.89	6.70	5.39	6.75	6.38	7.24	7.21	6.04	6.94	3.65	6.24	4.62	7.04	4.86	4.27
CaO%	10.85	9.49	8.86	7.06	8.75	8.58	10.61	10.45	9.96	9.70	9.88	11.01	7.35	9.63	8.80	9.88	7.66	8.01
Na_2O%	2.28	3.02	2.87	0.65	2.15	2.99	2.14	2.46	2.69	2.25	2.34	1.91	2.76	2.33	2.29	2.47	2.43	1.86
K_2O%	0.74	1.49	1.49	1.57	1.13	0.48	0.43	0.43	0.69	0.76	0.96	0.45	2.24	0.68	1.73	1.13	1.98	1.84
TiO_2%	1.26	1.32	1.34	1.40	1.42	1.43	1.49	1.51	1.58	1.58	1.64	1.64	1.74	1.95	1.76	0.80	3.58	2.06
P_2O_5%	0.14	0.25	0.25	0.19	0.14	0.47	0.11	0.15	0.17	0.16	0.43	0.10	0.24	0.18	0.35	0.19	0.63	0.39
SO_3%	0.02	0.01	0.00	0.02	0.01		0.03	0.01	0.03	0.00	0.02		0.00	0.01	0.02	0.00		0.02
LOI%	1.17	0.59	-0.35	1.91	0.50		-0.04	-0.66	0.16		0.27		-0.61	0.61	-2.94	-0.10		-0.40
TOTAL	100.22	100.70	99.90	100.14	100.19	100.82	100.48	100.40	100.27	100.85	100.09	101.16	100.17	100.12	100.26	100.27	100.24	100.76
Rb	31.6	84.1	48.0	95.620	83.9	3.0	13.7	14.7	23.106	24.0	46.4	10.0	122.4	38.6	56.9	30.0	68	65.1
Ba	116	236	533	234	234	127	126	148	194	258	268	131	452	244	671	728	901	762
Th	1.3	0.5	5.8	9.1	1.9		1.1	1.7	3.1		2.6		12.5	2.8	3.9	2.2		4.3
U	1.1	10.7	1.9	4.2	1.3		1.2	1.7	1.2		0.6		5.0	2.4	1.9	0.5		1.7
Nb	7.9	6.4	13.2	10.1	8.5	9.0	8.3	7.3	7.4	8.0	14.9	6.0	18.8	11.1	11.0	7.0	21	13.6
La	6	13	41	19	8	29	7	10	15	12.2	25	13	47	20	34	23.9		37
Ce	15	34	80	54	36	71	33	39	37	27	50	29	92	55	79	50.9		73
Pb	4.0	6.7	9.6	5.5	2.9		4.7	0.9	7.1		6.6		16.4	4.4	10.6	6.4		15.3
Sr	224.0	193.4	244.7	150.9	188.5	109	184.3	170.6	177.1	188	158.8	110	133.1	226.1	208.9	320	209	211.1
Nd	11.458	19	36	25.016	8	31	9	13	18.952	16.2	31	13.0	43	28	31.912	23.3		39
Zr	70	64	209	169	106	62	67	96	112	105	135	107	268	126	167	107	303	191
Sm	2.87			5.78					4.59	4.09					7.00	4.48		
Y	19.2	26.1	36.1	32.8	31.5	23	22.1	27.7	27.5	28	37.4	21	52.6	71.3	42.2	25	56	47.9
V	295	243	251	296	355	233	401	40	363	269	254	318	377	431	308	228		379
Sc	38.9	34.1	24.6	35.8	40.8	33.0	45.8	145.0	37.7	34.0	45.1	35.0	29.7	45.3	39.5	35.0	31	39.4
Cr	145	456	135	25	197	114	175	355.2	192	141	151	66	*	187	67	345		26
Ga	17.1	16.2	22.1	21.2	19.8		20	81.4	22.3		20.6		23.3	19.7	22.1	6.4		26.2
Cu	90	88	118	9	6		109	18.8	143		207		157	36	132			156
Zn	86	114	95	121	117		121	200	114		119		115	119	162			173
Ni	133	136	65	16	86	62	72	114	131		50	62	34	75	84			63
Co	73.1	67	53	69.5	84.5	114	76.7	84	68		100		64	63	100.2			74
Eu	1.058									1.41						1.28		
Gd	3.133									4.75						4.47		
Dy	2.893									4.93						4.22		
Er	1.627									2.93						2.68		
Yb	1.457									2.76						2.67		

Lithology	HBaT															Iron rich Tholeiites (FeRT)		
Type		Amphibolite	Amphibolite	Amphibolite	Amphibolite	Amphibolite	E leucosome amphib	W leucosome amphib		leucosome mafic	Even grained mafic	boudin neck	middle dyke	of even grained mafic	hb gt mafic	gt mafic	hb 2px gran	
Sample #	1028-8	D74	D48	D76	A27	B45	SEP-199D	SEP-199B	SEP-218A	SEP-196A	SEP-198	SEP-194B	SEP-199C	SEP-199F	1028-21	1028-10	1028-4	1028-48
Location	*C Catastrophe*	*Kirton Pt*	*Pt Boston*	*Kirton Pt*	*Kirton Pt*	*C Donington*	*Kirton Pt*	*Kirton Pt*	*E C Tournefor*	*Wanna*	*Wanna*	*Wanna*	*Kirton Pt*	*Kirton Pt*	*Kirton Pt*	*Lookout*	*C Catastrophe*	*C Catastrophe*
Source	Bendall, 1994	Mortimer, 1984	Mortimer, 1984	Mortimer, 1984	Mortimer, 1984	Mortimer, 1984									Bendall, 1994	Bendall, 1994	Bendall, 1994	Bendall, 1994
Easting							580790	580790	578460	577800	577740	577780	580790	580790				
Northing							6157000	6157000	6135060	6138400	6138420	6138600	6157000	6157005				
SiO_2%	53.87	52.82	54.11	54.35	58.00	51.84	55.54	57.92	55.52	55.43	54.55	52.45	56.86	57.01	58.32	48.10	49.72	49.53
Al_2O_3%	15.04	12.71	14.10	13.13	12.82	12.40	13.24	13.07	14.24	14.23	15.14	14.11	12.93	12.88	12.67	14.72	13.61	13.65
Fe_2O_3%	12.01	15.06	12.79	15.42	14.12	16.22	14.95	13.61	12.44	10.90	12.10	14.01	14.47	14.58	13.94	16.66	17.01	17.00
MnO%	0.16	0.21	0.19	0.22	0.19	0.21	0.20	0.18	0.18	0.16	0.16	0.18	0.18	0.19	0.15	0.21	0.23	0.23
MgO%	3.82	3.26	4.24	3.20	1.99	3.17	2.90	2.29	4.57	4.47	4.45	4.02	2.46	2.47	1.50	6.27	4.93	4.96
CaO%	7.99	7.08	7.78	6.94	5.50	7.22	6.78	5.76	8.30	7.22	8.45	7.28	6.11	6.13	4.80	8.68	8.95	8.89
Na_2O%	2.76	3.16	2.64	2.58	2.72	2.59	3.05	2.99	2.70	2.79	2.56	2.66	2.98	2.81	2.54	2.73	2.62	2.58
K_2O%	2.05	2.45	2.33	2.25	2.93	2.32	2.28	2.69	1.87	2.99	2.13	2.75	2.48	2.66	3.08	1.09	1.41	1.39
TiO_2%	1.23	2.50	1.31	1.72	1.44	2.75	1.49	1.37	1.05	0.90	1.22	1.45	1.48	1.49	1.60	1.81	2.08	2.10
P_2O_5%	0.31	1.04	0.33	0.32	0.33	1.20	0.34	0.30	0.24	0.20	0.31	0.36	0.32	0.32	0.66	0.20	0.26	0.25
SO_3%	0.01						0.01	0.01	0.01	0.02	0.00	0.00	0.02	0.02	0.02	0.01	0.03	0.02
LOI%	0.43						0.05	0.04	-0.27	0.48	-0.20	0.43	-0.09	-0.11	0.03	-0.52	-0.54	-0.56
TOTAL	99.69	100.29	99.82	100.13	100.04	99.92	100.83	100.23	100.85	99.79	100.87	99.70	100.20	100.45	99.32	99.95	100.31	100.05
Rb	82.5	97	84	82	109	81	70.9	89.2	65.9	123.6	77.0	130.5	89.0	105.9	159.9	40.8	57.4	56.8
Ba	776	1030	943	871	987	1047	789	815	819	873	886	947	965	984	1188	358	502	479
Th	9.5						11.6	14.1	8.2	13.6	8.7	10.1	10.9	12.7	14.3	3.4	5.1	4.9
U	3.8						2.3	3.1	2.2	6.5	2.8	3.1	3.6	4.1	4.0	2.2	2.9	2.7
Nb	11.1	15	11	12	13	15	17.9	14.3	9.9	13.1	11.8	13.3	14.9	14.9	16.6	9.6	11.8	12.4
La	17						72	71	46	32	50	62	60	60	73	19	26	67
Ce	100						131	132	91	68	102	113	120	117	147	47	69	67
Pb	12.5						20.2	20.1	10.2	23.6	14.8	14.0	21.7	18.6	25.4	5.7	12.5	6.1
Sr	270.2	287	252	267	233	288	246.3	195.6	275.6	239.7	264.1	224.7	245.5	249.2	256.4	183.1	164.6	162.2
Nd	40						55	53	38	29	46	47	50	52	64.0	20	26	26
Zr	208	251	220	203	257	234	228	226	176	150	204	254	236	242	281	144	170	175
Sm																		
Y	41.9	58	48	43	53	62	55.2	47.4	35.8	44.1	40.5	47.4	46.6	47.0	49.7	31.6	41.8	40.4
V	214						357	298	240	192	223	246	332	337	0	267	351	346
Sc	37.1	46	43	48	39	49	42.5	36.7	34.9	35.1	33.5	39.0	38.5	40.2	32.4	32.4	40.8	42.1
Cr	52						*	0	8	31	65	29	*	*	14	94	148	142
Ga	16.5						19.3	19.0	18.2	17.0	16.7	17.0	19.9	18.2	18.7	23	22.5	22.5
Cu	144						64	83	64	210	82	30	58	60	52	445	172	165
Zn	111						129	119	101	100	103	129	134	136	140	135	167	139
Ni	48						8	5	49	54	56	45	3	7	5	104	63	49
Co	59.6						79	82	61	57	87	65	86	65	82.2	80.9	76.3	76.1
Eu																		
Gd																		
Dy																		
Er																		
Yb																		

Lithology	FeRT														Sleaford Complex			
Type	G1 Tourn	mafic 315	Amphibolite	amphibolite	Gabbro norite		Amphibolite			mafic	hb gt mafic 340	mafic	gt mafic	hb gt mafic ?000	mafic	Sleaford	Sleaford	Coulta Granodiorite
Sample #	SEP-270	SEP-081	D54	1028-33	B82	1397	F37	1346	743	SEP-021	1028-13	SEP-035	1028-15	1028-12	446/F30	Leucogneiss	Augen gneiss	SEP-184
Location	*NW Will. Is Is*	*W West Pt*	*Pt Boston*	*Mine Ck*	*C Donington*	*Point Warna*	*C Colbert*	*Fishery Bay*	*Fishery Bay*	*Bolingbroke*	*Lookout*	*Massena Bay*	*Lookout*	*Lookout*	*Fishery Bay*	*Cape Carnot*	*Cape Carnot*	*Pt Drummond*
Source			Mortimer, 1984	Bendall, 1994	Mortimer, 1984	Bradley, 1972	Mortimer, 1984	Bradley, 1972	Bradley, 1972		Bendall, 1994		Bendall, 1994	Bendall, 1994	Turner et al., 1993	Turner et al., 1993	Turner et al., 1993	
Easting	588085	585840								601400		602440						
Northing	6123955	6128020								6179480		6183160						
SiO_2%	48.07	49.79	49.64	51.92	47.54	48.34	49.76	49.49	47.97	48.36	48.51	48.20	48.47	47.28	47.54	76.75	70.08	67.89
Al_2O_3%	13.19	13.63	13.08	14.60	13.43	13.87	13.94	14.36	12.91	12.84	12.39	12.54	12.16	12.77	13.03	12.87	14.97	14.21
Fe_2O_3%	17.93	16.75	17.66	15.97	17.40	16.53	16.81	17.70	18.22	17.81	18.44	18.37	19.47	18.65	17.77	1.77	3.59	5.11
MnO%	0.26	0.24	0.24	0.25	0.23	0.25	0.21	0.26	0.27	0.23	0.25	0.24	0.26	0.24	0.26	0.02	0.04	0.07
MgO%	6.42	5.29	4.56	3.45	6.06	5.85	4.48	6.06	6.05	5.00	3.74	4.60	4.30	4.68	6.83	0.40	2.08	1.38
CaO%	9.61	9.43	8.58	7.17	9.39	9.66	7.98	8.76	10.13	8.99	8.13	8.95	7.65	8.43	10.04	2.02	1.32	3.43
Na_2O%	2.38	2.61	2.50	1.52	2.32	2.38	2.54	0.84	1.52	2.01	2.44	2.48	2.02	2.32	1.64	3.75	2.79	3.88
K_2O%	0.51	1.13	1.29	1.94	0.91	0.89	1.22	0.33	0.29	1.13	1.52	1.19	1.49	0.94	0.25	2.31	5.50	2.60
TiO_2%	2.11	2.17	2.23	2.44	2.50	2.54	2.58	2.62	2.69	3.03	3.13	3.23	3.31	3.56	2.67	0.25	0.64	0.57
P_2O_5%	0.20	0.27	0.24	0.28	0.30	0.39	0.33	0.40	0.35	0.45	0.79	0.48	0.67	0.71	1.09	0.03	0.09	0.13
SO_3%	0.04	0.01		0.04	0.00					0.09	0.03	0.03	0.03	0.05				0.00
LOI%	0.06	-0.51		0.47						0.27	0.81	-0.17	0.47	0.48	-0.54	0.33	0.15	0.71
TOTAL	100.78	100.80	100.02	100.04	100.08	100.70	99.85	100.82	100.40	100.21	100.18	100.14	100.29	100.09	100.58	100.50	101.25	99.98
Rb	17.2	55.4	62	107.1	35	30	50	11.0	5.0	33.2	63.5	57.4	48.2	19.8	5.2	43.0	126.0	86.9
Ba	165	301	302	446	266	267	512	64	56	346	441	416	414	314	317	503	664	462
Th	3.0	6.0		17.2						5.3	6.7	4.2	4.6	5.7	1	11	52	13.9
U	0.1	2.3		3.5						2.2	2.3	1.8	2.7	2.9	0	0.2	2.3	4.2
Nb	9.7	12.7	14	18.8	12.0	13.0	16	18.0	16.0	18.1	16.4	15.9	14.1	14.7	17	6	7	9.4
La	15	21		109	21.8	21		34	21	34	5	34	73	35	37	39	88.3	37
Ce	41	59		109	49.9	49		85	50	68	83	68	39	74	70	70	214.64	79
Pb	4.9	8.5		18.2						14.1	10.5	10.0	4.6	8.1	3	14.9	40	14.4
Sr	164.7	135.5	162	146	177	162	254	52	59	137.2	143.3	144.8	145.2	143.1	61.4	135.0	140.0	143.3
Nd	18.875	26.338		46.0	28.2	21.0		45.0	21.0	37.0	38.0	43.0	22.0	37.0	28.8	17.1	40.2	31.1
Zr	130	203	196	287	150	174	209	169	170	230	221	205	185	183	170	171	275	222
Sm	5.04	6.63			6.90					8.27					7.49	2.64	6.78	6.50
Y	37.3	49.0	49	56.1	44	38	70	49	51	54.8	60.2	56.3	52.3	59.8	60	10	16	41.5
V	466	410		395	405	340		363	365	441	333	516	435	476	460	17	60	54
Sc	44.9	38.3	41	37.6	41.0	31.0	44	46.0	44.0	45.0	41.2	45.7	45.4	49.1	42.0	4.0	6.0	12.5
Cr	91	154		39	170	162		110	119	98	27	39	38	28	223	398	434	17
Ga	22.2	22.3		24.3						21.0	20.7	25.7	22	23.4	20	13	19	18
Cu	122	308		236						208	69	120	44	241				31
Zn	128	136		157						166	179	164	154	136				46
Ni	75	61		137		79		41	41	63	34	38	38	73	65	11	21	12
Co	71	62.7		50.6						58	55.1	58	46.8	68.5				48
Eu					2.24					2.279							1.06	
Gd					7.87					8.738							7.49	
Dy					7.78					8.520							3.41	
Er					4.61					4.972							1.24	
Yb					4.17					4.872							0.84	

Lithology	Sleaford Complex						?Miltalie Gneiss equivalents			Hutchison Group			
Type	Kiana Granite	mafic granulite	Waddikee	Kimba	Metapelite	Wangary Gneiss	Felsic Gneiss	Felsic Gneiss	Felsic Gneiss	Calc sil	Pelite	Yadnarie schist	Cook Gap Schist
Sample #	SEP-179	446/C142	Paragneiss	Paragneiss	SEP-188	SEP-181	SEP-160	SEP-247	SEP-263	SEP-075	SEP-117	1031-032	939-90-13
Location	*Pt Drummond*	*Cape Carnot*	*W. Eyre Pen.*	*W. Eyre Pen.*	*C Carnot*	*L Hamilton*	*S West Pt*	*S West Pt*	*NW Will. Is. Is*	*Trinity Haven*	*Trinity Haven*		*Lincoln*
Source		Turner et al., 1993	Turner et al., 1993	Turner et al., 1993								Simpson, 1994	Simpson, 1994
Easting							587500	587550	588036	602205	602205		
Northing							6125280	6125260	6123837	6187005	6187005		
SiO_2%	71.10	50.69	73.24	65.16	61.15	70.94	68.09		70.97	65.78	53.46	66.92	61.85
Al_2O_3%	14.24	14.57	14.30	16.06	16.35	14.99	15.08		14.53	14.00	20.81	15.03	15.76
Fe_2O_3%	2.95	12.94	2.45	5.40	11.57	2.40	3.10		2.35	3.72	10.30	6.17	8.07
MnO%	0.03	0.21	0.02	0.05	0.13	0.03	0.05		0.02	0.19	0.10	0.03	0.18
MgO%	1.01	7.77	0.69	1.75	4.69	2.59	0.98		0.29	1.59	4.18	2.32	2.92
CaO%	1.50	11.76	1.16	2.41	0.93	0.44	2.27		1.52	11.72	3.03	0.97	0.66
Na_2O%	3.55	0.94	3.24	3.32	1.14	2.39	2.69		2.66	0.77	2.98	1.90	1.82
K_2O%	4.11	0.65	4.62	4.46	2.31	3.99	5.94		6.51	0.38	3.03	3.67	4.72
TiO_2%	0.42	0.84	0.27	0.84	1.03	0.41	0.67		0.21	0.48	1.05	0.77	0.69
P_2O_5%	0.17	0.06	0.09	0.22	0.03	0.05	0.18		0.03	0.19	0.10	0.16	0.13
SO_3%	0.00				0.02	0.00	0.01		0.00	0.05	0.01	0.01	
LOI%	0.55	-0.01	0.27	0.48	0.61	1.37	0.34		0.23	1.46	0.78	1.77	2.42
TOTAL	99.63	100.42	100.35	100.15	99.96	99.60	99.40		99.32	100.33	99.83	99.72	99.22
Rb	230.2	19.1	177.1	138.0	117.7	164.1	245.0	142.7	196.7	21.8	173.4	184.4	229.2
Ba	576	203	415	1331	391	565	1161		1586	33	861	899	542
Th	36.5	1	32	18	13.6	36.2	34.1		13.4	15.2	39.6	19	24
U	4.2	0.7	14.4	0	0.8	5.9	1.3		1.3	5.7	8.1	2.1	6.1
Nb	13.3	4	12	13	8.3	13.7	20		1.7	14.8	19.9	13.8	17
La	57	6.58	28	51.58	22	46	165		60	43	85	45	50
Ce	122	16.92	61	130.48	42	105	300		111	81	168	89	93
Pb	29.8	6.6	31	27	15.7	14.3	30.3		31.4	14.3	22.4	10.6	1101
Sr	114.4	80.4	59.6	302.7	55.8	138.7	199.4	249.6	201.0	289.6	259.9	89.4	69.4
Nd	49.4	8.3	29.4	32.6	29.3	53.2	96.6	34.9	37.2	40.7	93.0	38.3	37.5
Zr	194	51	135	196	167	213	383		255	164	326	259	193
Sm	8.55	2.32	5.46	6.59	5.94	9.87	13.31	4.42	5.39		15.48	7.04	6.68
Y	15.6	24	12	12	35.8	22.3	28.7		9.0	36.3	40.2	30.9	36
V	42	278	27	106	201	38	24		6	40	188	110	96
Sc	5.7	43.0	5.0	9.0	14.7	9.5	8.8		4.7	11.1	22.1	17.4	12.0
Cr	21	368	240	209	265	26	5	b.d.		42	174	185	204
Ga	21.5	17	17.6	21	26.9	19.7	16.3		16.1	18.4	30.8	18.9	26
Cu	17				110	5	24		9	74	27	47	
Zn	59				237	33	47		24	113	173	72	
Ni	11	87	12	29	92	13	6		2	14	52	44	35
Co	46				62	28	67		45	56.6	42	30.5	
Eu		0.65		1.93									
Gd		2.86		5.83									
Dy		3.86		3.03									
Er		2.35		0.82									
Yb		2.43		0.45									

Appendix 3:

Compilation of isotopic data for southern Eyre Peninsula

	Quartz Gabbro Norite Gneiss					Memory Cove Charnockite						
Type	QGNG	QGNG	QGNG	QGNG	QGNG	MCC	MCC	MCC	MCC	MCC	MCC	MCC
Sample #	B203	B201	B205	B202	SEP-239	B143	SEP-154	B144	B25	SEP-074	SEP-147	SEP-073
Location	*C Donington*	*C Donington*	*C Donington*	*C Donington*	*Nth Taylors La*	*C Colbert*	*CC-Lookout*	*C Colbert*	*Surfleet Cove*	*Trinity Haven*	*Memory Cove*	*Trinity Haven*
Source	Mortimer, 1984	Turner et al., 1993	Mortimer, 1984	Mortimer, 1984		Turner et al., 1993		Mortimer, 1984	Mortimer, 1984			
Easting					590640		589500			602205	591020	602205
Northing					6145380		6127420			6187005	6129080	6187005
Stratigraphic age (T), Ma	*1848.1*	*1848.1*	*1848.1*	*1848.1*	*1848.1*	*1847*	*1847*	*1847*	*1847*	*1847*	*1847*	*1847*
Nd		28.80			70.843	50.9	47.449			41.968	46.162	37.950
Sm		5.68			12.926	9.58	8.646			8.420	8.516	7.226
$^{143}Nd/^{144}Nd$		0.511518			0.511431	0.511469	0.511477			0.51151	0.511483	0.511439
2σ		0.000024			0.000064	0.000013	0.000042			0.000058	0.000036	0.000018
$^{147}Sm/^{144}Nd$		0.1193			0.1104	0.1138	0.1102			0.1214	0.1116	0.1152
$T_{(CHUR)}$, Ga		2.2			2.1	2.1	2.0			2.3	2.1	2.2
$T_{(DM)}$, Ga		2.4			2.4	2.4	2.3			2.5	2.3	2.4
$\varepsilon_{Nd\ (0)}$		**-32.0**			**-33.7**	**-33.0**	**-32.8**			**-32.2**	**-32.7**	**-33.5**
$\varepsilon_{Nd\ (T)}$		-3.5			-3.1	-3.2	-2.2			-4.2	-2.4	-4.1
$\varepsilon_{Nd\ (1845)}$		-3.6			-3.1	-3.2	-2.2			-4.2	-2.4	-4.1
$^{87}Sr/^{86}Sr$	0.73753	0.738710	0.73602	0.74657	0.900624	0.79508	0.792497	0.81585	0.79949	0.838135	0.830676	0.832662
2σ		0.000049			0.000034	0.00004	0.000032			0.000030	0.000032	0.000040
Sr ppm	229	231	240	217	97.5	171	176.299	155	167	134.735	143.973	136.569
Rb ppm	97	102	97	117	234.6	201	205.909	223	207	228.711	239.454	221.811
Rb/Sr	0.424	0.442	0.404	0.539	2.406	1.175	1.168	1.439	1.240	1.697	1.663	1.624
$^{87}Sr/^{86}Sr_{(T)}$	0.704848	0.704637	0.704840	0.704932	0.712018	0.703932	0.701952	0.704062	0.703332	0.705957	0.701261	0.706259

	MCC	Megacrystic Charnockites								CRG		
Type	MCC	Megacrystic Charnockite	Megacrystic Charnockite	Megacrystic Charnockite	Megacrystic Charnockite	Megacrystic Charnockite	Megacrystic Charnockite	Megacrystic Charnockite	Megacrystic Charnockite	CRG	CRG	CRG
Sample #	B145	SEP-282	D108	SEP-249	A109A	D107	SEP-265	SEP-295	SEP-264	B153	B152	B154B
Location	*C Colbert*	*SE Will Is*	*Bolingbroke*	*S West Pt*	*C Donington*	*Bolingbroke*	*NW Will. Is. Is*	*NE Will. Is*	*NW Will. Is*	*Carcase R*	*Carcase R*	*Carcase R*
Source	Mortimer, 1984		Mortimer, 1984		Mortimer, 1984	Mortimer, 1984				Mortimer, 1984	Turner et al., 1993	Mortimer, 1984
Easting		589432		587520			588006	589279	588036			
Northing		6122718		6125760			6123978	6124074	6123837			
Stratigraphic age (T), Ma	*1847*	*1847*	*1847*	*1847*	*1847*	*1847*	*1847*	*1847*	*1847*	*1847*	*1847*	*1847*
Nd		49.570		37.185			49.075	41.972	60.805		33.8	
Sm		9.115		5.180			7.211	6.549	7.407		5.74	
$^{143}Nd/^{144}Nd$		0.511479		0.511168			0.511162	0.511205	0.511029		0.511728	
2σ		0.000032		0.00003			0.000024	0.000062	0.000039		0.000016	
$^{147}Sm/^{144}Nd$		0.1112		0.0843			0.0889	0.0944	0.0737		0.1027	
$T_{(CHUR)}$, Ga		2.1		2.0			2.1	2.1	2.0		1.5	
$T_{(DM)}$, Ga		2.3		2.2			2.3	2.3	2.2		1.8	
$\varepsilon_{Nd\ (0)}$		**-32.8**		**-38.8**			**-38.9**	**-38.1**	**-41.5**		**-27.9**	
$\varepsilon_{Nd\ (T)}$		-2.4		-2.1			-3.3	-3.7	-2.3		4.5	
$\varepsilon_{Nd\ (1845)}$		-2.4		-2.1			-3.3	-3.8	-2.3		4.5	
$^{87}Sr/^{86}Sr$	0.83575	0.79294	0.78881	0.76939	0.76575	0.788040	0.760319	0.768279	0.773451	4.0985	4.3548	4.3802
2σ		0.000032		0.00005			0.000068	0.00006	0.000418		0.00004	
Sr ppm	140	203.304	171	206.278	174	179	215.457	201.459	196.781	12	12	11
Rb ppm	238	236.604	185	177.029	135	193	156.441	161.160	172.002	397	413	442
Rb/Sr	1.700	1.164	1.082	0.858	0.776	1.078	0.726	0.800	0.874	33.083	34.417	40.182
$^{87}Sr/^{86}Sr_{(T)}$	0.703406	0.702714	0.704969	0.703008	0.705758	0.704489	0.704205	0.706408	0.705814	0.711078	0.764510	0.180822

	GG1	Megacrystic Granite Gneisses (GG2)										AFGG
Type	Even Grained Granite Gn.	Megacrystic Granite Gn.	Megacrystic Granite Gn.	Megacrystic Granite Gn.	Megacrystic Granite Gn.	Megacrystic Granite Gn.	Megacrystic Granite Gn.	Megacrystic Granite Gn.	Megacrystic Granite Gn.	Megacrystic Granite Gn.	Megacrystic Granite Gn.	AFGG
Sample #	SEP-252	SEP-142	B168	A88	A121	B164D	D21	B164E	B164B	B500	D205	B22C
Location	*S West Pt*	*Peake Pt*	*Engine Pt*	*McLaren Pt*	*Kirton Pt*	*Engine Pt*	*Kirton Pt*	*Engine Pt*	*Engine Pt*	*Billy Lights Pt*	*Kirton Pt*	*Carcase R*
Source			Mortimer, 1984	Mortimer, 1984	Mortimer, 1984	Mortimer, 1984	Mortimer, 1984	Mortimer, 1984	Mortimer, 1984	Mortimer, 1984	Mortimer, 1984	Mortimer, 1984
Easting	587530	593190										
Northing	6125760	6180040										
Stratigraphic age (T), Ma	*1847*	*1847*	*1847*	*1847*	*1847*	*1847*	*1847*	*1847*	*1847*	*1847*	*1847*	*1847*
Nd	52.501	47.236										
Sm	5.959	8.887										
$^{143}Nd/^{144}Nd$	0.510942	0.511477										
2σ	0.000038	0.000034										
$^{147}Sm/^{144}Nd$	0.0687	0.1138										
$T_{(CHUR)}$, Ga	2.0	2.1										
$T_{(DM)}$, Ga	2.2	2.4										
$\varepsilon_{Nd\ (0)}$	**-43.2**	**-32.8**										
$\varepsilon_{Nd\ (T)}$	-2.8	-3.0										
$\varepsilon_{Nd\ (1845)}$	-2.8	-3.1										
$^{87}Sr/^{86}Sr$	0.773248	0.822241	0.96317	0.83589	0.85265	0.95982	0.91619	0.98468	1.0248	0.96711	1.20906	5.3405
2σ	0.000054	0.000042										
Sr ppm	193.535	153.385	108	131	129	100	109	103	99	79	59	10
Rb ppm	168.725	233.907	361	235	244	323	293	370	414	263	371	448
Rb/Sr	0.872	1.525	3.343	1.794	1.891	3.230	2.688	3.592	4.182	3.329	6.288	44.800
$^{87}Sr/^{86}Sr_{(T)}$	0.705788	0.703679	0.699747	0.696234	0.705159	0.705352	0.705298	0.701002	0.693301	0.704651	0.701875	0.334889

	Alkali Feldspar GG		WIG	Selvages and partial melts				Jussieu Dykes				HMgT
Type	AFGG	AFGG	WIG	selvage/ charnockite	felsic selvage	felsic selvage	leucosome	Jussieu Dyke	Jussieu Dyke	Jussieu Dyke	Jussieu Dyke	ultramafic
Sample #	B159B	B154A	SEP-283	SEP-251	SEP-296	SEP-262	SEP-026	SEP-241	SEP-250	SEP-261	SEP-293	SEP-148
Location	*Carcase R*	*Carcase R*	*Williams Is*	*S West Pt*	*NE Will. Is*	*NW Will. Is*	*Bolingbroke*	*S McLaren Pt*	*S West Pt*	*NW Will. Is*	*NE Will. Is*	*Mem Cove*
Source	Mortimer, 1984	Mortimer, 1984										
Easting			589404	587520	589279	588036	600700	590740	587520	588036	589279	591020
Northing			6122608	6125760	6124074	6123837	6177960	6145460	6125760	6123837	6124074	6129080
Stratigraphic age (T), Ma	*1847*	*1847*	*1846*	*1846*	*1846*	*1846*	*1846*	*1846*	*1846*	*1846*	*1846*	*1812*
Nd			5.158	37.858	25.529	6.501	6.627	22.177	23.282	21.752	19.313	9.889
Sm			0.742	4.297	4.761	1.533	1.215	5.199	4.760	4.968	3.917	2.151
$^{143}Nd/^{144}Nd$			0.511182	0.510896	0.511415	0.511765	0.511454	0.511765	0.511825	0.511876	0.5117	0.51157
2σ			0.000034	0.00006	0.000032	0.000052	0.000073	0.000062	0.000052	0.000048	0.000062	0.00005
$^{147}Sm/^{144}Nd$			0.0870	0.0687	0.1128	0.1426	0.1109	0.1418	0.1237	0.1382	0.1227	0.1316
$T_{(CHUR)}$, Ga			2.0	2.1	2.2	2.5	2.1	2.4	1.7	2.0	1.9	2.5
$T_{(DM)}$, Ga			2.2	2.2	2.4	2.7	2.3	2.6	2.1	2.3	2.2	2.7
$\varepsilon_{Nd\ (0)}$			**-38.5**	**-44.1**	**-34.0**	**-27.2**	**-33.2**	**-27.2**	**-26.0**	**-25.0**	**-28.5**	**-31.0**
$\varepsilon_{Nd\ (T)}$			-2.4	-3.7	-4.0	-4.3	-2.8	-4.1	1.4	-1.0	-0.8	-5.7
$\varepsilon_{Nd\ (1845)}$			-2.5	-3.7	-4.0	-4.3	-2.8	-4.1	1.4	-1.0	-0.8	-5.5
$^{87}Sr/^{86}Sr$	4.3802	4.4532	1.431453	0.774299	0.856364	0.950661	0.861807	0.725881	0.747921	0.733507	0.723656	0.722115
2σ			0.000056	0.000044	0.000062	0.00008	0.00009	0.0001	0.000088	0.000128	0.000074	0.000048
Sr ppm	12	10	18.195	207.948	131.143	58.625	129.403	156.220	225.575	206.799	315.835	86.487
Rb ppm	437	440	172.934	190.049	262.626	188.968	256.492	42.819	132.052	79.751	83.129	18.512
Rb/Sr	36.417	44.000	9.504	0.914	2.003	3.223	1.982	0.274	0.585	0.386	0.263	0.214
$^{87}Sr/^{86}Sr_{(T)}$	0.574316	-0.169373	0.649390	0.703611	0.700238	0.697078	0.707197	0.704781	0.702759	0.703798	0.703399	0.705951

	High Magnesium Tholeiites			Unassigned Tholeiites								HBaT
Type	def mafic	Norite	Norite	Plag-phyric dolerite	mafic	Norite			gt hb mafic	Late Dyke	Gabbro norite	hb 2px granulite
Sample #	SEP-024	B58	B69	B52	1028-2	B16	SEP-220	SEP-034	1028-110	SEP-260	B36	1028-99
Location	*Bolingbroke*	*C Donington*	*C Donington*	*C Donington*	*E West P*	*Fisherman Pt*	*W West Pt*	*Massena Bay*	*Mine Ck*	*NW Will. Is*	*Surfleet Pt*	*W West Pt*
Source		Mortimer, 1984	Mortimer, 1984	Mortimer, 1984	Bendall, 1994	Mortimer, 1984			Bendall, 1994		Mortimer, 1984	Bendall, 1994
Easting	600740						585860	602280		588036		
Northing	6178020						6128024	6183240		6123837		
Stratigraphic age (T), Ma	*1812*	*1812*	*1812*	*1812*	*1812*	*1812*	*1812*	*1812*	*1812*	*1812*	*1812*	*1812*
Nd	6.240						24.3	11.458	25.016	18.952		31.912
Sm	1.654				4.40		4.89	2.871	5.782	4.594		6.999
$^{143}Nd/^{144}Nd$	0.512063				0.511989		0.511436		0.511876	0.512085		0.511627
2σ	0.000064				0.000037		0.000024		0.000059	0.000032		0.000059
$^{147}Sm/^{144}Nd$	0.1603				0.5324		0.1217		0.1398	0.1466		0.1327
$T_{(CHUR)}$, Ga	2.4						2.4		2.0	1.7		2.4
$T_{(DM)}$, Ga	2.7						2.6		2.4	2.2		2.6
$\varepsilon_{Nd\ (0)}$	**-21.4**				**-22.8**		**-33.6**		**-25.0**	**-20.9**		**-29.9**
$\varepsilon_{Nd\ (T)}$	-2.8						-6.1		-1.7	0.8		-4.9
$\varepsilon_{Nd\ (1845)}$	-2.6						-5.7		-1.4	1.1		-4.6
$^{87}Sr/^{86}Sr$	0.740074	0.71577	0.71318	0.71246		0.71544	0.717462	0.712916	0.751932	0.712885	0.7123	0.726084
2σ	0.000165	0.00006	0.00006	0.00015		0.00034	0.000026	0.00012	0.000049	0.000036	0.00005	0.000049
Sr ppm	80.243	112	165	58		182	248.553	224.035	150.898	177.105	188	208.945
Rb ppm	47.731	19	21	20		30	38.169	31.551	95.620	23.106	24	56.898
Rb/Sr	0.595	0.170	0.127	0.345		0.165	0.154	0.141	0.634	0.130	0.128	0.272
$^{87}Sr/^{86}Sr_{(T)}$	0.695075	0.702967	0.703577	0.686444	-0.004584	0.703000	0.705870	0.702290	0.703940	0.703041	0.702669	0.705512

	HBaT	**Iron rich tholeiites**		**Sleaford Complex**								
Type	Norite	G1 Tourn	mafic 315	mafic	Sleaford	Sleaford	Coulta Granodiorite	Kiana Granite	mafic granulite	Waddikee	Kimba	Metapelite
Sample #	B26	SEP-270	SEP-081	446/F30	Leucogneiss	Augen gneiss	SEP-184	SEP-179	446/C142	Paragneiss	Paragneiss	SEP-188
Location	*Surfleet Pt*	*NW Will. Is Is*	*W West Pt*	*Fishery Bay*	*Cape Carnot*	*Cape Carnot*	*Pt Drummond*	*Pt Drummond*	*Cape Carnot*	*W. Eyre Pen.*	*W. Eyre Pen.*	*C Carnot*
Source	Turner et al., 1993			Turner et al., 1993	Turner et al., 1993	Turner et al., 1993			Turner et al., 1993	Turner et al., 1993	Turner et al., 1993	
Easting		588085	585840									
Northing		6123955	6128020									
Stratigraphic age (T), Ma	*1812*	*1812*	*1812*	*2430*	*2430*	*2430*	*2517*	*2558*	*2430*	*2520*	*2520*	*2430*
Nd	23.3	18.875	26.338	28.8	17.12	40.24	31.052	49.400	8.34	29.37	32.62	29.338
Sm	4.48	5.04	6.626	7.49	2.64	6.78	6.503	8.553	2.32	5.46	6.59	5.940
$^{143}Nd/^{144}Nd$	0.511284	0.512313	0.512167	0.511981	0.510916	0.510933	0.511356	0.511134	0.51182	0.511377	0.511235	0.511229
2σ	0.000013	0.000036	0.000056	0.000026	0.000028	0.000028	0.000026	0.00004	0.000026	0.00002	0.000037	0.00005
$^{147}Sm/^{144}Nd$	0.1163	0.1615	0.1522	0.1573	0.0933	0.1019	0.1267	0.1047	0.1683	0.1125	0.1222	0.1225
$T_{(CHUR)}$, Ga	2.6	1.4	1.6	2.5	2.5	2.7	2.8	2.5	4.4	2.3	2.9	2.9
$T_{(DM)}$, Ga	2.7	2.1	2.2	2.8	2.6	2.8	2.9	2.6	3.8	2.5	2.9	2.9
$\varepsilon_{Nd\ (0)}$	**-36.6**	**-16.5**	**-19.4**	**-23.0**	**-43.7**	**-43.4**	**-35.2**	**-39.5**	**-26.1**	**-34.7**	**-37.5**	**-37.6**
$\varepsilon_{Nd\ (T)}$	-7.8	1.8	1.1	-0.5	-1.3	-3.7	-2.4	0.9	-7.1	2.7	-3.3	-4.3
$\varepsilon_{Nd\ (1845)}$	-7.4	2.0	1.3	-3.5	-9.2	-10.9	-8.5	-7.6	-9.3	-4.7	-9.8	-10.0
$^{87}Sr/^{86}Sr$	0.71087	0.710167	0.733129	0.71321	0.7432	0.7988	0.762447	0.911695	0.73215	1.0126	0.74719	0.887256
2σ	0.00003	0.00004	0.00012	0.00001	0.00003	0.00002	0.000018	0.000028	0.00007	0.00004	0.00007	0.000048
Sr ppm	320	164.702	135.544	61.4	135	140	143.287	114.425	80.4	59.6	302.7	55.774
Rb ppm	30	17.230	55.383	5.2	43	126	86.915	230.162	19.1	177.1	138	117.728
Rb/Sr	0.094	0.105	0.409	0.085	0.319	0.900	0.607	2.011	0.238	2.971	0.456	2.111
$^{87}Sr/^{86}Sr_{(T)}$	0.703798	0.702276	0.702240	0.704603	0.710733	0.706566	0.698245	0.692121	0.707961	0.690043	0.698950	0.669081

	Basement	**?Miltalie Gneiss**			**Metased**	**Hutchison Group and eqivalents**		
Type	Wangary Gneiss	Felsic Gneiss	Felsic Gneiss	Felsic Gneiss	Calc sil	Pelite	Yadnarie schist	CGS
Sample #	SEP-181	SEP-160	SEP-247	SEP-263	SEP-075	SEP-117	1031-032	939-90-13
Location	*L Hamilton*	*S West Pt*	*S West Pt*	*NW Will. Is. Is*	*Trinity Haven*	*Trinity Haven*		*Lincoln*
Source							Simpson, 1994	Simpson, 1994
Easting		587500	587550	588036	602205	602205		
Northing		6125280	6125260	6123837	6187005	6187005		
Stratigraphic age (T), Ma	*2479*	*2430*	*2430*	*2430*	*2430*	*2430*	*1860*	*1870*
Nd	53.157	96.579	34.941	37.170	40.65	92.960	38.281	37.48
Sm	9.867	13.313	4.418	5.393		15.481	7.040	6.68
$^{143}Nd/^{144}Nd$	0.511062	0.510964	0.511006	0.511196	0.511442	0.511312	0.511498	0.511405
2σ	0.000086	0.000074	0.000038	0.000082	0.000076	0.000028	0.000057	0.000031
$^{147}Sm/^{144}Nd$	0.1123	0.0834	0.0765	0.0878		0.1007	0.1112	0.1078
$T_{(CHUR)}$, Ga	2.8	2.2	2.1	2.0		2.1	2.0	2.1
$T_{(DM)}$, Ga	2.9	2.4	2.2	2.2		2.3	2.3	2.3
$\varepsilon_{Nd\ (0)}$	**-40.9**	**-42.8**	**-42.0**	**-38.3**	**-33.5**	**-36.0**	**-32.4**	**-34.2**
$\varepsilon_{Nd\ (T)}$	-3.9	2.7	5.7	5.9		4.1	-1.9	-2.8
$\varepsilon_{Nd\ (1845)}$	-10.8	-5.9	-3.4	-2.4		-3.2	-2.0	-3.0
$^{87}Sr/^{86}Sr$	0.813547	0.798519	0.748819	0.778371	0.711548	0.760362	0.85488	0.94741
2σ	0.000038	0.000044	0.000046	0.00003	0.00007	0.000052	0.000129	0.00006
Sr ppm	138.662	199.428	249.644	201.019	289.614	259.945	89.40	69.40
Rb ppm	164.062	244.958	142.651	196.689	21.800	173.443	184.39	229.20
Rb/Sr	1.183	1.228	0.571	0.978	0.075	0.667	2.063	3.303
$^{87}Sr/^{86}Sr_{(T)}$	0.689627	0.672643	0.690543	0.678295	0.703899	0.692238	0.692866	0.684252

Appendix 4:

Pressure-Temperature data used in figure 1.1

Continent	Orogeny	Age (Ma)	Duration (Ma)	P (kbar)	T (°C)	T/P
Australia	Kimban	1725	50	4	650	162.5
	Sleaford	2430	100	7	850	121.4
	Strangways	1755	50	8	885	110.6
	Musgravian	1150	150	12	860	71.7
	Musgravian	1200	150	8.5	820	96.5
	Olarian	1625	90	5	600	120.0
	Broken Hill	1650	300	6	800	133.3
	Delamerian	510	40	4	500	125.0
	Albany-Fraser	1290	20	5.5	800	145.5
	Mt Narryer	2700	100	5.5	622	113.1
	Shaw Batholith	2950	100	5.5	575	104.5
Antarctica	Prince Charles Mts.	1000	80	7	800	114.3
	Rauer	1015	30	8	840	105.0
	Commonwealth Bay	1275	100	6.5	875	134.6
	Napier-Napier	2600	200	5.5	850	154.5
	Napier-Scott	2600	200	9.5	980	103.2
	Napier-Tula	2600	200	7.5	980	130.7
	Rayner Complex	1050	300	9	850	94.4
Greenland	Ketilidian	1800	40	3.5	750	214.3
	Julianehaab (Ketilidian)	1740	20	3	725	241.7
	Buksefjorden	2750	100	9	750	83.3
	Isua	2850	120	5	550	110.0
North America	SW USA	1700	100	4.5	550	122.2
	Kapuskasing	2650	100	7.2	750	104.2
	Flin Flon	1850	100	5.5	550	100.0
	Amer Lake, W Churchill	2700	200	5	740	148.0
	Pikwitonei, Mantioba	2600	200	7.4	780	105.4
	Pikwitonei, Sipawesk	2600	200	9	900	100.0
	Slave	2600	100	3.5	550	157.1
	Wilson Lake, Ontario	1650	300	10	900	90.0
	Adirondacks- highlands	1050	300	7.5	775	103.3
	Adirondacks-lowlands	1050	300	6	730	121.7
	Ptarmigan, Labrador	1660	100	9.5	950	100.0
	New Quebec	2550	300	7	750	107.1
	Grenville	1050	300	7	780	111.4
	Grenville-early	1440	20	8	660	82.5
	Appalachians (Aldan)	397	20	4.5	600	133.3
	Colebrook	125	10	7.5	325	43.3
	Cascade River	75	10	9	600	66.7
	Cascades	95	10	6.5	600	92.3
	Abitibi	2660	30	3.5	400	114.3
	Acadian	335	20	8.5	570	67.1
South America	Margarita, Venezuala	95	10	12	550	45.8
UK/Europe	W Alps	110	40	19	550	28.9
	Trondheim-Bergen	425	100	15	700	46.7
	Scourie	2700	200	8.5	820	96.5
	Lofoten, Norway	2600	200	9	810	90.0
	Arendal, Norway	1650	300	7	800	114.3
	Rogaland, Norway	1050	300	5.5	920	167.3
	Inari, Finland	2025	250	6	730	121.7
	Hercynian	300	100	8	775	96.9
	Lindaas, Norway	440	5	10	690	69.0
USSR	Sharyzhalgay, Baikal	2600	200	6	750	125.0
	Maksyutov	378	10	14	600	42.9
India	Peninsular Gneisses	2600	200	8	850	106.3
	Sri Lanka highlands	1050	300	8	750	93.8
	Sri Lanka Vijayan	1050	300	7	700	100.0
China	Changle-Nanao	121	5	4.5	740	164.4
	Tianshan	400	20	9.5	450	47.4
Africa	Limpopo	2600	200	7.8	800	102.6
	Limpopo	2600	200	10	850	85.0
	Limpopo	2600	200	12	860	71.7
	Namaqualand	1050	300	4.8	820	170.8
	Okiep, S Africa	1100	100	6	800	133.3
	Aldan	2600	200	9	800	88.9

Appendix 5:

Manuscript: "The Jussieu and Tournefort Dykes of the southern Gawler Craton, South Australia"

The Jussieu and Tournefort Dykes of the Gawler Craton, South Australia

Bruce F Schaefer[1], J. Foden[1], M. Sandiford[1] and J.D Hoek[2]

1 *Department of Geology and Geophysics, University of Adelaide, Adelaide 5005, South Australia*
2 *School of Earth Sciences, University of Melbourne, Parkville 3052 Victoria.*

Abstract

Two phases of Palaeoproterozoic mafic magmatism are recorded in the southern Eyre Peninsula, on the Gawler Craton, South Australia.

The Jussieu Dykes are small volume syn-plutonic mafic dykes emplaced with the Lincoln Batholith, at ~1850 Ma. They range in $\varepsilon_{Nd(1850)}$ signatures from +1.5 to -4.0, and $^{87}Sr/^{86}Sr_{(1850)}$ from 0.70266-0.70473.

The Tournefort Dykes crosscut the Jussieu Dykes, but predate the Kimban Orogeny. Pb-Pb zircon geochronology places a minimum age of 1798±8 Ma with a preferred age of 1812±5 Ma on emplacement, of the same order as Rb-Sr whole rock data. Four geochemical groupings of the Tournefort Dykes are observed, all being continental tholeiitic in nature. Enriched LILE and LREE, and Nb, Sr and Ti anomalies with low Y levels are typical. Subgroups within the Tournefort include high Magnesium tholeiites with elevated MgO (>12 wt%), Iron rich tholeiites with > 16 wt% Fe_2O_3 and high Ba tholeiites (Ba > 650 ppm). Two distinct orientation groupings are observed, neither corresponding to specific chemical groupings. This situation is reflected isotopically, where high and low $\varepsilon_{Nd(1812)}$ (+1.9 to -1.6 and -2.8 to -6.0 respectively) dykes do not correspond with either geochemical or orientation classification. The Kimban Orogeny appears to have little effect in the bulk rock chemistry of the main dyke groups.

Examination of chemical and isotopic data for the least evolved Tournefort Dykes in each group suggests the LILE and LREE signatures are not features of emplacement level contamination. Indeed, the Tournefort Dykes show little evidence of crustal contamination, suggesting chemical and isotopic features observed reflect source characteristics. A two stage model is envisaged where the Tournefort Dykes are derived from a long lived, enriched lithospheric mantle reservoir due to the impingement of a plume at ~1800 Ma. The dichotomy of Nd model ages and ε values is attributed to derivation of the melts from either of these sources.

Keywords

geochemistry, geochronology, mafic dykes, Gawler Craton, Palaeoproterozoic

Introduction

Mafic dyke swarms are common in Precambrian terrains (eg, Kuehner, 1989; Zhao and McCulloch, 1993a, b; Mazzucchelli et al., 1995; Condie, 1997; Cadman et al., 1995, 1997; Hageskov, 1997). They have received considerable attention because their lateral continuity and

geologically short time scale of emplacement (LeCheminant and Heaman, 1989; Hoek and Seitz, 1995) makes them invaluable time markers. They also offer insights into the stress field and thermal state of the lithosphere into which they are emplaced (Hoek and Seitz, 1995). Additionally, they can provide geochemical information of deeper mantle reservoirs and processes (eg, Hergt et al., 1988; Sun and McDonough, 1989; Zhao and McCulloch, 1993a; Turner and Hawkesworth, 1994).

Many Proterozoic dyke swarms may be related to distinct geological features by virtue of their geometry, for example, the MacKenzie swarm in Canada radiates from a single point, believed to indicate a plume source (LeCheminant and Heaman, 1989). Other swarms of parallel dykes have been ascribed to lithospheric extensional events, such as rifting. In both cases, mafic dyke swarms may well represent the plumbing system of associated continental flood basalt magmatism (Fahrig, 1987). Distinguishing between mafic dyke swarms originating in subcontinental lithospheric mantle and those of mantle plume origin remains central to understanding the origin and persistence of geochemical reservoirs in the lithospheric mantle. However, identification of the source of mafic dykes is complicated by distinguishing between enriched lithospheric mantle sources and contamination with continental crust. Despite this, mafic dyke swarms rarely show geochemical evidence of such contamination (eg, Weaver and Tarney, 1981; Hergt et al., 1989; Tarney, 1992; Zhao and McCulloch, 1993a; Condie, 1997). Consequently such swarms provide excellent opportunities for identifying the geochemical signatures of mantle reservoirs and their evolution through time (Condie, 1997).

The following contribution uses the geometric, isotopic and geochemical attributes of the Palaeoproterozoic Jussieu and Tournefort Dykes of the southern Gawler Craton, South Australia, to assess the level of crustal contamination, constrain source region characteristics and speculate on the nature of subcontinental lithospheric reservoirs for Palaeoproterozoic continental mafic magmatism.

Geological setting and previous investigations

The Gawler Craton lies in central South Australia (figure 1) and is composed of Late Archaean to Mesoproterozoic sequences of varying composition and metamorphic grade. On southern Eyre Peninsula (figure 2), the Kalinjala Shear Zone (KSZ) separates Archaean granulite facies ortho- and paragneisses (the Sleaford Complex; ~2600-2400 Ma, Webb et al., 1986; Fanning et al., 1986; Fanning, 1997) and Palaeoproterozoic amphibolite grade metasediments (the Hutchison Group; ~1964-1859 Ma, Drexel et al., 1993; Fanning, 1997) to the west from variably deformed granitoid and mafic intrusions of the Lincoln Batholith and Tournefort Dykes (Mortimer et al., 1988a, 1988b; Hoek and Schaefer, in press) to the east (figures 2 and 3). To date, neither the Jussieu or Tournefort Dykes have been unambiguously correlated with mafic rocks on the western side of the KSZ, and the data presented within this contribution will be restricted to samples collected from within the Lincoln Batholith.

The Lincoln Batholith comprises a fractionated series of felsic magmas termed the Donington Granitoid Suite (DGS; 1850-1843 Ma,

Mortimer et al., 1988a) and syn-plutonic mafic dykes of the Jussieu Dykes (Hoek and Schaefer, 1998). The Tournefort Dykes post-date Lincoln Batholith magmatism and are intrusive into it. The term swarm has been dropped for both mafic suites due to implicit connotations of parallelism and hence cogenesis. As described below, field evidence clearly exists for more than a single phase of Tournefort emplacement.

The Jussieu Dykes were first identified on the basis of field criteria, and described in Hoek and Schaefer (in press). They are a volumetrically minor component of the terrain, however due to their syn-plutonic nature, they place important constraints on both the thermal and chemical evolution of the Lincoln Batholith. This study presents the first geochemical and isotopic data for this suite. On the basis of the comagmatic relationships, we conclude that the Jussieu Dykes were emplaced at ~1850-1840 Ma.

The Tournefort Dykes are composed dominantly of tholeiitic basalts and subordinate picritic tholeiites. Mortimer (1984) recognised three geochemically distinct suites of dykes, all of which were deformed to varying degrees by the Kimban Orogeny. This study presents additional geochemical and isotopic data, which, coupled with field observations from low strain zones, allow identification of discrete phases of magmatism and elucidation of possible source compositions. An evaluation of the effects of deformation on bulk rock composition in the Tournefort Dykes is also conducted.

Prior to this contribution, best estimates of emplacement ages were based on Rb-Sr whole rock isochrons in the range of 1572±99 Ma (Mortimer et al., 1988b) and 1500±200 Ma and 1700±100 Ma (two groups, Giddings and Embleton, 1976). However, refined regional scale geochronology (eg, Fanning et al., 1988; Fanning, 1997) indicates emplacement must have occurred prior to ~1750 but after 1850 Ma (Drexel et al., 1993).

The Kimban Orogeny was a term originally coined by Thomson (1969) and Glen et al. (1977) to identify the series of tectonic events recorded in the Hutchison Group. Subsequently the term has been applied on a craton wide basis to encompass any deformation that has taken place between the cessation of deposition of the Hutchison Group (1859±11 Ma, Fanning, 1997), and deposition of the Corunna Conglomerate, thought to be synchronous with eruption of the Gawler Range Volcanics (1592±2 Ma, Fanning et al., 1988). However, in the absence of a genetic link between deformational events correlated on the craton scale over a period of ~250 Ma, the term Kimban Orogeny in this contribution is restricted on southern Eyre Peninsula to encompass that deformation and metamorphism in the Hutchison Group with a common tectonic genesis; ie, during the period ~1750-1700 Ma. Development of an early, layer parallel schistosity in the Hutchison Group (D1) is considered contemporaneous with emplacement of the Lincoln Batholith (Parker, 1978, Parker and Lemon, 1982) at ~1850 Ma (and is indeed recorded in parts of it). However to date, no clear genetic link between this period of deformation and subsequent peak metamorphic conditions in the Hutchison Group has been made.

The Kimban Orogeny heterogeneously affected both the Jussieu and Tournefort Dykes, with preservation of dyke propagation features in low strain zones (figure 4a), wholesale retrogression and metasomatism in high strain zones (figure 4b), and preservation of peak metamorphic conditions in the form of garnet-hornblende±orthopyroxene assemblages in some Tournefort Dykes (Hand et al. 1995; in prep). There is no field evidence of post Kimban dyke activity, effectively placing a minimum age constraint on emplacement of the Tournefort Dykes at the cessation of the Kimban Orogeny, tentatively placed at ~1700 Ma with the intrusion of the undeformed Chinmina Syenite into the Hutchison Group (Fanning, 1997). Sm-Nd geochronology on peak metamorphic garnet and hornblende mineral separates constrain Tournefort dyke activity to predate 1748±25, 1717±65 and 1728±41 Ma for three separate samples over 100 km apart (Bendall, 1994; Hand et al., in prep).

Definition and distribution

The Jussieu Dykes

Identification of syn-plutonic mafic dykes within the felsic units of the Lincoln Batholith has lead to the definition of the *Jussieu Dykes*, a distinctive pre-Tournefort mafic episode (see Hoek and Schaefer, in press). Known outcrop of the Jussieu Dykes is limited to Williams Island, West Point and north of Taylors Landing (figure 2), with the bulk of localities on the extreme southern portion of Eyre Peninsula. Volumetrically they comprise a small component of Lincoln Batholith magmatism (<5%), however their distribution on offshore islands to the south of Eyre Peninsula is unknown.

The Jussieu Dykes are typically surrounded by a felsic selvage formed by melting and backveining due to propagation of mafic material through thermally perturbed felsic units (see Hoek and Schaefer, in press, for discussion on this process). Disaggregation and ultimately dissemination of commonly angular mafic enclaves (figure 5a) into curvilinear trains is observed along strike (figure 5b), which, coupled with the frequent association of felsic selvages along dyke margins act as criteria for distinguishing the Jussieu Dykes from the younger Tournefort Dykes in the field. The Tournefort Dykes always crosscut the Jussieu Dykes where such relationships are preserved (figure 6).

The Jussieu dykes are generally less than ~1m wide, although they may vary considerably in thickness along strike length in response to both differing degrees of subsequent deformation and the relative proportion of felsic material comprising vein networks within the dyke and surrounding selvage. There appears to be no preferred orientation of Jussieu dykes preserved in the field. Most contain aphyric textures with relict plagioclase + clinopyroxene ± orthopyroxene, with subsequent hornblende + quartz ± biotite static retrogression in areas of low strain. Identification of Jussieu Dykes becomes virtually impossible in high strain regions due to the obliteration of features such as the planar nature of enclave trains and selvages, along with accompanying retrogression and amphibolitisation of the mafics.

Contacts between the Jussieu and their surrounding selvages tend to be distinct, and often may be angular. A plagioclase + quartz ± orthopyroxene (± secondary hornblende) transition zone up to 1-2mm thick is common around the margins of Jussieu Dykes, while the bulk of the selvage material is composed of quartz + plagioclase + biotite ± hornblende ± orthopyroxene. Large plagioclase grains in the selvages typically contain distinct rims with hornblende inclusions, suggesting overgrowth of magmatic plagioclase during selvage formation.

The Tournefort Dykes

The Tournefort Dykes form a suite of gabbro to gabbronorite dykes and retrogressed equivalents, observed to crosscut all units of the Lincoln Batholith (including the Jussieu Dykes) were deformed and partly metamorphosed during the Kimban Orogeny, and in places (eg, West Point, Kirton Point) contain peak metamorphic assemblages. The timing of the Tournefort Dykes is thus bracketed by Lincoln Batholith magmatism (~1850 Ma) and peak Kimban metamorphism (~1730 Ma, Bendall, 1994; Hand et al., in prep.).

As noted by previous workers, such as Mortimer (1984) and Mortimer et al. (1988), two distinct types of mafic rocks occur on the southern Eyre Peninsula. These include gabbroic and picritic rocks with a clearly dyke like geometry preserving primary igneous textures as distinct from tectonically concordant boudins of amphibolite with appreciable or complete metamorphic recrystallisation. Detailed mapping has demonstrated that these amphibolites in the Lincoln Batholith preserve the same geometric relationships and are in a broad geochemical sense analogous to the Tournefort Dykes, but are generally found in zones of higher strain and metasomatism. Thus, in this contribution the amphibolites are considered to be retrogressed equivalents of the Tournefort Dykes. However, the bulk of discussion will focus on relatively pristine dykes from regions of low strain and deformation since such areas preserve the most information regarding petrogenesis and magmatic chemistry

Regions of low strain, particularly Williams Island, West Point and McLaren Point preserve a plethora of dyke propagation features, allowing distinction of two dyke emplacement events, characterised by NNW-SSE (~330-350°T) and NE-SW (~25-60°T) trending orientations (Hoek and Schaefer, in press). Crosscutting relationships on Williams Island suggest the NE trending set to be younger than the NNW trending dykes. Features such as arrested dyke tips, horns, steps, bridges and rafted bridge material (figure 7) are typical of dyke propagation (Hoek, 1994). While a range of other dyke and amphibolite orientations are observed along the coast of southern Eyre Peninsula (Giddings and Embleton, 1976; Hoek and Schaefer, 1998), these often reflect rotation due to Kimban deformation. Hence, while the orientation data is considered a useful tool in demonstrating the existence of several dyke emplacement events, it is by no means considered grounds for a definitive classification on the outcrop scale.

Localities such as Kirton Point (figure 8a) have been interpreted by some (eg, Tilley, 1921) to contain amphibolite gneiss which was engulfed and orientated by the intruding felsic gneiss. However, outcrops at Wanna demonstrate how discontinuous mafic bodies can be formed by deformation of initially planar dykes (figure 8b; Bales, 1996).

Geochemistry

Analytical methods

Major and trace element concentrations were determined at the University of Adelaide by Philips PW 148 XRF, with $^{87}Rb/^{86}Sr$ calculated from extended measurement routines of Rb and Sr. Total iron was calculated as $Fe_2O_3^T$, and *mg#* = (Mg/(Mg+0.8998Fe). REE analyses on samples prefixed SEP- were conducted by ICP-MS at Monash University following procedures recently described by Elburg and Foden (submitted). Nd and Sm concentrations and $^{143}Nd/^{144}Nd$ and $^{87}Sr/^{86}Sr$ isotopic compositions were carried out by thermal ionisation mass spectrometry on a Finnigan MAT 261 solid source mass spectrometer at the University of Adelaide. Elemental concentrations were determined on 100mg of sample dissolved in HF by bomb dissolution and spiked with ^{150}Nd-^{147}Sm tracer. Conversion to chloride by 6M HCl was followed by separation of Nd, Sm and Sr using a two stage cation exchange procedure, in essence the same as that described by Richard et al., (1976). Double Ta-Re, Re-Re and single Re filaments were used for Nd, Sm and Sr respectively, and data blocks of ten scans were collected until acceptable within run statistics were achieved (8-15 blocks for Sr with fixed double collector and 15-25 blocks for Nd with single collector). All Sr and Nd isotopic ratios were corrected for mass fractionation by normalisation of $^{88}Sr/^{86}Sr$ to 8.3752 and $^{146}Nd/^{144}Nd$ to 0.7219. Errors quoted on isotopic ratio measurements in this contribution are $2\sigma_{mean}$, and precision on Sm/Nd abundance ratios is about 0.1% relative deviation (1σ). Average blank levels during the course of this work were 1.7 ng Sr and 700 pg Sm and Nd. Neodymium model parameters are based on those of Goldstein et al. (1984), and are: depleted mantle $^{143}Nd/^{144}Nd$ 0.51316, $^{147}Sm/^{144}Nd$ 0.2137, and CHUR $^{143}Nd/^{144}Nd$ 0.512638, $^{147}Sm/^{144}Nd$ 0.1966.

The data generated in this study has been supplemented by data from unpublished theses by Bradley (1972), Mortimer (1984) and Bendall (1994), as well as data published in Mortimer et al., (1988b). In all cases, the supplementary data has been included for consideration only after rigorous cross checking of sample localities and, where possible, petrographic examination of samples.

Jussieu Dykes

Jussieu Dykes are known to outcrop in only three localities (north of Taylors Landing, the southern tip of West Point and Williams Island), however they display remarkable chemical homogeneity given such a spatial variation (table 1). They range between 48.9-51.6 weight % SiO_2, with a spread of *mg#* values from 61 to 48. Distinctive chemical features

include relatively enriched Rb and Pb, with Nb, Sr, Ti and P depletions (figure 9). Accompanying the low *mg#* values are low Ni (80-150 ppm) and covarying Cr (maximum of 840 ppm at *mg#* 61 down to 88 ppm at 48).

Overall, trace elements vary little from locality to locality (figure 9), with the notable exception of Th. Sample SEP-293 is from Williams Island and contains a distinctive Th depletion. In the absence of covarying U, which would be expected to be mobile with Th in the metamorphic environment, such a feature must be regarded as primary, and is indeed weakly mimicked in sample SEP-250 from West Point.

Despite the apparent chemical homogeneity, significant variation in Nd isotopic signature is observed. $\varepsilon_{Nd(1850)}$ values range from -4.0 north of Taylors Landing to +1.5 at West Point. Virtually no systematic isotope variation is observed with chemistry.

Tournefort Dykes

The Tournefort dykes are composed of four geochemical groups, reflecting both initial magmatic variation and variable subsequent metasomatic alteration associated with deformation and metamorphism during the Kimban Orogeny. However, all geochemical groupings possess (to varying degrees) negative Nb, Sr and Ti anomalies, along with depleted Y values.

High Mg Tholeiites (HMgT)

Dykes of this group range from picritic to gabbronorite in composition, with variable degrees of secondary amphibolitisation. Their chemistry is distinctive by virtue of very high MgO contents (12.1-24.1%) at low SiO_2 (46.2-53.3%) and CaO (3.9-11.0%). The HMgT also contain comparatively low levels of LILE and pronounced Nb, Sr and P depletions. They contain the lowest levels of LREE of any Tournefort Dykes (figure 10) and the highest Ni (382-1228 ppm) and Cr (1027-4166 ppm). Primitive mantle normalised patterns for elements more compatible than Sr tend to be fairly flat (figure 10), and in some samples the absolute abundances of Sm, Ti and Y is less than both N- and E- type MORB's.

Iron (Fe) Rich Tholeiites (FeRT)

The Fe rich tholeiites are a series of variously amphibolitised dykes with $Fe_2O_3^T$ > 16%, and elevated (up to 3.6%) TiO_2. They are slightly LREE enriched, and contain widely varying LIL element concentrations (eg, Ba = 56-502 ppm), a reflection in part of element mobility during amphibolitisation. FeRT dykes tend to high V concentrations with respect to the rest of the Tournefort Dykes, as well as containing elevated Rb, Ba, and Zr.

High Ba Tholeiites (HBaT)

This group of mafics typically outcrops as planar arrays of amphibolite rafts and boudins, commonly with partial melts and leucosomes generated in boudin necks and on raft margins (eg, centre of field in lower mafic in figure 8a, on tip of bottom portion of central dyke in figure 8b). Individual dykes are not as prevalent in this group as in the remainder of the Tournefort Dykes. The distinguishing character of these mafics is their high (>600 ppm) Ba, (figure 10). SiO_2 (49.3-58.3%), K_2O and Na_2O levels. They also contain high Rb, Th, Sr, Pb and LREE

concentrations. Although it is tempting to attribute many of these features to amphibolitisation, figure 10 compares the effects of different metamorphic assemblages on bulk composition for the main dyke groups. While there is some variation in chemistry within groups with increasing degrees of amphibolitisation, it is clear that overall trace element patterns broadly reflect initial compositions. The implications of this are discussed further below.

Unassigned Tholeiites

By far the bulk of the Tournefort Dykes fall into this category. A range of tholeiitic dolerites are observed, including plagioclase- and orthopyroxene-phyric dolerites, variably amphibolitised equivalents, and unaltered even grained dolerites. Due to both initial compositional variation and subsequent amphibolitisation, the tholeiite dykes possess a broad range of chemical compositions. SiO_2 values range from 47.0-53.1%, with moderate levels of MgO (5.1-9.7%) and the greatest values of CaO (8.6-12.5%) for the Tournefort Dykes. The bulk of unassigned tholeiites are Sr depleted with weakly developed negative Ti and Y anomalies, however absolute trace element abundances trend to higher values than for the HMgT. A wide spread in LILE (K, Rb, Ba) concentrations possibly reflects varying degrees of amphibolitisation and metasomatism during the Kimban Orogeny.

Nd isotopes define two distinct groups within the Tournefort Dykes. One group contains dykes with high $\varepsilon_{Nd(1812)}$ values (+1.9 to -1.6), with the other group containing $\varepsilon_{Nd(1812)}$ values in the range -2.8 to -6.0. This subdivision is independent of the previously described geochemical groups, an effect mirrored in their Sr isotopes. $^{87}Sr/^{86}Sr_{(i)}$ ratios show similar ranges for each geochemical group, ranging from 0.70304-0.70587 for the Unassigned Tholeiites through 0.70385-0.70551 for the HBaT. Only the FeRT show a narrow range (0. 70224 -0.70228) which probably reflect a sampling bias due to the small number (two) of analyses. Sample SEP-024 shows evidence of strong Rb enrichment during amphibolitisation of the HMgT (see below), resulting in anomalously low $^{87}Sr/^{86}Sr_{(t)}$ ratios. The two Nd isotopic groups are also present in the Sr isotope data, with samples containing low $\varepsilon_{Nd(1812)}$ values also containing correspondingly radiogenic $^{87}Sr/^{86}Sr_{(i)}$ signatures (>0.7045). Samples with high $\varepsilon_{Nd(i)}$ values typically have $^{87}Sr/^{86}Sr_{(i)}$ <0.7045 (table 2). Therefore, while the isotopic data contains little information within individual geochemical groups, the apparent coupling of the Nd and Sr isotope systems suggests the data reflects an important petrogenetic process.

Effects of amphibolitisation on bulk rock chemistry

From the preceding geochemical descriptions, it was suggested that some chemical variation within dyke groupings may be attributable to post emplacement metasomatism associated with the Kimban Orogeny. However, detailed analysis of the data suggests that chemical changes in bulk composition do not vary systematically with amphibolitisation, both on a regional scale and on the outcrop scale.

Figure 10 compares trace element chemistry of amphibolites and relatively unmetamorphosed dykes of all groups. In all cases, the amphibolites are hornblende+biotite gneisses, whereas the unaltered samples preserve primary pyroxenes and magmatic textures. One of the most striking characteristics of the HBaT and FeRT suites is the relatively minor changes in trace element chemistry observed during amphibole growth. Variations that are observed, particularly amongst the LILE, are usually systematic within a group, however no across group systematic variations are observed. Hence, amphibolitisation of HBaT appears to increase Th, U, Nb, K, Pb, LREE and Ti, whereas little variation in these elements from unaltered compositions is observed in the FeRT. By contrast, the Dolerite dykes preserve distinct decreases in Rb, Ba, Th, Nb, LREE and Ti, suggesting that compositional variation due to metasomatism is controlled in part by initial dyke composition, rather than systematically driven by the individual trace elements considered.

Dykes containing metamorphic garnet occur in three of the groups, and no systematic variation in bulk rock chemistry is involved with garnet growth (figure 10). In each group, garnet bearing mafics display bulk compositions that mirror those of unaltered samples, with limited non-systematic erratic element behaviour (eg U in the Dolerite dykes). This suggests garnet growth is not a response to pervasive metasomatism, but driven by ambient pressure and temperature conditions for a given bulk composition.

In an attempt to quantify smaller scale trace element variation with metamorphism, a series of samples across a boudin neck were collected at Kirton Point. The dyke sampled consisted of a recrystallised core mantled by leucosome bearing amphibolites. On approaching the boudin neck, the core and leucosomes became increasingly tectonised. Samples were collected in a transect across the boudin neck of the leucosome bearing amphibolites, and the central portion of the dyke in both the boudin neck and from a low strain zone 10m along strike. The amount of trace element variation is depicted as the HBaT amphibolite samples in figure 10. The two amphibolites contain the maximum and minimum range for amphibolites from Kirton Point. They vary little from the relatively undeformed central portion of the dyke, and indeed from the rest of the undeformed dykes of the same geochemical group. A garnet bearing mafic from the same locality possesses an indistinguishable primitive mantle normalised trace element pattern from the amphibolites (figure 10). Hence, trace element variations on the metre scale appear to be small, despite distinct changes in hand specimen appearance and total strain. It is therefore reasonable to conclude either that metasomatism took place on a large scale such the rocks sampled were essentially homogenised during amphibolitisation, or that amphibolitisation (at Kirton Point at least) resulted in little chemical variation in the mafics, even with moderate variations in strain. The latter hypothesis is favoured for the Kirton Point study as there is no evidence in the surrounding felsic gneisses for metasomatic processes acting on the scales required. However, whilst the observed variations are small, they are not trivial, and clearly with increasing strain (such as within the Kalinjala Shear Zone, or high strain

zones such as Lookout), masking of initial trace element patterns would be expected. Since such samples are not routinely collected in petrogenetic studies, this hypothesis remains unevaluated.

Therefore, only in the case of the Dolerite dykes does amphibolitisation appear to have radically altered both the pattern and absolute trace element concentrations. Clearly though, the least deformed and unaltered samples provide the best constraints for petrogenetic studies. Despite non-systematic behaviour of trace elements between individual geochemical groups of Tournefort Dykes, within group variation is broadly coherent. On the basis of whole rock trace element geochemistry, it may be concluded that the amphibolites of this study are indeed highly deformed and retrogressed equivalents of the Tournefort Dykes, consistent with petrological observations and field relation inference.

Geochronology

Mafic dykes are valuable geochronological markers due to their lateral continuity and their short period of emplacement (eg, Zhao and McCulloch, 1993b). Historically, however, precise age determinations of mafic lithologies has been fraught with difficulty. For example, the relatively low total concentrations of radioactive elements and minimal compositional variation result in a narrow range of parent/daughter ratios, producing large errors in fitting whole rock isochrons. Low levels of accessory phases (such as zircon) amenable to geochronology means mafic dykes pose problematic geochronological targets compared to more commonly studied felsic suites. Internal mineral isochrons have been used to constrain emplacement ages on comparatively unaltered and undeformed dyke suites (eg, Zhao and McCulloch, 1993b), however such an approach is complicated in the Tournefort Dykes due to the effects of the Kimban Orogeny (as observed in Hand et al., in prep).

Previous studies (eg Black et al., 1991; Lanyon et al., 1993) have made use of comagmatic felsic segregations within dykes as sources of radiogenic element bearing phases. Such segregations represent late stage fractionates of the mafic magmas emplaced in veins oriented perpendicular to dyke margins due to contraction during cooling. Their chemistry is often sufficiently siliceous to allow crystallisation of accessory phases such as zircon which are able to be dated by conventional techniques. Of utmost importance in such studies is demonstrating the comagmatic nature of the felsic segregations with the mafic dykes (as opposed to later generations of crosscutting veins), and being able to adequately discriminate between populations of potentially inherited phases (eg Black et al., 1991) and those associated with fractionation and crystallisation of the felsic segregation in question (eg, Lanyon et al., 1993).

Geochronology of the Tournefort Dykes

Pb-Pb zircon evaporation geochronology

A zircon bearing felsic segregation from a dyke in the low strain zone at McLaren Point (sample GC-99) was identified as a potential geochronological target. This sample preserved diffuse margins with the

host dyke (figure 11), does not continue beyond the dyke margins into the host Lincoln Batholith lithologies and is less siliceous than later (Kimban) felsic veins which crosscut both the dyke and host gneisses. This segregation therefore places a minimum age constraint on the host dyke containing it.

The Pb-Pb zircon evaporation technique as carried out in this study was developed by Kober (1986), with the method applied at Adelaide University outlined in Dougherty-Page and Foden (1996). The technique involves sequentially evaporating layers of zircon and analysing the Pb isotopic composition in a stepwise manner towards the core of the zircon. Ratios of $^{207}Pb/^{206}Pb$, $^{208}Pb/^{206}Pb$ and $^{204}Pb/^{206}Pb$ are thus obtained for each heating step, allowing calculation of a zircon age from the $^{207}Pb/^{206}Pb$ ratio which has been corrected for common Pb calculated from the $^{204}Pb/^{206}Pb$ ratio (Dougherty-Page and Foden, 1996). Coupled with the age determination is the ability to back calculate Th/U ratios for each analysis (Bartlett et al., in press), using the $^{208}Pb/^{206}Pb$ ratio. This $(Th/U)_t$ value is useful for discriminating separate zircon populations.

The limitation of the evaporation technique is that of demonstrating concordancy. However, using data obtained from many small sequential heating increments, and using only data plateaus in the sequence, discordance is minimised. That is, if a sequence of analyses were discordant, then successive heating steps would produce different measured ratios, and the data would not plateau. Age determinations are thus conducted only on the plateaus of data sets. Multiple analyses of zircons from within a single sample reproducing plateaus of corresponding $^{207}Pb/^{206}Pb$ and $(Th/U)_t$ ratios therefore imply a strong degree of concordance for the population in question.

Only a small number of zircons (~20) were retrieved from ~10 kg of sample GC-99, of which 5 zircons contained sufficient Pb to form a stable beam enabling analysis.

On the basis of $(U/Th)_t$, age and running criteria, two populations of zircon were identified in GC-99 (figure 12) which are not observed in any of the host Lincoln Batholith lithologies (Schaefer, 1998). The populations comprise a younger, high $(U/Th)_t$ population at 1798±8 Ma ($(U/Th)_t$ ~0.45), and a slightly older, low $(U/Th)_t$ population ($(Th/U)_t$ ~0.37) at 1812±5 Ma. Both populations are a marked contrast to magmatic Lincoln Batholith zircons from Tumby Bay and Wanna (1841±8 and 1841±9 Ma respectively, $(Th/U)_t$ ~0.40). U-Pb zircon analyses on the Quartz Gabbronorite Gneiss at Cape Donington and the Memory Cove Charnockite at Memory Cove by Fanning (1997) and Fanning and Mortimer (in prep) also show no evidence of zircon growth at 1798 -1812 Ma.

The reproduction of the age populations in multiple zircons and the marked absence of a Lincoln Batholith component in the zircons analysed, coupled with higher $(Th/U)_t$ ratios measured in GC-99, suggests the ages record reflect periods of new zircon growth. Thus, the youngest age obtained from the felsic segregation places a minimum age constraint on the mafic dyke. Both ages obtained are consistent with the lithological and structural controls on Tournefort Dyke emplacement.

Several scenarios can be envisaged for the presence of two unique zircon populations, including the younger age representing the time of dyke emplacement and the older component a mixing age beyond resolution of the evaporation technique with inherited zircons from the Lincoln Batholith. This is consistent with Lanyon et al. (1993) who noted a large component of inheritance in zircon studies from the Vestfold Hills. Alternatively, the younger age may be a mixing age formed by Kimban overgrowths with the magmatic emplacement age at 1812±5 Ma. At the time of writing it is difficult to distinguish between the two alternatives, except to note in passing that the high $(U/Th)_t$ ratio of the rims is consistent with metamorphic growth. Whilst there is evidence for this elsewhere in the Lincoln Batholith during the Kimban, the McLaren Point locality is a low strain area preserving fine scale magmatic relationships and typical bulk rock chemical and isotopic signatures. Also, as discussed above, the Tournefort Dykes have proved suprisingly robust to large scale metasomatism during amphibolitisation. In conclusion it would appear that the Tournefort Dykes can be no older than 1812±5 Ma, and no younger than 1798±8 Ma, both ages which are consistent with the regional geological constraints.

Rb-Sr whole rock geochronology

Previous attempts at whole rock Rb-Sr geochronology on the Tournefort Dykes have been inconclusive (Giddings and Embleton, 1976; Mortimer, 1984; Mortimer et al., 1988b). As an adjunct to an extensive palaeomagnetic survey of the Tournefort Dykes on Eyre and Yorke Peninsulas, Giddings and Embleton (1976) cite ages of 1500±200 Ma and 1700±100 Ma for the two palaeomagnetic groupings of dykes observed, however no data is presented. Mortimer (1984) calculated an age of 1539±251 Ma for his Group A mafics, and Mortimer et al. (1988b) reported ~1600 Ma for a number of regressions on the mafics in the Port Lincoln area.

Whole rock studies of mafic dykes are inevitably constrained by the narrow range of bulk compositional variation within a suite, the implicit assumption of cogenesis of parallel mafic dykes and subsequent mobility of Rb and Sr during metamorphism. The net result is that while whole rock Rb-Sr data may place broad constraints on the age of the Tournefort Dykes, detailed whole rock studies are unlikely to provide new insights.

In the course of petrogenetic sampling in this project, seven new whole rock analyses were generated, which, coupled with two previously unpublished analyses of Bendall (1994) and the existing data set of Mortimer (1984), prompted a re-evaluation of the status of whole rock Rb-Sr geochronology of the Tournefort Dykes.

Isochrons generated for each of the major geochemical groupings described above invariably returned a range of ages, some older than the Lincoln Batholith they were intruding (and obviously not of geological significance) and some of post-Kimban Orogeny age (table 3).

The seventeen least deformed members of the dataset viewed as a whole, define an isochron of 1817±43 Ma (2σ) with a MSWD of 38 and initial ratio of 0.70365. Whilst the error is clearly large and covers a range of geologically feasible events, including Lincoln Batholith emplacement

and initiation of the Kimban, the low initial ratio and large spatial diversity of samples used in construction of the isochron suggests cogenesis. Significantly, the isochron age is of the order of the 1812±5 Ma age determined by Pb-Pb zircon evaporation for Tournefort Dyke emplacement. While taken in isolation, little emphasis would be placed on the Rb-Sr whole rock isochron, coupled with the Pb-Pb data, it would appear to corroborate the emplacement age of the Tournefort Dykes.

Sm-Nd whole rock geochronology

The Tournefort Dykes form two groups of distinct isotopic signature. One group contains dykes with higher $\varepsilon_{Nd(1812)}$ values (~-2 to +1), with the other group containing $\varepsilon_{Nd(1812)}$ values in the range ~-3 to -6. These two groupings are also reflected in the depleted mantle model ages of the dykes, with the higher $\varepsilon_{Nd(1812)}$ group containing T_{DM} values of ~2.1-2.4 Ga, and the remainder containing older T_{DM}'s at ~2.6-2.7 Ga. While the absolute values of T_{DM} "ages" are strictly model dependent, and may have little strict geological relevance, they do place broad constraints on the crustal prehistory for a set of magmatic rocks. It must be stressed that in the case of the Tournefort Dykes, the two Nd isotopic groupings observed are independent of any of the previously discussed geochemical or orientation groupings, suggesting calculated model ages are artefacts of processes involved in both source and dyke generation.

Using the isotopic subdivision described above, two isochrons are generated from the available dataset. Those dykes with higher $\varepsilon_{Nd(1812)}$ values produce an array with an age of 2510±225 Ma (1σ), and comprise samples with a generally lower radiogenic component (figure 13), whereas the more evolved dykes define an older array (2864±134 Ma (1σ)) with lower $^{143}Nd/^{144}Nd$ components (figure 13).

While both ages are clearly too old to reflect emplacement ages, they clearly offer insights into the petrogenesis of the Tournefort Dykes, and will be discussed in this context below.

Tournefort Dyke geochronology summary

Pb-Pb zircon evaporation data from a felsic segregation interpreted to be comagmatic with Tournefort Dyke emplacement impose a minimum age of 1798±8 Ma and a likely emplacement age of 1812±5 Ma. Whole rock Rb-Sr data on the least deformed and metamorphosed samples of the suite as a whole define an isochron at 1817±43 Ma, of the same order as the Pb-Pb data. While the Pb-Pb age is likely to record crystallisation of a single dyke, the Rb-Sr data suggests this age is applicable to dykes within the larger Tournefort system. The coincidence of ages by independent isotopic systems on different rock samples suggests 1812±5 Ma is a best emplacement age estimate for the Tournefort Dykes, with a minimum age of 1798±8 Ma defined by a younger zircon population.

Sm-Nd whole rock data record no information of Tournefort emplacement. However, "isochrons" defined by the two isotopic groupings observed within the dykes may reflect a long lived enriched mantle source for the Tournefort Dykes.

Geochronology of the Jussieu Dykes

The age of the Jussieu dykes is tightly constrained by their comagmatic nature with the Donington Suite. Numerous U-Pb, Pb-Pb and Rb-Sr studies have been carried out on the felsic portions of the Lincoln Batholith (eg, Mortimer et al., 1988a; Fanning et al., 1988; Fanning, 1997), however in order to provide a temporal constraint independent of field relationships, three Jussieu Dyke-selvage pairs were analysed by Rb-Sr whole rock means.

The six samples thus analysed return an isochron of 1856±9 Ma (2σ) with a MSWD of 56 and initial ratio of 0.70349±0.00007. Despite the presence of excess scatter (as reflected in the MSWD), the age determined is within error of U-Pb and Pb-Pb zircon ages determined for the Lincoln Batholith (~1843-1852 Ma) from a range of localities (Mortimer et al., 1988a; Fanning et al., 1988; Fanning, 1997). This age is interpreted to reflect the time of selvage formation and dyke crystallisation, and is consistent with a Jussieu Dyke genesis that is comagmatic with the Lincoln Batholith.

Petrogenesis

The Tournefort Dykes show trace element patterns similar to that of the continental crust. They are LILE and LREE enriched, and distinctive by virtue of negative Nb and Sr anomalies, and also have depleted Ti and Y values (figure 4.3). One subdivision on the basis of isotopes preserves crustal signatures in the form of unusually negative initial εNd with correspondingly higher $^{87}Sr/^{86}Sr_{(i)}$ values for mafic dykes. At the time of emplacement, ε_{Nd} values of such Tournefort Dykes are more negative than the host gneisses of the Lincoln Batholith they intrude, and only slightly more evolved than the Sleaford Complex regional basement (figure 14), effectively ruling out emplacement level contamination. Therefore, elevated $^{87}Sr/^{86}Sr_{(i)}$ ratios coupled with evolved Nd isotopic signatures requires magma production from an environment that has an extended history of enrichment in incompatible elements, which is not preserved at the current erosion level.

With these constraints in mind, there is in essence two options for the generation of basaltic magmas with crust-like signatures; 1) mantle derived magmas contaminated during ascent through (and/or ponding in) the lower crust to a degree that essentially swamps source trace element characteristics; or 2) derivation from a portion of the mantle that has essentially crust-like isotopic and LILE signatures. The further option of emplacement level contamination seems limited in effect due to the extreme isotopic signatures, as noted above.

Constraints on crustal contamination

Samples most likely to have suffered crustal contamination are clearly those with strongly negative $\varepsilon_{Nd(i)}$ values. Samples from the HMgT, HBaT and Dolerite dykes are in this group, with FeRT restricted to more primitive $\varepsilon_{Nd(i)}$ values. In order to evaluate the amount of crustal interaction, the following discussion will centre on those dykes most likely to exhibit contamination, ie, those with more evolved Nd isotopic signatures (see table 2).

The absolute Nd concentrations in the least siliceous non cumulate members of the Dolerites and HMgT tend to low values (<19ppm, HMgT = 6-10 ppm). Typical oceanic and continental tholeiites contain ~7-10 ppm, compared to values typically >30 ppm in southern Gawler Craton crust. Therefore, in order to maintain low Nd concentrations in the melt, any potential crustal contaminant would need to be LREE depleted (ie, contain low Nd concentrations), or be mixed in small enough quantities to prevent significant perturbation of the Nd concentration. Since both the Sleaford Complex and Lincoln Batholith are comparatively Nd enriched (Nd ~30-70 ppm for large volume lithologies), the former seems untenable. Dykes containing evolved Nd signatures are distributed widely within the Lincoln Batholith, and comprise approximately half of the total dykes analysed for Nd isotopes. Such widespread and large scale variations in signature coupled with close proximity of dykes with more primitive Nd signatures at localities such as West Point argue against small volume mixing.

The Tournefort Dykes also maintain linear arrays on $\varepsilon_{Nd(1812)}$ vs Sm/Nd, 1/Nd and La/Sm plots (not shown). Such correlations are indicative of simple two component mixing. Situations involving more than two components, or more complex mixing processes (such as AFC) are likely to result in non-linear relationships (Zhao and McCulloch, 1993a). Furthermore, if simple two component mixing did take place, the linearity requires mixing with a crustal contaminant of unique composition. However, the most likely contaminant (the Sleaford Complex) displays a very heterogeneous nature, in both isotopic and trace element geochemical terms. Therefore, such trends would require contamination to have taken place within a specific (homogeneous) portion of the Sleaford Complex (figure 14), which seems unlikely given the spatial distribution of dykes defining the trends.

Contamination by silicic crust also fails to account for the low SiO_2 and high *mg#* of non-cumulate dykes in both the HMgT and Unassigned Tholeiite groups. So too, low $\varepsilon_{Nd(i)}$, HMgT samples display primitive mantle normalised patterns with values similar to or less than N-MORB sources for elements more compatible than Sr. This makes generating the required compositions by bulk mixing of crust with tholeiitic magmas difficult, particularly when trying to maintain a balance with incompatible elements, which are strongly depleted in N-MORB. Additionally, a number of key trace element ratios lie outside of N-MORB-crust mixing trends; eg Ti/V and Zr/Y for example are too low, and Sc/Y too high, to be a result of simple mixing. Therefore, while only comparatively small amounts of contamination are necessary for the LILE and some LREE, compatible elements such as Sm, Ti and Y require large proportions of contaminant to produce signatures observed in the HMgT.

This effectively leaves two possibilities; 1) the Tournefort Dykes have been contaminated by crust of a very specific composition, which is not exposed on the southern Gawler Craton or 2) the trace element and isotopic signatures reflect mantle source processes and have seen negligible crustal contamination. Regarding the former, given that the top of the Lincoln Batholith was at ~15 km during emplacement, and the

structural level of the batholith exposed in the Kalinjala Shear zone is a minimum of several kilobars deeper (Oussa, 1993; Bendall, 1994; Hand et al., 1995; Hand et al., in prep), the Lincoln Batholith occupies a portion of the middle to lower crust with exposed vertical relief of some 5-6 kilometres. With extension taking place during Lincoln Batholith emplacement, and again during Tournefort emplacement, only a comparatively thin and attenuated section of lower crust would have been available to act as a contaminant to the Tournefort Dykes. The composition of such lower crust is inaccessible by direct means, as the only enclaves observed within the Tournefort Dykes are locally derived Lincoln Batholith felsic gneisses. However Nd isotopes suggest that the only crustal contaminant available to the Lincoln Batholith was the Sleaford Complex (Schaefer, 1998). Hence, the only observable crustal contaminant available to the Tournefort Dykes either directly or indirectly (via a two stage process involving the Lincoln Batholith) was the Sleaford Complex. Since neither of the isotopic groupings within the Tournefort Dykes define mixing arrays with Sleafordian crust (figure 14), another source for this signature is required. Such a conclusion is consistent with the geochemical constraints discussed above.

Therefore, it would seem the apparent crustal signature of the Tournefort Dykes is a reflection of mantle source characteristics. The presence of enriched lithospheric mantle reservoirs beneath continental crust has been documented in many parts of the world, (eg, Menzies et al., 1987; O'Reilly and Griffin, 1988; Griffin et al., 1988 and references therein), and have been appealed to as sources for mafic magmatic events which preserve similar trace element and isotopic characteristics to the Tournefort Dykes (eg. Hergt et al., 1989; Zhao and McCulloch, 1993a). Enriched lithospheric mantle beneath the Gawler Craton is an appropriate chemical reservoir for the derivation of the Tournefort Dykes, as it is likely to be relatively enriched in incompatible elements, yet still relatively depleted in compatible elements. Isotopically however, samples of the subcontinental lithosphere from beneath the Gawler Craton in the form of xenoliths from kimberlites (Song, 1994), are not evolved enough to produce the signatures observed in the Tournefort Dykes. Instead, while the primitive Tournefort Dykes define mixing trends between the depleted mantle and lithospheric mantle (Figure 15), the low $\varepsilon_{Nd(i)}$ dykes trend towards an isotopically enriched source, such as that observed in the EM 1 ocean island basalts (OIB's). EM-1 is associated with plume magmatism at the Pitcairn and Tristan hotspots on the modern Earth (Hofmann, 1997), suggesting a role for plume related magmatism in Tournefort Dyke genesis.

Discussion

The origin of enriched mantle remains equivocal. However, only a comparatively small number of mechanisms may be envisaged which result in the formation and continued isolation of such reservoirs. There are essentially three general groups, viz:

1) subduction of continental crust into the upper mantle resulting in enriched lithospheric mantle (Hergt et al., 1989; Zhao and McCulloch, 1993a)
2) Plume driven, OIB type sources; some of which (eg HIMU) are not observed in mafic dyke swarms until the Neoproterozoic (Condie, 1997),
and 3) progressive enrichment of previously depleted subcontinental lithospheric mantle, either by continuous melt percolation from the asthenosphere (Erlank et al., 1987; McKenzie, 1989; Turner and Hawkesworth, 1995) or specific enrichment events.

The features outlined in the preceding section suggest that the Tournefort Dykes reflect the interplay between potentially three mantle sources; that of depleted mantle characteristics, one with a plume derived component and an enriched subcontinental lithospheric mantle.

A mechanism for generation of new continental lithosphere exists on southern Eyre Peninsula. Freezing of asthenosphere to the base of the lithosphere during sedimentation would allow the generation of a relatively primitive reservoir with MORB-like characteristics. However, the shallow nature of the Hutchison Basin (~3.5 km, N. Lemon, pers comm.), requires that the total volumes involved be relatively small, suggesting derivation of primitive Tournefort Dykes wholly from such a source is unlikely. The mixing arrays of the primitive dykes could therefore reflect interaction between relatively juvenile lithosphere with depleted mantle signatures, and the enriched subcontinental lithospheric mantle.

Additionally, the source of both heat and material for Tournefort magmatism may be derived independently of the local geology. Enriched asthenospheric sources for plume related magmatism may offer an alternative origin, (figure 15) however this merely moves the initial source of the enrichment one step further back, implying an effective mechanism existed for enriching, and more importantly, preserving chemical heterogeneities in the convective asthenosphere. Sun et al. (1989) note problems with returning (subducting) sufficient volumes of Archaean crustal material to establish large reservoirs early enough in the history of the Earth to source such magmatism. Despite this, portions of the Tournefort Dykes display trace element characteristics, such as flat compatible trace element patterns and arrays trending towards OIB (Ocean Island Basalt) sources (figure 15), consistent with derivation, at least in part, from a plume related source.

The origin and nature of a subcontinental lithospheric mantle reservoir remains equivocal. The Tournefort Dykes preserve a long history of enrichment prior to emplacement (~0.4 Ga); with the most evolved portions containing T_{DM} ages older than the those in the Lincoln Batholith they intrude (figure 16). As Zhao and McCulloch (1993a) note, subduction modified continental lithospheric mantle is likely to be readily extracted, particularly in regimes undergoing active extension and/or anomalous thermal activity. On southern Eyre Peninsula, the 150 million years prior to Tournefort emplacement was characterised by extension to allow deposition of the Hutchison Group from ~2000 Ma, and emplacement of the Lincoln Batholith, again probably in an extensional

environment at ~1850 Ma. It is only ~20-30 Ma *after* these protracted extensional and magmatic events that Tournefort Dyke magmatism from an enriched source took place. Therefore, the preservation of an ancient subduction modified enriched continental lithosphere for the duration of this tectonic activity seems unlikely.

Another view is that of enrichment of previously depleted peridotite beneath areas of stable continental crust. Turner and Hawkesworth (1995) argue for the establishment of large depleted reservoirs by crustal formation events, which are subsequently hydrated and enriched in incompatible elements. The ultimate source of incompatible elements and hydrous fluids has been suggested to be either the deep mantle (Erlank et al., 1992), or underplated oceanic crust (Tarney, 1992). In either case, lithospheric mantle thus developed is likely to remain isolated from the convecting mantle in the steady state due to its strength and buoyancy, features of its depleted nature.

O'Reilly and Griffin (1988) point out that once such a chemical reservoir is established, essentially primitive melts generated at depth beneath it are able to take on characteristics of the lithosphere it passes through. This "wall rock reaction" process may be analogous to crustal contamination processes, however the chemical signature is likely to be indistinguishable from the lithospheric mantle the melt transits. This scenario may work well if the initial melt is particularly depleted in incompatible elements, but will retain its initial compatible element distribution. The resulting isotopic signature however, is likely to reflect that of its primary primitive or depleted mantle source.

In the case of the Tournefort Dykes, the active regional prehistory of the terrain argues against the long term evolution of a single stage enriched mantle. T_{DM} values of the Tournefort Dykes fall neatly into two groups (eg, figures 14 and 16, table 2), an older group, which is indistinguishable from T_{DM} values of the Sleaford Complex (figure 16), and those younger at 2.1 to 2.2 Ga. This suggests the presence and persistence of an old lithospheric component, either formed or completely reset during the Sleafordian Orogeny (2.6-2.7 Ga), which sourced the HMgT, HBaT and parts of the Dolerite Dykes. The younger, more primitive lithospheric source is observed in the FeRT and remaining Dolerite Dykes (table 4.1, figure 15). Such a source is likely to be a relatively juvenile asthenospheric underplate formed during extension associated with Hutchison Group sedimentation. Additionally, trends suggesting interaction between enriched subcontinental lithospheric mantle and plume-type sources are observed on isotope vs HFS/LIL element plots such as figure 15. Hence, the older, more evolved (low ε_{Nd} dykes) source is partially attributed to a plume component, which also provided the necessary thermal input to drive remelting of the older lithospheric keel. Such a melting mechanism is necessary as decompression melting during continued extension is considered unlikely after removal of hydrous phases and volatiles from the lithospheric mantle during Lincoln Batholith generation. Since only ~20-30 Ma elapsed after Lincoln Batholith magmatism prior to Tournefort Dyke emplacement, it appears unlikely that the lithospheric mantle could

become sufficiently enriched in hydrous phases and incompatible elements to generate the Tournefort Dykes in this time.

Therefore, the diversity of chemistry within the Tournefort Dykes can be attributed to entrainment of both ancient and juvenile lithospheric mantle in an ascending plume, emplaced at ~1815 Ma.

In conclusion, the Tournefort Dykes place some constraints on the nature of the continental lithospheric mantle. They argue for the development and persistence of large volumes of ancient lithospheric mantle beneath stable cratonic regions, able to be sampled repeatedly during crustal evolution (eg, Miltalie Gneiss and Lincoln Batholith magmatism prior to Tournefort Dyke extraction). Their longevity also implies the existence of a mechanism capable of replenishing volatiles and incompatible elements in the lithospheric mantle. Mechanisms involving percolation of fluids from the lower mantle such as those invoked by Erlank et al., (1987); McKenzie (1989) and Hawkesworth and Turner (1995) are likely to be appropriate. Since the Tournefort Dykes were emplaced *after* protracted extension and thermal perturbations associated with Lincoln Batholith magmatism, a mechanism other than continued extensional melting is required. A mantle plume able to interact with the subcontinental lithospheric mantle provides the necessary of thermal energy to the lithospheric mantle and continental crust.

Acknowledgments

Martin Hand is thanked for numerous discussions, as well as assistance and support in fieldwork. This research was undertaken while BFS was on an APRA scholarship.

References

Bales, 1996. A structural analysis of Wanna, South Australia: The comparative behaviour of mafic dykes and granite during deformation. *Honours Thesis, University of Melbourne. Unpublished.*

Bartlett, J.M., Dougherty-Page, J.S., Harris, N.B.W., Hawkesworth, C.J. and Santosh, M., *in press*. The application of zircon evaporation and model Nd ages to the interpretation of polymetamorphic terranes: an example from the Proterozoic mobile belt of south India. *Contributions to Mineralogy and Petrology.*

Bendall, B.R., 1994. Metamorphic and geochronological constraints on the Kimban Orogeny, southern Eyre Peninsula. *University of Adelaide, Honours Thesis. Unpubl.*

Black, L.P., Kinny, P.D. and Sheraton, J.W., 1991. The difficulties of dating mafic dykes: an Antarctic example. *Contributions to Mineralogy and Petrology,* **109**, p.183-194.

Bradley, G.N., 1972. The geochemistry of a medium pressure granulite terrain at southern Eyre Peninsula, Australia. *Australian National University Ph. D. Thesis. Unpublished.*

Cadman, A.C., Tarney, J. and Baragar, W.R.A., 1995. Nature of mantle source contributions and the role of contamination and *in situ* crystallisation in the petrogenesis of Proterozoic mafic dykes and flood basalts, Labrador. *Contributions to Mineralogy and Petrology,* **122**, p. 213-219.

Cadman, A.C., Tarney, J. and Hamilton, M.A., 1997. Petrogenetic relationship between Palaeoproterozoic tholeiitic dykes and associated high Mg noritic dykes, Labrador, Canada. *Precambrian Research,* **82**, p. 63-84.

Condie, K.C., 1997. Sources of Proterozoic mafic dyke swarms: constraints from Th/Ta and La/Yb ratios. *Precambrian Research,* **81**, p. 3-14.

Dougherty-Page, J.S. and Foden, J., 1996. A Pb-Pb zircon evaporation date for the Charleston Granite: Comparisons with other zircon geochronology techniques. *Australian Journal of Earth Sciences,*

Drexel, J.F., Preiss, W.V. and Parker, A.J. (eds), 1993. The Geology of South Australia. Vol. 1. The Precambrian. *South Australian Geological Survey.* **Bulletin 54**.

Erlank, A.J., Waters, F.G., Hawkesworth, C.J., Haggerty, S.E., Allsopp, H.L., Rickard, R.S. and Menzies, M.A., 1987. Evidence for mantle metasomatism in peridotite nodules from the Kimberly pipes, South Africa. In: Menzies, M.A. and Hawkesworth, C.J. (eds), *Mantle Metasomatism.* Geological Series, Academic Press, New York. p.221-312.

Fahrig, W.F., 1987. The tectonic settings of continental mafic dyke swarms: failed arm and passive margin. *Geological Association of Canada, Special Papers,* **34**, 331-348.

Fanning, C.M., 1997. Geochronological synthesis of southern Australia. Part II. The Gawler Craton. *South Australia. Department of Mines and Energy. Open file envelope, 8918. Unpublished.*

Fanning, C.M., Cooper, J.A., Oliver, R.L. and Ludwig, K.R. 1986. Rb-Sr and U-Pb geochronology of the Carnot Gneisses: complex isotopic systematics for the late Archaean to Early Proterozoic Sleaford Complex, southern Eyre Peninsula, South Australia. *Geological Society of Australia. Abstracts,* **15** p. 69-70.

Fanning, C.M., Flint, R.B., Parker, A.J., Ludwig, K.R. and Blissett, A.H., 1988. Refined Proterozoic evolution of the Gawler Craton, South Australia, through U-Pb zircon geochronology. *Precambrian Research.* **40/41**, p. 363-386.

Giddings, J.W. and Embleton, B.J.J., 1976. Precambrian palaeomagnetism in Australia II: Basic dykes from the Gawler Block. *Tectonophysics,* **30**, p. 109-118.

Glen, R.A., Laing, W.P., Parker, A.J. and Rutland, W.R., 1977. Tectonic relationships between the Proterozoic Gawler and Willyama orogenic domains, Australia. *Journal of the Geological Society of Australia.* **24, Pt 3**., p. 125-150.

Goldstein, S.L., 1988. Decoupled evolution of Nd and Sr isotopes in the continental crust and the mantle. *Nature* **336**, p. 733-738.

Griffen, W.L., O'Reilly, S.Y. and Stabel, A., 1988. Mantle metasomatism beneath western Victoria, Australia: II. Isotopic geochemistry of Cr-diopside lherzolites and Al-augite pyroxenites. *Geochimica et Cosmochimica Acta,* **52**, p. 449-459.

Hageskov, B., 1997. Geochemistry and tectonic significance of late Gothian mafic dykes in the Østfold-Marstrand belt of S.E. Norway and W. Sweden. *Precambrian Research,* **82**, p. 287-309.

Hand, M., Bendall, B. and Sandiford, M., 1995. Metamorphic evidence for Palaeoproterozoic oblique convergence in the eastern Gawler Craton. *Geological Society of Australia. Abstracts.* **Vol 40**, p 59

Hand et al. in prep

Hergt, J.M., Chappell, B.W., McCulloch, M.T., McDougall, I. and Chivas, A.R., 1989. Geochemical and isotopic constraints on the origin of the Jurassic Dolerites of Tasmania. *Journal of Petrology,* **30(4)**, p. 841-883.

Hoek, J.D., 1994. Mafic dykes of the Vestfold Hills, East Antarctica. *University of Utrecht. Ph.D. Thesis. Unpublished.*

Hoek, J.D. and Seitz, H.-M., 1995. Continental dyke swarms as tectonic indicators: An example from the Vestfold Hills, East Antarctica. *In:* Dirks, P.H.G.M., Hoek, J.D. and Passchier, C.W. (eds). *Tectonics of East Antarctica, Precambrian Research.*

Hoek, J.D. and Schaefer, B.F. in press. The Palaeoproterozoic Kimban mobile belt, Eyre Peninsula: Timing and significance of felsic and mafic magmatism and deformation. *Australian Journal of Earth Sciences.*

Kuehner, S.M., 1989. Petrology and geochemistry of early Proterozoic high Mg dykes from the Vestfold Hills, Antarctica. In: Crawford, A.J. (ed). *Boninites and related rocks.* Unwin Hyman. London. p. 208-231.

Lanyon, R., Black, L.P. and Seitz, H-M., 1993. U-Pb zircon dating of mafic dykes and its application to the Proterozoic geological history of the Vestfold Hills, East Antarctica. *Contributions to Mineralogy and Petrology.* **115**, p. 184-203.

LeCheminant, A.N. and Heaman, L.M., 1989. Mackenzie igneous events, Canada: Middle Proterozoic hotspot magmatism associated with ocean opening. *Earth and Planetary Science Letters,* **96**, p. 38-48.

Mazzucchelli, M., Rivalenti, G., Piccrillo, E.M., Girardi, V.A.V., Civetta, L. and Petrini, R., 1995. Petrology of the Proterozoic mafic dyke swarms of Uruguay and constraints on their mantle source composition. *Precambrian Research,* **74**, p. 177-194.

Menzies, M.A., Rogers, N., Tindle, A. and Hawkesworth, C., 1987. Metasomatic and enrichment processes in lithospheric peridotites, an effect of asthenosphere-lithosphere interaction. In: Menzies, M. and Hawkesworth, C. (eds), *Mantle Metasomatism*, p. 313-361. Academic Press, UK.

Mortimer, G.E., 1984. Early to Middle Proterozoic, basaltic dykes and associated layered rocks of southeastern Eyre Peninsula, South Australia. *University of Adelaide, PhD. Thesis. Unpublished.*

Mortimer, G.E., Cooper, J.A. and Oliver, R.L., 1988a. The geochemical evolution of Proterozoic granitoids near Port Lincoln in the Gawler Orogenic Domain of South Australia. *Precambrian Research.* **40/41**, p. 387-406.

Mortimer, G.E., Cooper, J.A. and Oliver, R.L., 1988b. Proterozoic mafic dykes near Port Lincoln, South Australia: Composition, age and origin. *Australian Journal of Earth Sciences,* **35**, p. 93-110.

O'Brien, H.E., Irving, A.J., McCallum, I.S. and Thirlwall, M.F., 1995. Strontium, neodymium and lead isotopic evidence for the interaction of post-subduction asthenospheric potassic magmas of the Highwood Mountains, Montana, USA, with ancient Wyoming craton lithospheric mantle. *Geochimica et Cosmochimica Acta,* **59**, p. 4539- 4556.

O'Reilly, S.Y. and Griffin, W.L., 1988. Mantle metasomatism beneath western Victoria, Australia: I. Metasomatic processes in Cr-diopside lherzolites. *Geochimica et Cosmochimica Acta,* **52**, p. 433-447.

Oussa, S., 1993. Description of a granulite facies shear zone (Kalinjala Mylonite Zone), and inferred cooling rates following granulite facies metamorphism. *Honours Thesis, University of Melbourne, Unpublished.*

Parker A.J., 1978. Structural, stratigraphic and metamorphic geology of Lower Proterozoic rocks in the Cowell/Cleve district, eastern Eyre Peninsula. *University of Adelaide Ph. D. thesis. Unpublished.*

Parker, A.J. and Lemon, N.M., 1982. Reconstruction of the Early Proterozoic stratigraphy of the Gawler Craton, South Australia. *Geological Society of Australia. Journal,* **29**, p. 221-238.

Richard, P., Shimuzu, N. and Allegre, C.J., 1976. $^{143}Nd/^{144}Nd$, a natural tracer: An application to oceanic basalts. *Earth and Planetary Science Letters*, **31**, p. 269-278.

Thomson, B.P., 1969. Precambrian crystalline basement. *In:* Parkin, L.W. (Ed.) Handbook of South Australian geology. *Geological Survey of South Australia.* p. 21-48.

Tilley, C.E., 1921. The granite gneisses of Southern Eyre Peninsula (South Australia) and their associated amphibolites. *Quarterly Journal of the Geological Society of London,* **77**, p. 75-134.

Turner, S.P. and Hawkesworth, C.J., 1994. The nature of the sub-continental mantle: constraints from the major-element composition of continental flood basalts. *Chemical Geology*, **120**, p. 295-314.

Weaver, B.L. and Tarney, J., 1981. The Scourie dyke suite: petrogenesis and geochemical nature of the Proterozoic subcontinental mantle. *Contributions to Mineralogy and Petrology,* **78**, p. 175-188.

Webb, A.W., Thomson, B.P., Blissett, A.H., Daly, S.J., Flint, R.B. and Parker, A.J., 1986. Geochronology of the Gawler Craton, South Australia. *Australian Journal of Earth Sciences*, **33** p.119-143.

Wedepohl, K.H. and Muramatsu, Y., 1979. The chemical composition of kimberlites compared with the average composition of three basaltic magma types. In: Boyd, F.R. and Meyer, H.O.A. (eds). *Kimberlites, diatremes and diamonds; their geology, petrology and geochemistry*, Proceedings of the International Kimberlite Conference. 2, **Vol 1**, p. 300-312.

Zhao, J.X., and McCulloch, M.T., 1993a. Melting of a subduction modified continental lithospheric mantle: Evidence from Late Proterozoic mafic dike swarms in central Australia. *Geology,* **21**, p. 463-466.

Zhao, J.X. and McCulloch, M.T., 1993b. Sm-Nd isochron ages of Late Proterozoic dyke swarms in Australia: evidence for two distinctive events of mafic magmatism and crustal extension. *Chemical Geology (Isotope Geoscience Section),* **109**, p. 341-354.

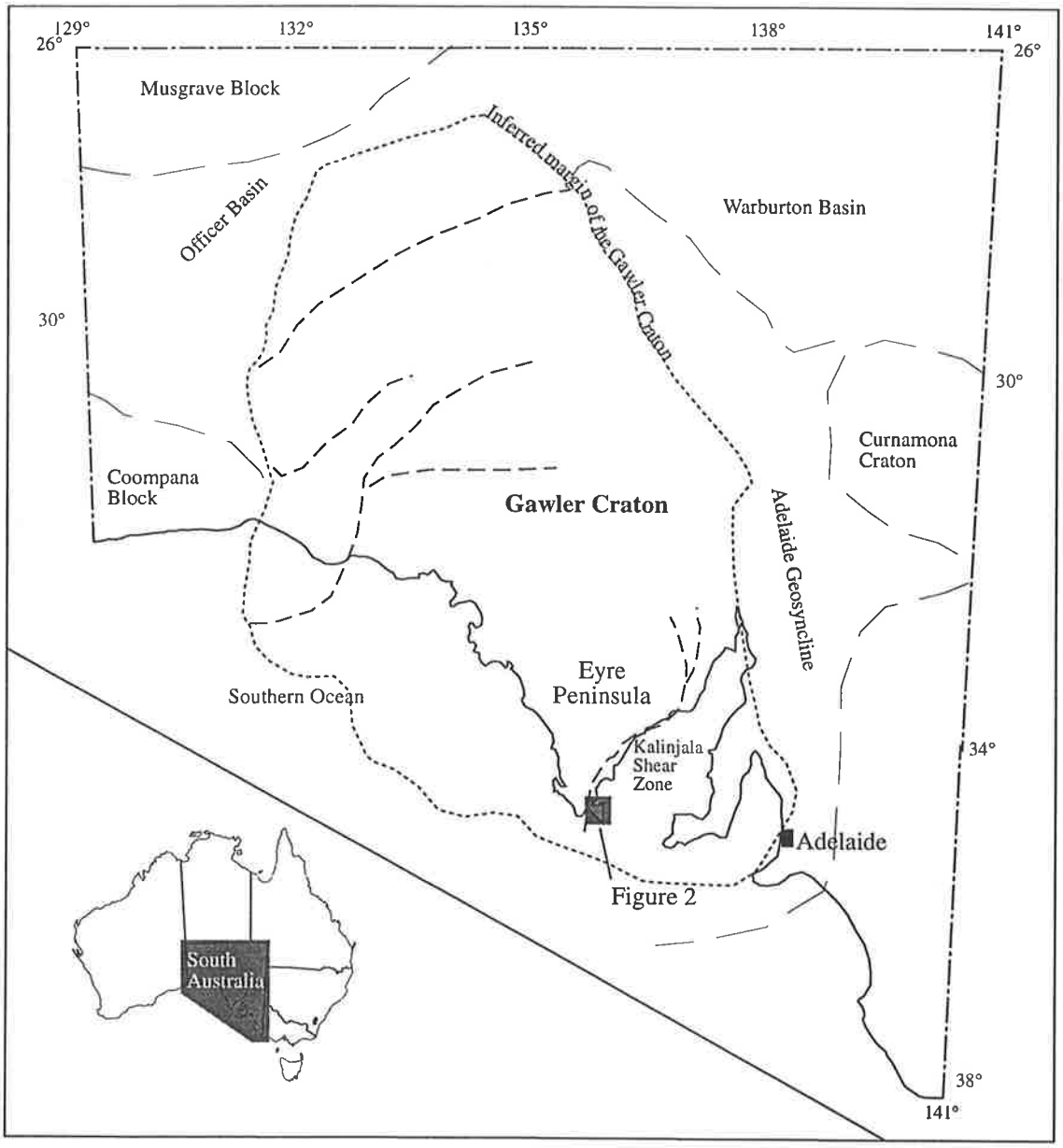

Figure 1: Location of the Gawler Craton and surrounding terrains.

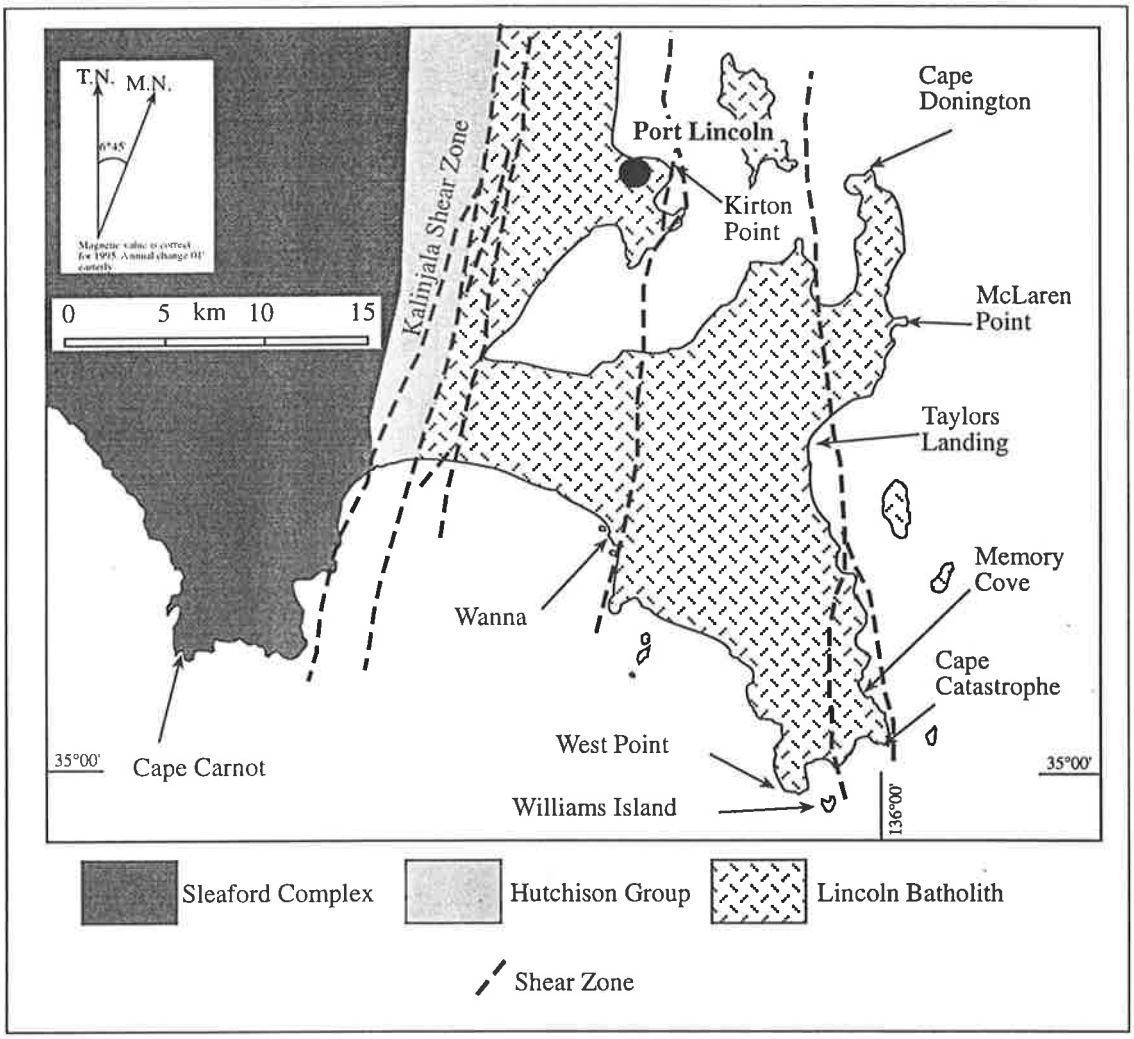

Figure 2: Major geological features and key localities on southern Eyre Peninsula.

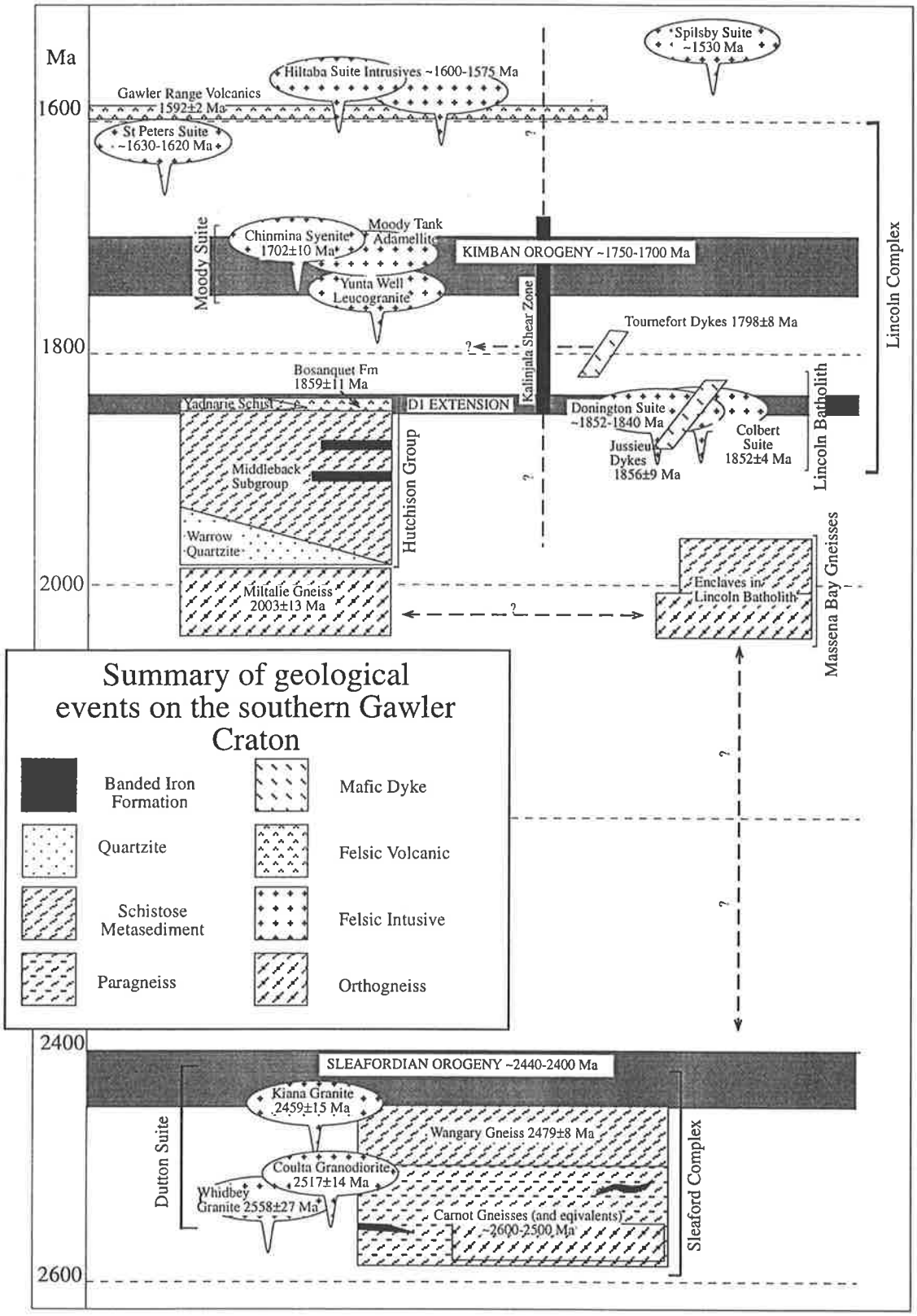

Figure 3: Summary of Precambrian stratigraphy and geological events on the southern Eyre Peninsula.

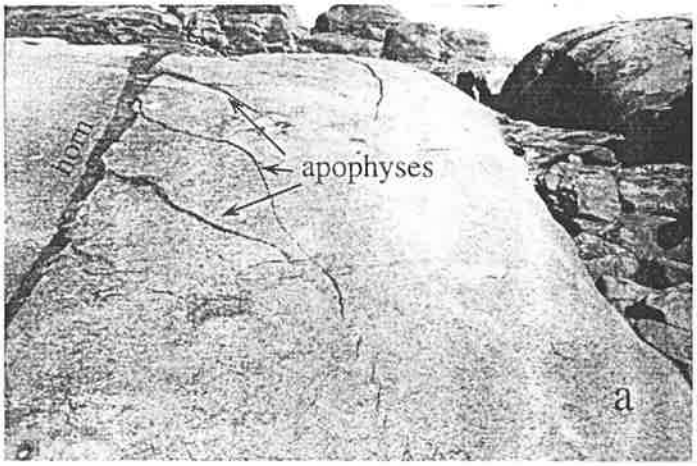

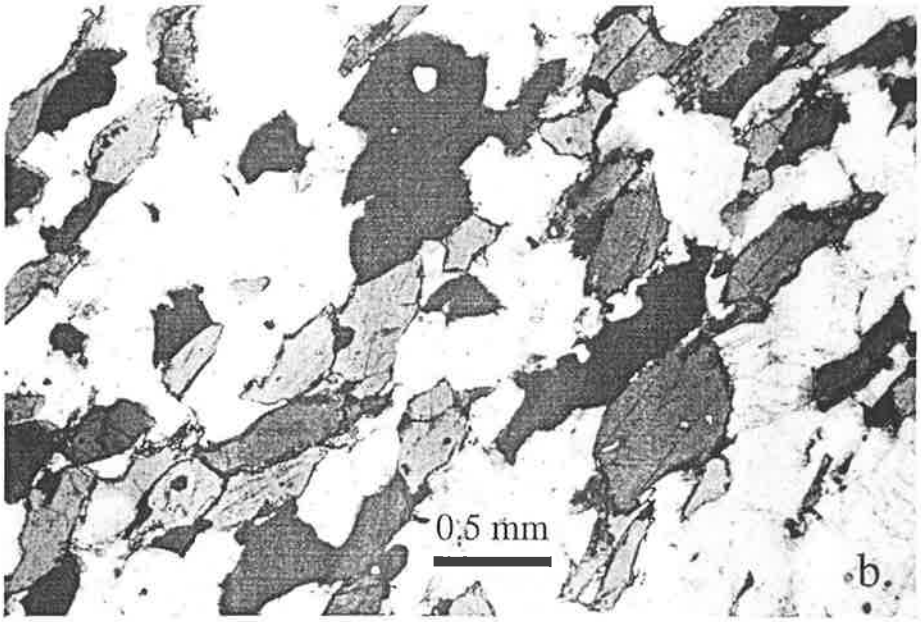

Figure 4: a) Preservation of dyke propagation features in Tournefort Dykes, northwestern Williams Island. Notebook is 15cm long. b) Photomicrograph of Tournefort Dykes metamorphosed to amphibolite gneiss. All ferromagnesian phases in field of view (dominantly hornblende) are secondary. Kirton Point.

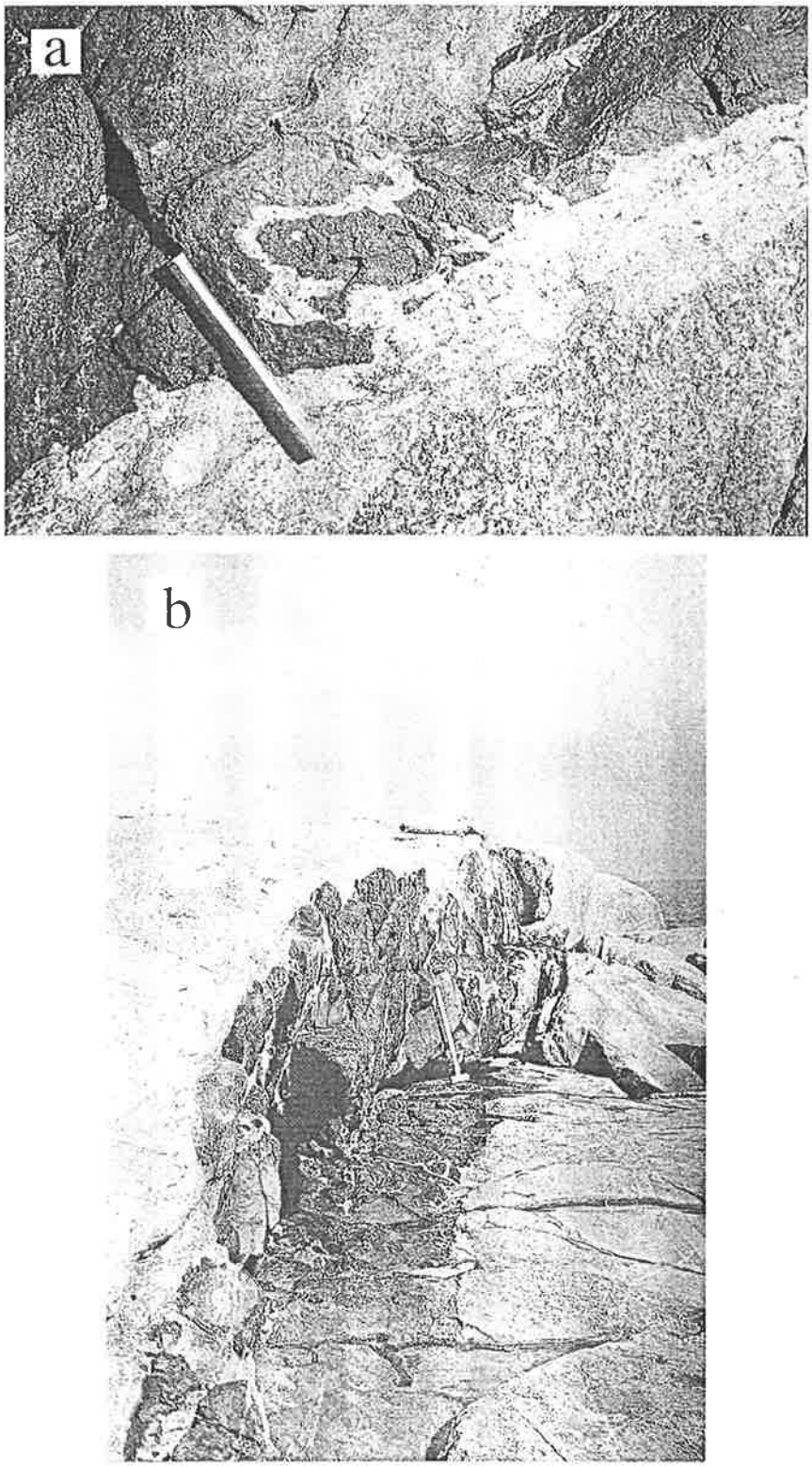

Figure 5: a) Jussieu Dyke margin displaying backveining of the dyke by felsic selvage generated during propagation. Incipient disaggregation into rounded and angular enclaves is present. Chisel ~15 cm. b) Backveined Jussieu Dyke maintaining planar character despite extensive selvage intrusion. Trend N-S, hammer ~1m. Both photographs from the west coast of Williams Island.

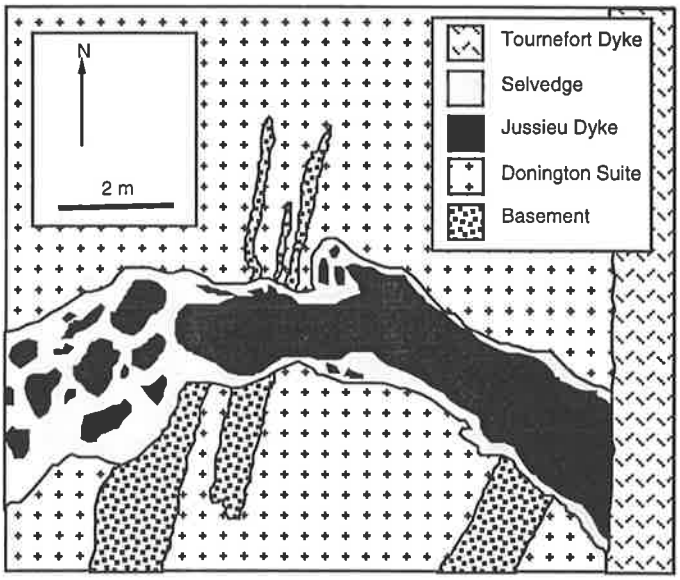

Fig 6: Crosscutting relationships between Jussieu Dykes, basement enclaves, Donington Suite felsics and the oldest set of Tournefort Dykes (trending roughly N-S). From an outcrop just off the northeastern point of Williams Island.

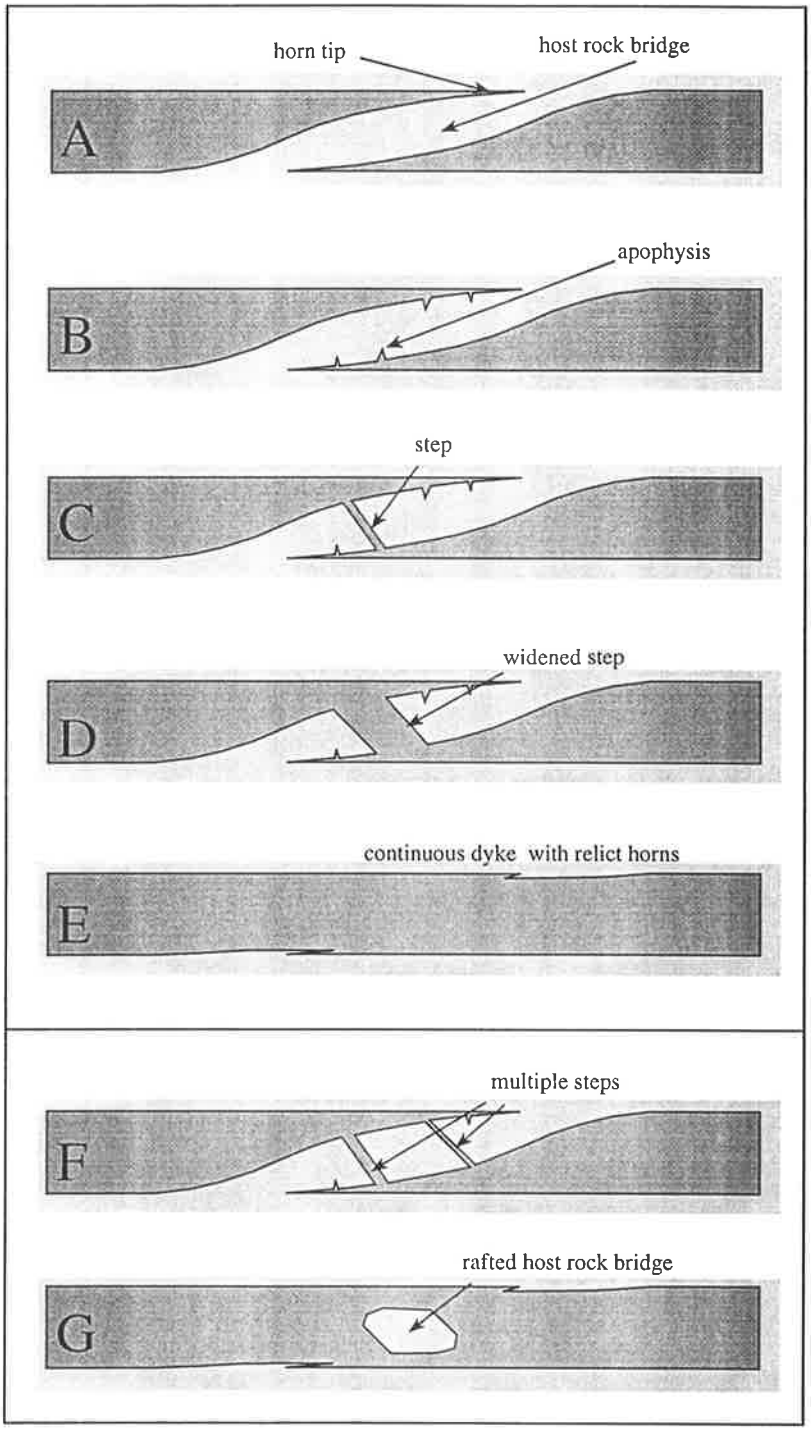

Figure 7: Evolution of dyke propagation features observed in low strain zones on southern Eyre Peninsula. Dyke tips propagate either vertically or laterally (A). Extension on the inner surfaces of the tips causes the formation of apophyses (B), which may ultimately breach the bridge of intervening country rock , forming a step (C). Continued passage of material through the step can cause it to widen (D), ultimately resulting in a dyke of original thickness, containing parallel margins with relict horn tips (E). In some cases, multiple steps may be formed (F), forming a raft of host rock material within the body of the dyke (G). Scale: from millimetres to tens of metres.

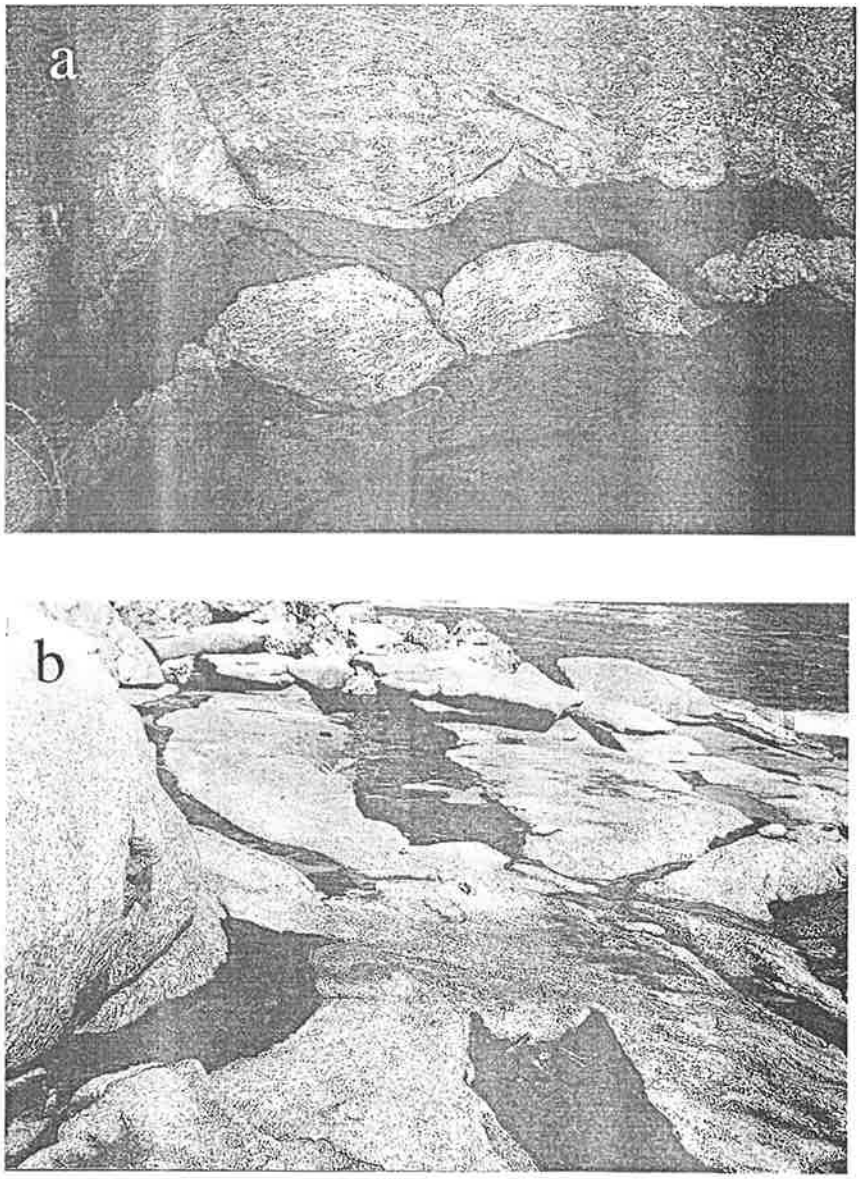

Figure 8: a)Boudinage of felsic gneiss between a mafic dyke and one of its horns. Note the presence of relict apophyses which have focussed strain during deformation. This situation is likely to be a deformed equivalent of that depicted in figure 7d. Kirton Point, pen ~10 cm. b) Pull apart of previously continuous planar mafic dykes to produce discrete mafic rafts. Continued deformation would result in isolated pods of mafic material preserving little evidence of a dyke-like origin. Wanna, broad dyke in centre is ~1 m wide.

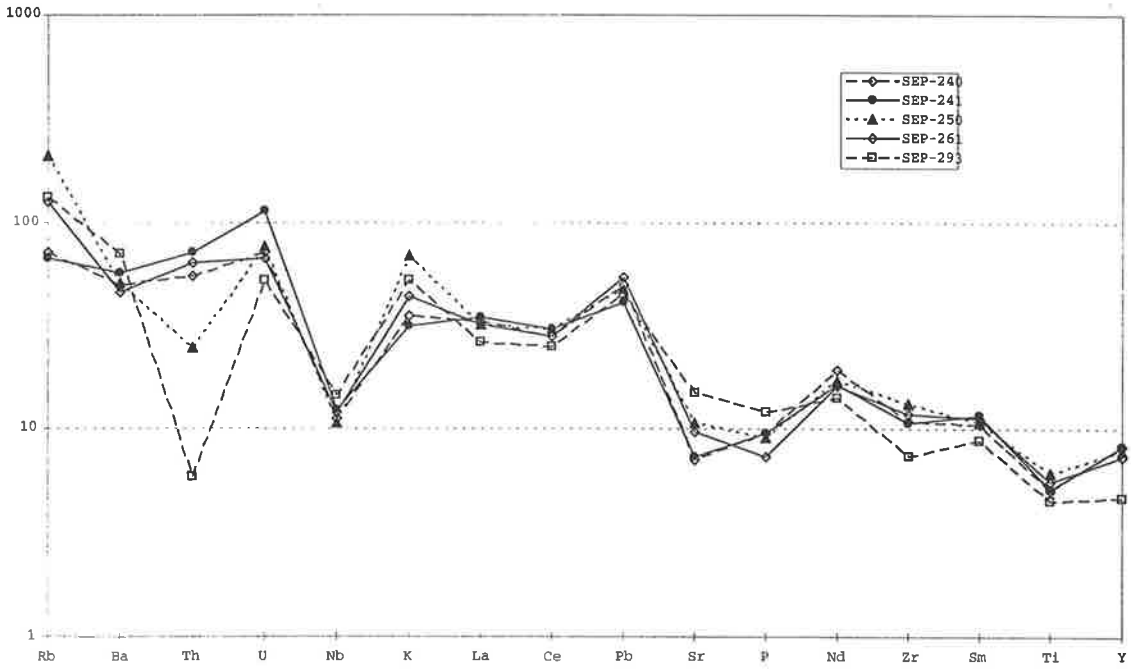

Figure 9: Trace element variation diagram for the Jussieu Dykes, normalised to primitive mantle values from Sun and McDonough, 1991.

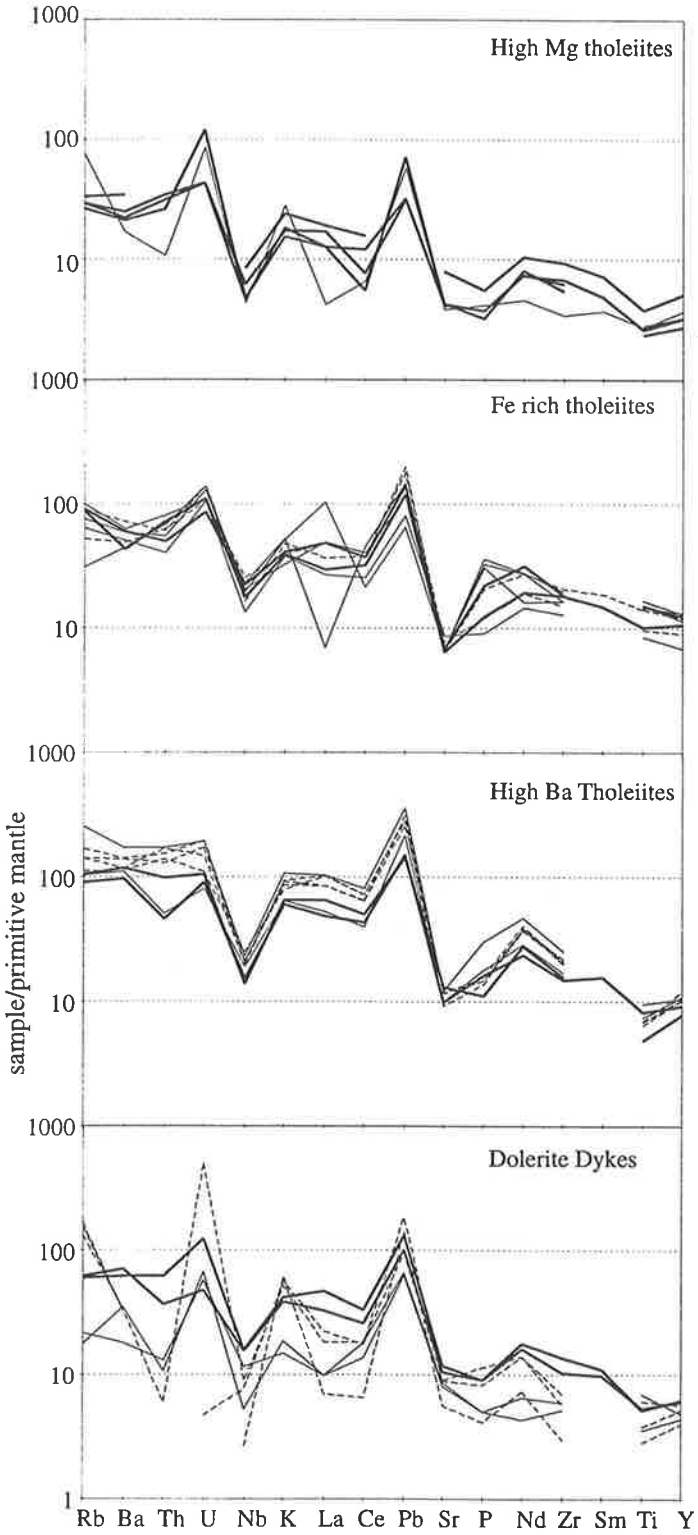

Figure 10: Comparative trace element variation diagrams displaying initial compositions and the effects of amphibolitisation of the Tournefort Dykes. Broad solid lines = undeformed dykes, narrow solid lines = hornblende+biotite amphibolites and dashed lines = gt bearing amphibolites.

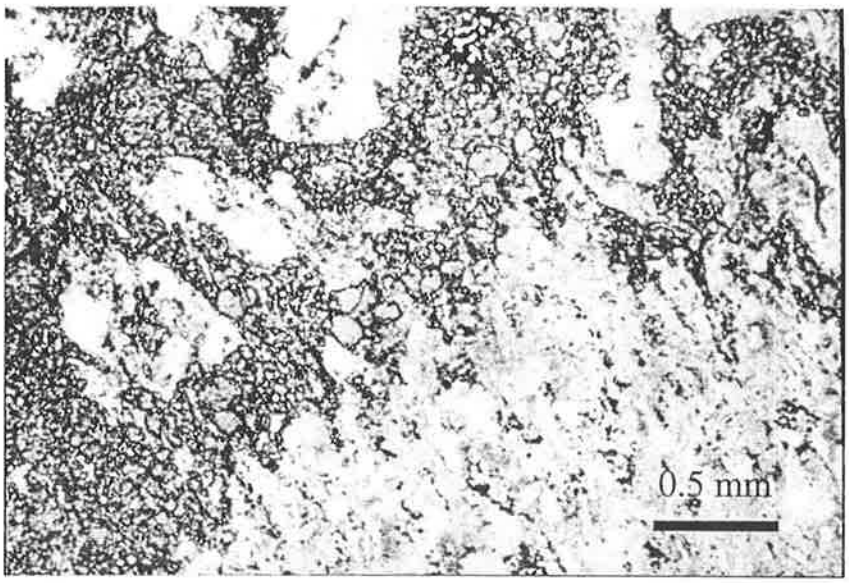

Figure 11: Photomicrograph of felsic segregation - Tournefort Dyke contact. Note diffuse and irregular margin of segregation. Such irregular margins are distinct from subsequent Kimban felsic veins which show sharp edges.

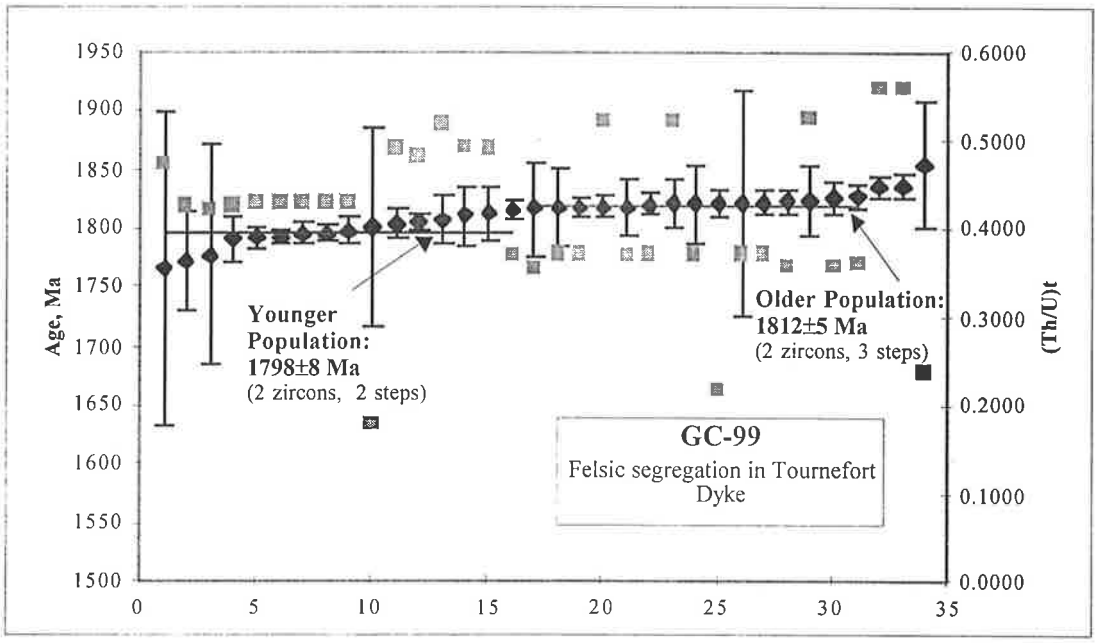

Figure 12: Summary of Pb-Pb zircon evaporation data from 4 zircons in sample GC-99 by block. Horizontal lines indicate mean values for the older and younger populations, error bars are 2σ. The data is arranged in ranked order of age calculated for each block analysed.

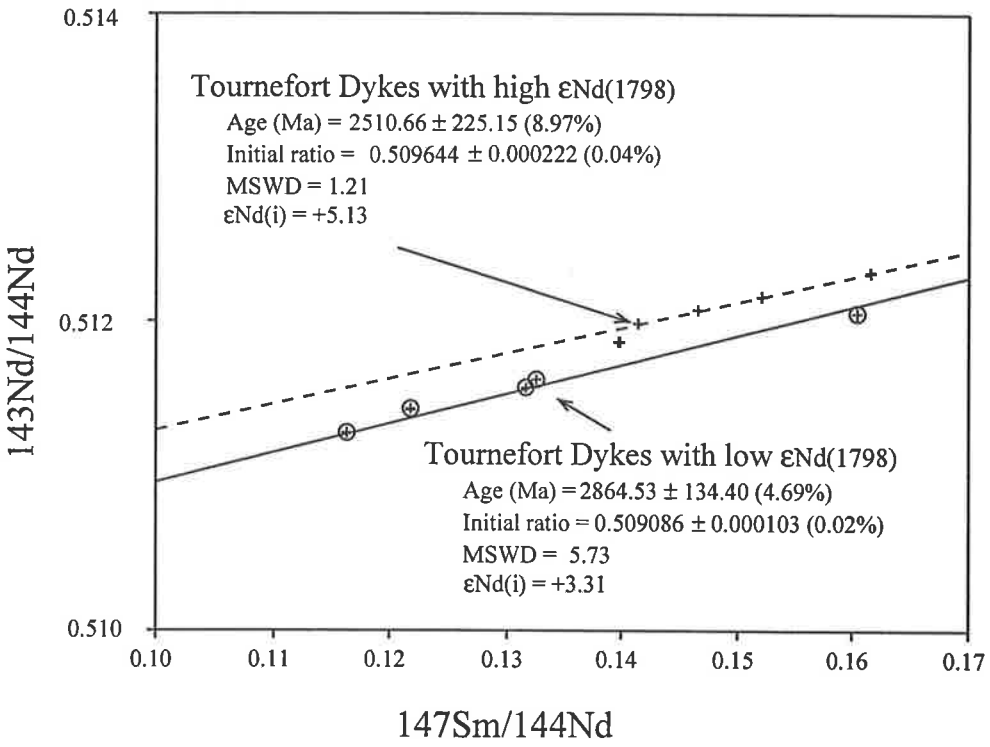

Figure 13: Isochrons generated for the two Nd isotopic groups of the Tournefort Dykes.

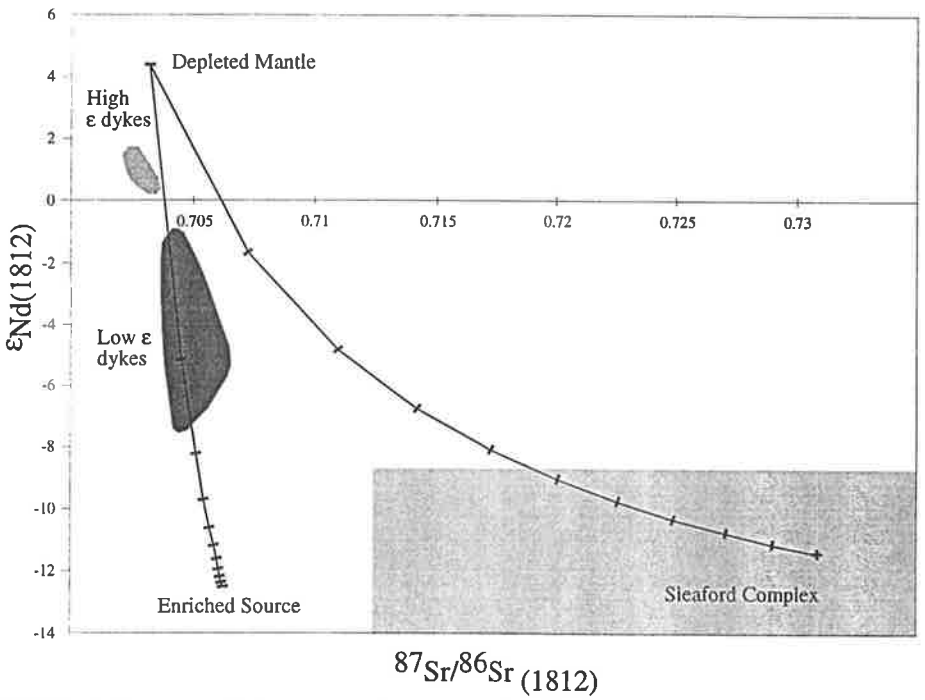

Figure 14: Nd-Sr isotope mixing curves between the depleted mantle, contemporary crust (ie, Sleaford Complex) and an enriched mantle source at the time of Tournefort emplacement. Mantle values from Sun and McDonough (1989), enriched (kimberlitic) source from Wedepohl and Muramatsu (1979). Tick marks at 10% intervals.

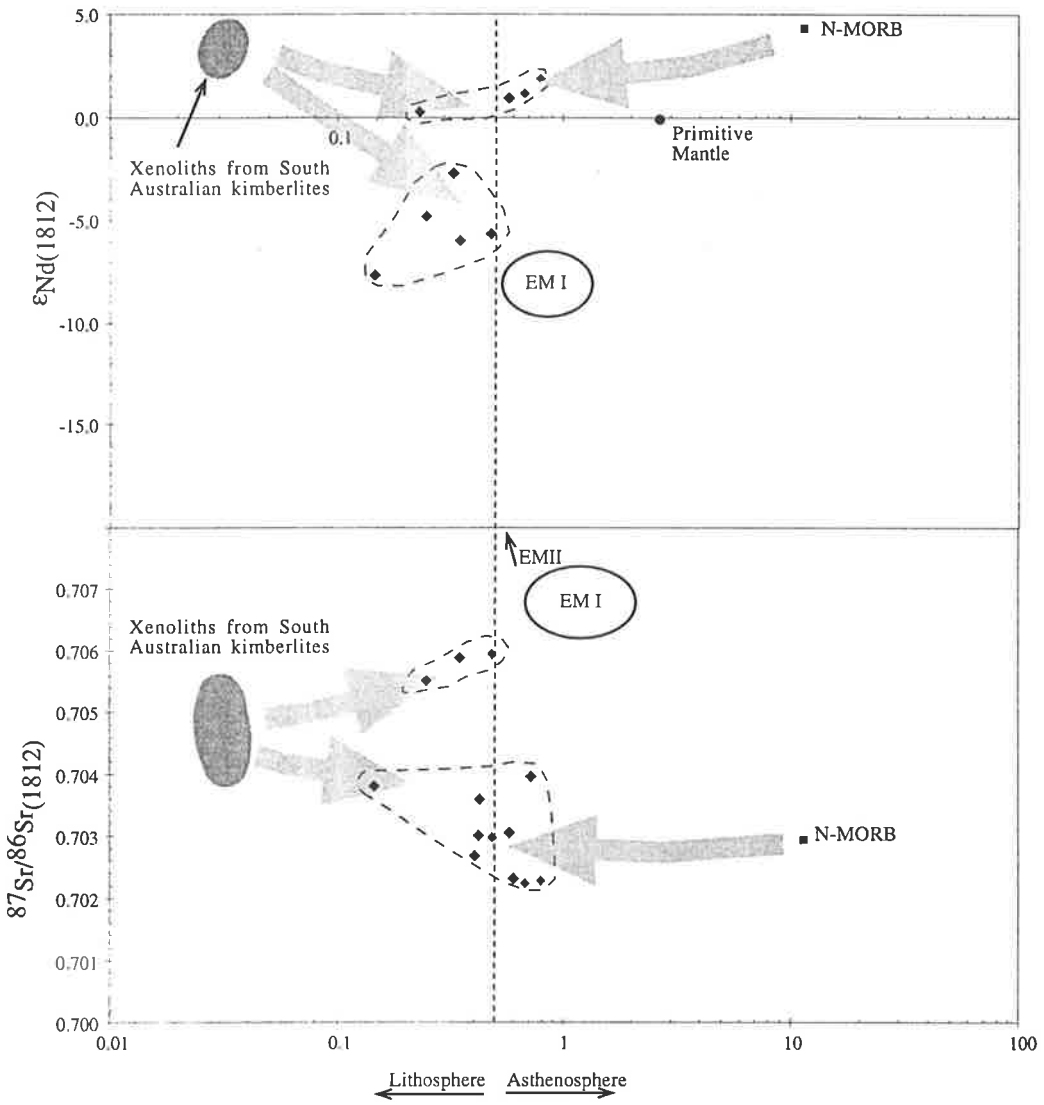

Figure 15: Isotopic variations with HFS/LILE ratio (Zr/Ba) with potential mantle reservoirs highlighted for the Tournefort Dykes. Note the tendency to scatter between an asthenospheric and subcontinental lithospheric source. Note also a trend for a subset of the Tournefort Dykes towards an OIB or plume related source. Cutoff Zr/Ba ratio = 0.5 arbitrarily derived from Hawkesworth and Gallagher (1993); Xenolith data from Song (1994). EM I = Enriched Mantle reservoir I, EM II = Enriched Mantle reservoir II, both subsets of OIB's (Ocean Island Basalts). N-MORB = "Normal" Mid Ocean Ridge Basalt.

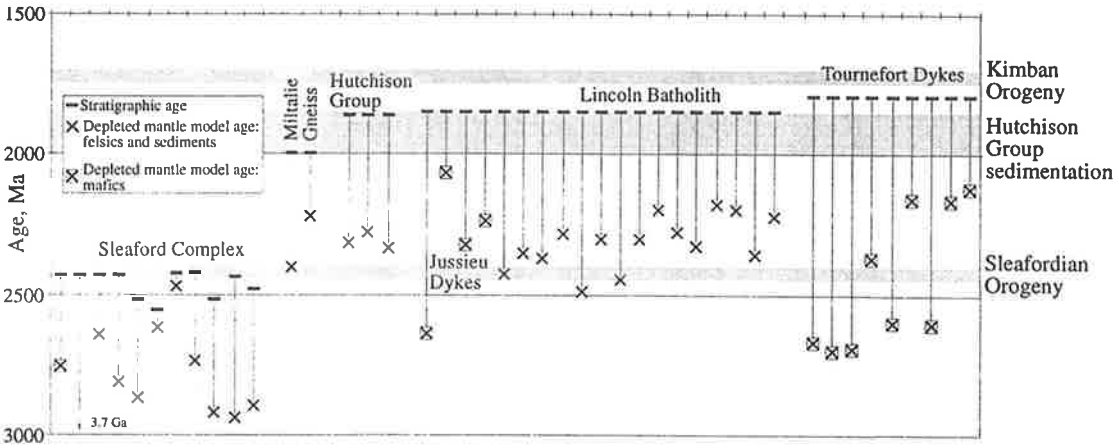

Figure 16: Summary of depleted mantle model ages as a function of stratigraphic age and lithotype for the southern Eyre Peninsula. Major geological events are shaded.

Lithology	Jussieu Dyke	Jussieu Dyke	Jussieu Dyke	Jussieu Dyke
Sample #	SEP-241	SEP-250	SEP-261	SEP-293
Location	Nth Taylors Lag	West Pt	Williams Is	Williams Is
Est Age (Ma)	*1850*	*1850*	*1850*	*1850*
SiO_2%	49.33	48.40	51.26	51.62
Al_2O_3%	15.99	16.37	16.12	14.45
Fe_2O_3%	13.41	13.07	13.14	10.57
MnO%	0.18	0.17	0.19	0.16
MgO%	7.36	6.08	6.06	8.29
CaO%	9.67	8.89	7.75	9.10
Na_2O%	2.53	3.16	3.20	2.83
K_2O%	0.95	2.04	1.32	1.57
TiO_2%	1.11	1.34	1.21	0.98
P_2O5%	0.21	0.20	0.16	0.26
SO_3%	0.02	0.03	0.02	0.02
LOI%	-0.06	0.26	-0.14	0.35
TOTAL	100.70	100.01	100.29	100.20
Rb	42.819	132.052	79.751	83.129
Ba	400	353	324	489
Th	6.1	2.1	5.4	0.5
U	2.4	1.6	1.4	1.1
Nb	8.8	7.6	8.6	10.4
La	24	22	22	18
Ce	54	54	50	45
Pb	7.6	8.8	10.0	8.4
Sr	156.220	225.575	206.799	315.835
Nd	22.177	23.282	21.752	19.313
Zr	119.5	149.0	133.7	82.3
Sm	5.199	4.760	4.968	3.917
Y	37.5	36.0	33.3	21.3
V	202	173	164	213
Sc	34.0	32.1	27.0	24.9
Cr	296	104	88	840
Ga	19.9	19.9	20.7	16.8
$^{143}Nd/^{144}Nd$	0.511765	0.511825	0.511876	0.511700
2σ	0.000062	0.000052	0.000048	0.000062
$^{147}Sm/^{144}Nd$	0.1418	0.1237	0.1382	0.1227
$T_{(DM)}$ Nd	**2.94**	**2.25**	**2.58**	**2.43**
$\varepsilon_{Nd(t)}$	-4.04	1.46	-0.99	-0.75
$^{87}Sr/^{86}Sr$	0.725881	0.747921	0.733507	0.723656
2σ	0.000100	0.000088	0.000128	0.000074
$^{87}Rb/^{86}Sr$	0.7944	1.7004	1.1186	0.7627
$^{87}Sr/^{86}Sr_{(t)}$	0.70473	0.70266	0.70373	0.70335

Table 1: Geochemical and isotopic data for the Jussieu Dykes.

Lithology	HMgT	HMgT Amphib.	HBaT Amphib.	FeRT	FeRT	Dolerite	Dolerite	Dolerite Amphib.
Sample #	SEP-148	SEP-024	1028-99	SEP-270	SEP-081	SEP-220	SEP-260	1028-110
Location	Memory Cove	Pt. Boling	West Pt	Williams Island	West Pt	West Pt	Williams Island	Tumby Hills
Est Age (Ma)	*1798*	*1798*	*1798*	*1798*	*1798*	*1798*	*1798*	*1798*
SiO_2%	49.07	47.39	51.00	48.07	49.79	53.33	47.70	56.71
Al_2O_3%	8.99	12.96	14.40	13.19	13.63	17.65	14.48	14.84
Fe_2O_3%	11.95	12.10	18.02	17.93	16.75	11.03	15.35	11.73
MnO%	0.19	0.19	0.22	0.26	0.24	0.15	0.22	0.17
MgO%	21.39	12.06	4.62	6.42	5.29	4.40	7.24	3.89
CaO%	6.74	10.96	8.80	9.61	9.43	9.49	9.96	7.06
Na_2O%	0.78	1.97	2.29	2.38	2.61	3.05	2.69	0.65
K_2O%	0.50	0.81	1.73	0.51	1.13	1.21	0.69	1.57
TiO_2%	0.55	0.58	1.76	2.11	2.17	1.12	1.58	1.40
P_2O5%	0.08	0.09	0.35	0.20	0.27	0.20	0.17	0.19
SO_3%	0.01	0.00	0.02	0.04	0.01	0.00	0.03	0.02
LOI%	-0.24	1.10	-2.94	0.06	-0.51	-0.20	0.16	1.91
TOTAL	100.01	100.21	100.26	100.78	100.81	101.43	100.27	100.14
Rb	18.512	47.7311	56.898	17.230	55.3827	38.169	23.106	95.620
Ba	154.0	118.0	671.0	165	301.0	432	194	234
Th	2.6	0.9	3.9	3.0	6.0	5.2	3.1	9.1
U	0.9	1.8	1.9	0.1	2.3	2.6	1.2	4.2
Nb	4.4	3.1	11.0	9.7	12.7	11.4	7.4	10.1
La	12	3	34	15	21	33	15	19
Ce	14	12	79	41	59	61	37	54
Pb	2.2	4.1	10.6	4.9	8.5	9.4	7.1	5.5
Sr	86.487	80.243	208.945	164.702	135.544	248.553	177.105	150.898
Nd	9.889	6.240	31.912	18.875	26.338	24.300	18.952	25.016
Zr	74.7	38.5	167.1	130.4	203.4	152.8	112.0	169.3
Sm	2.151	1.654	6.999	5.040	6.626	4.890	4.594	5.782
Y	14.6	16.8	42.2	37.3	49.0	28.5	27.5	32.8
V	186	254.5	307.5	466	410.3	215	363	295.8
Sc	25.7	36.8	39.5	44.9	38.3	23.2	37.7	35.8
Cr	3009	1262	67	91	154	86	192	25
Ga	9.6	13.7	22.1	22.2	22.3	22.0	22.3	21.2
Eu	0.588							
Gd	2.310							
Dy	2.287							
Er	1.382							
Yb	1.373							
$^{143}Nd/^{144}Nd$	0.511570	0.512063	0.511627	0.512313	0.512167	0.511436	0.512085	0.511876
2 σ	0.000050	0.000064	0.000059	0.000036	0.000056	0.000024	0.000032	0.000059
$^{147}Sm/^{144}Nd$	0.1316	0.1603	0.1327	0.1615	0.1522	0.1217	0.1466	0.1398
$T_{(DM)}$ Nd	**2.67**	**2.70**	**2.60**	**2.13**	**2.16**	**2.61**	**2.16**	**2.37**
$\varepsilon_{Nd(t)}$	-5.86	-2.86	-4.99	1.76	1.07	-6.20	0.75	-1.77
$^{87}Sr/^{86}Sr$	0.722115	0.740074	0.726084	0.710167	0.733129	0.717462	0.712885	0.751932
2 σ	0.000048	0.000165	0.000049	0.000040	0.000120	0.000026	0.000036	0.000049
$^{87}Rb/^{86}Sr$	0.6202	1.7265	0.7893	0.3027	1.1851	0.4447	0.3777	1.8413
$^{87}Sr/^{86}Sr_{(t)}$	0.70608	0.69543	0.70567	0.70234	0.70248	0.70596	0.70312	0.70432

Table 2: Geochemical data for Tournefort Dykes with new isotopic data.

Geochemical Group	Number of samples	Age (2σ error)	MSWD	Initial Ratio
HMgT	3#	1796±28	135	0.70559
HBaT	2*	~1976	-	0.70362
FeRT	2*	~1809	-	0.70229
Dolerite Dykes	10	1646±33	58	0.70475
All Tournefort	17#	1817±43	38	0.70365

Table 3: Summary of whole rock isochron ages for geochemical groupings in the Tournefort Dykes. * = two point "errorchron", #= discarding amphibolitised sample SEP-024 from regression.

Appendix 6:

Paper: "Palaeoproterozoic Kimban mobile belt, Eyre Peninsula: timing and significance of felsic and mafic magmatism and deformation"

Hoek, J.D. & Schaefer, B. F. (1998) Palaeoproterozoic Kimban mobile belt, Eyre Peninsula: Timing and significance of felsic and mafic magmatism and deformation. *Australian Journal of Earth Sciences 45*(2) 305-313

Appendix 7:

Abstracts arising from this study:

Schaefer, B.F., Hand, M., Bendall, B., Foden, J. and Sandiford, M. 1995. Chronology of magmatism and deformation in the Lincoln Complex; constraints on the Kimban Orogeny. *Geological Society of Australia. Abstracts.* **Vol 40**, p 149.

Schaefer, B.F. 1996. Geochemical evolution of magmatism and deformation in the Palaeoproterozoic Lincoln Complex, South Australia: Insights into orogenesis and tectonism during the Proterozoic. *Geological Society of Australia. Abstracts.* **Vol 41**, p 378.

Schaefer, B.F. Hoek, J.D. and Foden, J. 1997a. Physical and chemical characteristics of the Lincoln Batholith: Aspects of Palaeoproterozoic magmatism and potential analogues. *Geological Society of Australia. Abstracts.* **Vol 45**, p 82-84.

Schaefer, B.F., Foden, J. and Sandiford, M., 1997b. Palaeoproterozoic crustal evolution of the southern Eyre Peninsula, Gawler Craton, Australia. In *Seventh Annual V.M. Goldschmidt Conference,* p. 185, LPI Contribution No. 921, Lunar and Planetary Institute, Houston.

Schaefer, B. F., Hand, M., Benhall, B., Foden, J. & Sandiford, M. (1995) Chronolgy of magmatism and deformation in the Lincoln Complex: constraints on the Kimban Orogeny. *Geological Society of Australia. Abstracts 40,* 149

Schaefer, B. F. (1996) Geochemical evolution of magmatism and deformation in the Palaeoproterozoic Lincoln Complex, South Australia: Insights into orogenesis and tectonism during the Proterozoic. *Geological Society of Australia. Abstracts 41,* 378

Schaefer, B. F., Hoek, J.D., & Foden, J (1997a) Physical and chemical characteristics of the Lincoln Batholith: Aspects of Palaeoproterozoic magmatism and potentioal analogues. *Geological Society of Australia. Abstracts 45,* 82-84

Schaefer, B. F., Foden, J. & Sandiford, M. (1997b) Palaeoproterozoic crustal evolution of the southern Eyre Peninsula, Gawler Craton, Australia. In *Seventh Annual V.M. Goldschmidt Conference* (p. 185). LPI Contribution No. 921, Lunar and Planetary Institute, Houston.